DESIGN AND CONTROL OF LARGE-SCALE GRID-CONNECTED PHOTOVOLTAIC POWER PLANT WITH FAULT RIDE-THROUGH

ALI QASEM SALEH AL-SHETWI

Doctor of Philosophy

UNIVERSITI MALAYSIA PAHANG

UNIVERSITI MALAYSIA PAHANG

DECLARATION OF THESIS AND COPYRIGHT

Author's Full Name   : ALI QASEM SALEH AL-SHETWI

Date of Birth   : 1 January 1985

Title   : DESIGN AND CONTROL OF LARGE-SCALE GRID-CONNECTED PHOTOVOLTAIC POWER PLANT WITH FAULT RIDE-THROUGH

Academic Session   : SEM 1 2018/2019

I declare that this thesis is classified as:

    ☐ CONFIDENTIAL   (Contains confidential information under the Official Secret Act 1997)*

    ☐ RESTRICTED   (Contains restricted information as specified by the organization where research was done)*

    ☑ OPEN ACCESS   I agree that my thesis to be published as online open access (Full Text)

I acknowledge that Universiti Malaysia Pahang reserves the following rights:

1. The Thesis is the Property of Universiti Malaysia Pahang
2. The Library of Universiti Malaysia Pahang has the right to make copies of the thesis for the purpose of research only.
3. The Library has the right to make copies of the thesis for academic exchange.

Certified by:

_____

   (Student's Signature)   (Supervisor's Signature)

04001010   Ir.Dr. Muhamad Zahim Bin Sujod
New IC/Passport Number   Name of Supervisor
Date: Date:

NOTE : * If the thesis is CONFIDENTIAL or RESTRICTED, please attach a thesis declaration letter.

SUPERVISOR'S DECLARATION

I hereby declare that I have checked this thesis and in my opinion, this thesis is adequate in terms of scope and quality for the award of the degree of Doctor of Philosophy.

_____

(Supervisor's Signature)

Full Name   : IR.DR. MUHAMAD ZAHIM BIN SUJOD

Position   : SENIOR LECTURER

Date   : JAN 2019

STUDENT'S DECLARATION

I hereby declare that the work in this thesis is based on my original work except for quotations and citations which have been duly acknowledged. I also declare that it has not been previously or concurrently submitted for any other degree at Universiti Malaysia Pahang or any other institutions.

_____

(Student's Signature)

Full Name   : ALI QASEM SALEH AL-SHETWI

ID Number   : PEE15007

Date   : JAN 2019

DESIGN AND CONTROL OF LARGE-SCALE GRID-CONNECTED PHOTOVOLTAIC POWER PLANT WITH FAULT RIDE-THROUGH

ALI QASEM SALEH AL-SHETWI

Thesis submitted in fulfillment of the requirements
for the award of the degree of
Doctor of Philosophy

Faculty of Electrical & Electronics Engineering

UNIVERSITI MALAYSIA PAHANG

JANUARY 2019

ACKNOWLEDGEMENTS

ABSTRACT

Over the recent years, the installation of photovoltaic (PV) system and integration with electrical grid has become more widespread worldwide. With the significant and rapid increase of photovoltaic power plants (PVPPs) penetration to the electric grid, the power system operation and stability issues become crucial and this leads to continuous evaluation of grid interconnection requirements. For this purpose, the modern grid codes (GCs) require a reliable PV generation system that achieves fault ride-through (FRT) requirements. Therefore, the FRT capability becomes the state of art as one of the challenges faced by the integration of large-scale PV power stations into electrical grid that has not been fully investigated. This research proposes FRT requirements for the connection of PVPPs into Malaysian grid as new requirements. In addition, presents a comprehensive control strategy of large-scale PVPPs to enhance the FRT capability based on modern GCs connection requirements. In order to meet these requirements, there are two major issues that should be addressed. The first one is the ac over-current and dc-link over-voltage that may cause disconnection or damage to the grid inverter. The second one is the injection of reactive current to assist the voltage recovery and support the grid to overcome the voltage sag problem. To address the first issue, the dc-chopper brake controller and current limiter are used to absorb the excessive dc-voltage and limits excessive ac current, respectively, and therefore protect the inverter and ride-through the faults smoothly. After guaranteeing that the inverter is kept connected and protected, this control strategy can also ensure a very important aspect which is the reactive power support through the injection of reactive current based on the standard requirements. Feed-forward decoupling strategy based-dq control is used for smooth voltage fluctuation and reactive current injection. Furthermore, to keep the power balance between both sides of the inverter, PV array can generate a possible amount of active power according to the rating of grid inverter and voltage sag depth by operating in two modes, which are normal and FRT modes. These two modes of operation require fast and precise sag detection strategy to switch the system from normal mode to a faulty mode of operation for an efficient FRT control. For this purpose, RMS detection method has been used. In this research, the large-scale PV plant connected to the MV side of the utility grid, taking the compliance of TNB technical regulations for PVPPs into consideration has been modelled using MATLAB/Simulink with nominal rated peak power of 1500 kW. Analyses of the dynamic response for the proposed PVPP under various types of symmetrical and asymmetrical grid faults also had been investigated. As a conclusion, the PVPP connected to the power grid provided with FRT capability has been developed. The sizing of the suggested PV array is achieved in which the simulation results matched the sizing calculation results. Moreover, the results at the point of common coupling show that the proposed PVPP is compatible with TNB requirements, including the PV-grid connection method, PV inverter type, nominal voltage operating range, total harmonic distortion less than 5%, voltage unbalance less than 1%, frequency fluctuation within ± 0.1 Hz, and power factor higher than 0.9. In addition, the control simulation results presented demonstrate the effectiveness of the overall presented FRT control strategy, which aims to improve the capability of ride-through during grid faults safely, to keep the inverter connected, to ensure the safety of the system equipment, to ensure all values return to pre-fault values as soon as the fault is cleared within almost zero second as compared to the strategy without FRT control which needs around 0.25s, and to provide grid support through active and reactive power control at different types of faults based on the FRT standard requirements.

ABSTRAK

Dalam tahun-tahun kebelakangan ini, pemasangan sistem fotovoltaik (PV) dan integrasi dengan grid elektrik telah menjadi semakin meluas di seluruh dunia. Dengan peningkatan ketara dan pesat penyambungan loji janakuasa fotovoltaik (PVPPs) ke grid elektrik, isu-isu berkaitan operasi sistem kuasa dan kestabilan menjadi lebih penting dan membawa kepada penilaian berterusan terhadap syarat penyambungan ke grid. Untuk tujuan ini, baru-baru ini, kod grid moden (GCs) memerlukan sistem penjanaan PV yang boleh dipercayai dengan mencapai keperluan melangkaui ganguan (FRT). Oleh itu, keupayaan FRT menjadi sebagai salah satu cabaran yang dihadapi oleh stesen kuasa PV berskala besar bagi penyambungan ke grid elektrik yang belum disiasat sepenuhnya. Kajian ini mencadangkan keperluan FRT untuk sambungan PVPP ke grid Malaysia sebagai keperluan baru. Di samping itu, membentangkan strategi kawalan komprehensif PVPP berskala besar untuk meningkatkan keupayaan FRT berdasarkan keperluan sambungan GC moden. Untuk memenuhi keperluan penyambungan ini, terdapat dua isu utama yang perlu ditangani. Yang pertama adalah arus ulang alik (ac) terlebih arus serta arus terus (dc) terlebih voltan yang boleh menyebabkan pemotongan atau kerosakan pada penyongsang grid. Yang kedua ialah suntikan arus reaktif untuk membantu pemulihan voltan dan menyokong grid mengatasi masalah sag voltan. Untuk menangani isu pertama, pengawal brek dc-chopper dan penghad arus digunakan untuk menyerap voltan dc yang berlebihan dan mengehadkan arus ac berlebihan, membolehkan melindungi penyongsang dan melangkaui gangguan elektrik dengan lancar. Selepas menjamin bahawa penyongsang terus disambungkan dan dilindungi, strategi kawalan ini juga boleh memastikan ciri yang sangat penting iaitu memberi sokongan kuasa reaktif melalui suntikan arus reaktif mengikut keperluan standard. Tambahan pula, untuk menjaga keseimbangan kuasa antara kedua-dua belah penyongsang, PV boleh menjana jumlah kuasa aktif yang diperlukan berdasarkan kepada penarafan grid penyongsang dan kedalaman voltan sag dengan dalam operasi dua mod iaitu mod biasa dan FRT. Kedua-dua mod operasi ini memerlukan strategi pengesanan yang cepat dan tepat yang penting bagi sistem untuk beralih dari mod operasi normal ke mod operasi kawalan FRT. Untuk tujuan ini, kaedah pengesanan RMS telah digunakan. Dalam kajian ini, loji PV berskala besar yang disambungkan ke sisi MV grid utiliti, yang mengambil pematuhan peraturan teknikal TNB mengenai penyambungan PVPP telah dimodelkan menggunakan MATLAB/Simulink dengan nominal kuasa puncak tertinggi 1500 kW. Analisa tindak balas dinamik untuk PVPP yang dicadangkan di bawah pelbagai jenis gangguan grid simetri dan bukan simetri juga telah dijalankan. Sebagai kesimpulan, reka bentuk lengkap PVPP yang disambungkan kepada grid kuasa yang disediakan dengan keupayaan FRT telah dilbangunkan. Rekabentuk saiz PV yang dicadangkan berdasarkan pengiraan ukuran telah dicapai. Selain itu, keputusan di titik gandingan bersama menunjukkan bahawa PVPP yang dicadangkan adalah bersesuaian dengan syarat keperluan TNB termasuk kaedah sambungan PV-grid, jenis penyongsang PV, rangkaian operasi voltan nominal, jumlah harmonik gangguan kurang daripada 5%, ketidakimbangan voltan kurang dari 1% , julat frekuensi dalam ± 0.1 Hz, dan factor kuasa lebih tinggi daripada 0.9. Di samping itu, hasil simulasi kawalan yang dibentangkan menunjukkan keberkesanan strategi kawalan yang dicadangkan secara keseluruhan, meningkatkan keupayaan melangkaui gangguan elektrik grid dengan selamat, memastikan penyongsang sentiasa terhubung, memastikan keselamatan peralatan sistem, semua nilai kembali kepada nilai pra-gangguan sebaik sahaja gangguan dibersihkan dalam masa hampir sifar saat berbanding tanpa kawalan yang memerlukan sekitar 0.25s, dan juga memberi sokongan kepada grid melalui kawalan kuasa aktif dan reaktif pada pelbagai jenis gangguan elektrik berdasarkan syarat keperluan FRT.
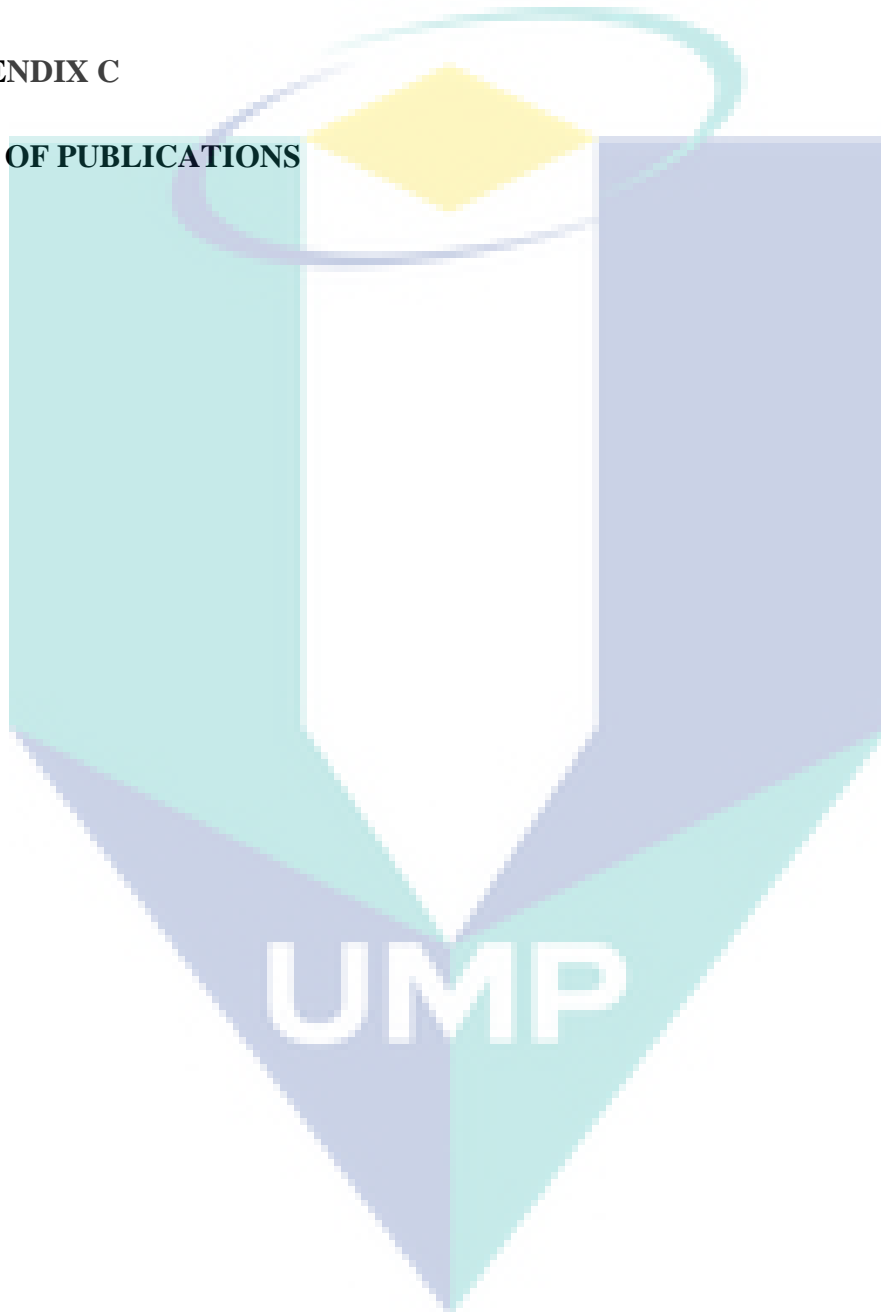
TABLE OF CONTENT

LIST OF TABLES

LIST OF FIGURES

xiv

LIST OF SYMBOLS

C_{dc}	DC-link capacitor
CO_2	Carbon dioxide
d/q	Components of that variable in SRF
f	Grid frequency
f_c	Switching frequency
$f_{carrier}$	Carries frequency
G	Sun irradiation
i_{abc}	Grid currents
i_{ia} i_{ib} i_{ic}	Inverter three-phase current
I_D	Diode current of the PV cell
I_d	Active current injected to the grid
I_d^*	Active current reference
i_{dref}	Active current reference of the inverter
$\tilde{i}_{dref}$	Output active current reference of the current limiter
I_{max}	Maximum current of the photovoltaic array
I_{mpp}	Current of the PV module/array at the maximum power point
I_n	Normal value of the inverter-rated current
I_P	Shunt current of the solar module
I_{Ph}	Photo current of the solar module
I_q	Reactive current injected to the grid
I_q^*	Reactive current reference
I_{qr}	Ratio of injected reactive current to the nominal current
I_{sat}	Reverse saturation current of the solar module
I_{sc}	Short circuit current
I_{THD}	Current total harmonic distortion
k_p, k_i	PI parameter of current loop
k_p, k_i	PI parameter of the voltage loop
L	Filter of the inverter
m	Modulation index
N_{cell}	Numbers of cells per module
N_{pv}	Total numbers of PV array modules (generators)

N_{pvs}	Number of PV modules in series
N_{pvst}	Number of the parallel strings
P	Instantaneous active power
P_{inj}	Active power injected to the grid
P_{max}	The maximum available output power
P_{mpp}	Power of the PV array at the maximum power point
P_{pv}	Generated power by the PV array
Q	Instantaneous reactive power
Q_{inj}	Injected reactive power to the grid
R	Filter of the inverter
R_{ch}	Chopper resistance
R_P	Equivalent parallel resistance of the solar module
R_S	Equivalent series resistance of the solar module
T	The Temperature
t	Time in second
V^+	Positive sequence of the voltage
V^-	Negative sequence of the voltage
V_{abc}	Grid voltage
V_d	Active voltage in SRF
V_d^*	Active voltage reference in SRF
V_{dc}	Dc-link voltage
V_{gn}	Nominal grid voltage
$V_{ia} \ V_{ib} \ V_{ic}$	inverter voltage
V_{max}	Maximum voltage of the photovoltaic array
V_{mpp}	Voltage of the PV module/array at the maximum power point
V_{oc}	Open circuit voltage
V_{pg}	Present grid voltage before faults
V_q	Reactive voltage in synchronous reference frame.
V_q^*	Reactive voltage reference
V_T	The thermal voltage
V_{THD}	Voltage total harmonic distortion
ω	Angular frequency
ΔP	Change in the power of MPPT

α/β	Components of that variable in stationary frame
θ_{PLL}	Phase angle of the PLL
α_v	Temperature coefficients of open circuit voltage
α_i	Temperature coefficients of short circuit current
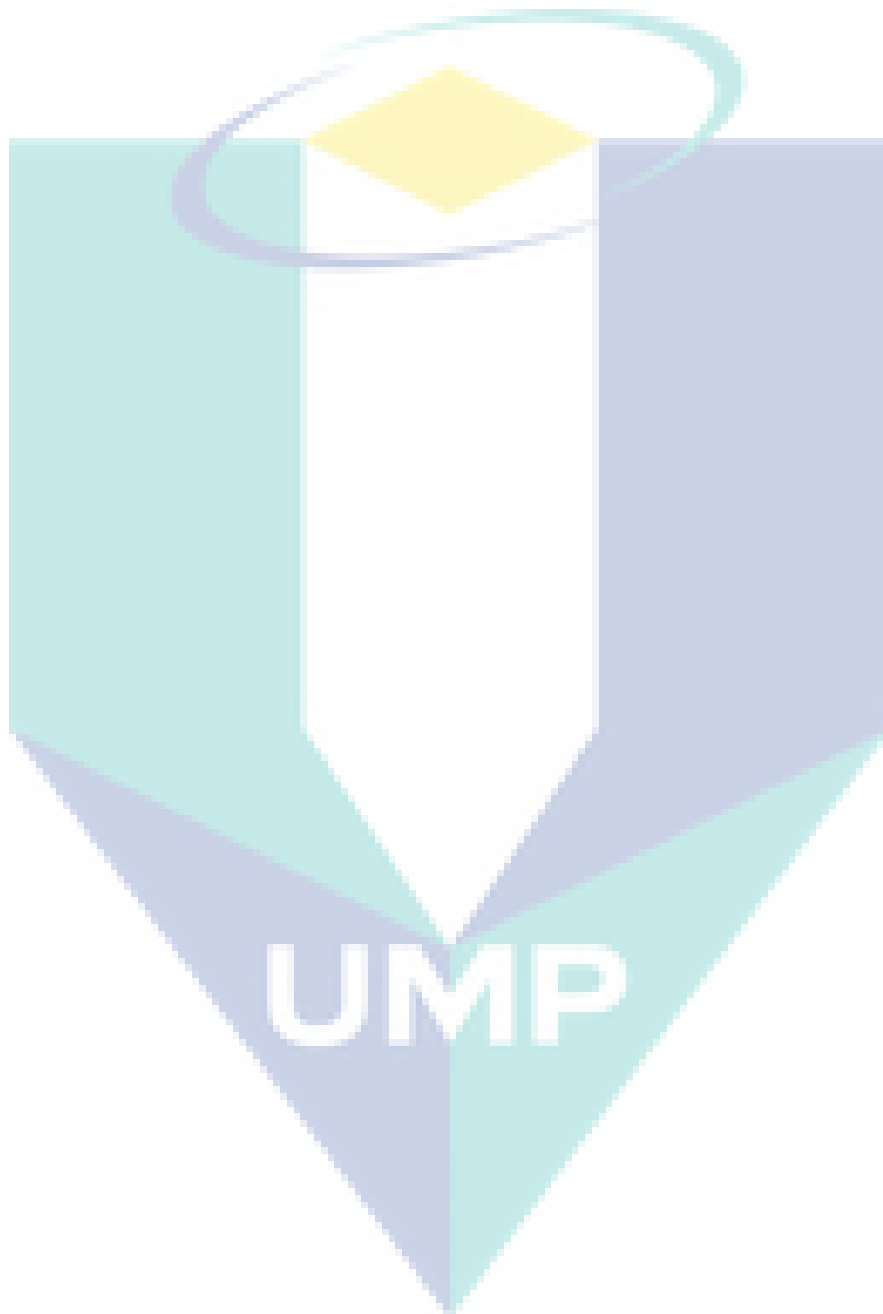
LIST OF ABBREVIATIONS

3-ph	Three phase
ac	Alternating current
AEMC	Australian Energy Market Commission
ANN	Artificial neural network
DCL	Adaptive dc-link
BDEW	German Association of Energy and Water Industries
CC	Constant current
CSI	Current Source Inverters
CV	Constant voltage
DB	Dead beat
dc	Direct current
DG	distribution generator
DPGS	Distributed power generation systems
DSO	Distribution system operators
DVR	Dynamic voltage restorer
DVS	Dynamic voltage support
ECM	Energy Commission Malaysia
FACTS	Flexible ac transmission system
FDP	Fuel diversification policy
FF	Fill factor
FFT	Fast Fourier transform
FiT	Feed-in-Traffic
FL	Fuzzy logic
FLC	Fuzzy logic control
FLS	Feedback linearization strategy
FL-GA	Fuzzy logic-genetic algorithm
FRT	Fault ride through
GA	Genetic algorithm
GB/T	Guobiao Standards/ recommended (Chinese national standards)
GC	Grid code
GCPPPs	Grid-connected photovoltaic power plants

GCPVS	Grid-connected photovoltaic system
GTO	Gate turn-off thyristor
GW	Giga watt
HC	Hill climbing
IEA	International Energy Agency
IEC	International Electro-technical Commission
IEEE	Institute of Electrical and Electronics Engineers
IGBT	Insulated-gate bipolar transistor
INC	Incremental conductance
IPP	Independent Power Producers
LL	Line to line
LLG	Line to line to ground
LV	Low voltage
LVRT	Low voltage ride-through
MDS	Main distribution substation
MOSFET	Metal oxide semiconductor field effect transistor
MPP	Maximum power point
MPPT	Maximum power point tracking
MV	Medium voltage
MVA	Mega volt-ampere
MW	Megawatt
P&O	Perturb and observe
p.u	Per unit
PCC	Point of common coupling
PI	Proportional integral
PID	Proportional integral derivative
PF	Power factor
PLL	Phase locked loop
PPU	Pencawang pembahagian utama-main distribution substation
PR	Proportional resonant
PSO	Power system operator
PV	Photovoltaic
PVPP	Photovoltaic power plants

PWM	Pulse width modulation
RC	Repetitive current
RE	Renewable energy
RM	Malaysian ringgit
RMS	Root mean square
SAPVS	Stand-alone photovoltaic system
SCESS	Supercapacitor energy storage system
SDBR	Series dynamic breaking resistor
SEDA	Sustainable energy development authority
SGCT	Symmetrical gate commutated thyristor
SLG	Single line to ground
sq km	Square kilometre
SRF-PLL	Synchronous reference frame phase-locked loop
STATCOM	Static compensator
STC	Standard test conditions
SVC	Static VAR compensator
THD	Total harmonic distortion
TNB	Tenaga Nasional Berhad
USANAERC	United States-north American electric Reliability Corporation
USAPREPA	United States-Puerto Rico Electric Power Authority
VAR	Volt-ampere reactive
VCO	Voltage controlled oscillator
VSI	Voltage source inverters
VUF	Voltage imbalance factor
WPP	Wind power plant
ZVRT	Zero voltage ride through

CHAPTER 1

INTRODUCTION

1.1   Background

Solar energy is a widely-available and clean source of energy that has been used to generate electrical power. The focus on electrical power generated by photovoltaic (PV) energy has remarkably increased due to the environmental problems from fossil fuels. Over the recent years, there was a sharp growth in both energy consumption and population. Whereas, the conventional energy source price is increasing and it's availability is dwindling. Global warming and greenhouse emissions are the main harmful results of fossil fuel consumption, and its impact can hardly be irreversible. Therefore, the attention is being paid to other alternative sources such as the nuclear and renewable energies to reduce the generation using combustible fuels. The electricity generation around the world can be divided mainly into fossil fuels, nuclear, and renewable energy (RE). The renewable electricity generation can be divided depending on the energy source used like wind power, hydropower, solar energy, biomass, and geothermal energy. Among these RE resources, wind and PV systems are the two most promising resources to produce electricity in large quantities. However, solar energy production is considered as one of the most important parts of the future energy generation (Honrubia-Escribano et al., 2018). The inclination towards solar energy arises because it is non-polluting, environmentally-friendly, less maintenance requirement when compared to other resources, easily available, accommodates to large-scale usage, does not contribute to sound pollution, and highly reliable (Kothari & Nagrath, 2003). The sun has produced free energy for billions of years where the solar radiation intercepted by the earth at each instant is a massive amount of power reaching about 1.8×10^{11} MW, which is much more than the total global consumption of power (Jain & Agarwal, 2007).

1

Over the past few years, there was a sharp growth in renewable energy development according to the global scale. Based on the recent renewable global status report made in the year 2016 (Global Status Report, 2017), the power generated by RE recorded highest annual growth ever in 2016, with an estimated 161 gigawatts (GW) of capacity added when compared to 2015 when 147 GW had been added. The overall worldwide capacity rose nearly 9% when compared to 2015, to nearly 2017 GW at year's end. The total worldwide capacity of RE is recorded as 1701, 1856, and 2017 GW in 2014, 2015, and 2016, respectively.

The last year was a phenomenal year for PV generation, as there was more power added by PV plants generation than any other kind of renewable energy technology. PV system in the first place, representing almost 47% of lately mounted renewable power capacity. The remaining capacity additions represented by wind (34%) and hydropower (15.5%), respectively. Figure 1.1 shows the global increase in solar PV installation capacity throughout 2005-2016 (Global Status Report, 2017). It can be observed that, until 2015, the highest annual growth of RE capacity occurred in the power sector is led by wind energy. But in 2016, the solar PV power recorded the largest annual increase in capacity ever with 75 GW higher than wind power which only increased by 54 GW.
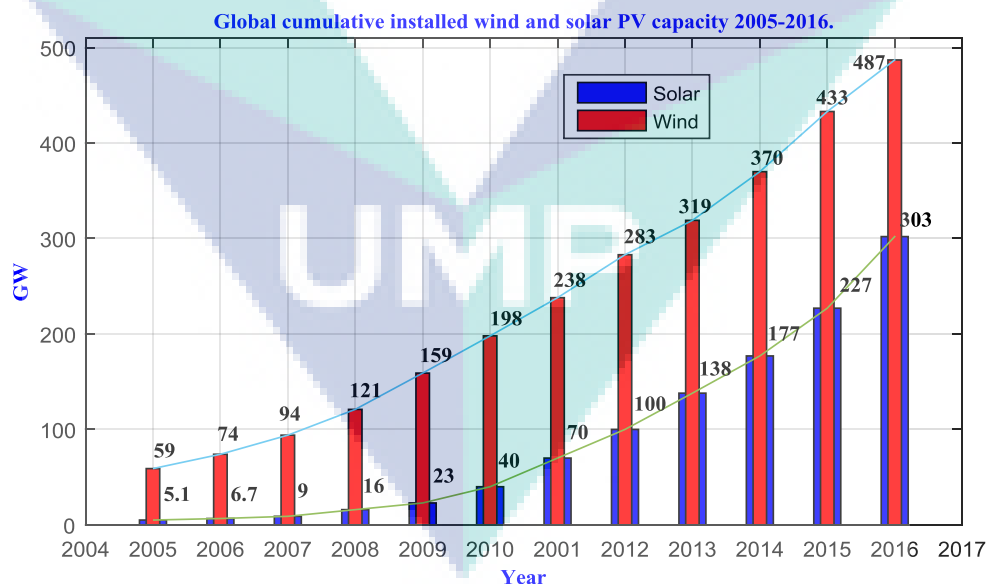
Figure 1.1   Global cumulative installed wind and solar PV capacity 2005-2016.

According to the latest reports by International Energy Agency (IEA) (International Energy Agency (IEA), 2017), by the end of 2016, the power generated by PV farms had crossed 300 GW to around 303 GW, and this amount is at least 50 times

higher than that of in 2006. In this regard, the top five countries with respect to the installed capacity annually are led by China and then followed by the USA, Japan, India, and the United Kingdom, respectively, as illustrated in Table 1.1. Additionally, there are four countries had installed more than 40 GW led by China that reached 78 GW, followed by Japan (42.8 GW) which rose to second place while Germany went down to third place by (41.2 GW). Germany is followed by the United States (40.3 GW), which is in the fourth place. Overall, Table 1.1 shows the list of top 10 countries regarding annual installation and total installed capacity of PVPPs by the end of 2016 (Foley & Olabi, 2017; Global Status Report, 2017; International Energy Agency (IEA), 2017)

Table 1.1   Annual & cumulative PV installed capacity: top 10 countries in 2016.

PV annual installed capacity (top 10 countries)			PV cumulative installed capacity (top 10 countries)		
No.	*Country*	*Generation in GW*	**No.**	*Country*	*Generation in GW*
1	China	34.5	1	China	78.1
2	USA	14.7	2	Japan	42.8
3	Japan	8.6	3	Germany	41.2
4	India	4	4	USA	40.3
5	United kingdom	2	5	Italy	19.3
6	Germany	1.5	6	United kingdom	11.6
7	Korea	0.9	7	India	9
8	Australia	0.8	8	France	7.1
9	Philippine	0.8	9	Australia	5.9
10	Chile	0.7	10	Spain	5.5

Source: Global Status Report (2017)

As a result, recently, the PV generation of electrical energy has become a reality. Consequently, there are thousands of photovoltaic power plants (PVPPs) integrated with power system in many regions and countries. In the past, the penetration of solar energy was very small when compared to the conventional generation system, but over the recent period, the grid connected-PV system increased dramatically (Mahela & Shaik, 2017).

PVPPs integration into the grid has various difficulties and problems due to the variation of the climate condition e.g., sun radiation, temperature, wind speed, humidity, pressure, etc. that results in fluctuations of the PV generated power leading to grid fluctuations in voltage and frequency. Grid fault is also one of the problems that PV farms control should take into consideration. It should be properly controlled to overcome grid faults that lead to voltage and frequency drop which in turn, causes instability of power grid. Therefore, the grid fault studies as well as improving the integration standards to

overcome the problems concerning grid stability and quality due to PV system integration have been taken seriously (Jenkins & Thornycroft, 2017). As a result, and in order to solve faults problems and keep the network stable and secure, most of the countries regulate these issues of grid-connected PV power plants (GCPPPs) by adding new requirements regarding PV penetration into their grid codes (GCs). Consequently, the new modern GCs requirements improved as long as GCPPPs penetration increased. But currently, the most advanced requirements imposed is the fault ride through (FRT) capability with reactive current injection to support the grid during faults. For this reason, the FRT capability control will be considered in this thesis.

1.2   Motivation and Significance of Study

Recently, the PV energy is becoming the most popular RE resource which has significant remarkable growth over the past years and is on the way to become an important part of electricity generation. In this regards, despite 33% of the earth's surface is covered by deserts with high amount of sun radiation. If just 4% of these ranges were utilized to install PVPPs, the result would be that the annual energy consumption would match the annual energy generation (Kurokawa, Komoto, van der Vleuten, & Faiman, 2007). Additionally, increasing efficiency of PV panels and decreasing manufacturing cost year after year, increasing environmental pollution and dwindling conventional resources has made solar energy to become competitive with conventional generators (Teodorescu & Liserre, 2011). Nowadays, the PVPPs penetration to the electric grid has been increased sharply around the world (Global Status Report, 2017). For instance, in 2016, there was a rapid increment in the capacity of PVPPs by around 75 GW as compared to 2015 whereby 50 GW had been added. In addition, PV systems production of electricity contribution reaches around 1.8% of electricity demand all around the world (International Energy Agency (IEA), 2017). In the past, GCs required PVPPs to disconnect directly from the grid as grid faults happened. However, recently, with this remarkable increase of PVPPs penetration to the utility grid, there appears some challenges concerning the operation, stability, and power quality. Thus, the disconnection of these PV farms is not permitted anymore due to the negative sequences of its disconnection to the grid and customers. As a result, this lead to the preparation of specific technical requirements as a part of grid code in some countries, which is known as the FRT capability or so-called low voltage ride-though (LVRT) capability, as the new

4

requirements. Whereas, some countries impose the reactive current injection during the fault as an additional requirement to support the grid during disturbances (Afshari, Farhangi, Yang, & Farhangi, 2017; Cabrera-Tobar, Bullich-Massagué, Aragüés-Peñalba, & Gomis-Bellmunt, 2016; Elrayah, 2017; Etxegarai, Eguia, Torres, Buigues, & Iturregi, 2017; Kim, Kang, Bae, & Park, 2013; Obi & Bass, 2016; Reddy, Babu, & Sanjeevikumar, 2018).

A large portion of the solar power plants is linked to the utility grid. The emergence of GCPPPs delivering large amount of MWs is an attestation of PV energy feasibility. The penetration of large-scale PVPPs to the utility grid can significantly affect the power system network. In addition to the intermittent nature of the PV system, these power generation plants bring about new requirements and regulations to the electric grid concerning the growing penetration level all over the power system (Teodorescu & Liserre, 2011). The grid code in most of the countries has been improved, as it is subjected to the new regulations which require complex control structures such as FRT capability, injection of reactive current, and active/reactive power control that are newly absorbed to face the large wind power plant (WPP) penetration in some countries such as Germany, Canada, Denmark, USA and Spain (Mohseni & Islam, 2012; Tohidi & Behnam, 2016). These requirements are being adopted for GCPPPs especially in Germany, Spain, China, USA, and Japan (Cabrera-Tobar et al., 2016).

In Malaysia, the PV penetration is also increased as a part of the PV revolution because of the tropical climatic which has abundant and high exposure of sunshine throughout most days (Chua & Oh, 2012), the high cost of electricity, and more CO_2 emissions resulting from coal and fuel plant combustion that expected to reach around 100 million ton from coal fired plant alone by 2020 (Johari, Hafshar, Ramli, & Hashim, 2011). Therefore, the interest on PV energy and the financial incentive programs have also been increased. Furthermore, the encouragement to adopt PV system by Malaysian government is to aim to generate around 200 MW from solar energy by 2020 (Economic Plan Unit, 2015). Moreover, the fund of this type of energy which started in 2011 has increased into 1.6% in 2014 (Ahmad, Ab Kadir, & Shafie, 2011). Although, the Malaysian GC and distribution GC that issued by the Energy Commission Malaysia (ECM) in 2010 and proved by parliament in 2011 included many regulations and standards for the national grid, these two codes still study to contain or address the new

regulation such as the FRT to regulate the PV penetration like other countries. As a result, this study will propose FRT as a new requirement for the Malaysia GC concerning PV penetration.

On the other hand, the national grid itself and due to the growing interest of PV system integration has led to the issuance of regulations regarding PV penetration to medium and low voltage (Azit et al., 2012). This regulation has been revised recently with a new version (Suruhanjaya Tenaga, 2016). However, these regulations are imposed to provide guidance on the requirements of PV interconnection method with the grid distribution system, operation, types of equipment, power quality issues, frequency, synchronization, and power factor, but still need to contain the FRT requirements or reactive current injection to regulate large-scale penetration in order to keep the grid secure and stable.

Furthermore, these Malaysian standards are similar to other international and national standard technical regulation and rules regarding the connection of PV systems to electrical grid that are applied by many countries around the world such as the IEEE 1547 series of standards (T. S. Basso & DeBlasio, 2004), which are updated in 2012 by (T. Basso, Hambrick, & DeBlasio, 2012) and European standards (IEC) (Cleveland, 2008). In addition to the national standards such as the Chinese standards (GB/T, 2012) and Brazilian standards for inverter-connected grid (Figueira, Hey, Schuch, Rech, & Michels, 2015) and etc. but, not found previous work considered the national grid standard to analyze the practical conditions and characteristics of PVPPs connection into the distribution system of the Malaysian grid sufficiently. No literature founded to indicate any PV system used to validate or test these requirements like the validations in place for the other standards. Thus, the proposed PVPPs in this research will be designed according to these regulations and should be compatible with it. In addition, based on the literature, the proposed PVPP-connected utility grid will be achieved properly. On the other hand, these regulations do not contain any new rules in case of grid fault such as the FRT and reactive current injection, but requires PVPPs to disconnect in case of grid faults.

This thesis will review the most essential interconnection issues that must be managed and propose solutions for enhancing the performance of PV system connected to utility grid. The main motivation of this research is to design and develop an efficient and comprehensive FRT controller in order to support the grid stability, security,

withstand different grid disturbances and auxiliary service arrangement, like a traditional power plant. Moreover, design PVPP connected to the medium voltage side of the utility grid considering the national grid technical regulation compatibility as well as to propose FRT capability as a new requirement in Malaysian grid code. Applying these issues concerning PV penetration is to make the PV connected to the power grid stable and secure, make the Malaysian grid code suitable to PV penetration and help to extend the reliable and safe implementation of such clean energy power generation in the world.

1.3 Problem Statement

In the past, when the PVPPs penetration was low, all regulation need these plants to disconnect directly as soon as a grid fault occurs. However, by the end of last year, PVPPs power generation reaches the first place among other RE resource. Therefore, when disconnected at the same time of grid disturbances will cause operational and stability problems and may lead to blackout (Honrubia-Escribano et al., 2018). To solve this issue, the FRT capability is becoming an essential capability of modern power system (Manikanta, Kesavarao, & Talati, 2017). As a result, many countries have added the FRT requirement into national grid codes such as Germany, Spain, USA, China, Japan, and Italy. Currently, Malaysian grid code and technical standards have not included FRT requirements. However, due to increasing installed capacity of PV power plants, the government under Suruhanjaya Tenaga has decided to investigate FRT capability as a new requirement in national grid code. So, this research proposed FRT requirement for Malaysian GC, FRT controller and reactive power injection during sag period also developed to assist the voltage recovery and grid support according to the FRT standards requirements.

During the sag events, there are two major issues that should be addressed by the PVPPs to achieve the full FRT requirements. The first one is the dc-link over-voltage in the dc-side of the PV inverter as well as the over-current that may occur in the ac side due to the imbalance between the incoming power from the PV side and the power delivered to the electrical grid. The second one is the injection of reactive current, which is considered as an effective solution for voltage recovery and to support the grid in order to overcome the voltage sag problems. Most recent studies focused only on ride-through the fault for either single or two stages grid-connected PV power plants. Although these studies have drawbacks such as using external hardware, focuses to enhance the output

7

waveform only, increases the overall costs and affects the reliability of the power system, the power balance had not been addressed, no specific time taken in consideration, all values take time to return to pre-fault values which cause instability issues, and the system's complexity increases, as described in detail in Chapter 2. However, not sufficiently deal with the reactive current injection during voltage sag for all types of the grid faults along with the fault-ride-through capability and inverter protection without many extra hardware and complex system. Therefore, this research develops a comprehensive control strategy that enables the PVPP to withstand grid faults, allow the inverter to remain connected, continuously produce electricity, and absorb excessive energy while injecting the required reactive power under different types of fault to meet the standard requirements. As compared to other methods, this method not only effectively suppresses the ac over-current as well as the dc-link over-voltage and protect the inverter during the voltage sag, but also support the grid via injection of reactive power. Furthermore, once the fault is cleared, all values will recover to pre-fault values directly. In addition, to switch the inverter operation from normal mode into FRT mode, the fast and precise sag detection strategy is a very essential feature for a more accurate and efficient FRT control.

1.4   Objectives of Research

In view of the problem statement and literature gap as well as the motivation and significance of the study, the aim of this study is to propose a FRT capability as a new feature in the Malaysian GC. In addition, this research develops an overall new control strategy for large-scale three-phase PVPP connected to the power grid based on TNB connection requirements on the faulty mode operation to ride-through the fault and support the grid according to the standard requirements. Moreover, the developed control strategy for the inverter is provided with a precise and fast fault detection unit as well as the reactive current injection capability to support the grid voltage stability while maintaining the connectivity of the inverter to the grid. These requirements are provided to supply the PV system with the control and rules that are essential for a safe, reliable, stable, and economic operation of the system. In conclusion, the high penetration level of solar energy into the electricity supply system could create issues of instability to the grid, which is not designed to receive such integration. The problem requires an immediate

attention in order to meet this high integration of PVPPs to the grid. Accordingly, the objectives of this research can be summarized as follows:

i. To design a comprehensive model of large-scale PVPP connected to the power grid based on TNB technical connection regulations using MATLAB/ Simulink.

ii. To propose FRT requirement for Malaysian grid code and design converter controller with the reactive current injection capability for voltage support at the grid during fault conditions according to the standard requirements.

iii. To design a protection method addressing the over-current, and over-voltage that occurs during the faults to guarantee the inverter connectivity.

iv. To analyze the performance of overall PVPP system during different grid fault types and levels.

1.5 Contributions of the Study

This research work studies the design and development of PVPPs integrated with the electrical power system and provide the system with FRT capability control. The main contributions in this research are as follow:

i. Large-scale PVPP connected to the distribution side of the power system and fulfilled the TNB standards regarding the connection of the PV system to the medium voltage side as first study can be conducted. The testing of these standards by simulation before applying in the real system could assist power system operators and PV designers to evaluate it like the other national and international standards. In addition, the proposed PVPP is designed in such a way to be capable of adding the FRT capability controller.

ii. The increase in penetration of PV farms into the utility grid poses great challenges in terms of system stability. Thus, forcing several countries to update their grid codes to accommodate the FRT capability of PV systems in order to stay connected into the grid and supply the reactive current to support grid voltage during grid faults. In line with this, the FRT requirements for Malaysian GC regarding PV penetration are proposed as new requirements. Moreover, a FRT

inverter controller is developed in this research for grid-connected PV system under symmetrical and asymmetrical grid faults with reactive current injection capability for voltage support at the grid during fault conditions according to the standard requirements. The proposed system has two modes- normal and faulty mode with grid support. So, in order to switch between these two modes, a fast, simple and precise fault detection method also has been proposed. A feed-forward decoupling current controller is designed for controlling active and reactive components under grid fault in order to deal with different faults. It permits the injection of the reactive current to the grid according to the reactive current requirement of grid codes during symmetrical and asymmetrical grid faults.

iii. The proposed strategy includes the dc-chopper protection method and current limiter in order to protect the inverter and keep its connectivity during the fault period to meet the requirements of the grid code. The controller at fault duration is designed in such a way that the inverter current never exceeds the current rating of the inverter in order to protect it during a grid fault. The dc-chopper breaker also will activate to suppress the dc over-voltage that occurs in the inverter dc side.

iv. The effectiveness of the proposed strategy had been verified using Matlab/Simulink simulation platform and the results show that the proposed LVRT strategy has a good performance under different grid faults, different fault periods and different GCs requirements.

1.6 Scope of Research

In this research, the design and development of single-stage large-scale PV farm interconnected to the utility grid using Matlab/Simulink environment are carried out. Modelling and simulation of PV module used in this research is Topsun S400 (TOPSUN solar modules, 2017) which allows the prediction of PV module's behavior and characteristics under different temperature and solar radiation. The sizing and configuration of the design of PVPP array should be calculated and presented theoretically and thereafter, verified using simulation. The maximum power point tracking (MPPT) will be utilized to extract the maximum available power from the array. The PVPP design can be divided into static and dynamic operation conditions. The

proposed PVPP is design and modelled according to nominal rated peak power of 1500 kW connected to the MV side (33 kV) of the power grid with TNB technical regulation compatibility. These technical regulations concerning PV penetration tested in this research are limited to connectivity issues such as PV-grid connection method, nominal voltage operating range, harmonics, voltage unbalance, MV penetration, PV inverter type, frequency, and power factor. Besides active power generation to meet the demand from the electric utility grid, dynamic support means the PVPP must be able to withstand a specific period of time and support the grid voltage during disturbances, faults, and voltage sags. It can be achieved by protecting the inverter from over-current, and over-voltage as well as by injecting reactive power using the inverter control. Additionally, for more efficient FRT control, fast and precise detection unit had been designed without any extra hardware. In this design, no particular equipment such as energy storage devices or reactive power compensators are considered to be utilized as a part of the PVPP to meet these prerequisites. Hence, the controllers will be developed to control the GCPPPs ought to address such necessities.

1.7   Outline of the Thesis

This thesis was arranged in a manner that clarifies the subject from all aspects; it provides details on the facts, gaps, arguments, effectiveness, and procedures to achieve the objectives. The thesis consists of six chapters. Chapter 1 includes the background and the advancement of the GCPPPs, motivation and significance of the study, problem statement, aim and research objectives, and contribution of the study as well as the scope of the research.

Chapter 2 discusses the previous studies related to the objectives of the present research. In addition, the chapter provides a relevant review of the literature concerning the penetration of PVPP to the utility grid with recent Malaysian and other international GCs standards and focuses on FRT capability control and injection of reactive current during disturbances. Also, the recent studies on protection of the inverter during FRT period and control applied to solve the problem of voltage sag as a result of grid faults. Additionally, determined the limitations and gaps of the previous studies.

Chapter 3 presents the design and modelling of the overall PVPP-connected distribution side of the grid and inverter control in the normal operation mode. The

description of the structure design and method used to achieve the stipulated goals for the research have been introduced. In addition, the Malaysian grid technical regulation concerning the penetration of PVPPs into the power grid side is determined. After designing and modelling the complete PVPP-connected grid and determining the parameters for main components of the whole system. The next stage is to add the proposed FRT capability control for single-stage inverter-based grid-connected photovoltaic power plant.

Chapter 4 explains the proposed FRT requirements as new requirements for the Malaysian grid code. Additionally, this chapter presents an overall new control strategy for a single-stage three-phase PVPP connected into the grid in the faulty mode operation to ride-through the fault and support the grid based on the proposed Malaysian LVRT requirements and GCs standard requirements. The newly proposed LVRT control strategy during fault conditions to avoid excessive ac-current, protect the inverter from excessive dc over-voltage, fault detection method, and injection of reactive power control also has been presented.

Chapter 5 presents the results and discussion of the fully-developed PVPP system connected to the utility grid and provided with the FRT capability control as well as the reactive power injection had been introduced. In this chapter, simulation results under all types of grid faults and comparison with the recently published results are presented to validate the performance of the proposed control strategy. The conclusion of this research and recommendations for the future works are presented in the Chapter 6.

CHAPTER 2

LITERATURE REVIEW

2.1   Introduction

A comprehensive overview of the past research in the grid-connected PV system components include static and dynamic studies. Static studies at the steady-state operation of the system are such as the PV cell characteristics and modelling, maximum power point tracking (MPPT) algorithms, PV inverter control and its typologies, and grid-connected PV typologies. On the other hand, dynamic studies (FRT study at faults) including review and comparison of the recent international grid codes integration requirements, voltage sag mitigation, and grid disturbances are presented in this chapter. In addition, the chapter provides a relevant review of the literature concerning the penetration of PVPP to the utility grid with the recent international GC standards, and focus on FRT capability control and injection of reactive current during disturbances. Moreover, the recent studies on the protection of the inverter during FRT period and control that applied to solve the problem of voltage sag as a result of grid faults. A review of other relevant research studies is also provided especially the national and international technical regulation and standards concerning PV penetration. As a conclusion, the literature review of previous studies with obvious gap is done extensively in order to tailor to the purpose of the current research properly and significantly add to the existing literature with regards to the trends of the research in the field.

2.2   Types of Solar PV System Configuration

The classification of the PV system is based on the operation requirements, the component configuration, and the connection method of the system to electrical demands and other source of power system. The categories of PV energy applications are: grid-connected PV system (GCPVS) which is linked directly to the utility power grid. GCPVS

is generally comprised of the PV array, maximum power point tracking, solar inverter which is considered as the main component in grid-connected PV system, filter, and utility grid connection equipment. It has lower initial and maintenance cost because there is no need for batteries or charge regulator (Center, 2001; Woyte & Goy, 2017). The second is a stand-alone PV system (SAPVS) which is also known as off-grid PV system that is suitable for low power applications and requires a battery bank to store the electrical energy. SAPVS is designed to operate independently without the electrical grid system and is almost used in rural or isolated areas where the electrical grid supply is unavailable or even impossible. The energy capacity of SAPVS is a few kWs of power. The stand-alone power plant works independently from the local network to provide electricity for households, irrigation systems, public lighting, water pumps, and etc. (Abu-Jasser, 2010; Ghaib & Ben-Fares, 2017).

The third category is the hybrid PV system that is connected to the grid with battery backup. The backup battery system is charged by both the PV array system and electrical grid. In the case of disconnection or outage, the backup storage devices should be switched on to provide the loads with electricity via either an automatic system or manually. The most important advantage of hybrid PV system when compared to the other two types above is that it can provide backup support during grid outage. On the contrary, it is equipped with the batteries which are expensive, require periodic inspection, and regular maintenance. As it is clear from the topic of this thesis, second and third category of PV system will not be discussed in this research, only the first type of GCPVS will be investigated. This is the focus because it has become the dominant part of the solar PV installed around the world and due to the new FRT requirement concerning this integration which is imposed by some of the modern GCs in order to contribute in power system stability. This type will be discussed in detail in Chapter 3.

2.3 Current Energy Situation Used in Power Sector in Malaysia

Before 1980, the energy sector in Malaysia was highly dependent on crude oil as the energy source. After the international oil crisis in 1979, the government introduced the four fuel diversification policy (FDP) to avoid depending on crude oil (Jafar, Al-Amin, & Siwar, 2008; Ong, Mahlia, & Masjuki, 2011). During this period, the natural gas, coal, and hydropower were the available alternative energy. After the implementation of the proposed four fuel diversification, the dependency on crude oil decreased from

61.1% to 38.22% in 1990 and 2008, respectively. In 2008, the natural gas became the main energy supply (43.4%), followed by crude oil (38.2%), while the coal and hydropower contributed 15.3% and 3.1%, respectively (Ahmad et al., 2011; Ong et al., 2011).

Today, Malaysia is taking up the five fuel diversification of energy that was introduced in 1999 (Jafar et al., 2008; Mekhilef et al., 2012). The fifth FDP was issued to reduce the dependency of fossil fuels (oil and gas) and achieve more balance in the energy mix. As a consequence, in the 9th Malaysian plan (2005-2010) the use of oil and gas had decreased from 77% to 55.9% (Mekhilef et al., 2012). Plan after plan, the government turns to focus on replacing fossil fuels by renewable energy resources. In the 8th Malaysia plan, the Malaysian government has included renewable energy as the fifth energy source with the aim to generate 5% of the country's electricity source. In this phase, the government estimated that using this 5% could save the country around RM 5 billion over a period of 5 years (Johari et al., 2011). As a result, according to this plan, the target was achieved and the generation from renewable energy reached to 350 MW in 2010. On the other hand, the 10th plan urges to achieve a renewable energy with a target of 985 MW by 2015. Under this initiative, solar power is expected to contribute at least 65 MW to the country's total capacity mix. Finally, in the 11th Malaysian plan (2015-2020), the country aims to generate around 2080 MW from renewable energy sources, whereby the PV generation contribution is expected reach to around 200 MW by 2020 (Economic Plan Unit, 2015). As a conclusion, the focus of this research will be on the PV energy as the main RE source in Malaysia.

2.3.1 Potential of solar energy in Malaysia

Malaysia is located in the South China sea between 1°-7' N Latitude and 100°-120' E longitude (Mekhilef et al., 2012). It consists of two main land area separated into two regions which are Peninsular Malaysia (West Malaysia) where this research is aimed to take place, and Borneo Island (East Malaysia) consisting of two states namely Sarawak and Sabah. The area of Malaysia is relatively large (330,000 sq km) where Peninsular Malaysia makes up 40% of the country's area, whereas the rest is covered by East Malaysia. Peninsular Malaysia consists of the majority of the population (76%) in the country (Mekhilef et al., 2012; Nugroho, 2010). Malaysia has a weather condition of generally heavy rainfall with constant high temperature and humidity. Except for

highlands, the humidity varies between 80% to 90%. Throughout the year, the temperature varies between 22ºC and 33ºC. The average daily temperature is 26.5ºC. There are two types of the monsoon winds in Malaysia, the first one is called the northeast monsoon that occurs between November and March when the wind moves from central Asia to South China sea through Malaysia. Meanwhile, the second one occurs in the period between May and September in the case of the wind moves from Australia across the Sumatra Island to Malacca and called southwest monsoon (Mekhilef et al., 2012), and in general, the solar energy extraction is affectedd by these monsoon.

Malaysia is situated in the equatorial region. Therefore, it receives a huge amount of solar irradiation every day. A variety of studies on solar irradiation in Malaysia were started by Chuah and Lee, (1981) which are considered one of the first studies in solar radiation estimation during (1975-1978) for three main towns including Kuala Lumpur, Penang, and Kota Bahru. Recently, there is a lot of study on irradiation estimation for many regions and towns in Malaysia that uses more recent technological devices. However, based on the tropical climate, generally, Malaysia has a high exposure to the sun throughout all year. According to Chua and Oh (2012), the average irradiance per year in Malaysia is 1643 kWh/m^2. Mekhilef et al., (2012) stated that the monthly average solar radiation in Malaysia is approximately in the range of 4.21 kWh/m^2 to 5.56 kWh/m^2 with an average sunshine duration ranging between 4-8 hours/day. This indicataes that, Malaysia receives sufficient solar energy to generate 11 years worth of electrical power (Tan, 2014). This incredible potential amount of energy clearly shows the possibility of it being utilized in Malaysia. The average daily solar irradiation is 5.5 kW/m^2, where the highest irradiation was estimated in August and September by around 6.8 kW/m^2, while the lowest was in December. The peak of electricity production by PV is usually during the period between 11:00 am and 03:00 pm (Ong et al., 2011). Figure 2.1 shows the average of annual irradiation for different states in Malaysia (Akorede, 2012). As a result of this thriving situation of potential solar energy in Malaysia, this research proposed FRT requirements for Malaysian GC and controls which can help to improve the stability of both PV systems and national grid due to this integration.
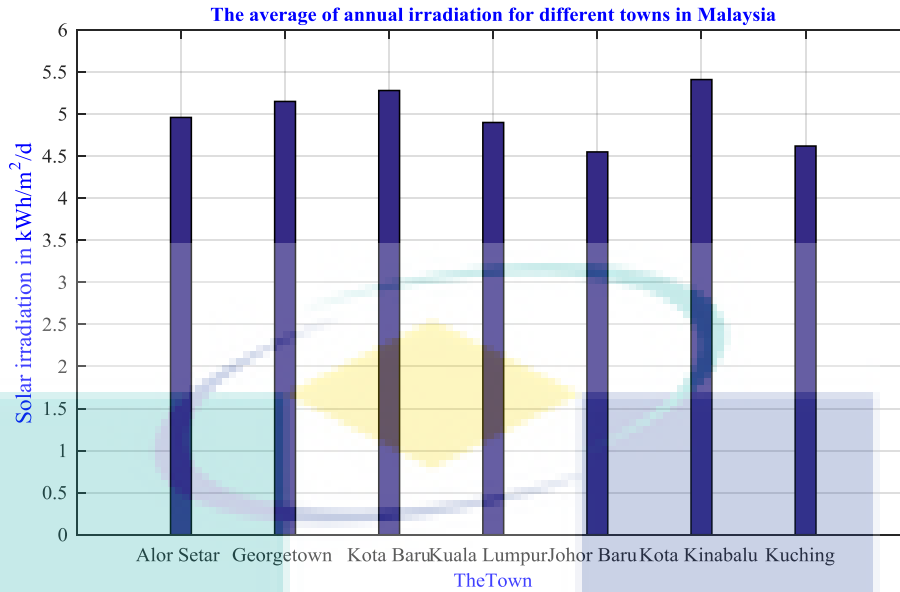
Figure 2.1   An average of annual solar radiation for different states in Malaysia.

2.4   Grid-Connected PV Power Plants

The grid-connected PV power plant (GCPPP) is briefly described in this section considering different classifications. In addition, the control structure of a typical grid-tie photovoltaic system is presented.

2.4.1   Configuration of grid-connected PV system

The sorting of GCPPPs from various aspects is mainly divided into two configurations of power electronic topology are described as follows:

2.4.1.1   Single-stage GCPPP topology

The direct connection from PV system array to the dc side of the inverter is called single-stage conversion. It can be seen in Figure 2.2 that the schematic diagram which describes the typical type of single-stage GCPPP conversion topology. In this case, as the term suggests, only consists of the inverter, meaning that there is no existing for the dc-dc converter stage. In one stage, the total voltage of PV series module in the array system should equal to the voltage of dc-link (Lee & Lee, 2013; Orłowska-Kowalska, Blaabjerg, & Rodríguez, 2014). Consequently, during the array sizing steps of the series connected modules and parallel strings should be built and determined according to the maximum dc-voltage of the inverter and rated power. The control strategy in this type is more complex than in the two stages because the inverter has to achieve all control objectives

alone. In the single-stage design, the inverter performs the MPPT function and the control of active/reactive current generation. The advantage of this type of GCPPP topology is that the single-stage conversion system can achieve a relatively high power efficiency with lower cost than the two-stage conversion system (Zhu, Yao, & Wu, 2011). As a result, the single-stage type is selected to be used in this study due the advantages offerred by this type as compared to two-stage type.
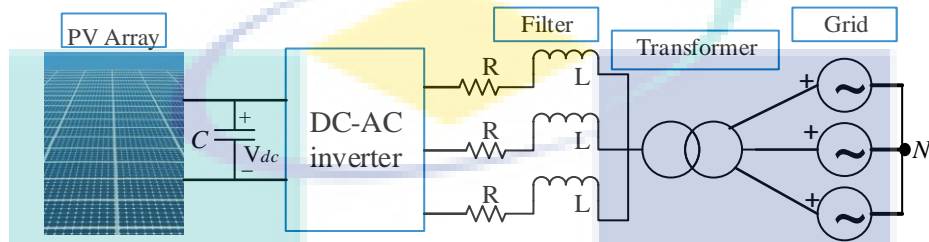
Figure 2.2   A typical schematic diagram of single-stage PV system topology.

2.4.1.2   Two-stages GCPVS topology

The two-stage conversion system consisting of firstly dc-dc converter part as a first stage exists between the PV array and the inverter then followed by the second stage, which is the inverter part to invert the available dc power to an ac power. A dc-dc converter stage is equipped between the PV source and the inverter which is responsible of voltage boosting, tracking the MPP and transfering the output power from PV array to the inverter. Wherease, the inverter stage is used to control the generated active and reactive current. The dc-dc conversion part often adopts a boost device or some other drives such as buck converter, buck-boost converter, etc. (M. R. Islam, Guo, & Zhu, 2014).
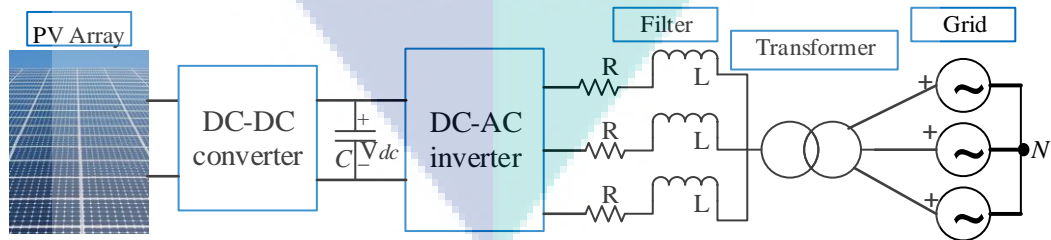
Figure 2.3   A typical schematic diagram of two-stage PV system topology.

The advantage of the two-stage type is the convenience during the control scheme designing. On the contrary, this type has to face more power loss when compared to the

single-stage type due to the increasing of circuit stages (Zhu et al., 2011). Figure 2.3 shows the typical two-stage conversion system of the GCPPP system.

2.4.2 The size of GCPPPs: classification

The size of PVPPs is determined depending on the voltage level of the grid connected to it. The PVPPs with lower power ratings (usually several kWs) are connected to low voltage distribution system while, the huge PV farms with tens of MWs are connected to high voltage. Generally, most of the PVPP are connected to the low and medium voltage distribution network as distribution generators (DGs) (Elrayah, 2017). However, the classification of maximum and minimum power at which the PVPP could be linked or integrated with any of the voltage levels is based on the grid conditions. For instance, in German GC, the PVPPs connected to the medium voltage side should have a possible power generation value in the range between 500 kW to 100 MW (Troester, 2009). In most of the cases, this issue can be defined by the grid system operator.

The PVPP-connected power grid can also be classified as small, medium, large, and in rare cases, very large scale sizes. The small-scale PV system refers to the system that is used for residential purposes with a rated power reach to 10 kW, while the medium-scale has a power rating ranging from 10 kW to 1000 kW and are usually used for commercial and large buildings (Kurokawa et al., 2007). The large-scale, which is the so-called utility scale, are the PVPPs that are interconnected to the conventional substations or feeder of the network with a power rating greater than 1 MW (Kurokawa et al., 2007). Nevertheless, according to the international energy agency (IEA) regulations studied by Theologitis (2011) stated that, the large-scale PV systems are those plants generating above 100 kW. The PVPPs with ratings ranging from 10 MW to several of GWs are classified as a very large scale PV system that are normally installed in deserts with high level of temperature and solar radiation (Kurokawa et al., 2007). On the other hands, based on the IEEE standard 929-2000 classification (IEEE Std. 929-2000, 2000), the PVPPs are divided into three categories: (*a*) small systems rated at 10 kW or less; (*b*) intermediate systems, rated between 10 kW and 500 kW; and (*c*) large scale, rated above 500 kW. It can be concluded that, all studies, classifications and grid code agreed that any PVPPs generate more than 500 kW considered a large-scale PVPP. Therefore, the study provided in this research is mainly concerned with FRT requirements and its control which are preferred to apply for this type of PV plants (Jenkins & Thornycroft, 2017),

Thus, the large-scale PVPP connected utility grid with rated power of 1500 kW is selected to be designed.

2.4.3   The basic structure of the inverter control based GCPPP

Power electronic inverter plays an important role in GCPPPs. So, the inverter is very essential part in order to convert PV array dc power into ac power to match the grid voltage and frequency. This importance comes since the inverter is needed to fulfil the power conversion and control optimization. In GCPPPs operation, the module's output is converted from sunlight to an inverter that converts dc voltage into an ac sine wave. A transformer is needed to step the voltage up to an appropriate level, at the point of common coupling (PCC). In general, grid connected pulse width modulation (PWM) voltage source inverters (VSI) is commonly used in a PV system, which at least have two capacities.

Firstly, the dc bus voltage of the inverter should be balanced out to a particular value due to output voltage of the PV panels fluctuates with weather conditions in addition to the impact of MPPT. Secondly, the energy should be fed from PV panels into the utility network by modifying the dc current into a sinusoidal waveform synchronized with the utility grid (Omar & Zainuddin, 2014; B. Yang, Li, Zhao, & He, 2010). The main typical control parts of VSI-based GCPVS including MPPT, the dc-link voltage regulation control, ac current control loop, and the synchronization of grid voltage. For the purpose of grid synchronization during the advancements of the distribution generators-based inverter connected grid, there are three main PLL strategies that have been utilized for synchronization purposes including, zero crossing method, synchronous rotating reference frame (SRF-PLL) and stationary reference frame. The SRF-PLL is one among the previously mentioned PLL with the best performance under unbalance system, frequency variation and non-ideal grid conditions (Kumar & Surekha, 2015), so the SRF-PLL technique is selected to be used in this PVPP system. The MPPT technique is used to extract maximum available power from the PV array and generates the dc-link reference voltage. The ac current control loop is designed for dynamic, current protection, and power quality issues such as harmonic compensation.The dc-link voltage regulation control is responsible for the balancing power flow in the system (B. Yang et al., 2010). The inverter controller parts in the single-stage GCPPP can be explained as follows:

2.4.3.1   Maximum power point tracking

The output power of solar PV modules is not constant as it changes according to the sun direction, solar radiation level, and temperature varying. Therefore, there is usually a unique point on the voltage-power (*V-P*) or voltage-current (*V-I*) curve of the solar module called maximum power point (MPP) as shown in Figure 2.4. This point cannot be identified based on those characteristics, but it can be located by using MPPT algorithms. As a result of the low efficiency of the PV module, it is desirable to be operated at MPP using MPPT techniques implemented to extract maximum power (P_{mpp}) available from the PV modules (Desai & Patel, 2007).
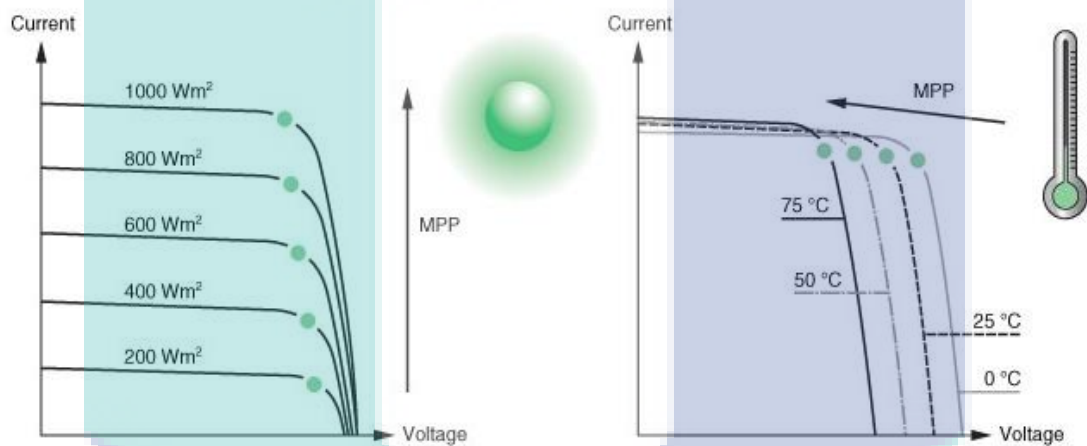
Figure 2.4   MPP for PV module at different level of radiation and temperature.
Source: Desai & Patel (2007).

There are a number of MPPT algorithms which have been used through the development of PV power systems. The grid-connected inverters generally employ MPPT to extract maximum available power from the PV array. It has been studied and addressed using different algorithms and techniques in the literature throughout the advancement of PV system. For instance, hill climbing (HC), incremental conductance (INC) method, perturb and observe (P&O) algorithm, look-up table method, constant voltage (CV) or constant current (CC). The aforementioned algorithms have been reported and compared by P.-C. Chen, Chen, Liu, Chen, and Luo (2015); Desai and Patel (2007); (Kamarzaman & Tan, 2014); Subudhi and Pradhan (2013). Over the recent years, different previous MPPT have been enhanced and proposed by the researchers in order to improve PV system efficiency such as the adaptive P&O, variable step size P&O, multivariable P&O, variable step size INC, and modified INC that reported and compared

in (Saravanan & Babu, 2016). In addition, there are high-efficient algorithms or the so-called intelligent MPPT techniques such as particle swarm optimization (PSO), artificial neural network (ANN), genetic algorithm (GA), fuzzy logic (FL) technique, and hybrid FL-GA based MPPT as investigated in (Khan & Mathew, 2017; Ram, Babu, & Rajasekar, 2017). On the other hands, these algorithms increases the system complexity. In general, all these methods have several advantages and drawbacks concerning oscillations, complexity, speed, the cost and extra hardware. The most widely utilized methods in GCPPP are P&O and INC because they are simple to be implemented on digital control when compared with other method and work reasonably well under most conditions. In this research, the P&O maximum power point tracking method will be implemented in the proposed GCPPP design steps due to its simplicity and ease of implementation.

2.4.3.2 PV inverter

The PV inverters can be categorized into different sorts according to the topology, operation principle, and the way of integration with the network. Taking into account the connection to the grid, there are lots of typologies. However, the most famous PV inverter-linked grid are: (*a*) Line-commutated; (*b*) Self-commutated. The first type is used (thyristor bridge or IGBT) as switching devices that control the switch-on time only, whereas the second one is more complicated than others and use (IGBT or MOSFET) as switching devices that control the switch-on/off time. The self-commutated is the prevailing technology in PV power system due to its ability to control the ac output signal (voltage and current), mitigate the harmonic current distortion, and regulate power factor (Theologitis, 2011). TNB allows only for grid connected inverters to be integrated with grid system. Therefore, for PV-grid connection, the regulation stipulates that self-commutated is preferred for MV and LV connection (Azit et al., 2012). For grid interfacing, self-commutated inverters are divided into voltage source inverters and current source inverters, depending on the type of pulse they control, either voltage or current (Ruiz, 2011; Theologitis, 2011; VanderMeulen & Maurin, 2010).

In general, in this research, self-commutated type of inverter will be used in the system design because it is imposed by the grid standards in addition to its ability to control the ac signal, mitigate harmonics, regulate power factor, and etc. Thus, the single-stage three-phase self-commutated voltage source inverter (VSI) is used in the proposed design to execute the power conversion and for control optimization purposes. In order

to control the VSI, there are two main control techniques: voltage control and current control. In current-controlled VSI, the injected active and reactive current components into the utility grid are controlled using PWM strategies. The current control method is faster in response, less sensitivity to grid voltage distortion, and voltage phase shifts. However, the voltage controller method is more sensitive to the harmonics and has small phase shifts (Bonaldo, Schiavon, Paredes, & Pomilio, 2017; Jana et al., 2016; Vu). As result, the current control method is used in the developed inverter control system.

a. *Voltage source inverters (VSI)*

In this type, the dc source (dc-side) is the voltage source of the inverter which remains constant and the output current is changing with the load. The inverter switches usually are insulated gate bipolar transistor (IGBT) semiconductor. VSI has a capacitor in parallel with the input. The voltage-source inverter is going to be used in this research.

b. *Current Source Inverters (CSI)*

In this type, the dc source (dc-side) is a constant current input and the voltage is changing with the load. The inverter switches usually are gate turn-off thyristor (GTO) or symmetrical gate commutated thyristor (SGCT) semiconductor. CSI has an inductor in series with the input.

2.4.3.3   Inverter control techniques

The inverter control can achieve the control process of the input side and grid side. The primary mission of the input controller is to obtain the maximum available power from the renewable energy systems while, the grid side controller deals with the active and reactive power that is transferred from renewable energy sources to the grid. Another responsibility of the grid-side controller is to ensure the grid synchronization as well as the quality of the delivered power into the network. Based on the literature overview, the voltage self-commutated inverter is preferred in all inverters. Whereas, the current-controlled inverters are more popular and utilized in grid-connected PV system when compared to voltage-controlled inverters as observed in Figure 2.5, because it achieves high power factor (Hassaine, OLias, Quintero, & Salas, 2014; Hojabri & Soheilirad, 2014; Parvez, Elias, Rahim, & Osman, 2016; Timbus, Liserre, Teodorescu, Rodriguez, & Blaabjerg, 2009). Depending on the operation of current-controlled inverter, the current

23

control approach can be categorized into the linear and nonlinear control strategies as follows:

Current and voltage controlled inverter ratio
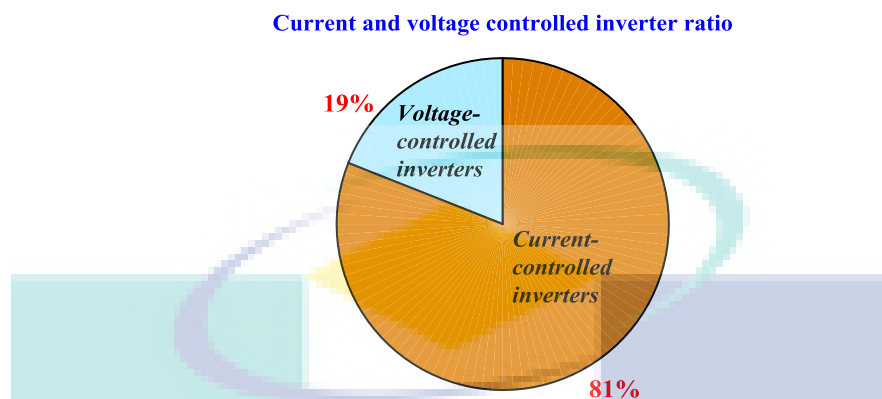
Figure 2.5   Share of the current- and voltage-controlled inverters in GCPPPs.

a.   *Linear current-controlled inverter for GCPPPs*

The most well-known linear current control strategies are the proportional integral (PI) controllers which are commonly associated with dq control approach, considering they are superior for controlling dc variables. The dq control is likewise known as a synchronous reference frame control which is described in detail by (Blaabjerg, Teodorescu, Liserre, & Timbus, 2006; Hassaine et al., 2014; Timbus et al., 2009). Proportional integral derivative (PID) also has been used (Hojabri & Soheilirad, 2014). Over the past years, inverter current proportional resonant (PR) controller's popularity for the GCPPPs has increased. In contrast to PI controller, this type of control is able to track the reference of sinusoidal current without phase error and steady-state value in the stationary reference frame known as ($\alpha\beta$ frame) (Cha, Vu, & Kim, 2009; Teodorescu, Blaabjerg, Liserre, & Loh, 2006).

The other famous linear type is the repetitive current (RC) controller, which has the ability to eliminate the steady-state error via controlling its components periodically. In addition, RC controllers are able to track the reference of the fundamental current and compensate a high order harmonic as introduced by (S. Chen, Lai, Tan, & Tse, 2008; Y. Yang, Zhou, & Blaabjerg, 2013). Nevertheless, the RC controllers is applied only for static operation mode and cause stability problems due to its slow dynamic response (Parvez et al., 2016). As a conclusion, despite the advantages of RC linear controller, this type performance is low during dynamic operation, while PI controller-based SRF is a

more robust type during disturbances so, this controller has been selected to control the inverter developed in this research for a more efficient FRT.

b. *Non-linear current-controlled inverter for GCPPPs*

The main two non-linear current controllers of the inverter linked GCPPPs are hysteresis controller and dead beat (DB) controller. Hysteresis control is a method which is used to control normally VSI wherein the grid current and the reference current are compared on an immediate basis to provide switching pulses for the inverter as described by (Kale & Ozdemir, 2005). Another kind is the DB controller that is applied as the control approach in lots of applications as described in detail by (Blaabjerg et al., 2006). Thus, this type of controllers are not selected due to the advantages of linear type controller, especially PI-based dq controller during dynamics operation.

2.5 Fault Types

One of the important parts in power system analysis is the fault study, which is the main causes of voltage sag. Insulation failure of equipment, flashover that initiated by a lightning, natural damage (falling of a tree, high-speed winds, earthquakes, etc.), or human error are the most common causes of faults in power system. These faults are divided into either three-phase balanced fault involving all three phases in a symmetrical way, namely symmetrical fault or unbalanced fault where usually one or two phases are involved in an unsymmetrical manner which is known as unsymmetrical fault (Kothari & Nagrath, 2003).

2.5.1 Symmetrical faults

A symmetrical fault is one that affects all three phases equally and is defined as the most severe fault. This type of fault involves large current and occurs infrequently in the power systems. In the balanced fault type, all three-phases are short-circuited to each other and often to earth, as illustrated in Figure 2.6 (Grainger & Stevenson, 1994; Kothari & Nagrath, 2003). This type will be used to test the proposed FRT controller as the most severe voltage sag.
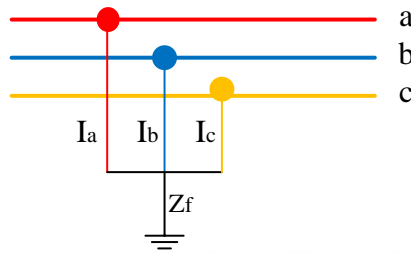
Figure 2.6 Symmetrical fault.

2.5.2 Unsymmetrical faults

Unsymmetrical faults are common fault, less severe than symmetrical faults, and occurs frequently in the power systems. In this type of fault, the three-phase lines become unbalanced. There are different types of unsymmetrical fault including single line to ground (SLG) fault, line to line (LL) fault, and double line to ground (LLG) fault. The most common unbalanced fault is SLG where 65-70% of the power system faults are of this type.

Figure 2.7 shows the unsymmetrical fault types. (Grainger & Stevenson, 1994; Seo, Kim, Yoon, & Jung, 2009b). All these types caused voltage sags at different levels. Therefore, it will be utilized to test the effectiveness of the proposed FRT controller to overcome these faults and support the grid according to the standard requirements.

(a) SLG Fault   (b) LL Fault   (c) LLG Fault
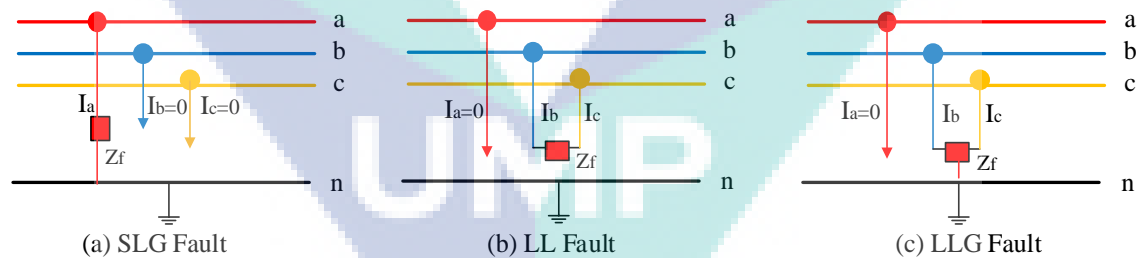
Figure 2.7 Unsymmetrical fault.

2.6 Voltage Sag

Voltage sags (dips) are probably one of the most important and severe power quality problems faced by the power industry as well as industrial and commercial customers (Singh, Chandra, & Al-Haddad, 2014). Voltage sags is defined as a reduction in the RMS supply voltage between 0.1 and 0.9 p.u at the power frequency for a short period of time (not exceeding one second). Although voltage sags are usually caused by

grid faults, it may also cause by starting large motors or energization of heavy loads (Fuchs & Masoum, 2011; Singh et al., 2014). Based on the fault type, voltage sags can be classified as a single phase, phase to phase, or three-phase sags.

2.6.1 Voltage sags detection methods

Most grids sag detection methods reported in the literature for GCPPPs are built into the inverter and are mostly intended for the purpose of connecting and disconnecting from the utility grid during disturbances or faults to prevent islanding (Pigazo, Liserre, Mastromauro, Moreno, & Dell'Aquila, 2009). Furthermore, it is used to activate the protection of the PV system array and modules from damage during low or high voltage events, identify a fault in a photovoltaic string or MPPT error, and report PV outcome status such as voltage, current, and power as introduced by (Charles et al., 2014; Chine, Mellit, Pavan, & Kalogirou, 2014; Silvestre, Chouder, & Karatepe, 2013). In the past, during abnormal conditions, the PVPPs must be disconnected directly. Thus, all these studies focused on detecting the voltage sag in case the inverter is disconnected during grid faults. But now, with the new GCs, the FRT requirement force the inverter to stay connected during faults. Therefore, the sag detection has become so much of an important feature, although the sag detection strategies for LVRT are not discussed in all references mentioned above.

Some of the fault detection methods for LVRT control strategy have been reported in the recent years, such as the peak value detection method, the missing voltage method, and the wavelet transform technique (Y. Yang & Blaabjerg, 2013; Y. Yang, Blaabjerg, & Zou, 2013). The peak value detection strategy computes the peak value of the input signal by utilizing a running average window of one cycle. It can be calculated according to the T/4 delay orthogonal technique. Hence, theoretically, this method will introduce one cycle delay until it reaches the correct value. The fault detection method using wavelet transform is becoming one of the most effective detection strategies as introduced in (Latran & Teke, 2015) due to its quick detection speed. Nevertheless, the use of this strategy is unfortunately difficult in real time. In this research, due the limitations of the above methods, RMS and positive sequence methods are going to be proposed, tested and compared. Next, the best method with good performance will be selected to use in the FRT control developed in this research.

2.6.2 Voltage sags mitigation techniques

The large costs associated with voltage sags can justify the use of sag mitigation strategies. This section describes some of the most common methods of voltage sag mitigation in the power system all around the world including Malaysia. A dynamic reactive compensation considers the famous solutions to mitigate the sags issues, including static synchronous compensator (STATCOM) and the static VAR compensator (SVC) which belongs to the flexible ac transmission system (FACTS) devices family. STATCOM device utilizes synchronous voltage sources in order to generate or absorb the reactive power and connected to the ac system via an interface transformer. A SVC can mitigate the voltage sag and support the grid voltage by injecting the loads by reactive current, which have been tested by (Foster, Xu, & Fox, 2006; Milanovic & Zhang, 2010). These traditional FACTS devices are being used to solve the FRT capability in renewable energy, which will be discussed in Section 2.10.

Another traditional device used to mitigate the sag events in the power system such as the uninterruptible power supply technique using energy storage devices to inject reactive current (Sannino, Miller, & Bollen, 2000) and dynamic voltage restorers (DVRs). DVR is a complicated device, which basically work on adding the lost voltage through voltage sag period as proved by (Patel, Goswami, & Singh, 2015). This means that the DVR injects voltage into the system to be able to bring the voltage returned as much as the level required. It is an automated impedance matching device designed to bring the system near unity power factor. Injection of voltage is completed by a switching system coupled to a transformer that is linked in series with the load, as introduced in (Patel et al., 2015). In general, all these techniques are expensive, increase the complexity of the system, and used for the traditional power system. Although using these devices and techniques, the voltage sag occurs and cause problems to the grid stability. Therefore, the FRT capability using the inverter controller presented in the current study will help in solving the sag problems and contribute to grid stability.

2.7 Global Standard Requirements Concerning the Integration of PVPPs

Due to the advancement of GCPPPs, the regulation and standard have been issued for the first time to regulate the connection using some simple requirements such as PV system design, operation and etc. Recently, these requirements become more stringent.

The old regulation includes international regulation, such as IEEE 1547 series of standards (T. S. Basso & DeBlasio, 2004), which is subsequently updated by (T. Basso et al., 2012) and European standards (IEC) (Cleveland, 2008). In addition to the national standards such as the Chinese standard (GB/T, 2012), Brazilian standards for inverter-connected grid (Figueira et al., 2015), and Malaysian standard issued by TNB for the connection of PVPPs to medium and low voltage (Azit et al., 2012). These standards did not contain FRT capability control, but require PVPPs to disconnect directly in case of grid faults.

2.7.1 National grid technical regulation concerning PV penetration

Early in 1996, TNB published the first technical regulation concerning the interconnection of synchronous distribution generator (DG) into TNB's distribution network. However, due to the rapid development of DG and implementation of the five fuel diversification of energy. Furthermore, the country encourages connections of RE-based DGs to the distribution network, led TNB in 2005 to stipulate the requirements regarding the connection of synchronous/asynchronous generator to the distribution network under the title of "technical guidebook for the connection of generation to the distribution network" (Tenaga Nasional Berhad, 2005). On 21 December 2010, the energy commission Malaysia (ECM) issued the Malaysian grid code and distribution grid code (Energy Commission Malaysia, 2010). Distribution grid code is a set of technical regulation and requirements which should be carried out to maintain the grid stable and ensure the distribution network is secure and reliable. As mentioned before, the government support as well as tropical climate are the driving factors for improving PV energy systems in Malaysia, in addition to the approval of the RE Act by the Parliament in 2011. These factors act as a catalyst for the entrance of privately-operated PV generation Companies into the utility grid, such as home owners that sell their excess energy generated for the network under the FiT scheme (Tenaga & dan Air, 2011). As a result, this growing interest has led to the issuance of the regulation regarding RE penetration to the utility grid (Energy Commission Malaysia, 2010; Tenaga Nasional Berhad, 2005).

More recently, due to the increasing power generation from solar energy and interconnection into the national electrical grid, TNB issued technical regulation concerning the penetration of PV system to medium and low voltage which is prepared

in compliance to the operational conditions terms as stated in the Malaysian distribution code and technical & operational requirements rules of RE (Azit et al., 2012) which was revised recently by (Suruhanjaya Tenaga, 2016). As a conclusion, all these technical regulation faced some issues such as the nominal voltage operating range, harmonics, frequency range, MV penetration, PV inverter type, voltage unbalance and power factor. However, it does not address or stipulate requirements regarding FRT capability, injection of reactive current, and active power control either for wind or PV plants. Consequently, this research proposed a new FRT as new requirements for Malaysian grid. Additionally, in the literature, no GCPPP had been used to validate or test TNB requirements like the other national and international standard. Therefore, these technical regulations of TNB regarding PV penetration to the national grid will be used as references in this research.

2.7.2   International and national standard requirements compliance studies

As mentioned above, standards are of significance to the development of GCPPPs. Therefore, the standardization process and discussion of national standard concerning PV penetration can be found in literature worldwide. Designing PVPP with a connection method control at PCC had been developed in (Klapp & Vollkommer, 2014) in order to comply with IEEE 1547 standard. In the same manner, the compliance of the connection of distribution generators in accordance with IEEE 1547 standard had been addressed by (de Carvalho et al., 2013) and (Liu, Lan, Lin, Chiu, & Chen, 2013). Another study tested and validated the Brazilian standard in comparison with IEEE 1547 and IEC 61727 rules introduced in (Figueira et al., 2015). Modeling and design of PVPP have been built in accordance with the national standard which is built based on the Chinese standard (GB/T, 2012) studied by (Y. Li, Li, Liu, Cai, & Dong). In a summary, the Malaysian standard (TNB regulations) is similar to the other national standard, but no previous work used these standard to consider and analyse the practical conditions and characteristics of present PVPPs connected to the distribution system of Malaysian grid sufficiently. Thus, this research will study the application of TNB technical regulation concerning the penetration of PVPPs to MV distribution system.

As a result, all the above mentioned standard requirements does not mention the new and advance requirements such as the FRT and injection of reactive current during grid disturbances especially, voltage sags. However, they require the PVPPs to disconnect

directly from the utility grid as soon as the grid faults happened. On the other hand, the modern grid codes have been imposed with the FRT requirements for the GCPPPs to support the grid and voltage recovery during sags events, as will be explained in the next section.

2.8   Modern Grid Codes Requirements

Grid codes are not new topics in the power system utilities. It began to appear 21 years ago. The grid codes differ from one country to another according to the characteristics, various regulations and laws of the national power system. In the beginning, the grid codes were applied to the transmission system as a set of operation specifications and technical guidelines for traditional power plants that are integrated with power system to comply with. On the contrast, GCs were mainly utilized to specify and set the rules that the distribution system operators (DSOs) should apply in the planning and improvement of distribution power systems (Preda, Uhlen, & Nordg, 2012). In today's context, the grid codes have been amended and improved by being subjected to the continuous changes and developments of renewable power system as distribution generators and new technical requirements such as FRT, reactive current injection and restoring active power.
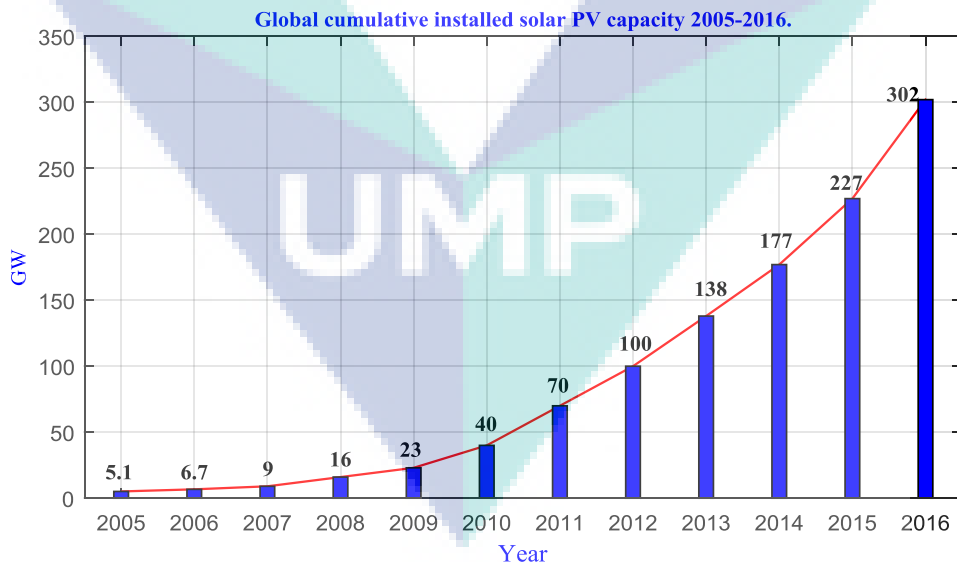
Figure 2.8   Global cumulative installed solar PV capacity 2005-2016.

These requirements have been newly absorbed to the GCs for large wind power plants (WPP) integration in some countries such as Denmark, Germany, UK, Canada, Ireland and Spain (Crăciun, Kerekes, Séra, & Teodorescu, 2012). Nowadays, these

requirements like FRT are being adapted for PV plants due to the rapid increase in PV installation and penetration and it is expected to continue to increase significantly, as observed in Figure 2.8. With the remarkable increase of PVPPs penetration to the utility grid, there appears some challenges where these power plants should overcome concerning the operation, stability, and power quality. However, few countries are aware of the importance of PVPPs as part of the utility system and how it can affect the network stability. Thus, the disconnection of these PV farms is not permitted due to the negative sequences of its disconnection to the grid and customers. As a result, this leads to prepare on specific technical requirements for the connection of large-scale PVPPs as a part of the grid code. Thus, these new requirements concerning the PV penetration to the utility grid have been imposed in some of leader countries in this field. The new requirements are the FRT, while some countries impose the reactive current injection during the fault as additional requirements (Afshari et al., 2017; Cabrera-Tobar et al., 2016; Elrayah, 2017; Etxegarai et al., 2017).

2.8.1 FRT as new requirements in grid codes for PV system connection

Nowadays, in light of the PV system thriving situation, the disconnection from grid during disturbances are no longer possible. Over the past days, during the abnormal grid conditions, PVPPs are needed to disconnect from the distribution system as soon as the fault happened for safety concern (Cabrera-Tobar et al., 2016; Shah, Mithulananthan, Bansal, & Ramachandaramurthy, 2015), and that is known as islanding protection. However, the effects of these PVPPs disconnections from the grid have newly gained growing attention and lead to new challenges for the power system operators (PSOs) and the PV inverter manufacturers in different aspects, like the system efficiency, the power quality and reliability. Therefore, in order to maintain both the excellence of power quality and high grid reliability, European countries such as German, Spain and Italy, which are considered as a leader in PV system marketing and installation, in addition to other countries like China, Japan and the United States have set a new standards and requirements to their GCs concern the PV penetration. The main requirements in the new grid codes and standards for GCPPPs is the FRT capability. Additionally, the PVPPs are required to inject the reactive current to the grid under faults occurrence, as imposed by some countries (Cabrera-Tobar et al., 2016; Crăciun et al., 2012; Perpinias, Papanikolaou, & Tatakis, 2015; Shah et al., 2015; Y. Yang, Enjeti, Blaabjerg, & Wang, 2013).

Like the traditional power plant, modern GCs require PVPPs contribution to support the grid stability, withstand different grid disturbances and auxiliary service arrangement. The main focus in the GCs is a fault ride-through requirements or the so-called low voltage ride-through (LVRT) and injection of reactive current (Bae, Vu, & Kim, 2013; Obi & Bass, 2016). In the literature, the issues of modern grid code requirements concerning the penetration of PVPPs have been explored. The new technical regulation in German grid codes was imposed by the German Association of Energy and Water Industries (BDEW) concerning PV connection to medium and high voltage which is considered as the first regulation worldwide (Bundesverband der Energieund Wasserwirtschaft (BDEW), 2008; Troester, 2009). Lately, these requirements are often used as references for other codes.

The Australian grid code requirements for PV integration was first presented by the Australian Energy Market Commission (AEMC) in 2014 (AEMC, 2015; Australian Energy Market Commission (AEMC), 2016; Badrzadeh & Halley, 2015). The technical regulations of Japan, China, US, Romania, and Spain were studied in (Bică, Dulău, Muji, & Dulău, 2016; García-Sánchez, Gómez-Lázaro, & Molina-García, 2014; GB/T, 2012; Gevorgian & Booth, 2013; Kobayashi, 2012). Italy recently issued a new requirement regarding PV penetration in the modern version of its grid code CEI 0-21 in 2014 (CEI-Comitato Elettrotecnico Italiano, 2014).

In Denmark, the individual technical regulation is defined to PVPPs that generate more than 11kW (Energinet, 2015). In South Africa, the grid code specifies technical criteria for PV power stations connected to both the distribution system and transmission system are studied (Magoro & Khoza, 2012). Finally, in Malaysia, on 21 December 2010, the grid code and distribution code have been issued by the energy commission Malaysia (ECM) (Energy Commission Malaysia, 2010), but these two codes did not address the FRT capability or dynamic voltage support either for wind or PV integration. Therefore, this study will propose FRT as a new requirement for Malaysian GCs to improve the system stability and reliability.

2.9   Global Trend of FRT Capability in GCs as New Requirements

2.9.1   FRT or LVRT capability requirements

Low voltage ride-through capability, defined as the PV inverters' capability to remain connected to the grid in the event of grid failures due to grid faults, to supply active and reactive power during a grid fault, and to deliver active power directly after clearing the fault, thus stabilizing the grid. The second aspect also relates to LVRT, but refers to the additional capability of injecting reactive power in the grid in case of grid fault, with the purpose to ensure the voltage support during fault conditions.

LVRT requirements are specified in the modern GCs, which require the PVPPs to withstand grid voltage sag to a certain percentage of the nominal voltage (down to zero in some grid codes) for a specific duration. In this duration, PVPP should operate normally. After faults clearance, PVPP must restore active and reactive power fast enough to the pre-fault values. In some countries, the PV system is required to operate like the traditional synchronous generators where reactive current should be fed into the grid to support the voltage stability (Hasanien, 2016; Obi & Bass, 2016). Normally, the international GCs containing LVRT curves are relatively similar to Figure 2.9. However, their characteristic may vary from one system to another.
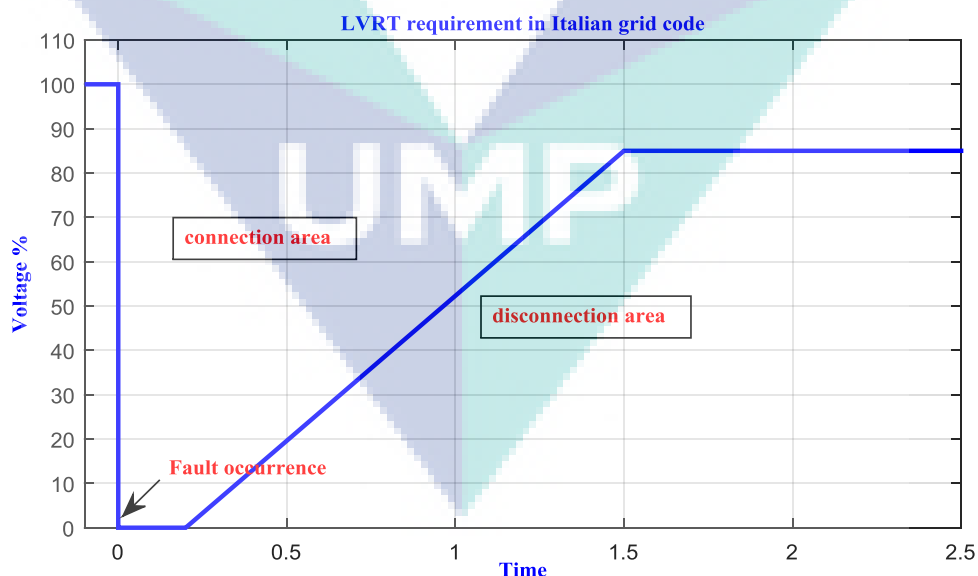
Figure 2.9   Italian LVRT requirement during grid faults.

Italian FRT requires the PVPP to withstand faults and still connected to the system within 200 ms when the voltage at the connection point of PV system drop down to zero as illustrated in Figure 2.9. If the voltage at the connection point recovered to 85% of the rated voltage within 1.5 s after the fault occurrence, the PV units shall remain under continuous operation without tripping off (CEI-Comitato Elettrotecnico Italiano, 2014).

2.9.2   FRT requirements in different GCs

The LVRT features can vary from one country to another, depending on the power company operator requirements and the reliability of the national grid (J. Hossain & Mahmud, 2014). For instance, the German GC (Troester, 2009) required that each PVPP should remain connected to the system within 0.15 s when the voltage at PCC drop to zero of the rated voltage, which is the so-called zero voltage ride through (ZVRT). No tripping off operation is allowed within this period. If the voltage at the connection point could recover 90% of the pre-distributed value within 1.5 s, the PVPP shall remain under continuous operation without tripping off. The Italian GC requires the PVPPs to withstand grid faults with voltage drop to zero for 0.2 s, accompanied by voltage restoration to 90% of its nominal value during the next 1.0 s after the voltage drop occurrence (CEI-Comitato Elettrotecnico Italiano, 2014).

The Chinese GC stipulates that the PVPPs must remain connected during voltage sag down to 20% within 0.625 s, and the voltage should be restored to at least 90% of its level available before the sag within 2 s (Cabrera-Tobar et al., 2016; Ding et al., 2016; GB/T, 2012). The Spanish GC imposes that PVPPs must withstand the drop in voltage to 20% of the rated value for 0.5 s, and then rise to 85% at PCC within the next 0.5 s (García-Sánchez et al., 2014). The more rigid LVRT requirement was enforced by Australian GC which requires PVPPs to withstand a voltage drop down to zero at PCC and return to 80% at the same time (Australian Energy Market Commission (AEMC), 2016). Table 2.1 summarizes the parameters of LVRT requirements in different GCs. The comparison of these LVRT requirements in different international grid codes with respect to the integration of PVPPs to the utility grid is shown in Figure 2.10. It is worth to note that these requirements have small differences between different countries and should be applied at PCC.

Table 2.1   LVRT requirements in different international grid codes.

Country Grid code	Fault time		After Fault	
	$V_{min.}$ (%)	$T_{max.}$ (s)	$V_{min.}$ (%)	$T_{max.}$ (s)
Germany	0%	0.15	90%	1.5
Spain	20%	0.5	80%	1.0
China	20%	0.625	90%	2.0
USA- PREPA	15%	0.60	85%	3.0
USA- NERC	15%	0.625	90%	3.0
Japan	20	1.0	80	1.2
Australia	0%	0.45	80%	0.45
Italy	0%	0.2	85%	1.5
South Africa	0%	0.15	85%	2.0
Romania	15%	0.625	90%	3.0
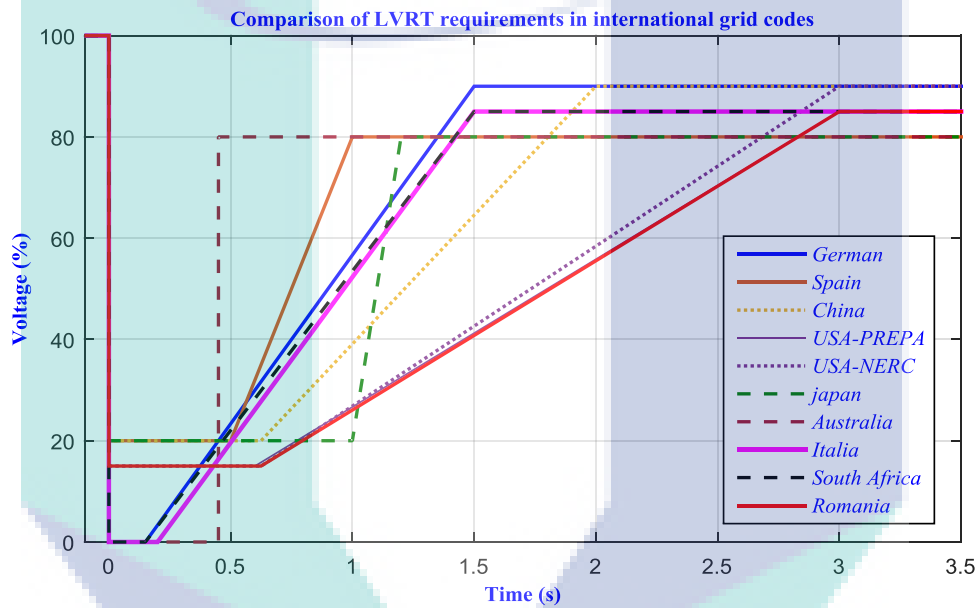
Figure 2.10   Comparison of LVRT requirement at different GCs.

2.9.3   Reactive current support

Despite many grid codes requiring the PV farms to remain connected to the grid during disturbances for a certain period of time as described in the previous section, a few codes require these plants to support grid voltage recovery by injecting reactive current during grid faults (Diaz-Franco, Vu, El Mezyani, & Edrington, 2016). For instance, the German grid code defines the injection of reactive current as fast as possible to support the grid voltage according to the standard requirements shown in Figure 2.14(a). It specifies that the amount of reactive current should be injected based on the depth of voltage sag. Typically, the voltage works in a band of ±10% of the nominal voltage. So, when the rated voltage is between 0.9 p.u -1.1 p.u, the system is in a steady state operation and therefore no change is required. For a voltage drop between 10% and 50% of its

nominal value, the amount of injected reactive current should be 2% of the rated current for each percent of the voltage drop. In case the amplitude of grid voltage drops below 50% of the rated value, PVPPs should inject the rated amount of reactive current (1 p.u) (Afshari et al., 2017; Neumann & Erlich, 2012).

The PV system has to support the grid by generating reactive power during a network fault and to increase system stability as stated in the Spanish grid code (García-Sánchez et al., 2014; Red Electrica, 2008). It requires the PV stations to inject reactive current during faults according to the saturation limits depicted in Figure 2.14(b). The reactive current can be reduced to zero in case voltage falls to lower than 50% of the rated voltage. USA-PREPA stipulates that PVPPs cannot inject reactive current for dead band within ±15%, otherwise it must be injected with a variable slope from 1% to 10% (Cabrera-Tobar et al., 2016; Gevorgian & Booth, 2013). Four percent of the rated current should be injected within 1% drop of the voltage at PCC, as imposed by Australian grid code (Australian Energy Market Commission (AEMC), 2016).
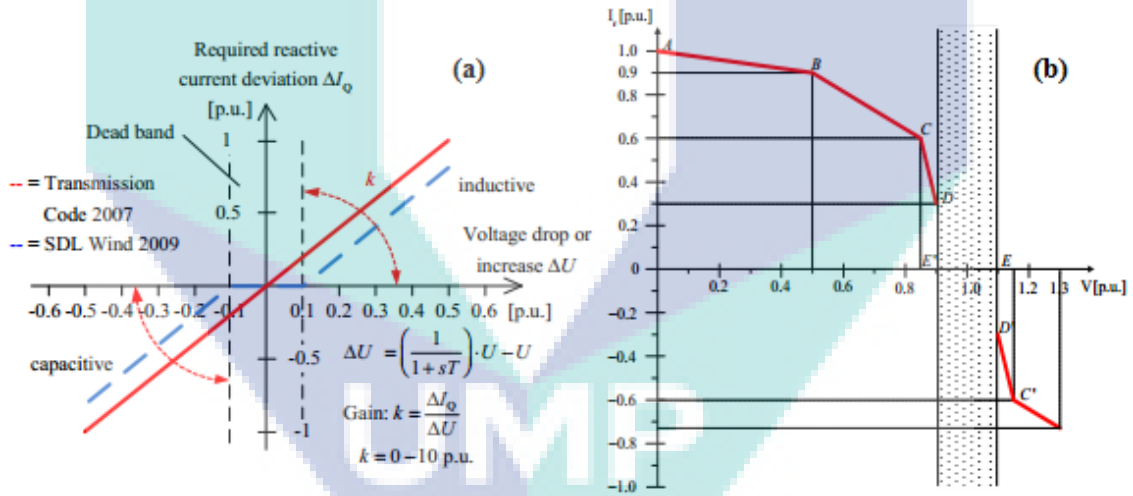
Figure 2.11   Reactive current injection requirement of FRT(a) German, and (b) Spain. Source: (a): Neumann & Erlich (2012), and (b): Red Electrica (2008).

2.10   FRT Capability Control Strategies – Gap Analysis

As above mentioned, these days, modern grid codes and power system operators are requesting PVPPs to act as traditional power plants as much as possible by providing FRT capability during voltage sag. Accordingly, the PVPPs ought to deal with the problems of inverter disconnection and support the grid by reactive current during disturbances. Therefore, developers and researchers should provide the proof of

verification and compliance with the FRT requirements that are already included in the modern grid codes. This section will introduce the state-of-the-art of some compliance solution and controls of FRT.

In one of the first literature studies for FRT capability presented by Azevedo, Vazquez, Luna, Aguilar, and Rolan (2009), the authors designed a new control strategy to allow the PV solar system operate during the grid faults without exceeding the rated current and resulting sinusoidal currents. Contrary to PV classic control which still delivers the same amount of power during fault time, the current can increase to dangerous values over the time. This study proposed control for 3 kW PV system simulated using PSCAD/EMTDC based on the stationary reference frame using proportional resonant current control. The authors dynamically calculate the maximum active power that should be delivered by the inverter and use this value as limiter of the reference power. Based on the positive sequence of voltage, they calculate the current references in the proper way to result in balanced values even in the occurrence of voltages unbalanced caused by grid faults. As a conclusion, this study ride-through the fault by a new control method and overcome the disadvantages of conventional PV inverter control by permit it to ride-through the fault. On the other hand, there is no specific time taken into account by the authors in the proposed control method to disconnect the inverter and this may cause problems especially in case of disconnection from the grid by protection relays. In addition, there is no injection of reactive current to support the grid voltage during the fault as stated in the GCs or addressing of dc over-voltage.

Another study proposed by (Viet & Yokoyama, 2010) to measure the transient stability as impacts of FRT characteristics for high penetration of GCPPPs. The authors focused to describe the effects of withstanding the inverter to the voltage sag with different cases of power generated, either a few or large amount and ignore the mention of the control that is used in this study. The results of this study explained that the large-scale PVPPs may make critical power transient stability under grid disturbance. In addition, emphasize that the need to use reactive current injection which is stated by some modern GCs and will be applied to the solar power plant which will be developed in this thesis. Dynamical current limitation (DCL) was adopted by (Benz, Franke, & Fuchs, 2010) in order to limit the current of a 5 kW station to protect the inverter and other

semiconductor devices from damage, but the issue of power balance, injection of reactive current, and dc over-voltage still needs to be addressed. A new control based on the feedback linearization strategy (FLS) proposed by Zhang, Ma, and Zheng (2011) to ensure that the inverter has the ability to ride-through the fault by remaining current levels within the designated limits. The proposed control allows the PV inverter to operate without exceeding the current limits and producing a sinusoidal wave under any fault. This study has drawbacks in case the fault maintains more than voltage sag time and maybe still gets connected, whereby islanding phenomena could happen. In addition, there is no support to the grid voltage during this period. A new FRT control scheme that limits fault current within the limits of the system is presented by Jayakrishnan and Sruthy (2015). This study introduced micro-grid system consisting of two wind sources and one PV source. The model is studied under normal and fault conditions. Master-slave control is adopted for the source to enable the power sharing and fault ride-through capability should address the current limits only.

(Carrasco et al., 2013) developed an experimental test in the laboratory using 500 kW test bench in order to test the solar inverter, as first test of LVRT experimentally. The bench test is based on two inverters, one used as a sag generator while the other as solar inverter under test as shown in Figure 2.12 to validate the requirements of the German BDEW standard. The results of this study show the effectiveness of this study under various types of grid fault and sag width. This method serves to prove that the FRT can be applied practically, but no use of PV system, fault detection or the inverter protection capability to stay connected have been tested.
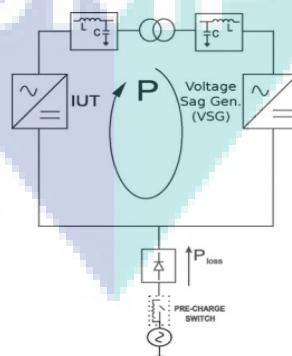
Figure 2.12   Single line diagram of the test bench.
Source: Carrasco et al. (2013).

Some research has used energy storage system (ESS) as external devices which are installed in the GCPPPs to offer ancillary services, such as active power balance and protect the inverter from excessive ac-current in the ac side of the inverter as well as the excessive dc voltage in the dc-side throughout the period of grid faults until ride through the faults smoothly. Energy storage function using supercapacitor was proposed by (Kim et al., 2013; Worku & Abido, 2015). Supercapacitor energy storage system (SCESS) control had been used during fault to store the generated power from the PV array for later use and for a fault ride-through. SCESS is connected to the dc-link via bi-directional buck-boost converter to deal with this issue using complicated control (Worku & Abido, 2015). It is important to mention that, this method has been used in the literature for wind energy before the PV system to integrate storage devices, either batteries or supercapacitor, for LVRT capability and smoothing power fluctuation in WPP-connected grid by Gkavanoudis and Demoulias (2014) and Yibre and Abido (2013). The main drawbacks of this method are the high cost of the additional energy storage system as well as the fluctuation of values before and after the fault, whether battery or supercapacitor.

Similarly, the batteries energy storage system (BESS) control is introduced by (K. Li, Qian, Wu, Li, & Yang, 2015; Manikanta et al., 2017) to store energy during the fault in order to address the over-voltage of the dc link. The control proposed by (Manikanta et al., 2017) utilize the bidirectional dc-dc converter which is connected to the batteries. So, it will be in off-mode during normal operation. Whereas, during the faults, the dc-link voltage is going beyond the limits specified. The controller detects this increase and activate the buck mode of bidirectional dc-dc converter to send more charge available at the dc-link to charge the batteries. On the other hand, if the voltage across dc-link is decreased to lower than required voltage, then the controller operates bidirectional dc-dc converter in boost mode and the dc-link receives charge from battery. By a similar way, the study proposed by (K. Li et al., 2015) used the BESS for LVRT control. In this study, a method of dc voltage control is adopted. Therefore, during the period of LVRT, the duty cycle of the boost circuit is adjusted to reduce the output power of the PV battery in order to restrain the dc side voltage. It can be noted from the behavior of these two methods that there are some fluctuation before and after grid fault, but the strategy control proposed by (Manikanta et al., 2017) addressed only a very high dc-link voltage. Whereas, a few increment and overshooting still exists and this may cause power

imbalance between both sides of the inverter. Although the above research on FRT control strategies using ESS solved the excessive dc-voltage with different efficiency and some drawbacks, all these studies are not dealing with the injection of reactive current to support the grid and voltage recovery which are imposed by some of grid codes. However, this type of technique is hard to be extensively applied in the industry because of high investment price, short lifestyles cycle of energy storage units, and increased complexity of the system.

A novel method using adaptive dc-link (ADL) voltage control to control the excessive voltage until ride-through different grid fault is applied by (Ding et al., 2016). Although this method used bidirectional dc-dc converter to change the voltage reference of the dc-link by MPPT control, there is a fluctuation in the dc-link voltage during the unsymmetrical faults, while high fluctuation appeared during 3-ph fault. Additionally, this method increased the complexity of GCPPPs. As a result, this control does not deal with excessive ac current in the ac-side as well as the injection of reactive current to support the grid and voltage recovery imposed by some grid codes.

The series dynamic breaking resistor (SDBR) is a resistor connected in series between the PVPP and grid connection point to improve the FRT capacity by protecting the system during the fault period against the excess voltage. In (M. K. Hossain & Ali, 2014), the SDBR was employed in GCPPPs to contribute to the system balance as a part of the FRT control. During a fault, the voltage increases in the inverter dc side. Subsequently, the energy is wasted in the SDBR, and stopping the dc-link voltage to increase sharply and overcome the overvoltage incident. As a conclusion, the SDBR address over-voltage to enhance the FRT, but not dealt with the over-current and injection of reactive current.

Although most of the above studies focused on ride-through the fault by protecting the inverter, a few studies dealt with reactive current injection, which is the most and recent capability enforced by some grid codes. For instance, the study introduced by (L. Yang, Liu, Peng, Chen, & Xu, 2016) used the coordination between the PV system and the STATCOM to deal with the grid fault. It can be noticed that the STATCOM inject the required reactive current to support the voltage recovery during the fault and addressed the excessive dc-link voltage. In addition, the static VAR compensator (SVC) also has the ability to inject reactive power and consequently compensate voltage sags,

as presented in (Castilla, Miret, Camacho, Matas, & de Vicuña, 2014). In general, these FACTS devices are effective to inject reactive currents and to enhance the FRT capability. However, it increases the complexity and cost due to adding an external hardware to the system, while not deal with the inverter protection.

On the other hand, the most control used the inverter itself to meet FRT requirements without extra hardware is the control introduced by (Merabet & Labib, 2017; Saad, El-Sattar, & Mansour, 2016). The simulation results presented in (Saad et al., 2016) show the effectiveness of the particle swarm optimization (PSO) strategy to enhance the FRT capability as computational method, mitigate voltage sag by addressing excessive dc voltage, and ride through the grid fault safely without reactive current injection. The control proposed by (Merabet & Labib, 2017) addressed the excessive ac current and excessive dc voltage as well as injected the required amount of reactive current by modified inverter controller (MIC) using a dual mode operation control, but an oscillation and overshooting appears in the results because of the use of an anti-wind-up technique dc-link voltage regulation via dc-dc converter, respectively, also can causes harmonics at the PCC.

In the literature, the major strategies proposed have addressed the FRT requirements of PVPPs connected to the power grid mentioned above are illustrated in Figure 2.13. The two fundamental approaches of FRT capability control can be divided into the FRT control using external devices and modified controller approaches. Energy storage systems either BESS or SCESS, flexible alternating current transmission system (FACTS) devices either STATCOM or SVC, in addition to some other methods such as the SDBR, are the FRT capability control strategies using external devices. The modified inverter controllers, computational methods, and others such as including DCL, FLS, and ADL are modified controller strategies without additional devices.
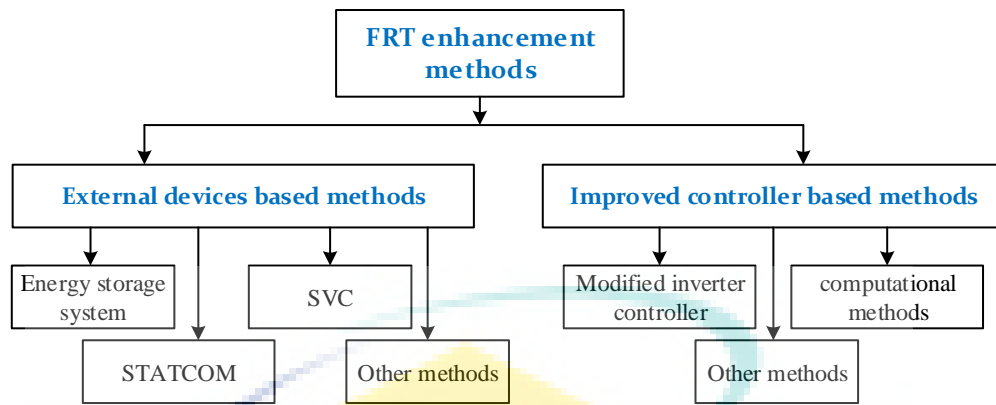
Figure 2.13 Categorization of prior-art control methods to enhance the FRT performance for grid-connected PV systems.

In sum, as comparison of different FRT strategies discussed above in terms of complexity, economy, additional device, and addressing the two main issues of FRT capability to meet the modern GC requirements are summarized in Table 2.2. The two main issues include the protection from overvoltage and overcurrent during faults and the reactive current injection based on grid codes requirements. It is important to mention that some FRT strategies are more expensive than others. In line with this, the cost of these strategies is classified into high, medium, and low. FACTS devices, either STATCOM or SVC usually require a coupling transformer and include many switches, and therefore are considered as the most expensive strategy. Furthermore, the ac over current and dc overvoltage have not been addressed by STATCOM or SVC, respectively. In addition, the difficulty in controlling their switches will increase the complexity of these FRT techniques.

Table 2.2   Technical, economy, and complexity comparison of FRT methods.

| Techniques | The cost | The complexity | Fulfillment of grid code requirements | | | Extra devices |
			Overvoltage in dc-link	*AC overcurrent*	*Reactive current injection*	
BESS	High	Medium	Yes	No	Low	Yes
SCESS	High	Medium	Yes	No	Low	Yes
STATCOM	High	High	Yes	No	Good	Yes
DVR	High	High	No	Yes	Good	Yes
SDBR	Medium	Medium	Yes	No	No	Yes
MIC	Low	Medium	Yes	Yes	Good	No
FLC	Low	Medium	Yes	No	Low	No
DCL	Low	Low	No	Yes	No	No
FLS	Low	Low	No	Yes	No	No
ADL	Medium	Low	Yes	No	No	No
Current study	Low	Low	Yes	Yes	Good	No

Another high-cost FRT strategy is the ESS such as the BESS or SCESS because it is equipped with batteries and super capacitors, respectively, which are expensive, require periodic inspection, and regular maintenance. Moreover, although ESS strategies have been used to suppress the excessive energy and therefor protected the inverter and ride through the faults, the injection of reactive current have not been addressed. Since the SDBR strategies have less switches as compared to FACTS and utilize high power resistors, they are the less expensive techniques among the FRT control based on external devices. Finally, modified controller based techniques are more economic FRT strategies, due to the fact that these method do not use extra devices in their structures. Regarding the grid code compliance, these method not sufficiently dealt with it to achieve an efficient and comprehensive FRT. Therefore, the current study comes to overcome the drawbacks and fills the gap.

2.11   Summary

This chapter discussed the most recent international grid code standards concerning PVPPs penetration to the utility grid, including FRT capability and injection of reactive current during voltage sag caused by grid faults. Likewise, this chapter summarized the main concept and definition related to the study as well as the related studies in FRT control, international and TNB standard and regulation as well as GCs requirements regarding PV penetration. An overview of the previous studies conducted in FRT capability control and injection of reactive current with their advantages and disadvantages have been presented. In addition, the PV inverter control of GCPPPs, voltage sag mitigation and detection methods have been illustrated. Obvious gaps in the comprehensive and effective FRT capability control to protect the inverter from high ac current and dc voltage as well as injection of reactive current without increasing the cost, using extra hardware, smooth return of the power parameters without fluctuations have been highlighted. In addition, the gap of Malaysian GC regarding FRT and compliance of TNB technical regulation is illustrated. Therefore, this research has addressed these problems to fill the gap, and this will be discussed in the following chapters. The next chapter will present the designing steps and modeling of the proposed PVPP connected to the power grid.

CHAPTER 3

DESIGN OF THE PROPOSED LARGE-SCALE PVPP-CONNECTED TO THE UTILITY GRID

3.1   Introduction

This chapter presents the method utilized to achieve the objectives of the research. In addition, the design and control of a large-scale single-stage PVPP connected to the electrical power grid with the developed FRT inverter controller are presented. For a more accurate design, the overall performance and reliability are important to the PV system. Consequently, proper modeling and control design permits the development and smooth performance of FRT capability control. The complete design and modeling of the proposed PVPP and its control can be divided into several subsystems to facilitate the control operation. Firstly, the design and modelling of the large-scale PV array steps are presented in detail. It includes, the modeling of the PV modules equivalent circuit to represent the PV arrays, sizing steps of the PV array, and MPPT algorithm to ensure that the maximum available power is captured and converted. Secondly, the voltage source inverter (VSI) control strategy of the PVPP and integration with the power system have been introduced. For control and analysis purpose, the control structure of the VSI including the mathematical modeling, inner and outer loops of the control, and the pulse width modulation of VSI control are synchronized to the distribution network via a synchronous rotating reference frame-phase locked loop (SFR-PLL). Thirdly, the decoupling of the three-phase ac current and voltage to dq coordinates, which is much easier to design and control especially for the proposed FRT technique, will be considered. Lastly, the compatibility with TNB technical requirements concerning the penetration of PVPP into MV side of the power grid are discussed.

3.2   Research Methodology

This section describes the structure of the research design and methodology adopted to achieve the stipulated goals of the research. The technique implemented in this thesis was based totally on creating an enough background through a literature overview. All essential information has been filtered and used to provide a theoretical assessment over the grid linked photovoltaic systems, technical regulation, standard requirements, grid codes, and FRT with a discussion on the technical compliance and simulation effects. The method applied can be briefly explained through several fundamental and essential phases which are addressed in an acceptable sequence as illustrated in Figure 3.1. The research framework consists of three phases which are planning, designing and implementation, and evaluation phase. Each phase includes sub-components which have a brief explanation in the following sub-sections.

3.2.1   Planning phase

This is the first phase of the proposed research framework. It is a way to set a plan before implementing this work in order to determine all aspects of the research. The main sub-component in the planning phase is literature review which is considered as one of the most critical phases in the research framework. This is due to the importance in determining the limitations of existing studies and defining the problem statement of this research. In addition, the objectives, significance, scope, and contribution of the research are determined in this stage as well. Moreover, the planning phase delivers the research Gantt charts which illustrates the predicted period to achieve this work and the domain of the study. This phase has been clarified clearly in chapter one. The purpose of the research plan can be summarized as: (*a*) providing a brief description of the research problem; (*b*) finding the limitation of current studies that relate to the problem of research; (*c*) identifying the objectives of research based on the current studies; (*d*) determining the procedures and steps that followed in addressing the problem of research; (*e*) detecting the platform, data, and design tools needed to achieve the goals; and (*f*) developing a way to address the problem in identifying research methods that will be used in this thesis.
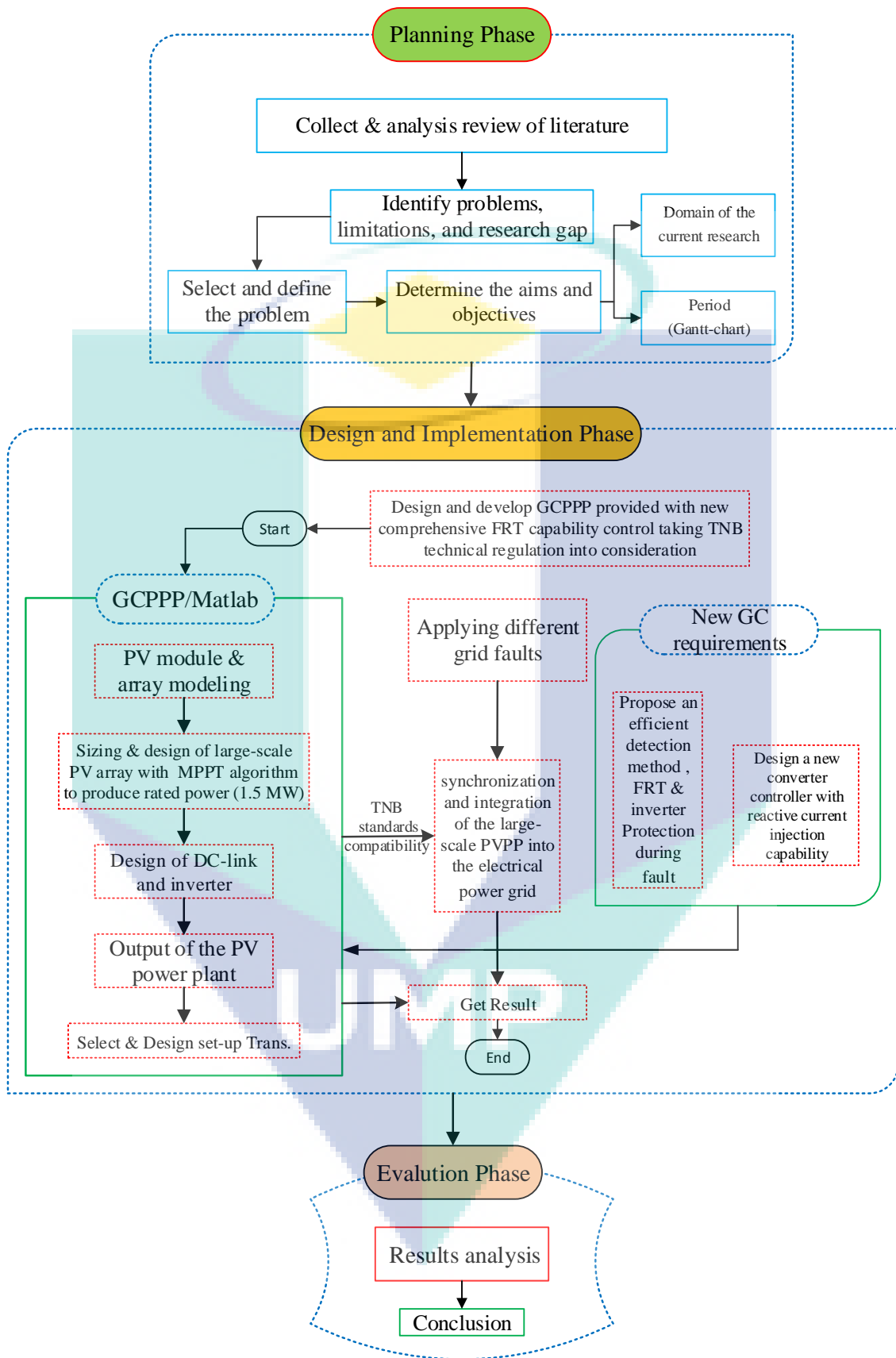
Figure 3.1   The study framework.

3.2.2 Design and Implementation Phase

Designing steps describe the strategy that followed in order to address and achieve the finding and objectives, respectively. As can be seen in Figure 3.1, this research proposed method consists of a sequence of steps. First of all, this thesis aims to provide investigation information on FRT capability and propose this requirement for Malaysian grid code. It also focuses on design and development of converter controller for the PV system provides the FRT capability. FRT capability in some countries will be first obtained and compared. The most suitable FRT capability will be proposed and implemented. The system will be modelled in MATLAB/Simulink and simulation will run under various grid fault conditions to investigate the effect of FRT capability to the power system quality and stability. Moreover, to achieve and apply the developed FRT capability control of the PV inverter-connected grid, the data of chosen distribution side at medium voltage which determine the domain has been selected to use in this work. Afterwards, TNB technical regulations compatibility imposed regarding the interconnections of PV system to the medium and low voltage should be applied at the PCC (Azit et al., 2012; Suruhanjaya Tenaga, 2016). However, during designing and modeling of the large-scale PVPP that preferred to apply these type of requirements will pass through many of stages. The first step should be modeling of the selected PV module that will be utilized in this research depend on the mathematical modeling of the PV circuit to verify its specifications, as has been done in Section 3.3.1.

Next, sizing and design of the PV array to produce required power of large-scale system. The sizing will pass through theoretical calculation phase then verified by using Matlab/Simulink. MPPT algorithm which is very essential method for any PVPP to get maximum available power from the array according to weather condition is considered. Then, dc-link design. At this point, dc part of the PV plant will be achieved. On the other hand, to connect this PV system into the selected side of the utility grid, the ac part including self-commutated inverter and its control, synchronization using rotating reference frame will be designed based on most recent standard and should be compatible with TNB rules. Furthermore, the PVPP will connected to the distribution grid side of the power grid via set-up transformer. At the point of common coupling (PCC), the regulation of TNB regarding the penetration of PV system to the MV side should be fulfilled.

Finally, this research proposes a FRT capability as new requirement of the Malaysian GC and implements this feature by proper ride-through control based on the literature gap. In addition, to apply the reactive current injection capability control based on the standard requirements at different types of grid faults, it is important to keep the inverter stay connected during the faults. This can be achieved by protecting the inverter from excessive ac-current that can occur at the ac side as well as excessive dc-voltage at the dc-side of the inverter (Afshari et al., 2017; Etxegarai et al., 2017; Mahela & Shaik, 2017; Obi & Bass, 2016; Perpinias et al., 2015; Reddy et al., 2018; Y.-K. Wu, Lin, & Lin, 2017). As described above, the inverter will operate with two modes of operation. The first mode is the normal operation without FRT control, while the other is the faulty mode of operation with FRT capability control. It is worth mentioning that, fault detection unit is so essential part in this system to detect grid faults and then to inform the inverter in which mode should operate. As final stage, different types of grid faults will be created to show the effectiveness of the proposed control.

3.2.3 Evaluation Phase

In this research, different type of faults will be applied to test and evaluate the proposed control. The PVPP array sizing and design will be verified by matching the theoretical mathematical results to Simulink results. Additionally, the effectiveness of the proposed control will be verified by matching the standard requirements, protect the inverter and inject the required amount of the reactive current to support the grid stability and quality during fault time based on the FRT curve. The comparison of results before and after using the controller will be presented as well. In conclusion, the overall results of this study will be compared with the results of recent published studies to show the effectiveness of the proposed control as well as its consistency with other previous study.

3.3 Modelling and Design of the Single-stage Three Phase PV System

The schematic diagram of Figure 3.2 shows the power stage of a 1500 kW single-stage PVPP modelled in this research using Matlab/Simulink. A three-phase grid-connected PV system contained the PV array, perturb and observe (P&O) maximum power point tracking (MPPT), and the grid inverter with its control as well as the transformer that linked to the medium-voltage (MV) side of the distribution grid. The incoming feeders from the PVPP to the distribution system were linked via a step-up

transformer (0.4 kV/33 kV), and two feeders supplied a series of main distribution substations (MDSs) or loads (IEEE power and energy society, 2009).
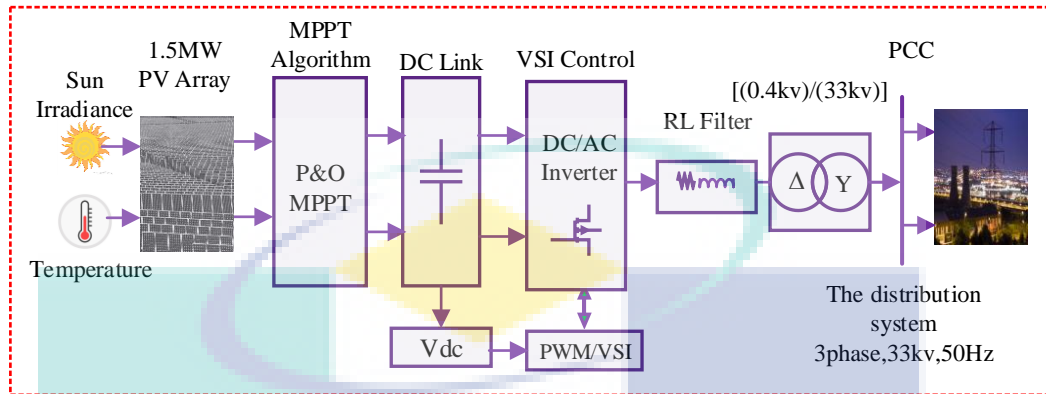
Figure 3.2   PV power station connected to the power grid.

The MPPT stage controlled the output dc power generated from the PV array to an appropriate level so that delivered to the inverter. The PV inverter stage controlled the dc-link voltage and then delivered the necessary current into the distribution network via several voltage and current control loops (Jana, Saha, & Bhattacharya, 2016; Ünlu, Camur, Beser, & Arifoglu, 2015). The details of developing, sizing and testing the modeled PV power station connected to the power grid are presented in the next sub-sections.

3.3.1   Design, sizing and modelling of the PV array

As mentioned above, in order to study the PV system in GCPPPs, a modelling and analysis for the PV module of the array system is an essential. In PVPPs, the PV array considers as the complete power generating unit, comprising of many modules linked in series and/or parallel together to yield high voltage, current, and power. The modelling, sizing, and design of the PV array will be described below.

3.3.1.1   Modelling of the PV module

The fundamental device of a solar system is the PV cell, which directly converts daylight into electricity. Typically, a PV cell produces voltage around 0.5 to 0.8 depending on the semiconductor type and the developed technology (Villalva, Gazoli, & Ruppert Filho, 2009b). This amount of voltage is insufficient and cannot be put to use. Therefore, the cells are linked together to consist a PV module which is the smallest unit

that can be utilized to generate a useful amount of PV power. The modules can be connected in parallel and/or in series to form the PV array. Due to the nonlinear characteristics of the PV modules and its dependency on the solar irradiation and temperature, it is important to model it for the proper design, simulation of MPPT, and better understanding of its working.

In this research, a TopSun TS-S400 PV Monocrystalline module has been selected to use in the proposed PVPP design. Every single module produces maximum power of 400 W at STC, the other electrical and mechanical specification of the module such as ideally factor of diode (m), open circuit voltage (V_{oc}), short circuit current (I_{sc}), maximum power voltage (V_{mp}), maximum power current (I_{mp}) along with temperature coefficients of open circuit voltage and short circuit current (α_v, α_i), respectively are provided in the datasheet by the manufacturers (TOPSUN solar modules, 2017) as listed in Table 3.1.

Table 3.1   TopSun TS-S400 PV module specifications.

The parameters	The value
Maximum power	P_{max}=400 W
Maximum power voltage	V_{mp}=49.78 V
Maximum power current	I_{mp}=8.04 A
Open circuit voltage	V_{oc}=60 V
Open-circuit-current	I_{sh}=8.56 A
Numbers of cells per module	N_{cell}=96
Temperature coefficient of I_{sc}	α_i=0.043/C°
Temperature coefficient of V_{oc}	α_v=-0.367/C°
Parallel & series resistance (R_p,R_s)	389.9 Ω,0.33 Ω
Ideally factor of the diode	m=1.02

Source: TOPSUN solar modules(2017).

Figure 3.3 shows an equivalent circuit of the PV module which consist of several PV cells. It includes a current source generates photo current that depends on the irradiation, a big diode which is equivalent to the p-n transition area of the solar cell, the voltage losses represented by series resistance while parallel resistance representing the leakage current. The output voltage and current relationship of a PV module can be expressed by the following equation (Bellia, Youcef, & Fatima, 2014; Wang et al., 2017):
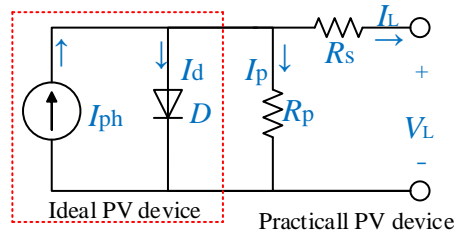
Figure 3.3   Equivalent circuit of a solar cell.

By using Kirchhoff's laws:

$$I_{Ph} - I_D - I_P - I_L = 0 \implies I_L = I_{Ph} - I_D - I_P \qquad 3.1$$

$$(V_D = V_P) = V_S + V_L \implies V_D = R_S I_L + V_L \qquad 3.2$$

where $I_P = \dfrac{V_P}{R_P} = \dfrac{V_D}{R_P}$, substitute by V_D from equation (3.2):

$$I_P = \frac{I_L R_S + V_L}{R_P} \qquad 3.3$$

The diode current (I_d) can be expressed as follows (Bouraiou et al., 2015):

$$I_D = I_{sat} \left(e^{\left(V_D / m N_s V_T \right)} - 1 \right) \qquad 3.4$$

where $V_T = \dfrac{KT}{q}$, substitute by V_T in equation (3.4), yield:

$$I_D = I_{sat} \left(e^{\left(q V_D / m N_s KT \right)} - 1 \right) \qquad 3.5$$

By substituting equations (3.3) and (3.5) in equation (3.1), the load current can be expressed based on the following equation:

$$I_L = I_{Ph} - \underbrace{I_{sat} \left(\exp\left(\frac{q V_D}{m N_s KT}\right) - 1 \right)}_{Id} - \frac{I_L R_S + V_L}{R_P} \qquad 3.6$$

52

The I_{Ph} , I_D , I_P and I_{sat} are the photo current, the diode current of the PV cell, shunt current and the reverse saturation current of the solar module, respectively. Ns is the number of cells connected in series, V_T is the thermal voltage which equals to 25.7V at 25ºC (298K) and m is the ideal factor of the diode (1-5(V_T)). K is the Boltzmann constant (1.381×10^{-23} J/K) and q is the charge of the electron (1.6021×10^{-19}C) (Bellia et al., 2014). R_S and R_P are the equivalent series and parallel resistance of the solar module, respectively. It is well-known that the I_{Ph} is affected by sun irradiance and temperature. Therefore, the influence of these two factors on the photo current can be expressed by the following equation (Villalva et al., 2009b):

$$I_{ph} = \left(I_{sc} + \alpha_i (T - 25) \right) \frac{G}{G_{ref}}$$
<div align="right">3.7</div>

It is worth mentioning that, I_{Ph} is the photo current at nominal PV standard test condition (STC) (normally T=25ºC and G=1000 W/m^2) for temperature and irradiation, respectively. I_{sc} is the nominal short circuit current of the module. G and G_{ref} are the amount of actual and nominal irradiation, respectively. T is the temperature degree in Kelvin (K) and α_i is the current temperature coefficient. The I_{sat} and I_{sc} can be obtained according to the following equations (Villalva et al., 2009b):

$$I_{sc} = I_{sc,ref} \left(\frac{R_P + R_S}{R_P} \right)$$
<div align="right">3.8</div>

$$I_{sat} = \frac{I_{sc,ref} + \alpha_i (T - 25)}{e^{q \left(V_{oc,ref} + \alpha_v (T-25)/N_s mKT \right)} - 1}$$
<div align="right">3.9</div>

where $I_{sc,ref}$ and $V_{oc,ref}$ are the short circuit current and open circuit voltage of the module at STC, respectively, whereas α_v is the open circuit voltage temperature coefficient. Normally these values are evaluated by the manufacturer. The output voltage and current of the module can be expressed using the following equation:

$$I_L = \left(I_{sc} + \alpha_i (T - 25) \right) \frac{G}{G_{ref}} - I_{sat} \left(e^{\left(qV_D/mN_sKT \right)} - 1 \right) - \frac{I_L R_S + V_L}{R_P}$$
<div align="right">3.10</div>

Based on equation (3.10), a Matlab/Simulink model was developed to represent theses equations of the PV circuit. Most of the equation parameters are obtained from the manufacturer's data sheet (TOPSUN solar modules, 2017) shown in Appendix A.

For the equivalent model of the PVPP array that consist of a different number of PV modules based on the required output power, the following set of equation is developed (G. M. S. Islam, Al-Durra, Muyeen, & Tamura, 2011):

$$I_L = N_p I_{Ph} - N_p I_{sat} \underbrace{\left(\exp(\frac{qV_D}{mN_M N_s KT}) - 1 \right)}_{Id} - \frac{I_L R_{S(eq)} + V_L}{R_{P(eq)}} \qquad 3.11$$

$$and \ I_{sat} = \frac{N_p I_{sc,ref} + \alpha_i (T - 25)}{e^{q(N_M V_{oc,ref} + \alpha_v (T-25)/N_s N_M mKT)} - 1} \qquad 3.12$$

where N_p is the number of parallel strings and N_M is the number of series modules connected in a string. In addition, $R_{S(eq)} = (N_M \times R_S / N_P)$ and $R_{P(eq)} = (N_M \times R_P / N_P)$.

3.3.1.2   Array sizing of the PVPP

In this research, a large-scale PVPP which is the most suitable type of PV plants to be provided with the FRT capability (Lammert et al., 2017) should be designed, simulated, and connected to the utility grid based on the standard requirements. Therefore, in order to accomplish the proposed single-stage large-scale PVPP with peak power of 1500 kW, the PV module described above is selected to build the PV array. The PV array system or the power generating unit considers as the main part in any PVPPs that should be designed based on the required output power of the system. The following steps were taken for proper design of the PV system (PV generators or dc-part) to generate the required amount of power. The required number of modules that will be used as generators (PV array) can be obtained by dividing the needed amount of power by the maximum power of the PV module using the following equation (Mahmoud & Ibrik, 2006):

$$N_{pv} = \frac{1.5 \times 10^6}{400} = 3750 \ modules \qquad 3.13$$

In the proposed design and for single-stage concept, the PV array arranged in a certain way (paralleled strings) in which links to the central inverter without dc-dc converter stage. This type of inverter, normally three-phase, is the widely used for utility-scale or large-scale PVPPs. But, this central inverter needs of high dc-link voltage, typically (550-850) V. Thus, the system dc-link in this design is rated at 800 V to reduce the output current ripple and regulate the voltage at the dc-side of the inverter (Jana et al., 2016; Lee & Lee, 2013; Orłowska-Kowalska et al., 2014). Consequently, the necessary number of PV modules in series (N_{pvs}) is obtained by dividing the dc-nominal voltage of the system over maximum power point voltage of the module as follows:

$$N_{pv_s} = \frac{800}{49.78} \approx 16 \ modules \qquad\qquad 3.14$$

whereas the number of the parallel strings (N_{pvst}) of the photovoltaic array can be obtained by dividing the total number of PV array modules (N_{pv}) by number of modules in series (N_{pv}) according to the following relation:

$$N_{pv_{st}} = \frac{3750}{16} \approx 235 \ strings \qquad\qquad 3.15$$

As a result, to generate a nominal rated power of 1500 kW at STC, 3750 TopSun TS-S400 modules with maximum power of 400 W have been selected and distributed as 16 series modules and 235 parallel strings to consist the PV array of the proposed large-scale PV system.

The actual maximum voltage (V_{mpv}) and the actual maximum current (I_{mpv}) of the PV system (dc-part) can be obtained by multiplying the number of series module by maximum power point voltage (V_{mpp}), and number of strings with maximum power point current (I_{mpp}), respectively, as expressed in the following equations:

$$V_{mpv} = \left(N_{pv_s} \times V_{mpp} \right) \Rightarrow V_{mpv} = 16 \times 49.78 = 796.4 \ V \qquad 3.16$$

$$I_{mpv} = \left(N_{pv_{st}} \times I_{mpp} \right) \Rightarrow I_{mpv} = 235 \times 8.04 = 1889.4 \ A \qquad 3.17$$

Therefore, actual maximum generated dc power of the PVPP will be obtained as follows:

$$P_{dc} = V_{mpv} \times I_{mpv} = 796.4 \times 1889.4 = 1504718.1 \ W \qquad 3.18$$

On the other hand, the array's open circuit voltage is calculated by multiplying the number of array's series modules with open circuit voltage (V_{oc}) of the module, whilst the short circuit current of the system array is obtained by multiplying the number of array strings with short circuit current (I_{sh}) of the module, respectively, as follows:

$$V_{pv(oc)} = \left(N_{pv_s} \times V_{oc} \right) \Rightarrow V_{pv(oc)} = 16 \times 60 = 960 \ V \qquad 3.19$$

$$I_{pv(sh)} = \left(N_{pv_{st}} \times I_{sh} \right) \Rightarrow I_{pv(sh)} = 235 \times 8.56 = 2011.6 \ A \qquad 3.20$$

It is important to mention that all these values are obtained at STC, in case the irradiation and temperature changes, the output of the PV system will be changed accordingly.

3.3.2 Perturb and observe MPPT algorithm

There are many of MPPT algorithms have been utilized through the advancement of PV energy system. The issues of using MPPT to extract the maximum available power from the PV array have been studied and addressed using different algorithms in the literature. In this research, the focus will be put on the FRT and how to reflect the new modern grid codes requirements which are the state of art in this filed. Thus, a P&O MPPT technique which is common algorithm and widely used in PV system due to its ease of implementation and small number of measured parameters required, is used in this study to extract maximum available power from the PV array. The theory of this method was proposed in the literature (Ishaque, Salam, & Lauss, 2014; Mohammad, Quamruzzaman, Hossain, & Alam, 2013).

Table 3.2   Operational way of the P&O MPPT algorithm.

The Perturbation	Output Power	Next perturbation
Increase	Increase	Increase
Increase	Decrease	Decrease
Decrease	Increase	Decrease
Decrease	Decrease	Increase

This method operates by increasing or decreasing the array voltage using fixed step value. In case PV array voltage perturbed at any direction and produce increases in terms of power value, this indicates that the operating voltage should be further perturbed in the same direction, otherwise the direction of the perturbation must be reversed. The summary of the operation of this method is illustrated in Table 3.2 (Mohammad et al., 2013). It can be observed from Figure 3.4 that depending on the irradiation level and terminal voltage of the PV array. Thus, the maximum power point is obtained when the slope of the power curve is zero (*dp/dv*=0). The power curve slope (*dp/dv*) can be expressed by the following equation:

$$\frac{dp}{dv}(n) = \frac{P(n) - P(n-1)}{V(n) - V(n-1)}$$ 3.21
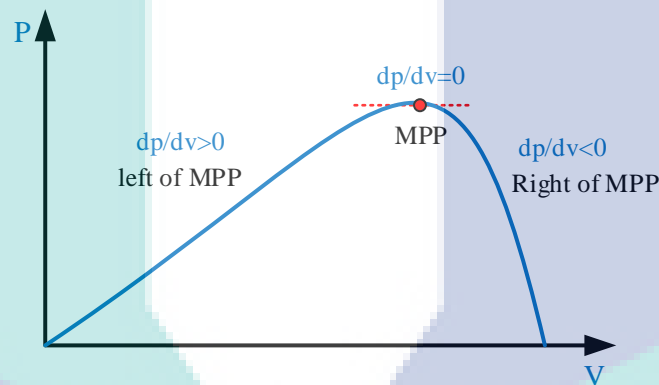
Figure 3.4   PV array power curve characteristic.

There are two options in case the operating voltage of the PV generators (PV array) is perturbed by a fixed step (ΔV), and then caused changes in the power by (ΔP). First, if ΔP is positive (*dp/dv*>0), the next perturbation of the voltage must be in the same direction. Second, if ΔP is negative (*dp/dv*<0), this means the operating voltage of the system moved away from the MPP and therefore the operating voltage of the PV array must move towards the opposite direction (Villalva, Gazoli, & Ruppert Filho, 2009a).

The flowchart of the P&O MPPT technique in basic form is depicted in Figure 3.5 for more explanation about its performance. Although the P&O method has many advantages such as ease of implementation, less complex when compared to other methods and the fewest number of measured parameters required. It has some disadvantages, like slow response speed and oscillation around MPP in case of steady-

state operation and unable to track rapidly increasing and decreasing irradiance conditions (P.-C. Chen et al., 2015; Saravanan & Babu, 2016).
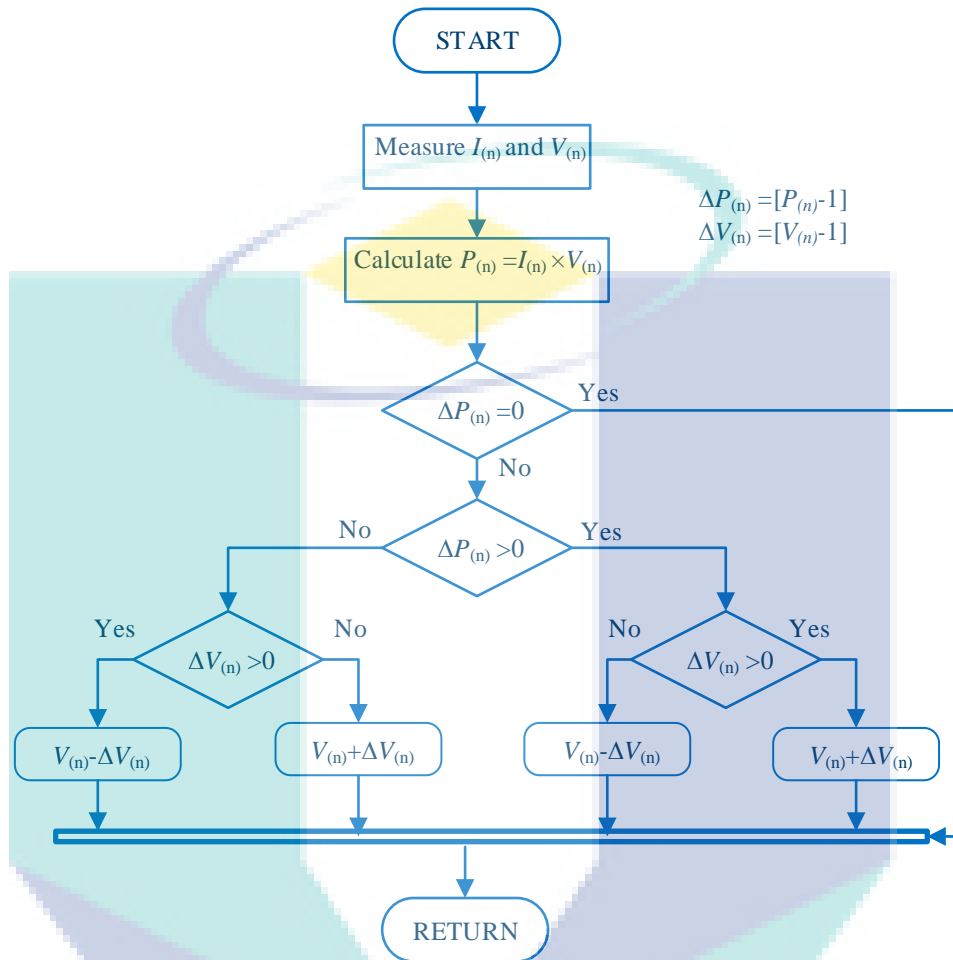
Figure 3.5   Flowchart diagram of the P&O MPPT method.

3.4   Inverter Control Strategy of the Grid-Connected PVPP

For grid integration, the output dc-power should be converted into three-phase ac power and therefore the three-phase inverter is used to convert the generated dc power into ac power until can interface with distribution network. Therefore, the inverter is considered as the most important part for GCPPPs. As a result, in this study, a single-stage three-phase self-commutated voltage source inverter (VSI) is used in the proposed design to execute the power conversion and for control optimization purposes. With a view to control the VSI, the current controlled VSI is selected to be used in the proposed PVPP due to its advantage explained in Section 2.4.3.2. The inverter control frame consists of all basic control requirements for grid-connected PV system which is designed to be compatible with Malaysian grid technical regulation for MV connection (Azit et al.,

2012; Energy Commission Malaysia (ECM), 2017; Suruhanjaya Tenaga, 2016; Tenaga Nasional Berhad, 2005). The dc-link voltage in single-stage VSI inverter should have a value in the range of 550-850 volt (Orłowska-Kowalska et al., 2014). Thus, the selected dc-link voltage in the proposed system is 800 V. Moreover, this value is near to maximum output voltage of the array (796.4 V) in order to reduce current ripple and regulate the voltage at the dc side of the inverter.
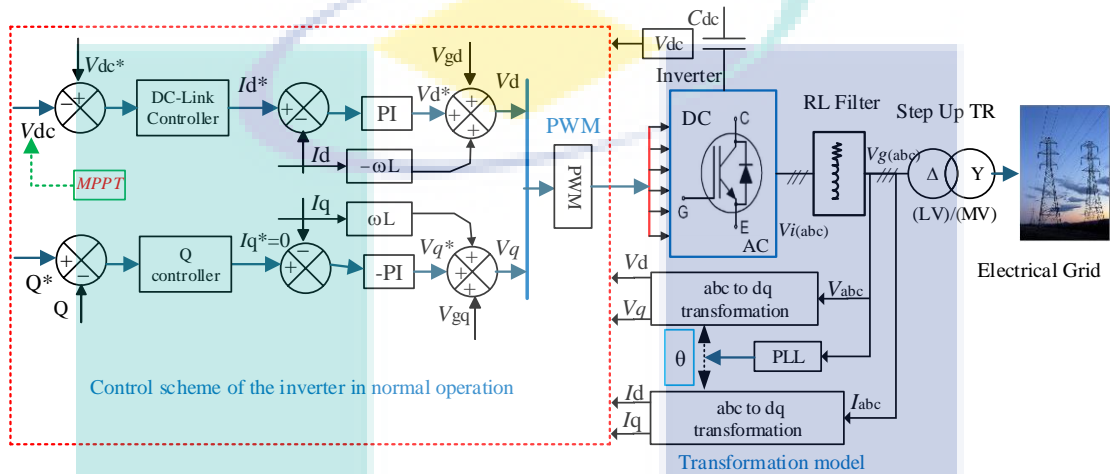
Figure 3.6   Schematic diagram of a three-phase inverter with synchronous rotating frame control (dq-control).

In normal operation, the schematic diagram of the inverter control is depicted in Figure 3.6. The current control system-based VSI adopts a double loop control mode. It consists of an inner current loop (active current (I_d) as well as reactive current (I_q)) and outer voltage loop. The outer loop is utilized to stabilize and manage the dc-link voltage (V_{dc}). It is important to mention that the voltage loop output is used as the active current reference (I^*_d) whilst the reactive current reference (I^*_q) is set at zero during normal operation to achieve the unity power factor as much as possible. The typical proportional-integral (PI) controllers are utilized in both loops to regulate the grid current and the dc-link voltage (H. Wu & Tao, 2009). For easier control of active and reactive current parameters, the feed-forward decoupling strategy is applied. The main parameters of the proposed inverter-connected grid are listed in Table 3.3.

Table 3.3   The main parameters of the inverter-connected grid.

Parameters of the inverter	The value
Effective voltage of the grid	V_g=33 kV
DC-link-voltage	V_{dc}=800 V
DC-link-capacitor	C_{dc}= 0.2130 F
Grid frequency	ω=2π*50 rad/s
R filter of the inverter	R=1.25Ω
L filter of the inverter	L=0.1 mH
Switching frequency of the inverter	f_c=2 kHz
PI parameter of current loop	K_p=0.3, K_i=20
PI parameter of the voltage loop	K_p=2, K_i=400
Transformer	0.4/33kv, 50Hz

Additionally, for the purpose of grid voltage and phase angle synchronization, the phase locked loop (PLL) based on (*d-q*) synchronous reference frame (SRF-PLL) is applied to lock the grid frequency and to support the reference synchronization signal for the VSI control system. The phase angle (θ_{PLL}) is obtained through the SRF-PLL that is used for *abc* to *dq0* transformation. The inner loop PI controllers of VSI control mode produce active voltage reference (V^*_d) and reactive voltage reference (V^*_q). Active and reactive voltage references are used for *dq0* to *abc* transformation in order to get V_{abc}. Lastly, V_{abc} is sent to a PWM signal generator to obtain switching pulses for the VSI. The VSI control strategy will be introduced in detail in the following sub-sections:

3.4.1   Current control structures of the inverter

The generated PV energy is transformed into power through the VSI in which the input side of the inverter is utilized to extract the maximum available energy from the PV array and the output side controller is utilized to control the active and reactive power provided to the grid. There are different types of inverter controller, but the current-controlled inverters are more efficient as compared to other inverters controls discussed in the literature for GCPPPs, especially under grid disturbances (Bonaldo, Schiavon, Paredes, & Pomilio, 2017; Hassaine, 2016; Parvez et al., 2016; Vu, Tuyen, & Bang, 2016). In this study, the feed-forward decoupling PI current controller-based synchronous rotating reference frame (d-q control) current controller is used to control the connection of the proposed PVPP into the grid. The structure of the three-phase inverter with synchronous rotating frame control (dq-control) using decoupling and voltage feedforward terms is described briefly as follows:

60

3.4.1.1 Mathematical model of the inverter controller

Voltage equations of the grid inverter considering the access to the power grid as shown in Figure 3.7 are driven as follows:
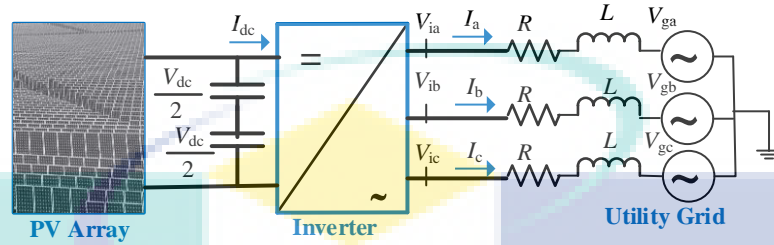
Figure 3.7   Grid connected voltage source inverter; three-phase view.

$$V_{ia} = L\frac{di_a}{dt} + Ri_a + V_{ga}$$

$$V_{ib} = L\frac{di_b}{dt} + Ri_b + V_{gb} \tag{3.22}$$

$$V_{ic} = L\frac{di_c}{dt} + Ri_c + V_{gc}$$

Where "V_{ia}, V_{ib}, V_{ic}", "i_a, i_b, i_c", and "V_{ga}, V_{gb}, V_{gc}" are the inverter voltage, inverter current, and grid voltage, respectively. After the rotational transformation using synchronous reference rotating frame, the mathematical model of the grid inverter in *d-q* synchronous frame at the line frequency can be obtained as:

$$V_{id} = L\frac{di_d}{dt} + Ri_d + V_{gd}$$

$$V_{iq} = L\frac{di_q}{dt} + Ri_q + V_{gq} \tag{3.23}$$

In terms of power calculations, active and reactive power equations of the grid side in space vector form are expressed as follows:

$$P = \frac{3}{2}(V_{gd}I_d + V_{qd}I_q) \tag{3.24}$$

$$Q = \frac{3}{2}(-V_{gd}I_q + V_{qd}I_d) \tag{3.25}$$

Where "V_{gd}, I_d" and "V_{qd}, I_q" denote the d and q axis voltage and current at the grid side in d-q synchronous reference frame, respectively. As mentioned above, in normal operation mode, the system has to operate at unity power factor. Then, by neglecting power losses, V_{qd} is zero for a balanced system. Thus, equations (3.24) and (3.25) become as follow:

$$P = \frac{3}{2} V_{gd} I_d \qquad\qquad 3.26$$

$$Q = -\frac{3}{2} V_{gd} I_q \qquad\qquad 3.27$$

The decoupling control is realized for the active (P) and reactive (Q) power of the PVPP as indicated by equations (3.26) and (3.27). The active and reactive power are affected by I_d and I_q, respectively, and therefore any adjustment of I_d and I_q can manage the output active power and reactive power independently, and this is what has been exploited in this study for FRT capability to achieve the required injection of active and reactive power according to the standard requirements.

3.4.1.2   Proportional-integral (PI) in d-q controller

Most of the PI controllers are commonly related to dq control method, because they are preferred for controlling dc variables. The dq control is likewise known as an SRF control. This control converts the grid currents in abc natural frame into a dq reference frame which rotates with the grid voltage synchronously by the angular speed of ω (Lauria & Coppola, 2014). The transformation equations known as Park's transformation are described in Appendix C. A standard shape of the dq control is shown in Figure 3.8. The dq representation is considered as a simplified way of representing a set of three sinusoidal-varying phase currents and voltages using only two values to control the grid current and voltage efficiently. As a consequence, it is a great simplification of the three-phase system and therefore it can be controlled using only two values.
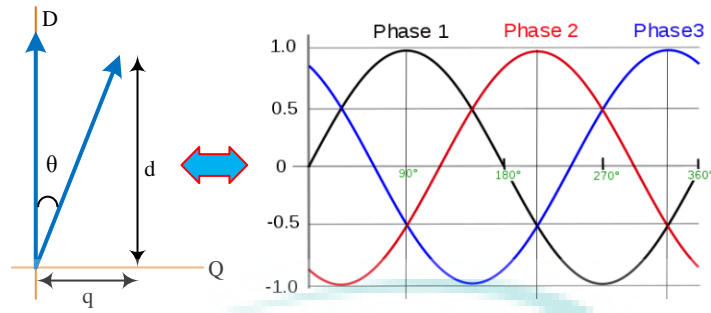
Figure 3.8   The *d-q* Coordinates.

Outer loop controller is used to generate the active reference current that represents the active power component. On the other hand, depending on the requirement for the reactive power, the reference reactive power is set to zero at normal operation (Orłowska-Kowalska et al., 2014). A PI controller gain is described through the transfer function in *dq* coordinates form as the following equation:

$$G_{PI}(s) = K_P + \frac{K_I}{s}$$ 3.28

Where proportional and integral gain of the PI controller are represented by K_p and K_i, respectively. The feed-forward *dq* control structure involving decoupling the grid current and grid voltage is described in Figure 3.6. It is expected that the control's dynamics would be high in the period of grid voltage fluctuations, so the grid voltage feed-forward used in this structure of the control (Huang, Shi, Sun, & Wang, 2014; Timbus et al., 2009).

3.4.1.3   VSI inner control loop

In order to simplify the controller design especially for LVRT capability, a feed forward decoupling control strategy is adopted in the inner loop control to decouple the active (I_d) and reactive currents (I_q). The simplification process of the internal loop control is illustrated in Figure 3.9. The control system collects the instantaneous value of dc-link voltage, grid-connected current and grid voltage timely, and then calculates the control pulse width of each bridge arm, and tracks the given value of grid-connected power obtained by dc voltage outer loop. The phase locked loop (PLL) can guarantee that the grid-connected current and grid voltage has the same frequency as well as same phase. It is important to mention that the inner loop takes the reference active current generated by

63

the outer loop control to achieve PV system current source integration. Meanwhile, the reactive current reference is set to zero because at normal operation, the reactive reference power of grid inverter is maintained zero (Timbus et al., 2009). Thus, the inverter usually operates around unity power factor and this feature agrees with TNB regulation which requires leading or lagging power factor higher than 0.9 (Azit et al., 2012; Suruhanjaya Tenaga, 2016).
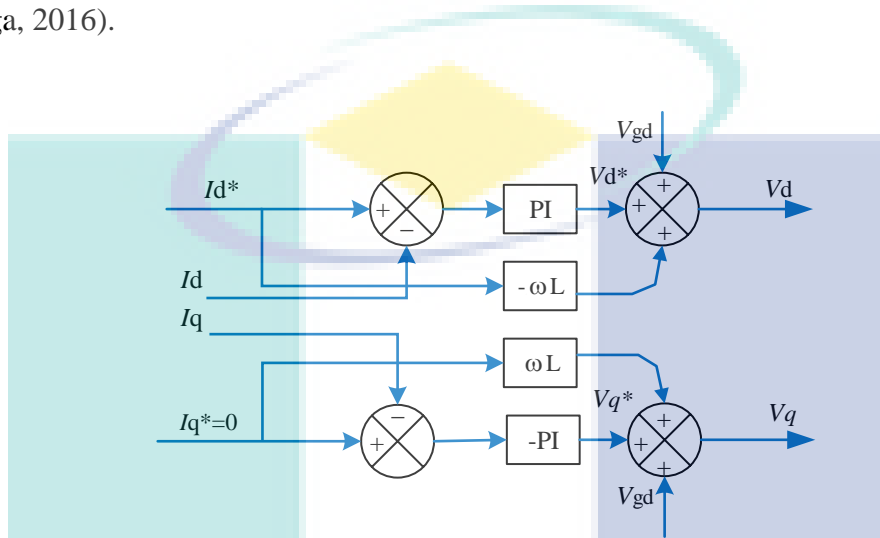
Figure 3.9   Inner loop control mode of the inverter.

3.4.1.4   VSI outer control loop

Outer loop of the VSI is known as dc-link voltage regulation that provides active current reference for the inner loop control and stabilize dc-link voltage (V_{dc}) to its rated value. The dc-link voltage is regulated using typical proportional-integral (PI) controller. The schematic diagram of the outer loop is simplified in Figure 3.10.
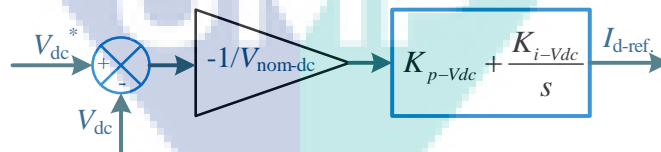
Figure 3.10   DC-link voltage control scheme.

As the voltage of the dc-link normally operates at the maximum power point, the output power is supplied to the ac-side. The power delivered to the inverter is calculated based on equation (3.29), likewise the injected power from the VSI to the utility grid is as described in equation (3.30), as follows:

$$P_{input-inv.} = I_{mpp} \times V_{dc} \qquad\qquad 3.29$$

$$P_{out-inv.} = I_d \times V_d + I_q \times V_q \qquad\qquad 3.30$$

3.4.2 Sinusoidal pulse width modulation

The VSI power converter basically converts the input dc-voltage to a three-phase ac output voltage. The output ac voltage is created by turning on and off appropriate insulated gate bipolar transistors (IGBT) within the VSI using PWM signals. The sinusoidal PWM is essentially a carrier-based PWM technique. In this technique, the fundamental sine wave is considered as the modulating signal and the high frequency triangular wave is the carrier signal.
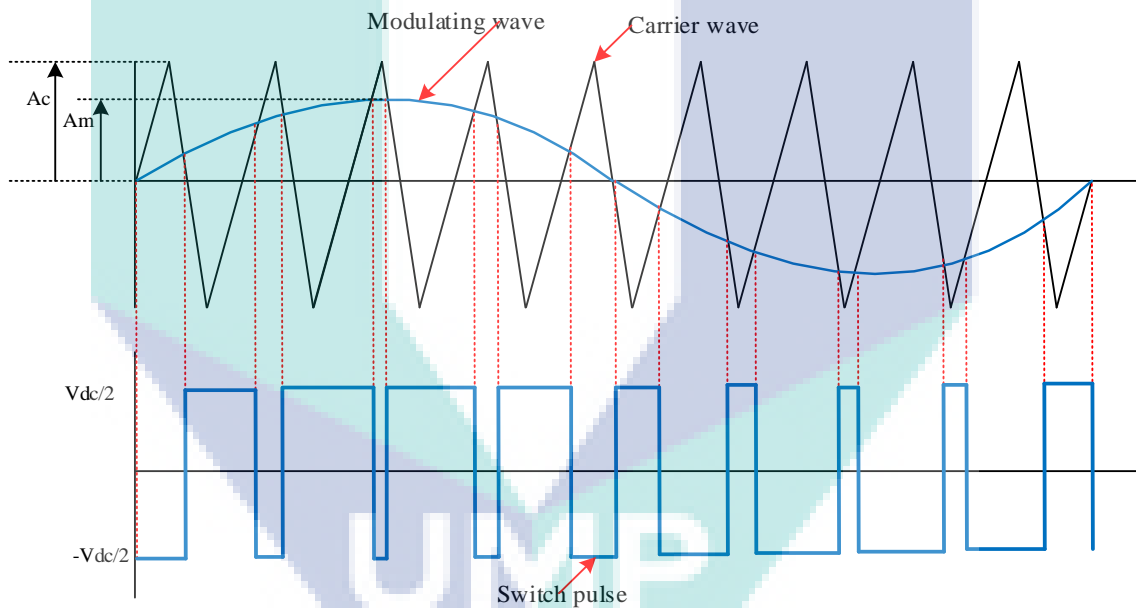
Figure 3.11   The principle of sinusoidal PWM control for VSI.

The general concept of SPWM explained in Figure 3.11, in which the modulating wave (which is a fundamental frequency sine wave) is compared with the high frequency triangle carrier wave. Thus, the points of intersection determine the switching times of the switches. The reference signal is the input of the PWM controller to be used as a reference in order to produce PWM signals and then controls the switches of the inverter and produces a PWM waveform coming from the PV array. The produced wave passes through a filter to produce pure sine wave as much as possible.

The PWM controller shown in Figure 3.11 can compare the magnitude of V_{ref} or modulating wave with the magnitude of triangle carries signal every time and at every point, if the reference signal is higher than carrier, then the switch pulse would be on (1) and the output voltage of the inverter leg will be connected to the positive side of the dc-link. If the reference signal is lower than the carrier, then the switch pulse should be off (0) and the output voltage of the inverter leg will connect to the negative side of the dc-link.
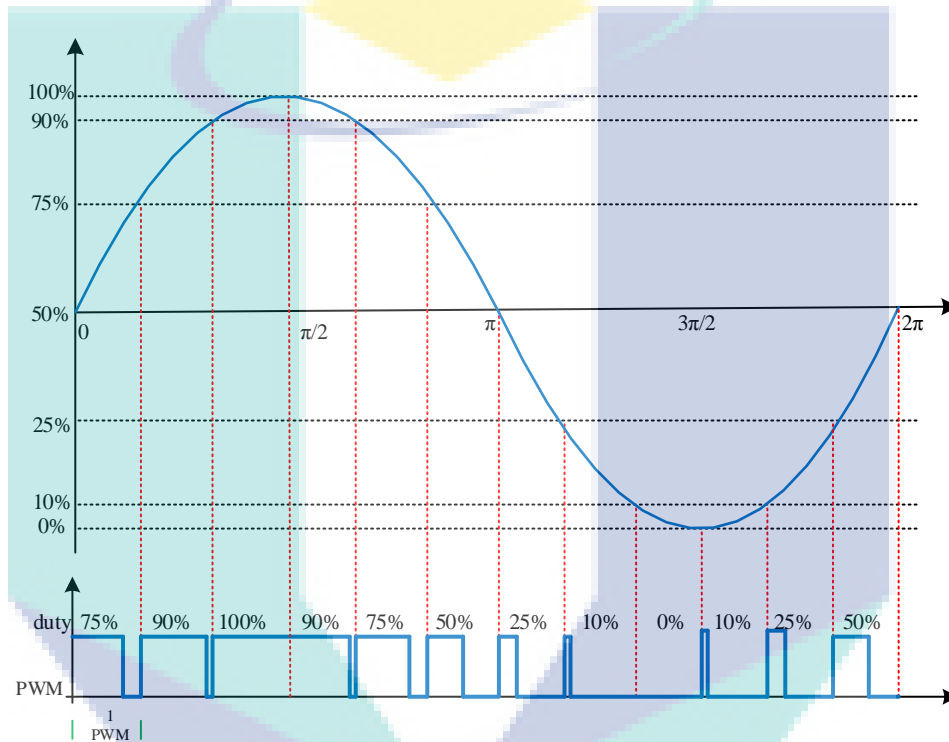
Figure 3.12   Sample of sine wave points via corresponding PWM modulated signal.

The generated 50 Hz square wave should be converted to a sinusoidal wave that can be connected to the ac power system. Simply, output signals of the PWM are built by comparing two control signals, a modulation signal and a carrier signal. This is known as the carrier-based PWM. The carrier signal is a high frequency (switching frequency) triangular waveform. The reference sine wave is the modulation signal. The output will follow the shape of the modulation signal in case the peak of the modulation is less than the peak of the carrier signal. Thus, it encodes the voltage into a fixed frequency carrier wave. The frequency of the PWM would be fixed while the duty cycle will range between 0% and 100%. The percentage of the on-time period will be proportional to the output signal voltage. For example, a 0% duty cycle produces a 0 V output while a 100% duty cycle produces a peak-to-peak voltage, as illustrated in Figure 3.12.

The PWM of the inverter switches (timing of the switches) indicate the modulation of the switching pulses. By using the duty cycle information, the value of sine wave can be defined. As it can be seen in Figure 3.12, at the top of sinewave, the duty cycle is 90-100%, therefore the sinewave is the maximum, but when the duty cycle is almost zero (the switch almost off), the sinewave is minimum. While at π, the duty cycle is almost 50%, and therefore the sinewave is in the middle. Consequently, the sine wave value is encoded in the duty cycle of this PWM. As a result, the duty cycle of PWM is proportional to the reference signal value.

3.4.3 Phase locked loop (PLL) and grid synchronization

After generating a sine wave from a modulating signal reference using PWM, it is important to match frequency with the grid and lock on like any other generator using grid voltage phase angle synchronization, and this aspect is classified as one of the main issues in grid-connected PV inverters. For this purpose, the method of phase locked loop (PLL) is considered as one of the well-known and extensively utilized technologies (Guo, Wu, & Gu, 2011; Kumar & Surekha, 2015).
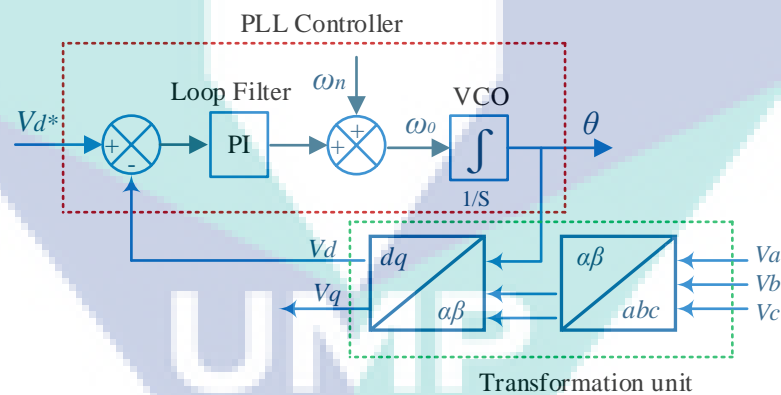
Figure 3.13   The structure of the SRF-PLL.

The SRF-PLL control, also named d-q control, is a non-linear closed loop system with a PI-controller tracking the phase angle. Input of the SRF-PLL feed-back system is the 3-phases of the power system voltage and the output is the phase angle. According to the block diagram of the 3-ph PLL shown in Figure 3.13, it detects the phase angle and creates an error signal by comparing the reference signal (input signal) with the output signal. Additionally, the loop filter eliminates unwanted harmonics terms from the error signal, while the voltage controlled oscillator (VCO) in turn generates the output signal

whose frequency differs around the system frequency depending on the output of the loop filter.

In this method, the 3-ph voltage vectors are transformed from the natural reference frame (*abc*) to the stationary reference frame (*αβ*) using Clarke's transformation, and then translated to *dq* rotating frame by Park's transformation (C. Lu et al., 2016), as shown in Figure 3.13. The equations of Clarke's and Park's transformation strategies are described in Appendix C

3.5   The Distribution System: A Case Study

The distribution system according to Malaysian grid code specification is the system of electrical lines with voltage less than 66 kV and the MV is defined as the voltage equal to or above 1 kV but not exceeding 50 kV (Azit et al., 2012; Energy Commission Malaysia (ECM), 2017). As described earlier in this thesis, the distribution side selected to link the proposed large-scale PVPP is the MV side and therefore, the available area of the distribution system which was examined in this research was 'A–S/S–Z–D/L' at grid medium voltage (33 kV) (IEEE power and energy society, 2009) interconnected to the proposed PVPP (A and Z represents the names of the substation bus-bars and feeders, whereas S/S and D/L indicates the substation and the distribution line, respectively).

Figure 3.14   The schematic diagram of PVPP system connected to 'A–S/S–Z–D/L' distribution system.

On the medium voltage side of the distribution grid, the proposed PVPP is connected to 33 kV bus-bar in the distribution system via the step-up transformer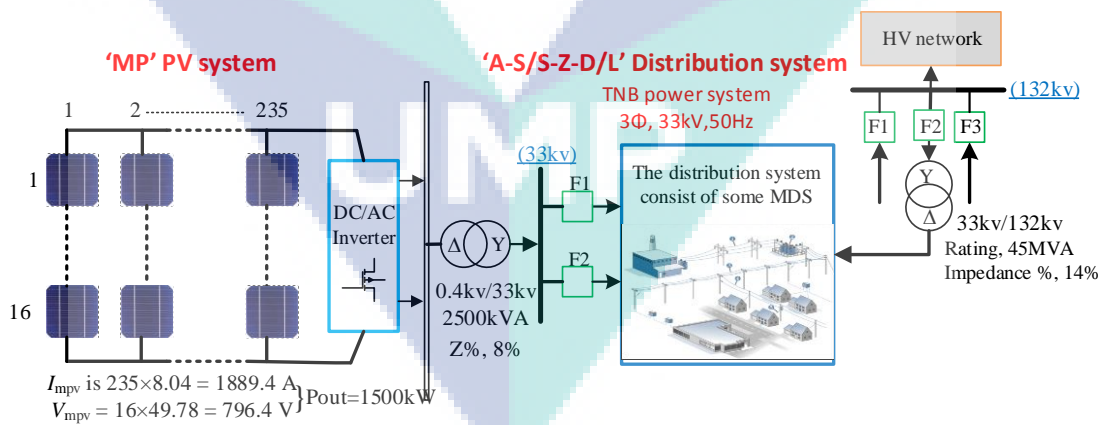 (0.4/33) kV and two feeders are going to supply a series of PPUs (Pencawang Pembahagian Utama or Main Distribution Substations). This is because TNB technical regulation imposes that, any PV plant connected to the MV should be connected to a bus-bar at substation, and the connection to an overhead lines or cables are not permitted (Azit et al., 2012; Suruhanjaya Tenaga, 2016). Therefore, the proposed PVPP in this study is integrated into the Malaysian grid via a bus-bar at the main distribution substation (PPU) of 33 kV, as imposed by the regulation. The main step-down substation (in Malaysia, it is normally called main intake substation) is connected to the grid at nominal voltage of 132 kV. The main intake substation has another voltage transformation 132/33 kV, and a data of 45 MVA transformers as shown in Figure 3.14.

3.6   Technical Requirements Concerning of Grid-Connected PVPPs

Lately, the usage of GCPPPs system has increased significantly. Therefore, manufacturers and distribution system operators are still very concerned on the mechanism operation and performance characteristic of the PV system units that are connected to the distribution system (Azit et al., 2012; Foley & Olabi, 2017; Y.-K. Wu et al., 2017). In Malaysia, PV system has developed quickly in the recent years. Several PVPPs have been built and put into operation, and many others are under design or construction. In light of this thriving situation, national grid has been issued technical regulation concerning the penetration of PV system to medium and low voltage to be in compliance with operating conditions and terms as stated in the Malaysian distribution code and technical & operational requirement rules (Azit et al., 2012; Suruhanjaya Tenaga, 2016). In summary, these technical regulations regarding PV penetration to the Malaysian utility grid will be used as references in this study. For any PV integration, the following rules were produced to fulfil the connection to the distribution network. In this research, it should be fulfilled in a manner that will allow the PV plants to perform smoothly as expected and be installed at a reasonable cost while not causing operational or safety issues of the utility grid.

3.6.1 PV-grid connection scheme and interconnection method

The connection scheme of PVPPs connected to the Malaysian utility grid must be subjected to some considerations such as safety, compliance to regulatory necessities, cost, and connection with the slightest adjustment to the existing system. According to TNB conditions, any PVPP connected to the MV network should be connected to a busbar at substation and the connection made directly to an overhead line or cable is not permitted. The feeding strategy can be sub-arranged as direct feed in which the PV plant is linked to a point at TNB and indirect feed where the connection point is at a customer. However, indirect feed method is only applicable at LV side. The feeding methods can be observed in Figure 3.15. In this study, the designed PVPP is linked to the grid via 33 kV bus-bar at substation as a direct feed to be compatible with these regulations.
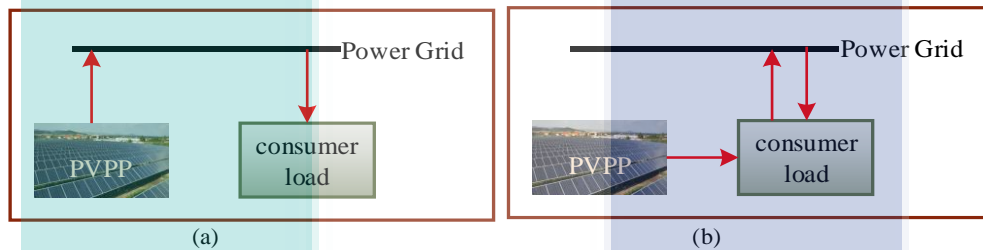
Figure 3.15   Electical grid Feeding method: (a) Direct feed, and (b) Indirect feed.
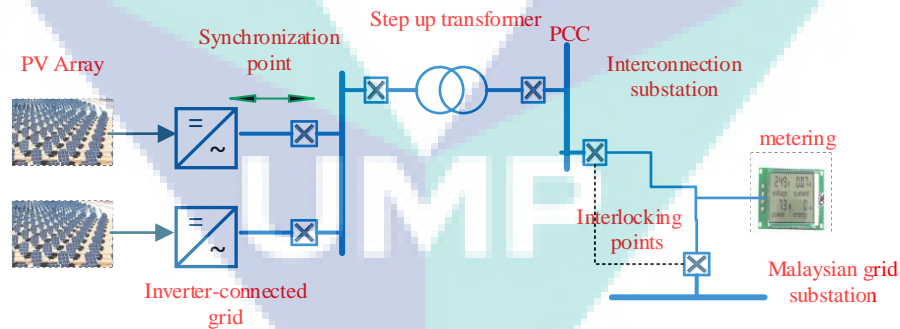
Figure 3.16   Connection configuration scheme on MV connection.

The most important connection requirement is that the quality of power parameters, especially voltage and harmonics at the grid interface or PCC should comply with TNB and Malaysian distribution grid code technical regulation (Energy Commission Malaysia (ECM), 2017). In MV-PV inverter connection, the most critical part is the interconnection feeder at the PCC. The distance between the inverter and PCC should be

considered by the designer to avoid power losses and significant drop in voltage. It is where the control sequence of operation is adopted between the grid and PV system side. The connection scheme configuration of MV integration is illustrated in Figure 3.16 (Suruhanjaya Tenaga, 2016). As a result, the proposed PVPP is connected into the grid side accordingly.

3.6.2 Nominal voltage operating range

During the normal operation, the PV system injects the current into the electrical grid but does not regulate the voltage. Concerning the penetration of photovoltaic systems to the MV level of the distribution network, TNB had imposed that in normal operation, PVPP connected to the MV e.g (6.6 kV, 11 kV, 22 kV, and 33 kV) should operate at PCC within the voltage limits without exceeding ±5% of its nominal value (Azit et al., 2012; Suruhanjaya Tenaga, 2016; Tenaga Nasional Berhad, 2005). Thus, these values have been considered as reference in this study.

3.6.3 Short circuit level

The short circuit level ratings specified that the network's maximum three-phase symmetrical short circuit should be within 90% of the apparatuses' nominal short circuit. The typical equipment ratings in the distribution network are stated in Table 3.4. The requirements specified by TNB regulations impose that the short circuit level should be within the equipment rating (Azit et al., 2012; Suruhanjaya Tenaga, 2016). Therefore, the PVPP connected into 33 kV should stay under the rated voltage and fault current are limited under the stated value using the current limiter.

Table 3.4   Typical equipment ratings in the distribution network.

Nominal Voltage (kV)	Rated Voltage (kV)	Fault Current (kA)
0.4	1.0	31.5
11	12	20
22	24	20
33	36	25

3.6.4 Harmonics and voltage unbalance

Photovoltaic power plants connected to the distribution network can improve the operation of power system by enhancing the voltage profile as well as by reducing the distribution feeders' energy losses, operating and maintenance costs in addition to

reducing electricity bills and the loading of transformer tap changers during peak hours (Farhoodnea, Mohamed, Shareef, & Zayandehroodi, 2013). However, because of the significant increase of PVPPs integration to the power grid, low power quality issues such as voltage and current harmonics, voltage unbalance, and power factor at the point of common coupling (PCC) can impose some adverse effects to the distribution system, especially to nearby loads. For instance, power electronics inverters of large-scale PV system can insert current harmonics to the associated bus and consequently pollute the power quality of nearby power systems and connected loads (S.-y. Lu, Wang, Ke, Chang, & Yang, 2014). Therefore, it is very important to apply strict power quality regulations concerning the penetration of distributed energy generators which are imposed by either national grid codes (GCs) such as in Malaysia (Azit et al., 2012) or international standard requirements such as the IEEE standards and IEC standards.

The harmonics can be measured by calculating total harmonic distortion (THD) or by the percentage of fundamental frequency (Farhoodnea et al., 2013). TNB technical rules regarding the connection of PV generators to distribution network state that the PV system output should have low current distortion levels in order to ensure that no harmful impacts are caused to other equipment connected to the utility grid. Thus, the THD shall be less than 5% at rated inverter output at PCC (Azit et al., 2012; Suruhanjaya Tenaga, 2016).

The ratio of negative voltage sequence component to the positive voltage component is defined as the voltage unbalance. TNB imposes that the voltage unbalance should be 2% for a one-minute duration at the PCC when different single-stage PV units are installed. On the other hand, the Malaysian distribution grid code requires the voltage unbalance not to exceed 1% if there are no abnormal conditions (Azit et al., 2012; Energy Commission Malaysia (ECM), 2017; Suruhanjaya Tenaga, 2016).

It is well-known that most traditional power systems are designed in a manner where generating stations are far away from the load centers and therefore utilize the transmission and distribution network as pathways. The normal operation of conventional power systems does not contain generation plants in the distribution system or in the customer's side of the network. Nevertheless, the integration of PVPPs into distribution systems changes the normal operation of power systems and poses a few problems on the power system quality (Cabrera-Tobar et al., 2016; Farhoodnea et al., 2013). Therefore,

power quality issues such as harmonics and voltage unbalance analysis of installing large-scale grid-connected PVPPs on the performance of electric network is important. This evaluation is necessary since it can give a possible solution for potential operational issues that PVPPs can bring about to the other components in distribution networks (Abdul Kadir, Khatib, & Elmenreich, 2014; Farhoodnea et al., 2013). Therefore, more analysis study has been applied for the proposed GCPPP based on TNB technical regulation in detail.

a. *Harmonic distortion*

Harmonic distortion in an electrical power system is a serious power quality problem. It is described as a distortion of the normal electrical voltage or current waveform and is then adjusted from the original shape or characteristics (Farhoodnea et al., 2013). As it is well known that the PV system consists of different power-electronic devices that produce distortion, the inverters that are considered the main part in GCPPP are no exception. Two of the most important characteristics of the PV inverters-connected grid are the efficiency and the electricity supply quality. Therefore, the electricity supply quality can be studied from the current and voltage total harmonic distortion. It is utilized to measure the presence of harmonics in a power system. The THD for a voltage or current waveform is a measurement of the harmonic distortion present and is defined as the ratio of the sum of all magnitudes of voltage or current harmonic components to the voltage or current magnitude of the fundamental frequency. It can be calculated using the following expression (Ayub, Gan, & Kadir, 2014; de Souza, Alves Filho, & de Oliveira, 2016):

$$THD = \frac{\sqrt{\sum_{n=2}^{k} h_n^2}}{h_1}$$

3.31

Where h_2, h_3,…,h_n denote the effective value of the harmonics for the orders 2,3,4, …,k, while h_1 is the fundamental component. The n and k represent the harmonic order and last harmonic series, respectively. It is worth mentioning that if the wave is an ideal sinusoidal, the total harmonic distortion is zero. Furthermore, more particular measures for the quantitative analysis of the components, either the voltage distortion or the current distortion in percentage can also be expressed for a more exact view using the following equations, respectively (de Souza et al., 2016):

$$V_{THD}\% = \frac{\sqrt{|V_2|^2 + |V_3|^2 + |V_4|^2 + ...}}{|V_1|} \times 100\% \qquad 3.32$$

$$I_{THD}\% = \frac{\sqrt{|I_2|^2 + |I_3|^2 + |I_4|^2 + ...}}{|I_1|} \times 100\% \qquad 3.33$$

Malaysian distribution GC mentioned that the inverters should operate at PCC with current THD not exceeding 5%. TNB standard also requires I_{THD} to be less than 5% at a rated inverter output in PCC and the individual harmonics should be limited to the limits listed in Table 3.5 (Azit et al., 2012; Suruhanjaya Tenaga, 2016). In this study, these values have been considered as a reference.

Table 3.5   Current distortion limits.

The Harmonics		Distortion limit
Odd	3-9	< 4%
	11-15	< 2%
	17-21	< 1.5%
	23-33	< 0.6%
Even	2-8	< 1.0%
	10-32	< 0.5%

Regarding voltage distortion, the IEEE Standard 519-1992 indicates that voltage distortion at PCC is limited to 3% for individual harmonic content and only 5% for voltage bus rated 2.3-69 kV, as illustrated in Table 3.6. It is recommended that the voltage distortion of the system should be lower than 2.5% before a distributed generator such as PV is integrated with the system (Blooming & Carnovale, 2006). The TNB technical regulation and Malaysian distribution grid code require that voltage distortion for all distribution generator connected utility company unless abnormal conditions prevail, shall not exceed: (*a*) at 33 kV, 22 kV, 11 kV and 6.6 kV : a THD of 6.5%, and (*b*) at 400 V and below, a THD of 5% (Azit et al., 2012; Suruhanjaya Tenaga, 2016). Therefore, these values have been used as reference in this study. In sum, the high THD for either current or voltage have been limited to values under the 5% by increasing the switching frequency and proper design of the RL filter, as explained in Section (5.4.1.1). The proper RL filter can be defined using the following formula:

$$f_c = \frac{\omega_c}{2\pi} = \frac{R}{2\pi L} Hz \qquad 3.34$$

Table 3.6   Voltage distortion limits % at PCC.

Bus Voltage	Individual Voltage Distortion (%)	Voltage THD (V_{THD} %)
2.3-69 kV	3	5
69-161 kV	1.5	2.5
>161 kV	1	1.5

b. *Voltage unbalance*

Voltage unbalance is defined as the ratio of the negative sequence voltage component to the positive sequence voltage component. Voltage unbalance occurs when the three-phase voltage varies in magnitude and/or in the normal 120º phase difference (Shahnia, Majumder, Ghosh, Ledwich, & Zare, 2011). According to IEEE standards, the recommended practice for monitoring electric power quality is the percentage voltage unbalance factor (VUF %). The true definition in many of different standards of VUF % is given by the following equation (Shahnia, Majumder, et al., 2011; Smith, Hensley, & Ray, 1995):

$$VUF\ (\%) = \frac{V^-}{V^+} \times 100$$

3.35

Where V^+ and V^- are the positive and negative sequence of the voltage and can be calculated in the three-phase system as expressed in (4.36) and (4.37), respectively.

$$V^+ = \frac{1}{3}(V_a + aV_b + a^2V_c)$$

3.36

$$V^- = \frac{1}{3}(V_a + a^2V_b + aV_c)$$

3.37

Where a is the operator that shifts the vector counter-clockwise by an angle of 120 degrees, while a^2 fulfills a phase shift by 240 degrees counter-clockwise.

According to the grid technical regulation (Azit et al., 2012), the limits for voltage unbalance are based on United Kingdom Energy Networks Association Engineering Recommendation P29, which limits the whole voltage unbalance of the network to 2% and 1.3% at PCC and the load point, respectively. Other than the abnormal operations, the Malaysian distribution grid code requires the voltage imbalance at steady state not to exceed 1% (Energy Commission Malaysia, 2010). In this study, these limits have been

considered as a reference. Therefore, this study measured the unbalance of the voltage at the PCC using equations (3.35-3.37) to be within the required limits.

3.6.5 MV penetration and PV inverter

TNB allows only for grid-connected inverters to be integrated with TNB system. Therefore, for PV-TNB connection, the regulation stipulates that self-commutated type is preferred for MV and LV connections (Azit et al., 2012; Suruhanjaya Tenaga, 2016) and therefore this PV inverter type has been used in the proposed design, as described in detail in Section 3.4.

3.6.6 Frequency, synchronization, and power factor

One of the most important factors in power quality is the frequency. In the past, the frequency fluctuation caused by the small size PV system can be neglected as compared to other RE resources such as wind farms. Nowadays, this issue becomes more severe than before due to the high penetration of large-scale PVPP to the utility grid. Therefore, it is necessary to determine the frequency difference limits between electrical grid and PVPP. A PV system connected into a TNB distribution network shall operate in synchronism with TNB frequency. The TNB utility grid operates at nominal frequency 50 Hz with margin of ±1 Hz. On the other hand, the synchronization is the process of matching the voltage and frequency with the network. For this purpose, the SRF-PLL described in Section 3.43 is used for the synchronization with TNB, whereas the PV system matches the grid supply parameters within allowable limits illustrated in Table 3.7 (Suruhanjaya Tenaga, 2016; Tenaga Nasional Berhad, 2005).

Table 3.7   The required synchronization parameters.

Voltage Difference	Frequency Difference	Voltage Angle Difference
Less than 10%	Less than 0.2 Hz	Less than 10 deg.

Practically, the power factor is constantly under 1 as all circuits contain capacitance and inductance to a certain degree (Gonen, 2016). The TNB technical regulation stipulates that the PVPPs connected to the MV shall have a leading or lagging power factor higher than 0.9 (Azit et al., 2012; Energy Commission Malaysia (ECM), 2017; Suruhanjaya Tenaga, 2016). Therefore, these values are considered as a reference in the proposed design of this study. In order to achieve these limits, the current controlled

VSI described in Section 3.4.2 has been designed. So, the inner loop sets the reactive current to zero in order to achieve unity power factor at the PCC.

3.7   Summary

The details of PV system design and simulation modelling are presented in this chapter. Design and modelling of the PVPP-connected to the power grid is a first stage in this work. It describes the methods in order to design the large-scale PV array and produce the output power of dc part. Secondly, as far as the inverter control is concerned, this stage explained all required structure of the proposed three-phase inverter with synchronous rotating frame control (*dq*-control) using decoupling feedforward strategy. The designed PVPP also has been linked to the distribution side of the utility grid. In addition, the TNB technical regulation concerning the penetration of PVPPs into the power grid side is determined and the use of proper design is to be fulfilled, including the PV inverter type, connection method, frequency and power factor, harmonics and voltage unbalance. All these issues are designed to be within the required limits. Finally, the PV array system as well as the inverter integrated into the distribution system of the grid via a step-up transformer. Until this point, designing and modelling the complete PVPP-connected grid and determining the parameters for main components of the system are achieved. The next chapter discusses the addition of the developed FRT control of the inverter to support the grid voltage recovery based on the proposed Malaysian FRT and the standard requirements. Thus, when the voltage sags occur, a few control adjustments have been proposed to make the PVPP ride-through different types of grid faults as will be described in detail in the next chapter.

CHAPTER 4

FAULT RIDE-THROUGH CAPABILITY CONTROL

4.1   Introduction

This chapter presents the proposed FRT requirements concerning the penetration of the PVPP to the Malaysian grid code as new requirements and the developed FRT capability control for single-stage inverter-based grid-connected photovoltaic power plant. Thus, an overall control strategy for a single-stage three-phase inverter of PVPP connected to the grid in the faulty mode operation to ride-through all types of grid faults according to the standard requirements is presented. To achieve these FRT requirements, there are two major issues that should be addressed by the PVPPs during grid faults. The first one is the dc-link over-voltage in the dc-side of the PV inverter as well as the over-current that may occur in the ac side. The second one is the injection of reactive current, which is considered as an effective solution for voltage recovery and to support the grid in order to overcome the voltage sag problems according to the GC requirements. As a result, this study proposes an efficient control strategy that enables PVPP to withstand grid faults, keep the PV inverter to stay connected with the grid and continuously produce electricity.

Furthermore, suppressing excessive ac current as well as excessive dc voltage and then injecting the required amount of reactive current based on the standards requirements. The excessive dc voltage is superseded using appropriate dc-chopper brake circuit controller, while the ac-current is limited using current limiter control. Therefore, over-voltage on the dc-link voltage as well as over-current that may occur on the ac side are limited. Apart from that, when the fault is cleared, all values will recover to pre-fault values. After guaranteeing that the inverter is still connected without any problem, the control will inject the grid by an amount of reactive current necessary to support the voltage stability during fault condition according to the proposed Malaysian requirements

and other grid codes (GCs). An accurate and fast fault detection method is used to convert the operation of the inverter from normal operation mode into the FRT operation mode as fast as the occurrence of the fault.

4.2 Voltage Sag

Voltage sags (dips) are probably one of the most significant and severe power quality problems faced by both power industry as well as industrial and commercial customers (Singh et al., 2014). The severity of this power quality issue arises and therefore, it may generate interruptions in industrial processes or electrical equipment used in modern industrial plants. Voltage sag is defined as a reduction in the RMS supply voltage between 0.1 and 0.9 p.u at the power frequency for a short period from 0.5 cycles to one minute. Recently, as described earlier, the GCs requires the PV system to take an action during the occurrence of this problem by achieving FRT requirements. The sag event mostly occurs by grid faults. Therefore, depending on the fault type, voltage sags can be classified as single phase sags, phase to phase sags, or three phase sags as shown in Figure 4.1. It illustrates single, two, and three-phase voltage sag caused by grid faults and causes the nominal voltage to decrease from 100% to 50% during 0.15 s.
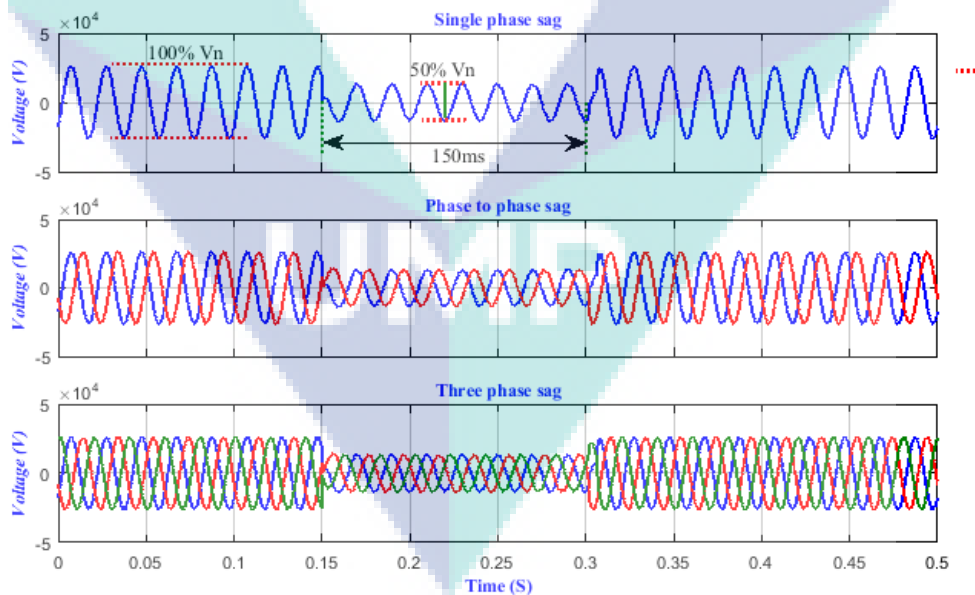

Figure 4.1   Voltage sag with 50% reduction of nominal voltage during 150 ms.

4.3 Fault Ride-Through Requirements

In the recent years, there is a sharp increase in the integration of photovoltaic power plants (PVPPs) to the utility grid. This significant increase in the PVPPs integration to the electric grid is expected to continue developing rapidly in the future (Petrović, Šimić, & Vražić, 2014). During the disturbances, it was required that these plants should to disconnected speedily to prevent islanding problem, but as the penetration of PVPPs to the electricity grid increases, disconnections of these plants during faults are undesirable, as this will lead to the loss of a large amount of PV-generated power, which may cause problems in the stability and operation of the power system (Y.-K. Wu et al., 2017). Consequently, many countries have put in efforts to establish specific technical requirements as a part of their grid code (GC) related to the integration of PV farms. The main focus in the new grid code requirements is the fault ride-through (FRT) capability which so called low voltage ride-through (LVRT) capability. The FRT specifies the range of the grid voltage level under nominal values in which the PVPPs have to remain connected to the power grid. Additionally, some countries require advance feature which is the injection of reactive current to support the grid and voltage recovery as a part of FRT requirements (Cabrera-Tobar et al., 2016; Y.-K. Wu et al., 2017).
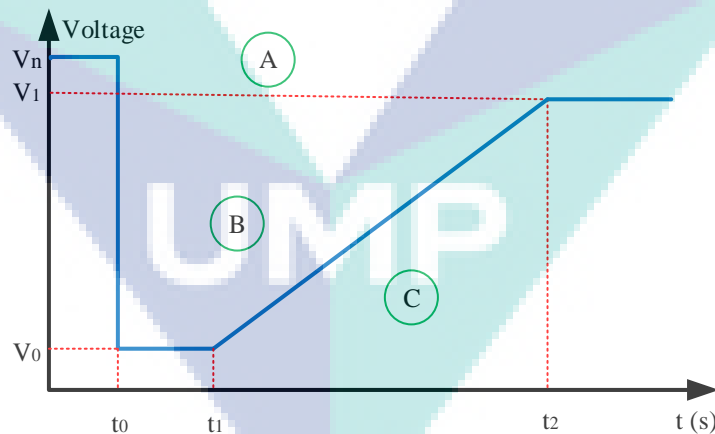
Figure 4.2   General curve limits for low voltage ride-through requirements.

Figure 4.2 shows the general FRT requirements for grid-connected photovoltaic power plants (GCPPPs). The GCPPP is required to work continuously in area A, which represents the nominal voltage at the connection point that is the point of common coupling (PCC). However, if the voltage is in area B, the GCPPP have to withstand voltage sag and remain connected to the system for a period of time ($t_0 \rightarrow t_1$); otherwise,

they have to be disconnected. In case of the voltage at the connection point in area C recovers to V_1 within time t_2 after a fault has cleared, it is mandatory for the PVPP to remain under continuous operation without disconnection. The values of V_0, V_1, t_1, and t_2 differ from GC to another based on the standards and characteristics of the national grid (Merabet, Labib, & Ghias, 2017).

4.4   Proposed Malaysian FRT Requirements

As Malaysia is planning to increase the PV generation as mention in Chapter 2, this requirement is still under investigation by Suruhanjaya Tenaga. Therefore, this research aims to provide investigation information on FRT capability for PV power generation in Malaysia and propose this requirement for Malaysia grid code. Thus, FRT requirements are proposed as shown in Figure 4.3 which is similar to is the US FRT requirements.
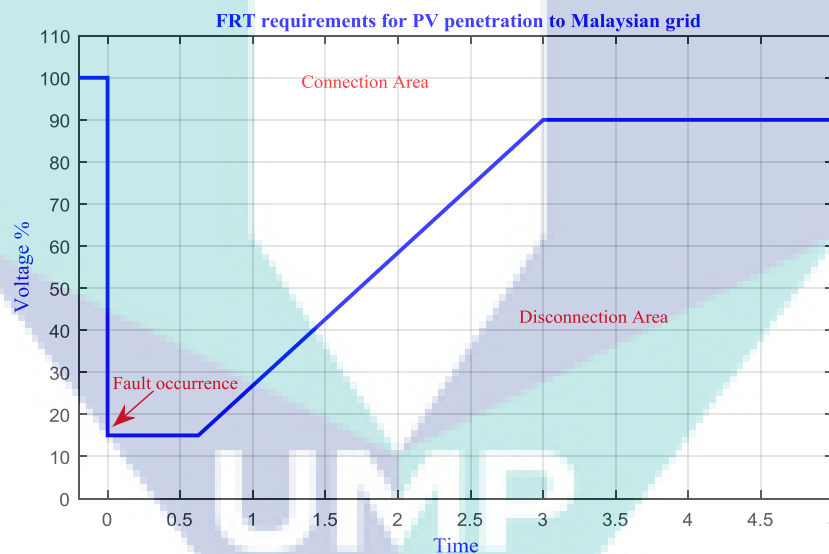

Figure 4.3   The proposed Malaysian fault ride-through requirements.

It proposes that the PVPP has to withstand the grid faults and stay connected to the grid when the voltage decreases to 15% of the nominal voltage at PCC within 0.625 s. On the other hand, when the voltage at PCC is below the blue line (disconnection area), PVPP can trip out from the grid. It is worthy to mention that the changes in FRT requirements from country to country are usually in the depth and duration of voltage sag.

Based on the literature, the FRT capability available for all countries are obtained and compared. The most suitable FRT capability for Malaysia is the US due to many

criteria e.g., (*a*) Denmark and Ireland applied the German FRT standards concerning wind penetration because they have same unit transformers which are connected to the generating units (Mohseni & Islam, 2012). In this regard and based on the Malaysian distribution code, national grid has almost the same unit transformer ratio as the US; (*b*) The US distribution system applied IEEE 1547 standards for the grid-connected distribution generators (DGs) and TNB follows these standards for DGs connection; (*c*) According to TNB regulation (Suruhanjaya Tenaga, 2016), for power quality especially for voltage sag, the average permissible time based on the percentage of remaining voltage during sag event is 0.6 s and this value is near to the curve proposed; (*d*) most counties choose the FRT period based on the operation time of protection relay, in Malaysia grid code (Energy Commission Malaysia (ECM), 2017), under-voltage relaies disconnect in range of one second and this is suitable of the prosed FRT disconnection; and (*e*) most new FRT standard under test consider the maximum time of FRT (0.625 s) to support the grid during sag event as long as possible as suggested by Romania and China.

4.5   Overview of the Developed FRT Control

The main objective of FRT capability is to protect the power inverter and ride-through grid faults during voltage sag time without disconnecting the PV power station. Moreover, inject the required amount of reactive current based on the standard requirements rapidly as soon as the grid faults happens. When voltage sags occur, the output power generated from the PV side and power following to the electrical grid is imbalanced. The imbalance between both sides will lead to transient excessive voltage and over-current at the dc-side and ac-side, respectively (Etxegarai et al., 2017; Obi & Bass, 2016). In order to avoid the damage and protect power electronic devices from excessive dc-voltage and ac-current, the FRT control strategy is applied to force the PVPP stay connected and ride-through voltage sag by decreasing both the over-voltage and over-current. Not only this, but also the proposed control strategy can support the voltage recovery as well as the grid stability during the fault time through the injection of active and reactive power based on the depth of the voltage sag. The control scheme of the proposed FRT control strategy during voltage sag is depicted in Figure 4.4.
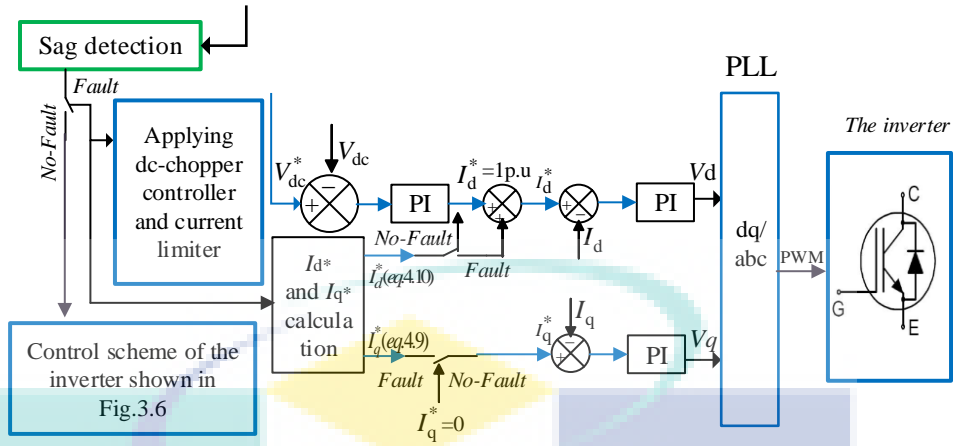
Figure 4.4   The schematic diagram of the proposed FRT control strategy.

This figure includes voltage sag detection (fault detection) unit, due to the fact that fast, automatic, and precise sag detection strategy has to be used in order to switch the system from normal operation to faulty mode of operation for an efficient FRT control. It also contains dc-link brake chopper circuit, ac current limiter, active and reactive current controller in order to protect the inverter from the excessive dc-voltage on the dc-side, excessive ac-current on the ac-side, and injection reactive power according to the standard requirements, respectively.

The PVPP must work in an MPPT mode during the normal operation whilst the chopper circuit stay in off mode. On the other hand, when the voltage sag is detected, dc-chopper circuit scheme will switch to operation mode while current limiter in turn will limit the non-normal ac-current in order to keep the system in balanced situation and protect the power electronic devices until ride-through the voltage sag duration. These two features are used to keep the system in a balanced situation and protect the power electronic devices until ride-through the voltage sag duration and to return all values of the PVPPs to pre-fault values as soon as the fault is cleared.

In addition, the inverter will inject the required active and reactive current according to the standard requirements for the contribution of grid support and voltage recovery. The overall proposed FRT control strategy operation principle is explained in the flowchart shown in Figure 4.5 and will be discussed in order in the following sub-sections:
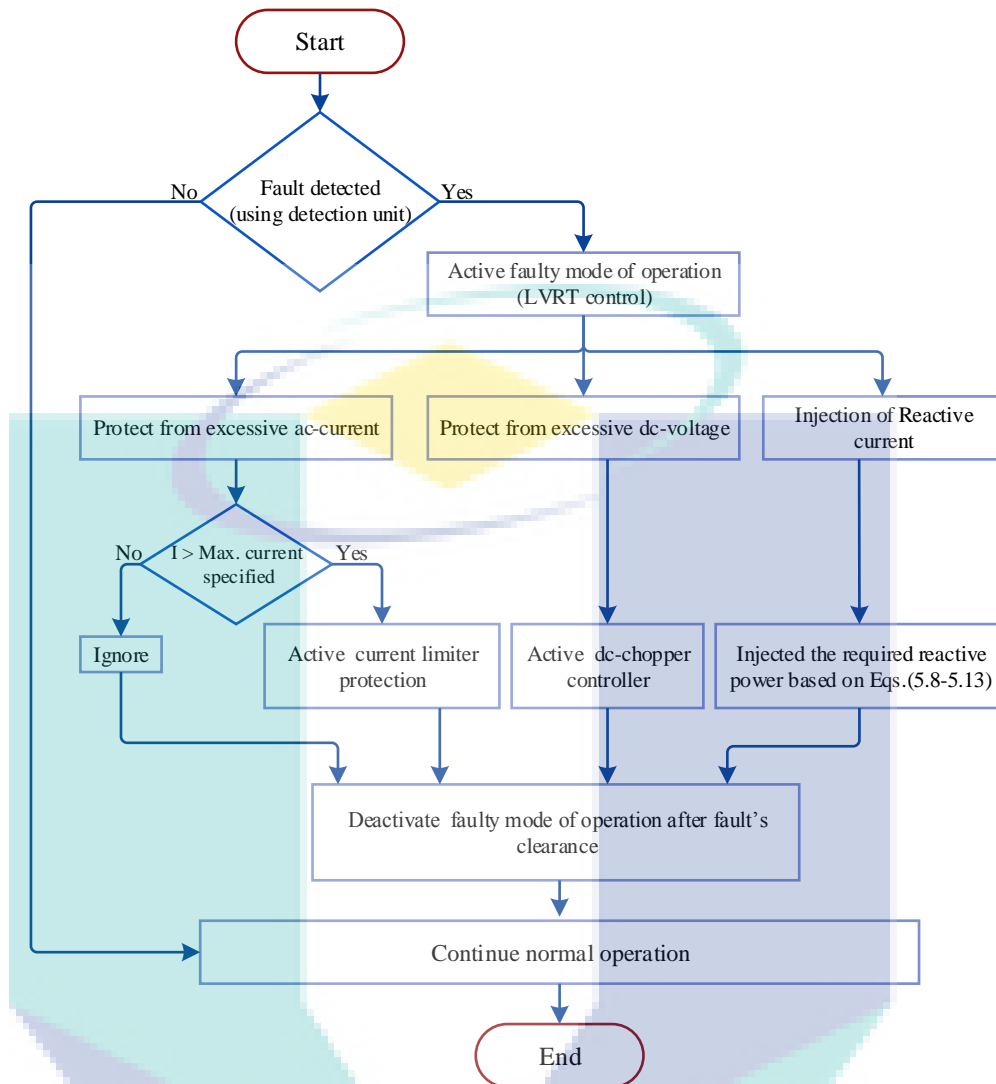
Figure 4.5   Flow diagram for the proposed FRT control.

4.5.1   Grid fault detection method

In order to achieve FRT requirements, the PV inverter should have two modes of operations. The first one is the conventional or normal operation mode without any additional controller during grid steady state conditions. The other one is the grid faulty mode of operation with FRT capability control when the occurrence of grid voltage sag is caused by short circuit fault. Thus, once the voltage sag occurred, an essential task of FRT control is that, the system has to switch normal operation mode to grid faults (FRT) operation mode immediately. In view of the above discussion, it is obvious that the sag detection method has a significant effect on the performance of GCPPPs under grid faults. Therefore, the fast and precise sag detection strategy is a very essential feature for more accurate and efficient FRT control.

As a result, in the developed control, the method of root mean square (RMS) is adopted to detect the grid fault as a first stage of the control system. It monitors the RMS value of the *d-q* grid voltage components from the PLL. This detection strategy calculate the present grid voltage (V_{gp}) using equation 4.1 without any additional transformation or extra hardware.

$$V_{gp} = \sqrt{V_{gd}^2 + V_{gq}^2}$$

<div align="right">4.1</div>

Where V_{gd} is the *d*-component and V_{gq} is the *q*-component of the grid voltage, respectively. It is also important to mention that, there was proposed another detection method which is the positive sequence method. This second detection method tested to be used in this research is based on calculating the positive sequence component magnitude of the three-phase grid voltage as expressed in the following equation:

$$V_{gp} = \frac{1}{3}(V_a + aV_b + a^2V_c)$$

<div align="right">4.2</div>

Where *a* is the operator that shifts the vector counter-clockwise by an angle of 120 degrees, and a^2 fulfils a phase shift by 240 degrees counter-clockwise. After testing the two methods founded that the RMS detection method is faster and more accurate than the positive sequence method, Therefore, this detection algorithm is preferred to use in the proposed control for a more accurate and efficient FRT control. The description, operation, and full comparison between theses two detection methods are provided in Appendix B.

4.5.2 Excessive ac current protection

It is well-known that the PV inverter connected-grid has a specified value of maximum ac current that should not be exceeded. In case any current exceeds such value, it will lead the inverter to be disconnected from the grid. Under a grid fault condition, the *d*-components of the current in the SRF-PLL starts to increase. This increase is due to the fact that the controller is trying to maintain the grid voltage constant during sag period. Furthermore, the *q*-components of the current in the SRF-PLL increases as well because of the inverter must inject reactive current during voltage sag to meet the LVRT requirements. As a result of the increasing *d* and *q* current components, the inverter may

be disconnected from the grid by over-current protections. To overcome this problem the current limiter shown in Figure 4.6 is proposed to keep the current value within the required limits.
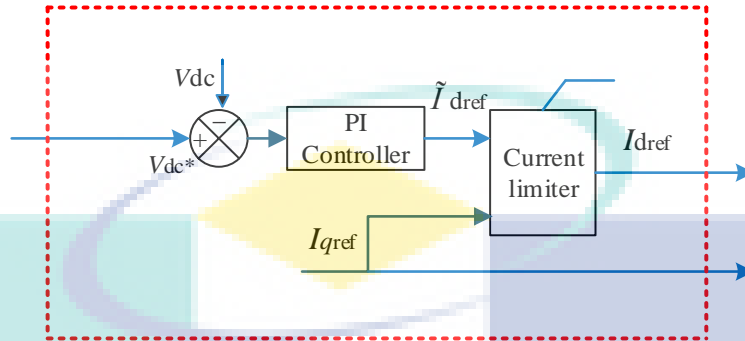

Figure 4.6   The control of current limiter.

4.5.3   Protection from excessive dc voltage for FRT

When the fault occurs and causes imbalance between the PV array side and grid side, the dc-link voltage will increase due to the accumulation of energy in the dc-link capacitors, which may damage power electronic devices. During voltage sag, the increasing of dc-link voltage leads the maximum operating point of the PV array (I-V) curve to move towards the open circuit voltage (V_{oc}) which in turn leads array output current to decrease, as explained in Figure 4.7:
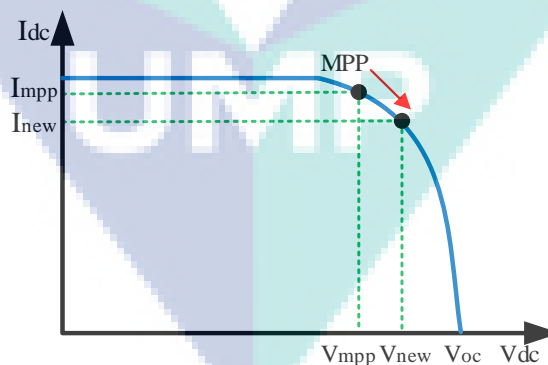

Figure 4.7   The change in (I-V) curve operating point under grid fault.

Additionally, another problem may appear due to the deviation of MPP during voltage sag. The problem is, when the voltage sag is being cleared, values such as dc-link voltage, PV array current and voltage, and output power take a long time to come to the pre-fault values. To overcome the significant increase of dc-link voltage which causes

these problems and to protect the inverter from being damaged or disconnected by over-voltage protection, this study proposed the dc-chopper circuit protection scheme shown in Figure 4.8.
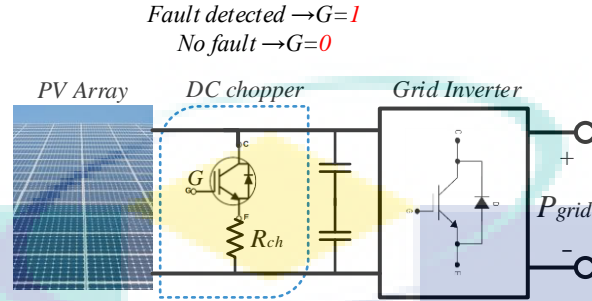

Figure 4.8   Chopper brake circuit for FRT protection devices.

The dc chopper circuit is a simple protection device that is connected in parallel with the dc-link capacitors, as illustrated in Figure 4.8. It consists of resistance (R_{ch}) and an insulated-gate bipolar transistor (IGBT). This protection scheme is used to protect the inverter from over-voltage caused by the increasing of dc-link voltage during voltage sag. Therefore, it works only when the fault is detected by switching on the gate pulse of the IGBT whereby the resistor will absorb the extra power generated by the PV array to protect the inverter and keep the power balance between dc and ac sides of the inverter. In addition, it keeps the MPP of the array working normally at its rated value. The chopper resistor is calculated according to the equation 4.3 as follows:

$$R_{chopper} = \frac{V_{dc\text{-}link}^2}{P_{dc}}$$

4.3

Where P_{dc} represents the output power of the PV array. The behavior of the inverter dc-voltage can be defined according to the following equation:

$$\frac{dV_{dc}}{dt} = \frac{\Delta P_{dc}}{V_{dc} \times C_{dc}}$$

4.4

Where

$$\Delta P_{dc} = P_{inv} + P_{chopper} - P_{inv-losses}$$

4.5

$$P_{inv} = (v_{inv,d} \times i_{inv,d}) + (v_{inv,q} \times i_{inv,q})$$

4.6

$$So, P_{chopper} = \frac{V_{dc}^2}{R_{chopper}} \Rightarrow when\ chopper\ circuit\ is\ on\ and,$$

4.7

$$P_{chopper} = 0 \Rightarrow when\ chopper\ circuit\ is\ off.$$

It is also important to mention that the inverter losses are generally small (roughly 1% of rated output power) (Pannell, Zahawi, Atkinson, & Missailidis, 2013) and therefore it has been neglected for the desired stability type of simulations.

4.5.4   Reactive power injection control during voltage sag

Once the voltage sag is detected, the standards require the grid inverter to have the LVRT capability, which imposes reactive power injection to help voltage recovery and grid support. Thus, the standard requirements specified the amount of injected reactive current into the grid for the PV station under voltage sag as depicted in Figure 4.9 which depend on the depth of voltage sag (Neumann & Erlich, 2012).
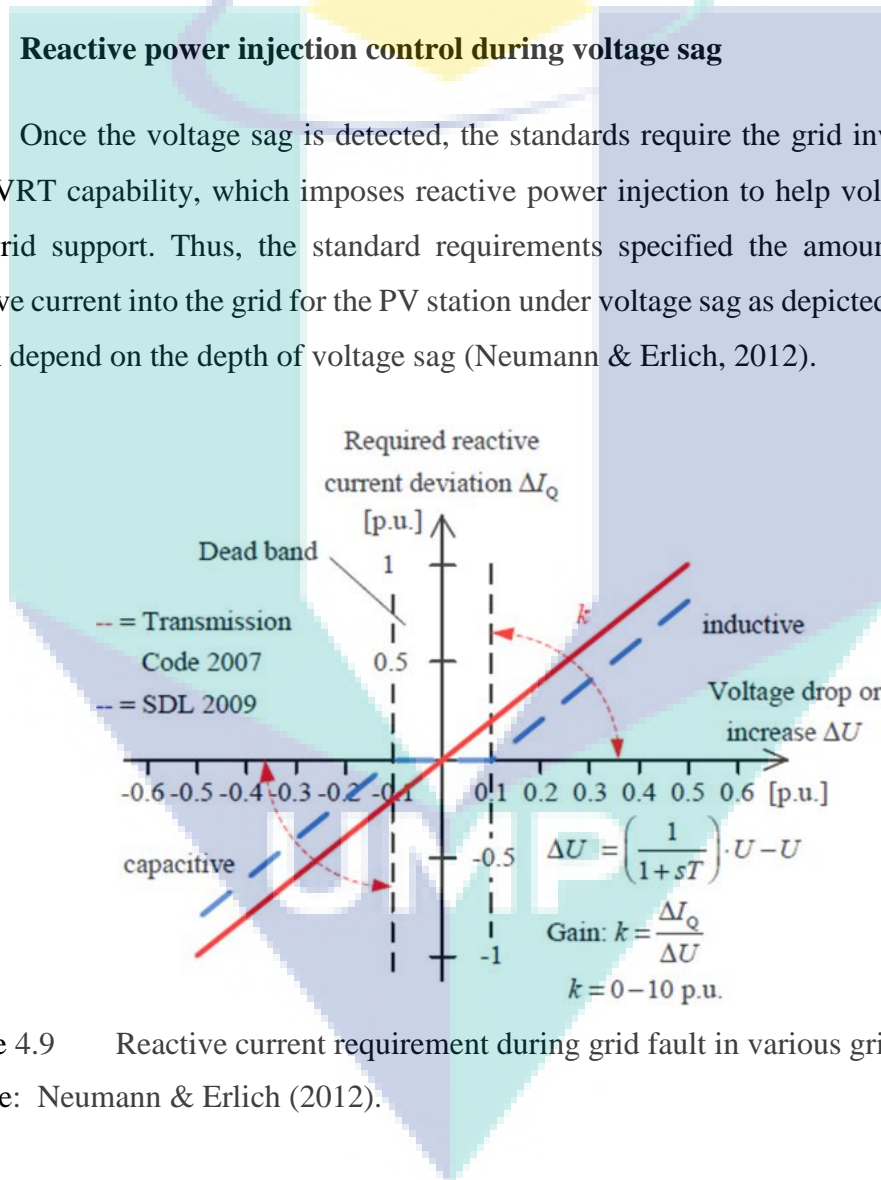

Figure 4.9   Reactive current requirement during grid fault in various grid conditions.
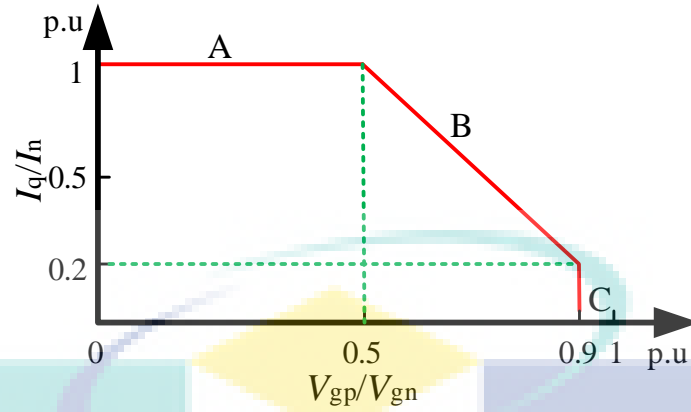Source: Neumann & Erlich (2012).

Figure 4.10   Illustration of the amount for reactive current during grid faults.

Based on the grid code regulations (Figure 4.9), the amount of injected reactive current calculation is the key to meet these requirements during voltage sag as simplified in Figure 4.10. Therefore, depending on the depth of voltage sags, the ratio of the required active current to the rated current (I_{qr}) can be represented by three regions as follow: (*a*) area C, which is defined as normal grid operation condition as long as the amplitude of the present grid voltage is higher than 0.9 p.u of the nominal voltage; (*b*) line B defines the amount of I_{qr} when the voltage during grid fault is less than or equal to 0.9 p.u and higher than 0.5p.u; and (*c*) line A is considered as the most severe situation due to decreasing the voltage under 0.5 p.u from its nominal value and therefore, the injected reactive current I_{qr} has to equal the nominal current. In other words, when the amplitude of grid voltage is between 0.9 p.u and 1.1 p.u, the system should stay in normal operation mode and the inverter injects only active current (no injection of reactive current is needed). Whereas, when the amplitude of grid voltage drops below 0.9 p.u, the inverter control must be switched to LVRT control and therefore the ratio of injected reactive current to the nominal current (I_{qr}) can be defined piecewise, depending on the magnitude of voltage sag as follows:

$$\begin{cases} I_{qr} = 0 & , \ V_{gp} > 0.9V_{gn} \\ I_{qr} = -2\dfrac{V}{V_{gn}} + 2 & , \ 0.9V_{gn} \geq V_{gp} > 0.5V_{gn} \\ I_{qr} = 1 & , \ V_{gp} \leq 0.5V_{gn} \end{cases} \qquad 4.8$$

Where V_{gp} and V_{gn} are the amplitude values of the present voltage during the fault and the normal grid voltage, respectively. On this basis, the reference value of the reactive current during voltage sag is defined as:

$$I_q^* = I_n \times I_{qr} \qquad 4.9$$

Where I_n is the normal value of the inverter-rated current. As a conclusion, during voltage sag, the inverter should inject the specified reactive power to help voltage recovery based on the LVRT requirements. For this purpose, the proposed control sets the reference value of the reactive current according to (4.8) and (4.9) as soon as the voltage sag is detected. Otherwise, at normal operation mode, the reference value of the reactive current is set to zero to achieve unity power factor.

Regarding the active power calculation and control during voltage sag, it would be better to generate active power as much as possible during this period to increase the energy caught from the PV array. According to the depth of the voltage sag, the allowed maximum injected active (d-axis) current into the power grid during faults can be calculated from the following equation:

$$I_d^* = \sqrt{1 - I_{qr}^2} \times I_n \qquad 4.10$$

It is worth to point out that, in all cases, both active and reactive current must not exceed the normal value of the inverter rated current, which can be derived from the following relation:

$$\sqrt{I_d^2 + I_q^2} = (I_n) \qquad 4.11$$

Hence, the maximum allowed active power (P_{inj}) and reactive power (Q_{inj}) reference flowing through the grid inverter in the faulty mode operation are given as:

$$P_{inj.} = \frac{3}{2} V_{gd} I_d^* \quad , and \qquad 4.12$$

$$Q_{inj.} = -\frac{3}{2} V_{gd} I_q^* \qquad 4.13$$

4.6 Summary

This chapter explained the proposed FRT requirements as new requirements for the Malaysian grid code by simulation. Additionally, an efficient new comprehensive FRT control of the inverter to support the grid voltage recovery based on the proposed FRT and standard requirements has been discussed. Thus, when voltage sag is detected by the proposed detection unit, a few control adjustments have been proposed to make the PVPP ride-through different types of grid faults. These adjustments include sag detection unit that is an essential part to inform the inverter to convert from normal operational status to FRT mode of operation, applying a dc chopper brake circuit and current limiters, which efficiently protect the system from over-voltage and -current, respectively, and also improve the FRT capability by injecting required amount of the reactive current to support voltage recovery based on the depth of grid faults. The effectiveness of the proposed method will be validated through simulation results in the next chapter. Much further, the next chapter will also focus on the results and discussion of the full developed system.

CHAPTER 5

RESULTS & DISCUSSION

5.1   Introduction

In this chapter, the results and discussion of the fully photovoltaic power plant (PVPP) system connected to the utility grid and provided with a fault ride through capability (FRT) control are introduced. Firstly, analysis of design, sizing and modelling results of the PV module and the array has been investigated. Secondly, modeling and design results of the PVPP connected to the medium voltage side of the grid with TNB technical regulation compatibility regarding PV penetration to medium voltage, in addition to the dynamics of this PVPP under different fault conditions are presented. After that, a comprehensive coverage of all the results that have been obtained at all stages of the FRT control is presented. The results of improving the capability of ride-through faults safely and keeping the inverter connected via suppressing the ac over-current as well as the dc-link over-voltage and protect the inverter during voltage sag are explained. Furthermore, once the fault is cleared, all values are recovered to pre-fault values directly. In addition, the results of the injection of reactive current control to provide grid support through active and reactive power control at different type of faults based on the standard requirements are presented. The performance of the FRT strategy is evaluated by developing Simulink models. Whereas, different parameters have been assessed through modification or performance enhancing strategies. Finally, the results of the research are compared with the published results of other investigators or other methodologies, both the experimental results and simulated results, are presented in this chapter. MATLAB Package version 7.17.0.634 (R2015a) is used to obtain the Simulation results.

5.2   Overview of the PVPP Connected to Utility Grid with FRT

The PVPP model that is designed in this research has been developed using Matlab/Simulink as the general block diagram illustrated in Figure 5.1. A three-phase grid-connected PV inverter contains the PV array, P&O maximum power point tracking (MPPT), the grid inverter with its control and transformer linked to the MV side of the grid. The MPPT stage controls the output dc power of the PV array to an appropriate level so that the inverter can work regularly. The PV inverter stage controls the voltage of dc-link and then delivers the necessary current to the distribution network through multiple voltage and current control loops. In addition, the TNB technical regulation concerning the penetration of the PV system to medium and low voltage distribution system of the national grid has been applied to this model for compliance purpose. Finally, a new comprehensive FRT capability control has been applied to this model based on the proposed FRT as well as standard requirements and other GCs. The performance of the control is tested under different types of the grid faults. It overcomes the problems of over-current, over-voltage, return all values to pre-fault as soon as the fault is cleared, achieve system balance, and inject the required amount of reactive current according to the standard requirements. A detailed developing, sizing and testing results of the model under TNB rules and FRT control of the PV system will be introduced in the upcoming sections.
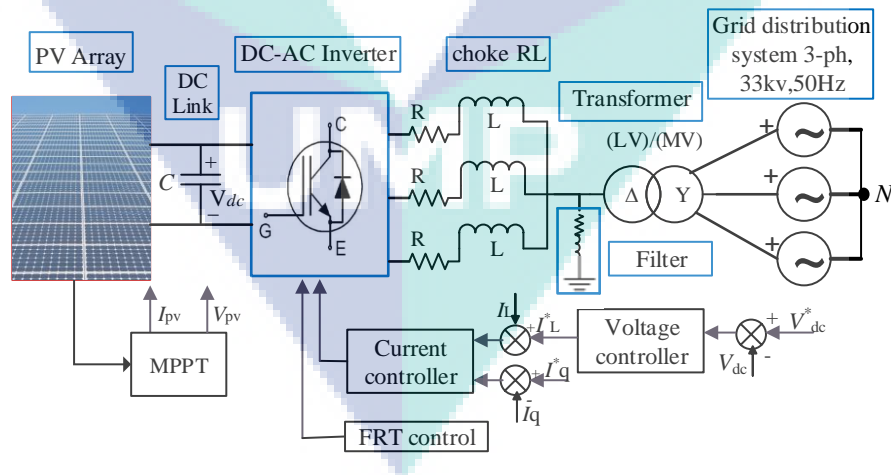

Figure 5.1   Schematic block diagram of the general PVPP system with FRT.

5.2.1 Modelling of the PV module

In this research, a TopSun TS-S400 PV Monocrystalline module has been selected to use in the proposed PVPP design. Every single module produces maximum power of 400 W at STC, the other electrical and mechanical specification of the module are provided in the datasheet by the manufacturers (TOPSUN solar modules, 2017) as listed in Table 3.1. The selected PV model is simulated and modelled based on the mathematical model explained earlier in sub-section 3.3.1.1. As a result, the current-voltage (*I-V*) and power-voltage (*P-V*) characteristic curves of the PV model at STC (*G*=1000 W/m^2, *T*=25ºC) are verified through Simulink as shown in Figure 5.2. It is clear that, the results shown in the figure matched the manufacturer datasheet provided in Table 3.1 and Appendix A.
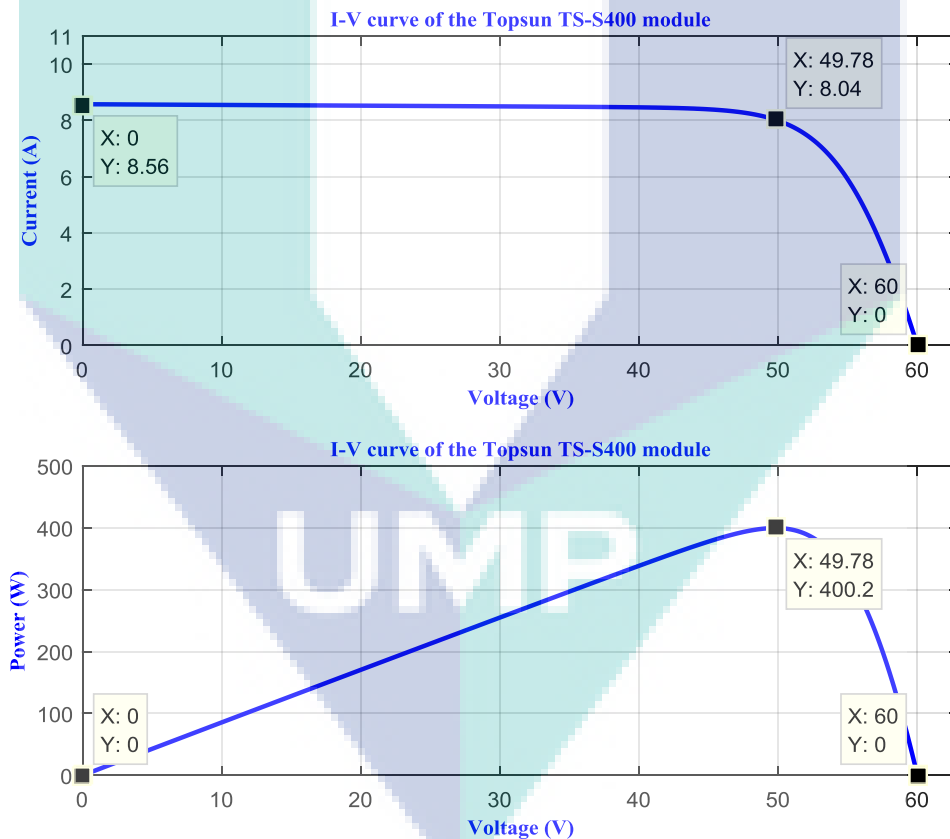

Figure 5.2   Characteristic curve of PV Topsun S400 module at STC: (a): I-V curve and (b): P-V curve.

It is well-known that the output current, voltage, and power are highly dependent on the solar irradiation and ambient temperature. These two factors have become of very importance for PV system design. For this reason, the predication of the selected module's

behavior and characteristics based on mathematical modelling of the equivalent circuit using Matlab/Simulink platform under different temperature and solar radiation readings have been introduced in Figure 5.3 and Figure 5.4, respectively. *I-V* and *P-V* characteristics of the module at different level of irradiation and constant temperature are illustrated in Figure 5.3. It can be seen that there is a direct relation between the output voltage, current, and power generated with sun irradiance. Once the irradiation increases, the three parameters increase and vice versa. For instance, the power has an increment of about 80 W when the irradiation increases by 200 W/m^2. In addition, the PV current produced decreases proportionally by around 2 A as long as irradiance decrease.
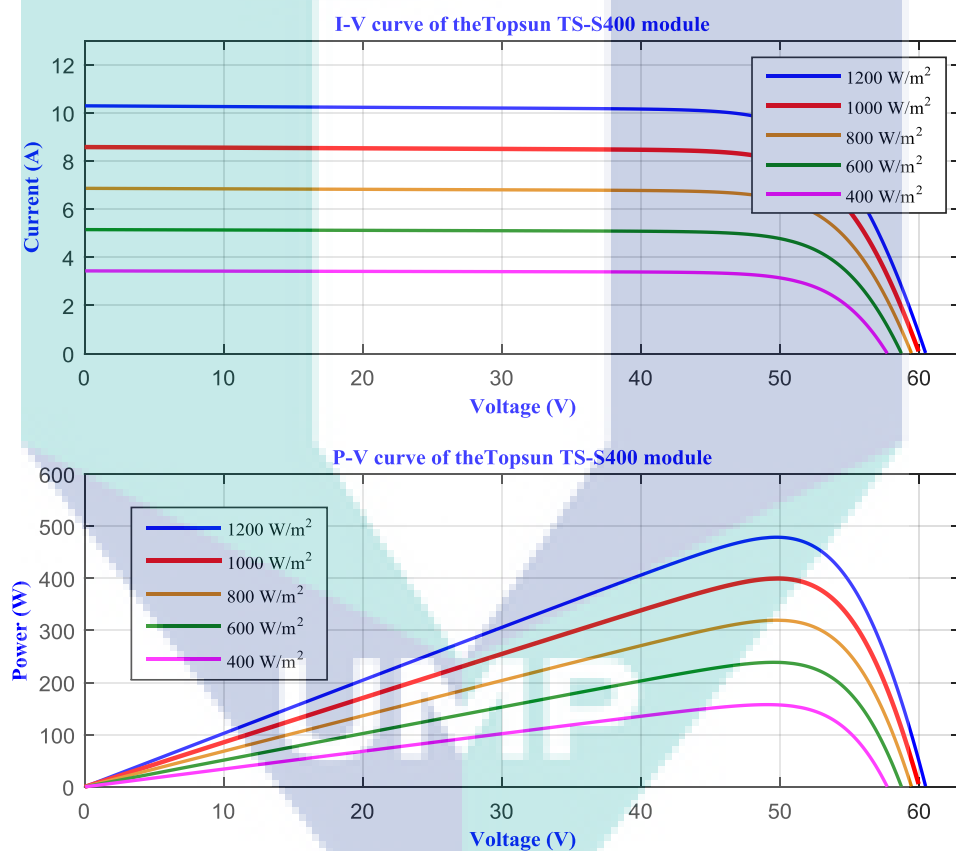
Figure 5.3   I-V and P-V curves at different levels of sun irradiance and constant temperature 25°C.

On the other hands, the output voltage and power generated are inversely proportional to the ambient temperature (Bouraiou et al., 2015). Generally, at any value of solar radiation, in case the module temperature increases, the short circuit current (I_{sc}) will slightly increase whereas open circuit voltage (V_{oc}) decreases. Consequently, the

maximum generated power increases as long as the temperature decrease, this behavior is accurately tested and presented as shown in Figure 5.4.
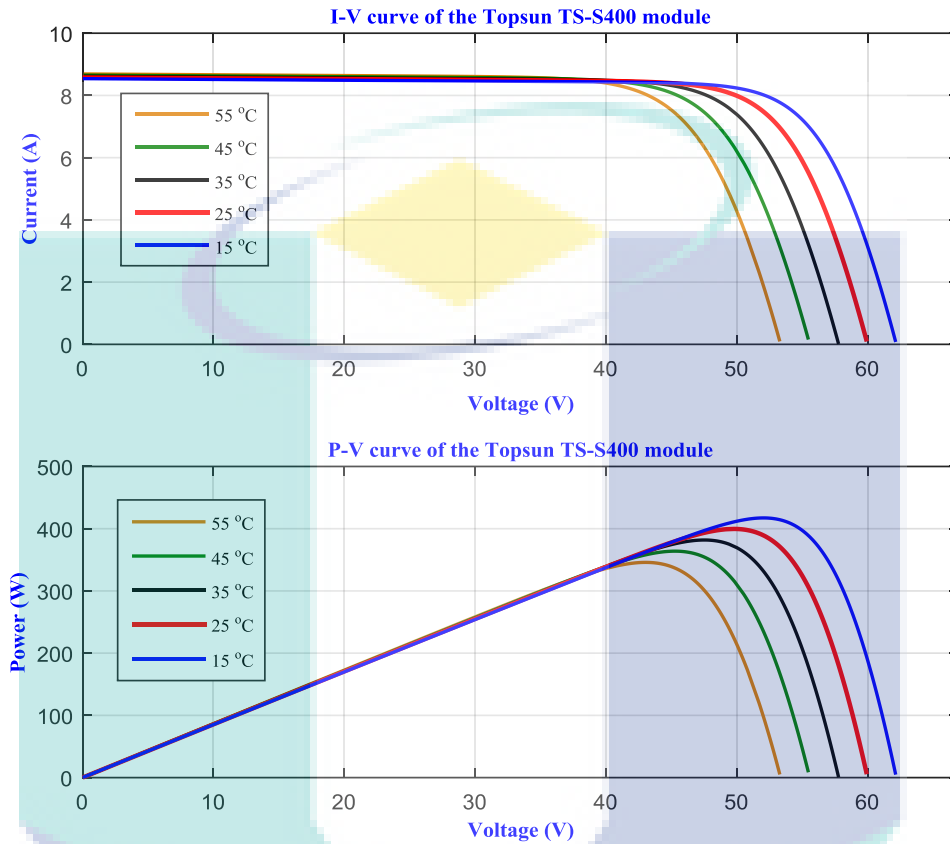

Figure 5.4   I-V and P-V curves at different values of temperature with constant sun irradiance 1000 W/m^2.

5.2.2   Matlab/Simulink PV array sizing results with MPPT

Theoretical sizing and design of the PV array in sub-section 3.3.1.2 requires that, to accomplish the proposed GCPPP with a nominal peak power of 1500 kW at STC, 3750 Topsun (Ts-S400) modules are selected to build the PV system array. The modules distributed as 16 series modules and 235 parallel strings to form the PV array, as it can be seen in Figure 5.5. This configuration also shows the other important values which have already been obtained by calculation in the design steps such as maximum voltage, current, and power in addition to the open circuit voltage and short circuit current of the proposed PVPP system.

I_{mpv} is $235 \times 8.04 = 1889.4$ A

$I_{pv(sh)} = 235 \times 8.56 = 2011.6$ A

$V_{mpv} = 16 \times 49.78 = 796.4$ V

$V_{pv(oc)} = 16 \times 60 = 960$ V

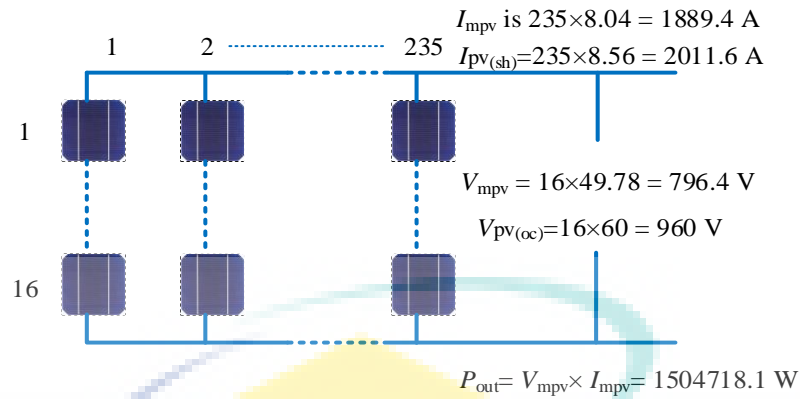$P_{out} = V_{mpv} \times I_{mpv} = 1504718.1$ W

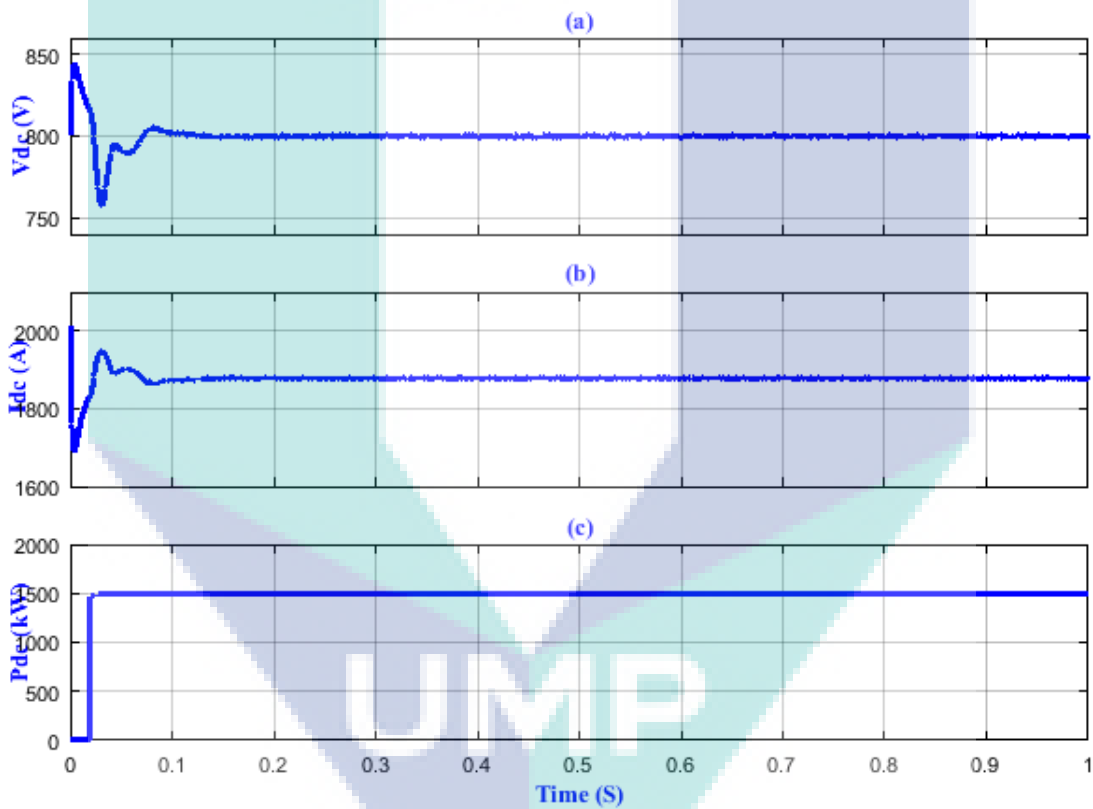Figure 5.5   Configuration of the array in the proposed PV system.

Figure 5.6   Maximum output of the PVPP array at STC: (a) voltage; (b) current; and (c) power.

After theoretical sizing calculation of the proposed PVPP, validation of the array sizing with Simulink is carried out. Using the same number of panels and implementing of P&O MPPT technique which is used to ensure that the solar energy is captured and converted as much as possible, the PV modules operate at its maximum power point as the temperature and irradiation vary by tracking the maximum current (I_{max}) and maximum voltage (V_{max}) of the photovoltaic array, and consequently the maximum

available output power (P_{max}) is obtained. Figure 5.6 illustrates that at STC, the PV array delivers a maximum power of around 1500 kW. Whereas, the maximum voltage and current are 798.6 V and 1881 A, respectively, which comply with the calculation sizing results in Figure 5.5 and chapter 3.
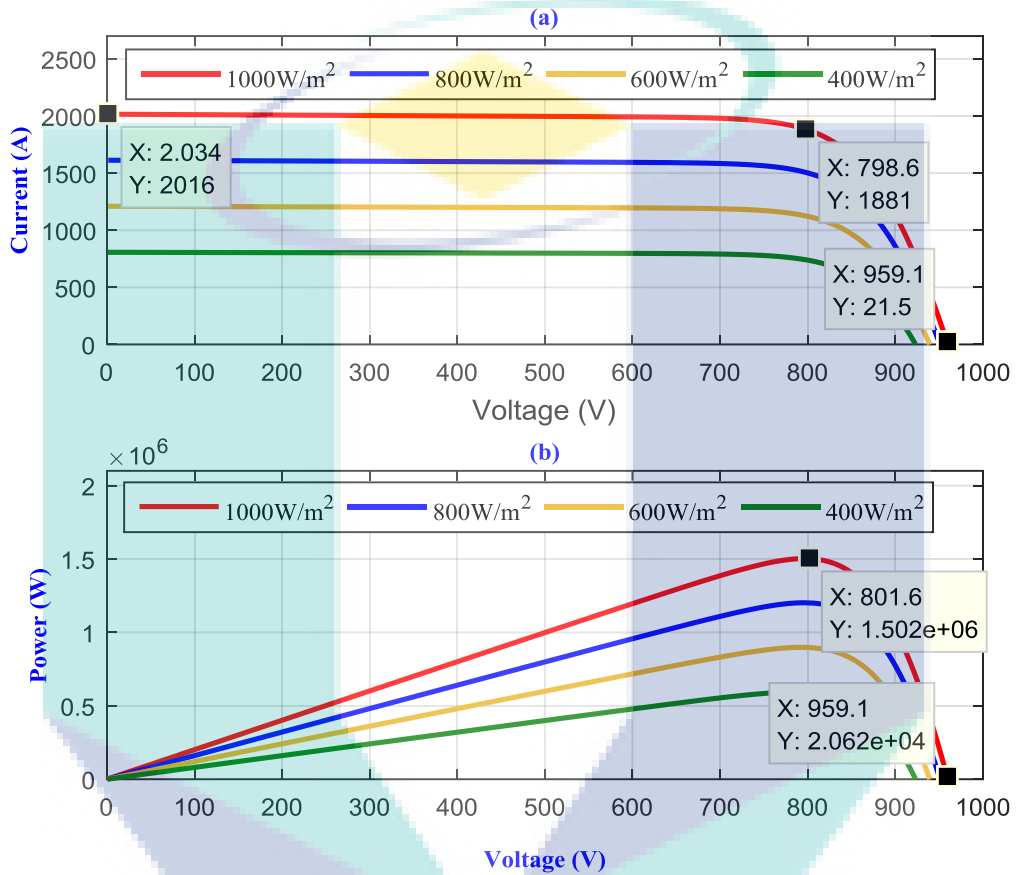

Figure 5.7   Characteristic curve of the PV array system consists of 235 parallel strings and 16 series modules at different level of irradiation and constant temperature (25°C): (a): I-V curve and (b): P-V curve.

In addition, the results of the sizing calculation demonstrated that the actual maximum open circuit voltage was $V_{oc} = 960\ V_{dc}$ and the actual maximum current short circuit current I_{sh} was 2011.6 A, which are equivalent to the simulation results shown in Figure 5.7. It provides the (I-V) and (P-V) characteristic of the PV array used in this design to explain the behavior of the proposed PV array at different levels of irradiation. These results prove that the simulation result has matched the theoretical sizing study since the values are equivalent.

The figure also showed the PVPP array with different sun radiation to provide the system operator with a background by the amount of the power and current of the system

which could be generated in case of increasing or decreasing the radiation levels. It can be summarized that according to the results shown in Figures 5.6 & 5.7, the simulation results are the same as the theoretical results calculated in Section 3.3.1. Thus, theoretical findings were verified using Matlab simulations.

Figure 5.8 shows the output power of the PV system at three different levels of radiation. It starts at 1000 W/m^2, decreases to 400 W/m^2, and then increases up to 800W/m^2 at a constant temperature of (25°C). The power produced under STC is around 1500 kW whereas the maximum power is 600 kW and 1200 kW when the radiation levels are 400 W/m^2 and 800 W/m^2, respectively. In conclusion, the simulation results based on the mathematical modeling described in Section 3.3.1, has matched the data provided from the PV module.
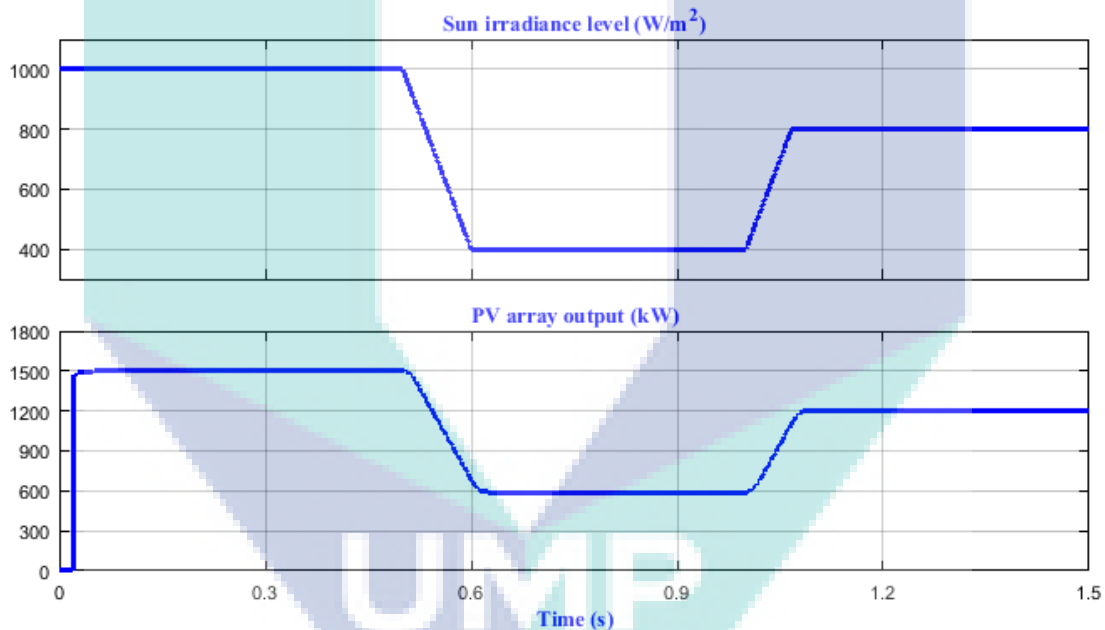
Figure 5.8   Output power of the PVPP array (dc generators) at different levels of radiation.

5.3   Grid-Connected PV Inverter

In normal operation, based on the analysis of operating principle of single-stage grid-connected PV inverter discussed in Section 3.4, the mathematical model of three-phase grid-connected inverter under *dq* synchronous rotating reference frame is set up, the feed-forward decoupling control strategy of three-phase photovoltaic grid-connected inverter is achieved, and the overall control strategy of single-stage grid-connected

inverter is developed in this thesis. The control strategy consists of MPPT loop, dc voltage outer loop, ac current inner loop. This control strategy not only realizes the decoupling control of active power and reactive power, but also has the characteristics of simple control as well as high control accuracy. Finally, the control strategy proposed is applied for 1500 kW grid-connected PV inverter. Given that the focus will be on the new proposed FRT control during abnormal operation, only some of the results at inverter normal operation will be discussed in the following sub-sections:

5.3.1 The dc-link voltage

A dc-link is widely used in GCPPPs. In a single-stage large-scale PV system, the dc-link capacitor should have a value near the maximum array voltage in order to reduce the output current ripple and regulate the voltage at the dc side of the grid inverter (Lee & Lee, 2013). Therefore, in this research, the dc-link voltage designed with 800 V comprises of capacitors, C_1 and C_2, which are split into ±400 V. The inverter has the same nominal voltage of the dc-link and should be compatible with the array voltage to withstand its maximum values, as the V_{oc} of the array (960 V) is within the inverter voltage range. The dc-link voltage of the system is shown in Figure 5.9.
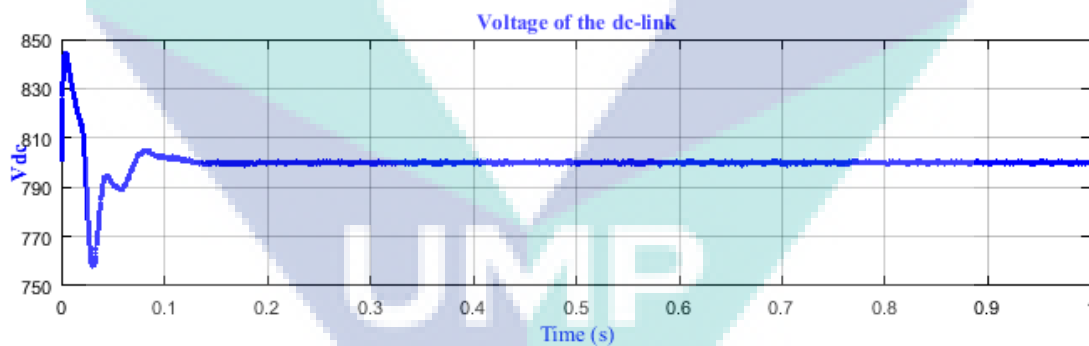
Figure 5.9   DC-link Voltage (V_{dc}).

5.3.2 Inverter simulation results

In this research, a self-commutated inverter type has been used as stated by integration rules and due to its advantage for large-scale PVPPs mentioned previously in order to execute the power conversion and control optimization. Figure 5.10 shows the output of the inverter line voltage. The value of sine wave encoded in the duty cycle of the PWM is shown in Figure 5.11. Input of the PWM control is the reference signal shown

in Figure 5.12. Then, the output of the inverter passes through the filter to get a pure sine wave as described in detail in Section 3.4.2.
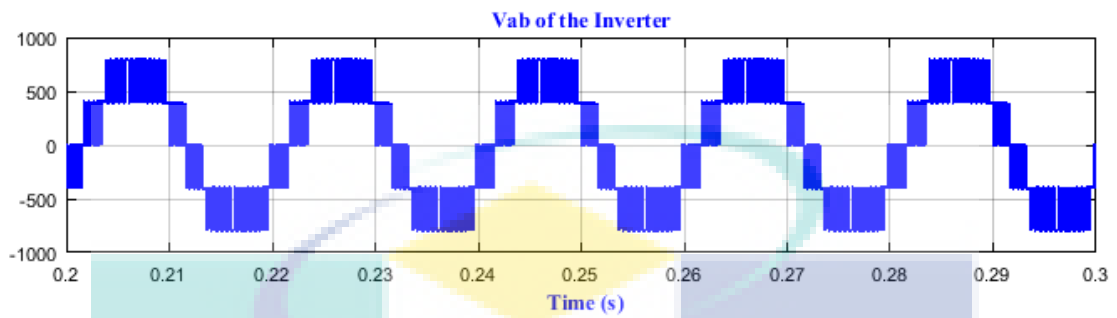

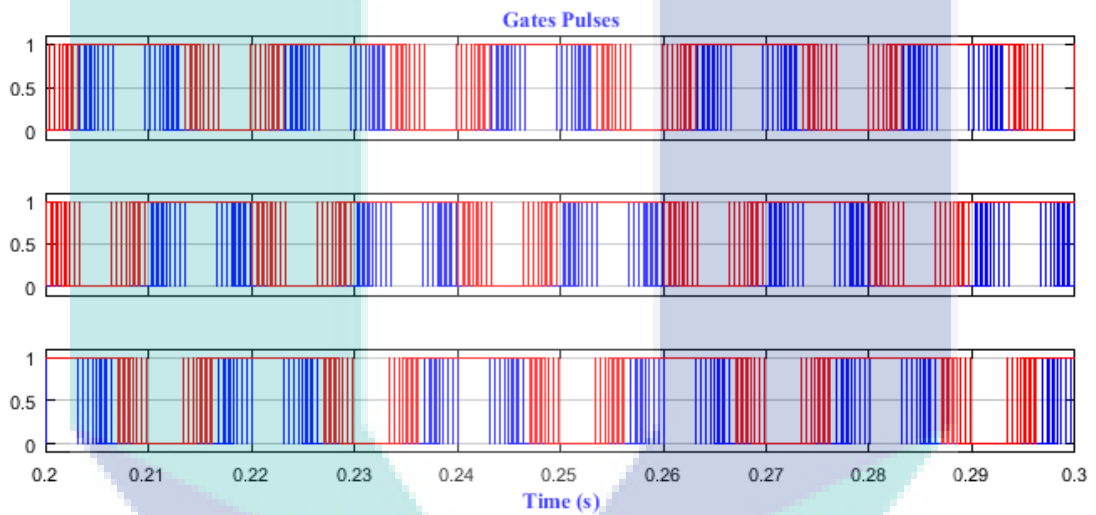Figure 5.10   Inverter output voltage (V_{ab}).
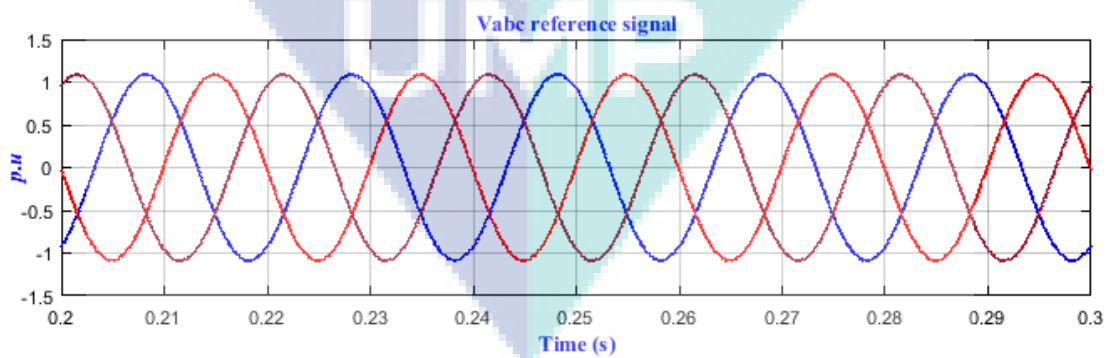

Figure 5.11   The duty cycle of the PWM.

Figure 5.12   Reference signal of the 3-ph voltage for synchronization.

Figure 5.13 and Figure 5.14 show the q-axis and d-axis of the current and voltage of the decupling control at normal operation, respectively. It can be noticed that the current of the q-axis is kept zero and d-axis current is set at rated value (1 p.u) as the output of the dc-link controller (outer loop) during steady state operation due to the fact that the inverter always operates at almost unity power factor (Parvez et al., 2016). The feed forward decoupling control is applied for smooth fluctuations of the dc-link and to decouple the active and reactive current. The *dq* control transforms the *abc* frame to *dq0* frame rotates in synchronous with grid voltage. In conclusion, in normal operation the values of I_d and I_q are 1 and zero per-unit, respectively to achieve unity power factor.
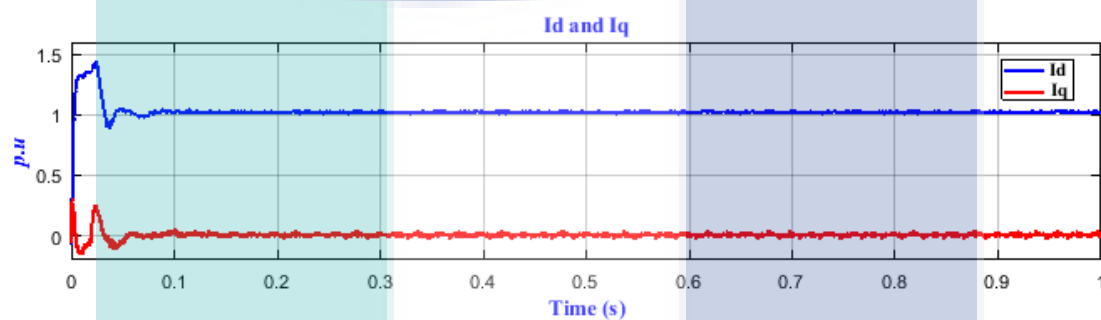
Figure 5.13   Active and reactive current of (*dq*-control).
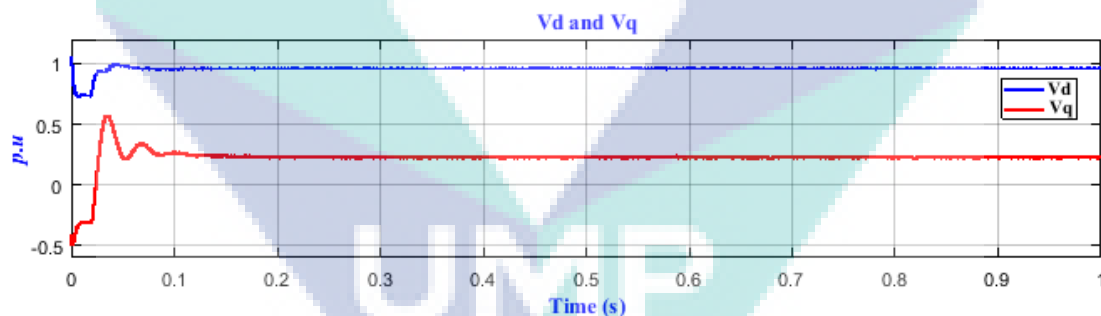
Figure 5.14   Active and reactive voltage of (*dq*-control).

5.4   TNB Technical Regulation Compatibility of the Developed Grid-Connected PVPP

Increasing penetration of photovoltaic power plants to the electrical grid leads to continuous evaluation of grid interconnection requirements. For this purpose, Malaysian grid representative from TNB issued the technical rules and requirements concerning the connection of photovoltaic system to low and medium voltage networks, as described in Section 3.6 and its sub-sections. Thus, this Section mainly focuses on the results of

applying TNB technical regulation concerning the penetration of large-scale PV plant into MV side of the electrical power grid with nominal rated peak power of 1500 kW, taking the compliance of TNB technical regulations into consideration based on the analysis of the practical conditions and characteristics of both PV system and Malaysian distribution system. These requirements, including PV-grid connection method that achieved by connecting to bus-bar at 33 kV substation, self-commutated PV inverter type which used in the PVPP design based on these technical regulations, TNB nominal voltage operating range, and power factor, while more focuses will be on harmonics and voltage unbalance. The following simulation results show the proposed PVPP model's ability to reflect the important requirements that a PVPP should have and be compatible with based on TNB rules for MV connection.

Figure 5.15 shows effective voltage, current, and the generated ac power (1466 kW) from the PVPP at the connection point. It is worth to mention that, the generated power is reduced from 1.5 MW to around 1.46 MW due to power losses.

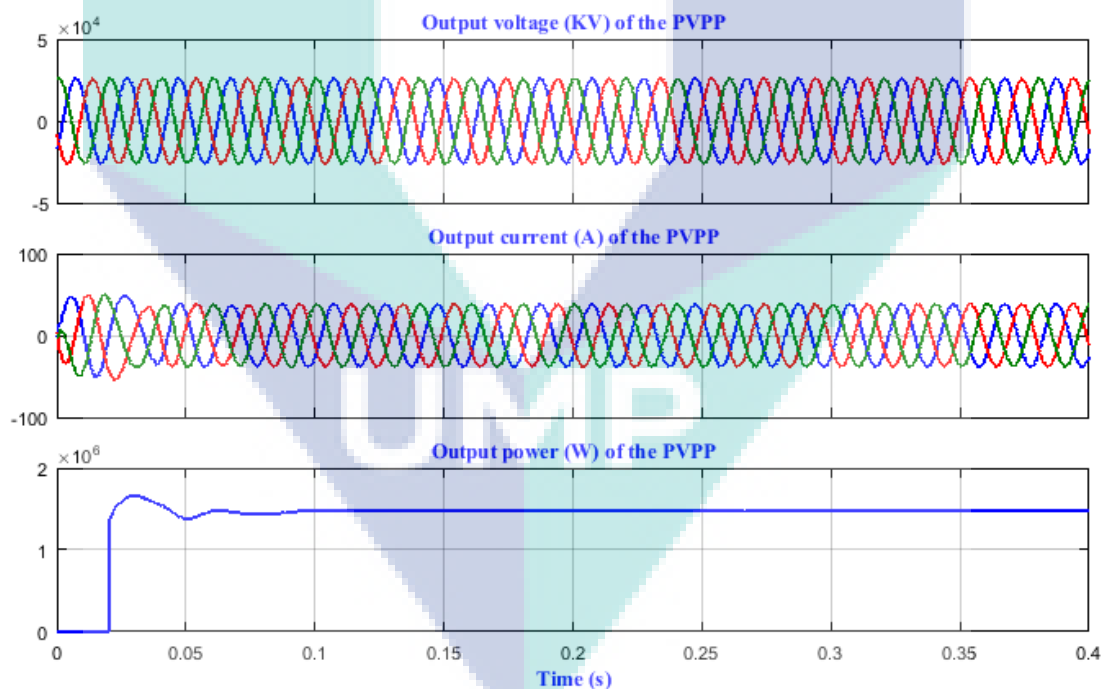Figure 5.15   Voltage, current, power of the PV generators at the PCC.

TNB nominal voltage operation range as described in Section 3.6.2 stipulates that the voltage limits at normal operation in 33 kV side is ±5%. In this design, the distribution system of 33 kV operates at voltage level less than the standard value due to known system losses. It can be seen in Figure 5.16 that the PV system voltage matched these

103

requirements at steady state conditions in which its voltage operates within the permitted voltage limits.
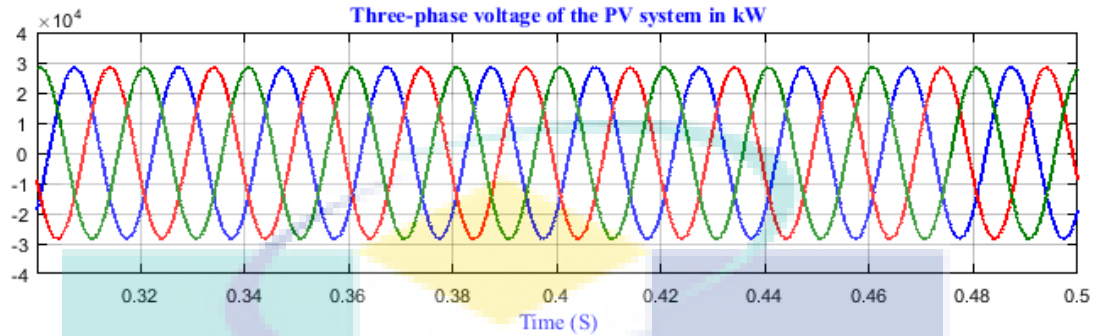
Figure 5.16   PV system voltage at the PCC.

Most of the PV inverters are designed for grid interconnection services operating close to unity power factor (PF) since, in normal operation, the reactive power reference is kept at zero. It can be clearly seen in Figure 5.17 that the response of PF of the proposed PVPP is near to unity PF (reactive power equals to zero) and this matches the TNB requirements that require leading or lagging PF higher than 0.9.
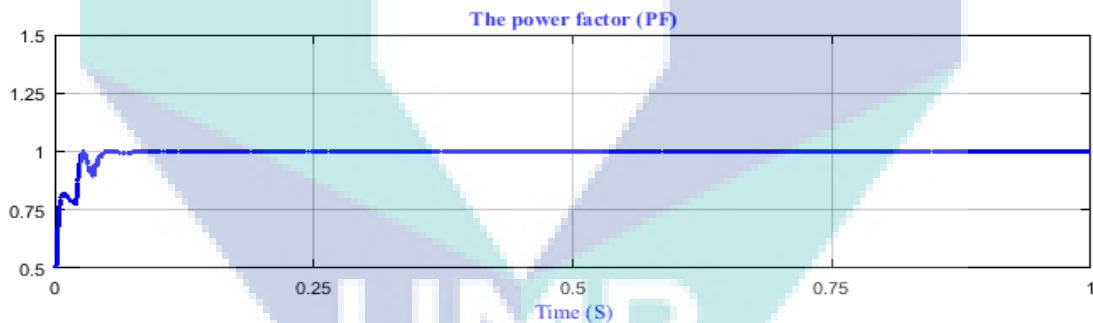
Figure 5.17   PF of the PV power system at rated inverter output power.

According to TNB technical regulation, PVPPs connected national utility grid should operate at nominal frequency 50 Hz during normal operation and be permitted with a margin of ±1 Hz during disturbances. Therefore, to test the maximum deviation of the system frequency during disturbances, symmetrical three-phase (3-ph) fault on the utility power grid that serves as the most severe fault is utilized for frequency performance test during abnormal conditions. The fault duration is 0.1 s, occurred between 0.15 s and 0.25 s. The total simulation is done within 0.4 seconds. It can be seen in Figure 5.18 that the frequency dynamics stay within the required limits of TNB, even during the period of disturbances.
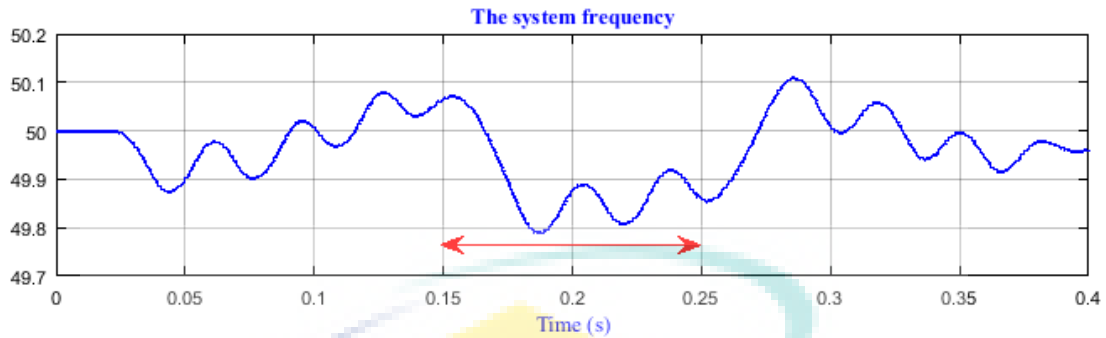
Figure 5.18   Dynamics behaviour of the system frequency.

5.4.1.1   Harmonic distortion and voltage unbalance

To accurately analyze the effects of installing large-scale grid-connected PVPP station on the power quality issues such a current and voltage harmonic distortion as well as voltage unbalance, the proposed PVPP model connected into the power grid is used to analyze these power quality issues based on the Malaysian grid standard requirements at different level of irradiation. The simulation results show that the THD and voltage unbalance are modified and degrades to the standard defined levels. As mentioned in Section 3.6.4, it is recommended that the THD at the PCC should comply to the standard requirements especially TNB standards at PCC (Azit et al., 2012; Energy Commission Malaysia (ECM), 2017). At this point, the output of the PV system should have low THD levels either for current or voltage to guarantee that no adverse impacts are caused to other equipment connected to the grid. In order to calculate the THD, the fast Fourier transform (FFT) tool in Simulink was used to record the THD of the output voltage and current waveform with the fundamental frequency at 50 Hz.

Figure 5.19 and Figure 5.20 show the THD of the current and voltage at PCC measured at STC (G=1000 W/m^2, T=25 ºC). It can be observed from the figures that the THD of current and voltage (I_{THD} and V_{THD}) waveform are oscillating around 9.2% and 2.8%, respectively. It is evident that the I_{THD} is higher than the 5% limit, whilst the V_{THD} is lower than the 5% limit, established by the previously discussed standard. Even after using three-level voltage source inverter and an efficient current control (Vu et al., 2016), the I_{THD} still higher than these limits. Thus, to solve this issue, a proper RL filter in the PV inverter had been used and PWM switching frequency increased. Therefore, the values of RL filter parameters used for calculation of harmonics suppression are 1.25 Ω

and 0.1 mH, respectively at switching frequency (f_c) equal to 2000 Hz, based on the formula described in equation 3.34:

Figure 5.19   THD level of the current waveform at STC before filtering.
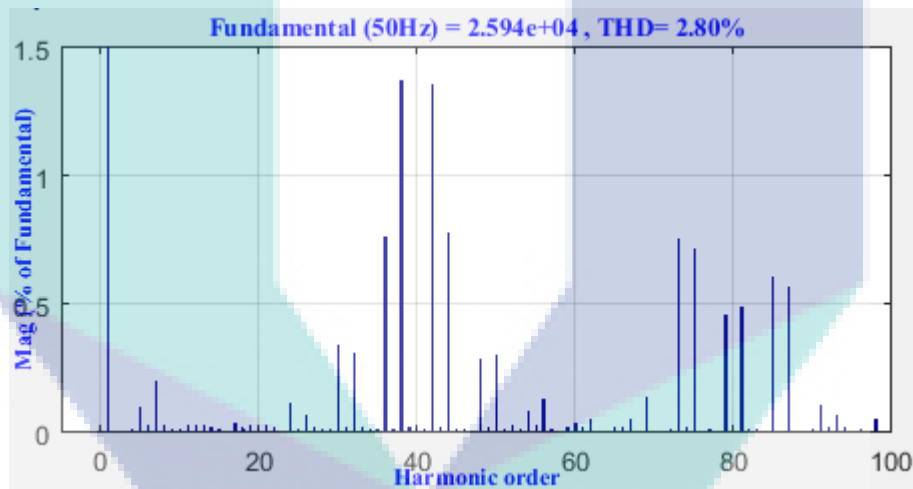
Figure 5.20   THD level of the voltage waveform at STC before filtering.

The effectiveness of this filtering is shown in Figure 5.21 and Figure 5.22 in which the I_{THD} and V_{THD} have been decreased to lower values of 0.74% and 0.15%, respectively, and these values are much lower than the value of the 5% limit. Figure 5.23 illustrates the three-phase current waveform of the PVPP at PCC before and after using the filter and adjusting of switching frequency. When comparing the sub-plot of this figure, in the time domain, it is evident that before filtering, the distortion was high and clear as shown in part (*a*), while in part (*b*), the shape of the current waveform is smoother than waveform in part (*a*) due to using a proper RL filter and increasing the PWM switching frequency. As a result, the FFT results (Figure 5.21 & Figure 5.22) show that the waveforms after

filtering have less THD and meet the desired limit than before the filtering case (Figure 5.19 and Figure 5.20).
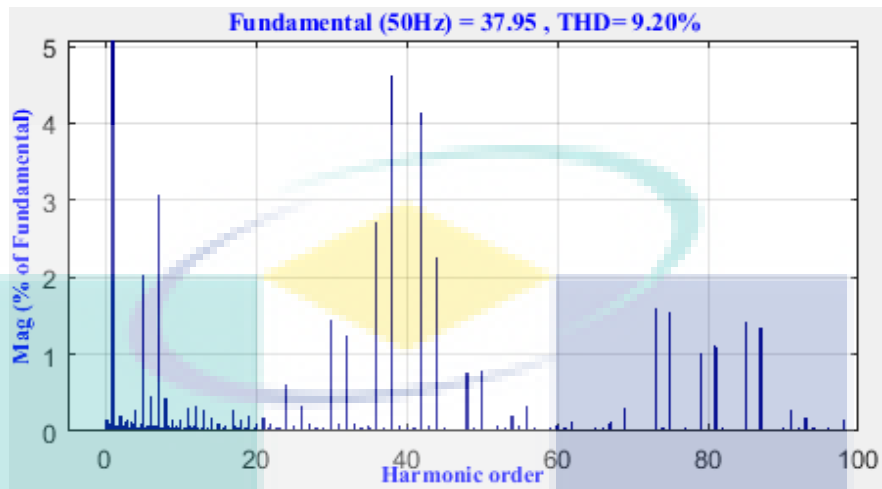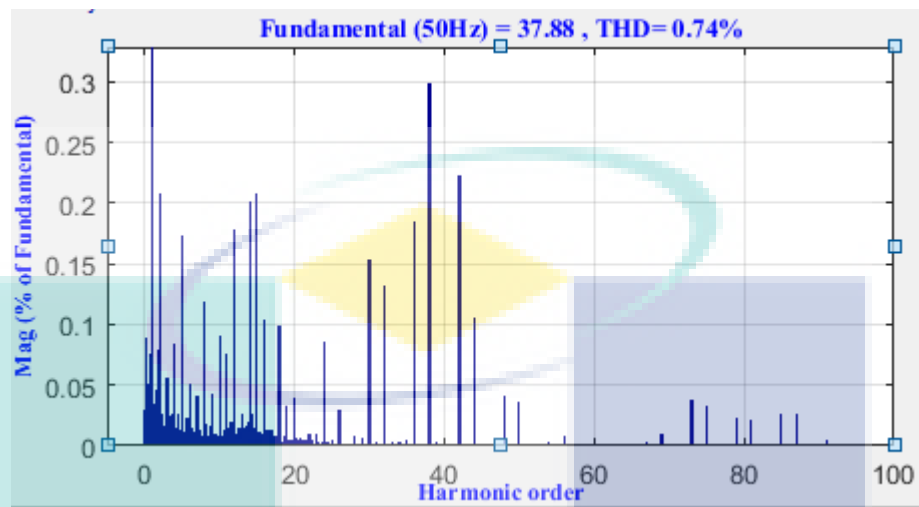

Figure 5.21   THD level of the current waveform at STC after filtering.
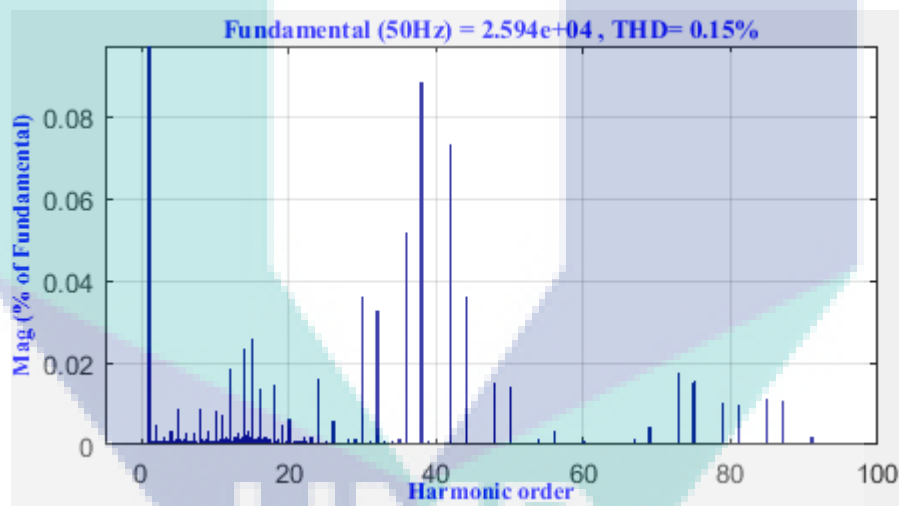
Figure 5.22   THD level of the voltage waveform at STC after filtering.
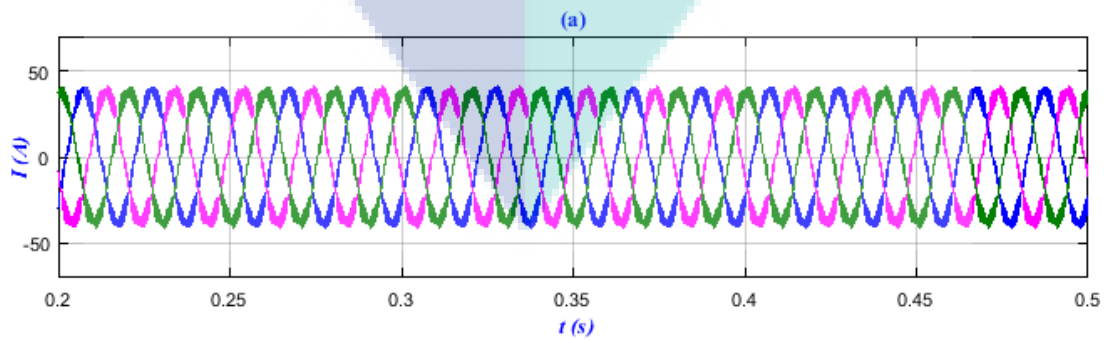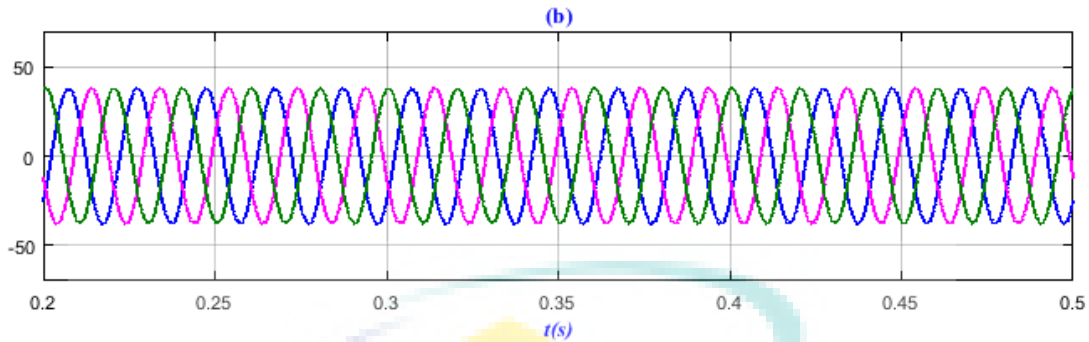
Figure 5.23   The three-phase waveform of the current at PCC: (a) before using RL filter and (b): after the implementation of RL filter.

In order to test THD of the proposed PVPP connected to Malaysian grid under different levels of solar irradiation, the I_{THD} and V_{THD} values of the PVPP at PCC were illustrated at 500 W/m^2 irradiation values as observed in Figure 5.24 and Figure 5.25, respectively. It is shown in Figure 5.24 that by decreasing the solar irradiation value to 500 W/m^2, the I_{THD} values were increasing. On the other hand, there is a small noticeable effect of decreasing solar irradiation on the V_{THD} value which remains almost constant, as shown in Figure 5.25 as compared to Figure 5.22. Therefore, one could conclude that the I_{THD} analysis is more significant than the V_{THD} analysis in the case of GCPPP operating under different solar irradiation. Moreover, the GCPPP injects more current harmonics into the utility grid when operating under low solar irradiation than at high irradiation values. In conclusion, as the solar irradiation increases, the THD reduces and vice versa. This occurs because the THD tends to increase, when the modulation index (m) decreases, however the THD is minimum with modulation index equal to one (m=1) (Barge & Jagtap, 2013). Therefore, when irradiation decreased to 500W/m^2, the THD is increased as compared to 1000 W/m^2 because the generated current and voltage is lower than the rated value, and this means the modulation index is less than one. To illustrate the effectiveness of the proposed method for individual harmonics, the value of each current harmonic in Figure 5.21 and Figure 5.24 is compared to the range given in Table 3.5, and the value of each individual voltage harmonic in Figure 5.22 and Figure 5.25 is compared to the range given in Table 3.6 and it was found that none of the individual harmonics violates the specified limits.
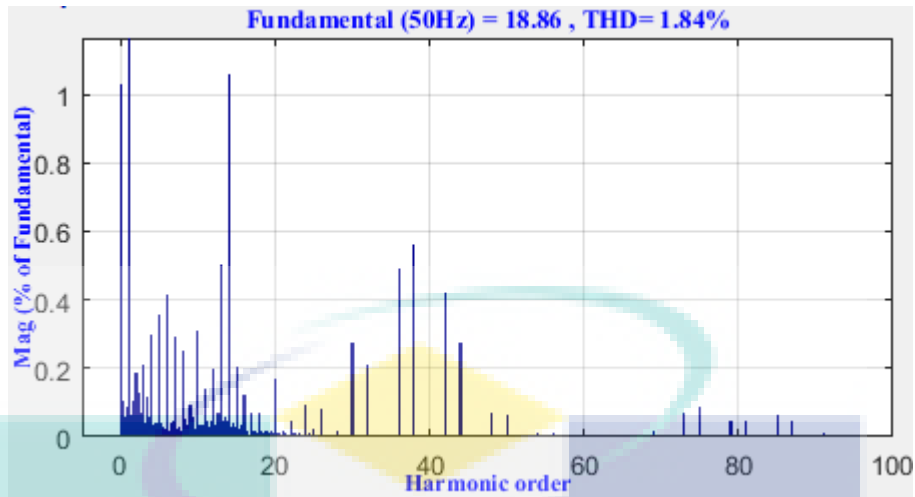
Figure 5.24   THD level of the current waveform at 500 W/m² solar irradiation.
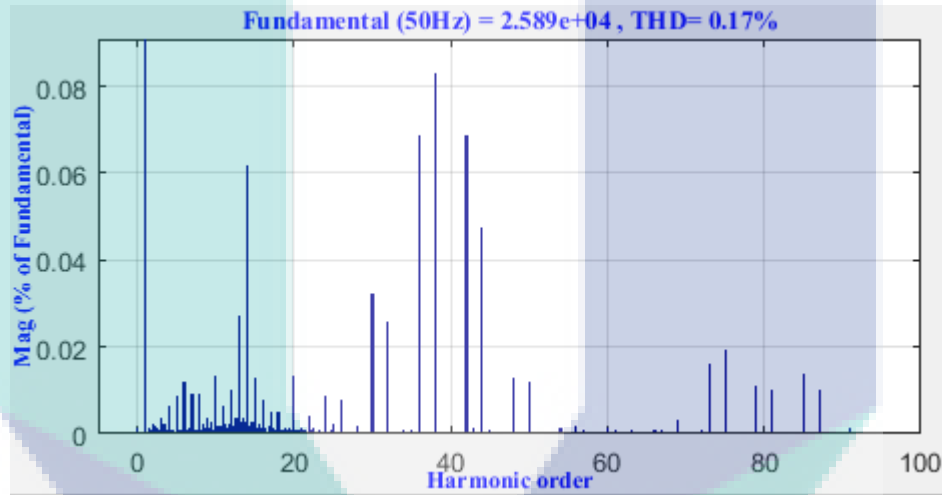
Figure 5.25   THD level of the voltage waveform at 500 W/m² solar irradiation.

Voltage unbalance mostly occurs in the low voltage distribution level especially at the user end, and therefore it is more common in the individual customer load due to the unbalance of load phases (T.-H. Chen, Yang, & Yang, 2013). Despite the fact that voltages are well balanced at the supply side, the voltage at customers' level can turn out to be unequal due to the unequal impedance of the system, incorrect distribution of single phase loads by the three phases of the system, or large quantities of single phase transformers (Shahnia, Ghosh, Ledwich, & Zare, 2011). As a result, these issues are out of the scope of this study and it is the responsibility of the distribution system operator to overcome this problem by rearranging or distributing the residential loads equally among the three phase distribution feeders or by installing dynamic voltage restorer (DVR) for better outcomes (Kanjiya, Singh, Chandra, & Al-Haddad, 2013). Therefore, in this study, the voltage unbalance problem analysis is focused and tested at the PCC to ensure that

non-unbalance three phase voltage is injected into the distribution system. The standard mentioned in Section 3.6.4(b) requires the VUF% to remain under 2% whilst at the abnormal operations, the Malaysian distribution grid code requires the voltage imbalance at steady state not to exceed 1% for one minute duration. Figure 5.26 illustrates that the VUF % at STC is 0.2% within 0.1s, whereas at low level of irradiation (500 W/m^2), the corresponding value is 0.16% within 0.1s, as observed in Figure 5.27. It is evident that the VUF % in both cases is much less than the standard limits.
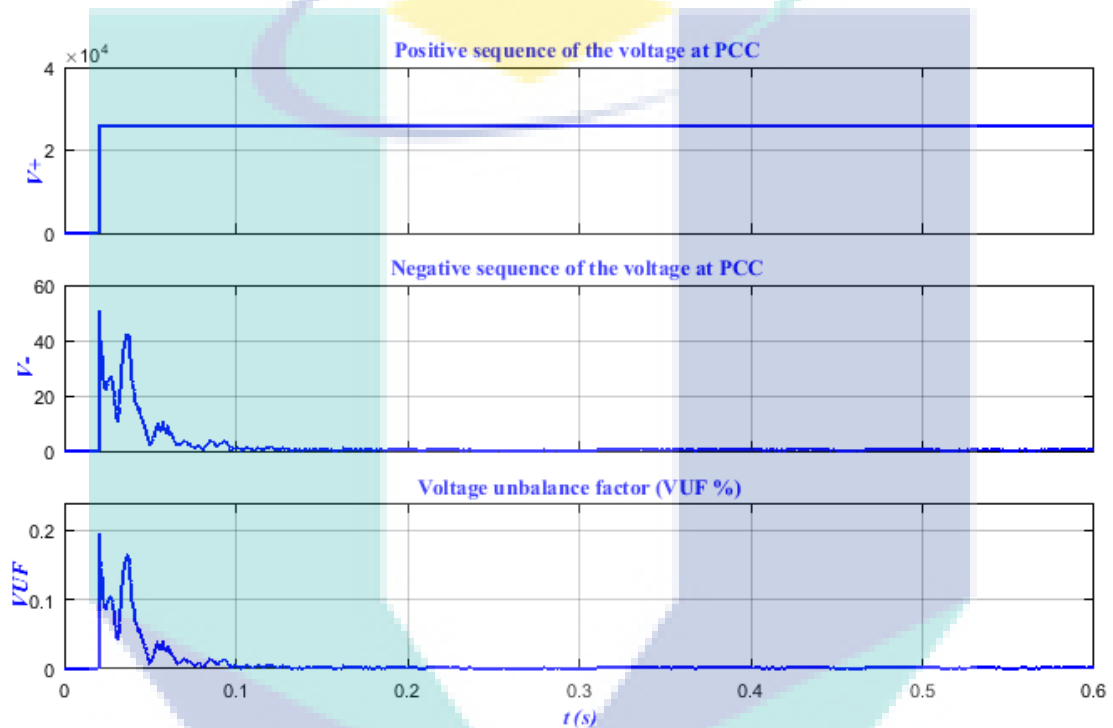
Figure 5.26   Voltage unbalance factor of the PVPP-connected grid at STC.

110
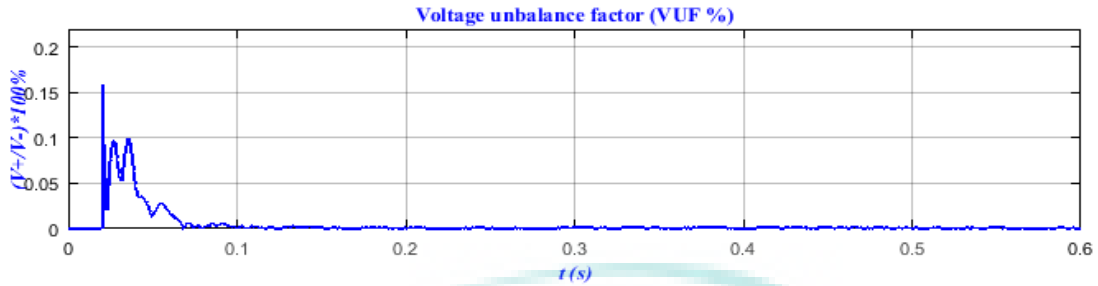
Figure 5.27   Voltage unbalance factor of the PVPP-connected grid at 500 W/m^2.

5.5   Dynamics of the GCPPP under Different Fault Conditions

In order to analyze the dynamics of the GCPPP throughout grid faults on the utility grid, the Simulink model is run under normal conditions (G=1000 W/m^2 and T=25°C) with different fault types, i.e., single line to ground (SLG) fault, line to line (LL) fault, line to line to ground (LLG) fault, and symmetrical three-phase (3-ph) fault at the power grid side. The fault duration is 0.1 s which occurred between 0.15 s and 0.25 s, and the fault resistance is equal to 1 Ω. The total simulation is done within 0.4 seconds. The main simulation results are listed in Table 5.1 and is shown in the Figures (6.28-6.31).

Table 5.1   Parmerters values of the PVPP during fault period (0.15–0.25s) at different types of faults.

Type of the Fault	PV array Output			VSI	Effective voltage (kV)			Effective current (A)			Voltage Dip level	Active Power (kW)	Grid Frequency (Hz)
	Voltage (V)	Current (A)	Power (kW)	dc-link voltage	V_a	V_b	V_c	I_a	I_b	I_c			
Steady state	799.5	1897	1502	800	28.1	28.2	28.1	40	40.2	40.1	0%	1474	50.01
(SLG) Fault	782.3	1815	1499	782	2.3	28.6	29.9	304	390	261	25%	1471	50.03
(LL) Fault	848.4	1666	1285	850	15.5	11.1	25.25	52.2	52	60.7	50%	1152	49.97
(LLG) Fault	875.7	1433	1042	875	2.76	2.67	30.04	195	271	209	60%	921	49.96
(3Ph) Fault	946.4	310.1	300	945.3	2.93	2.91	2.92	52.5	53	55	85%	231.7	49.87

The following figures depict the response and behavior comparison of three-phase photovoltaic system operation connected to the MV of the power grid (distribution levels) during different types of faults including non-symmetrical short circuit grid fault (unbalanced fault) and symmetrical grid faults (three-phase fault). The four different faults are simulated under the same conditions and time duration when the fault occurred on the grid side.

Figures (5.28-5.30) depict the PVPP operations when applying the unsymmetrical faults i.e., SLG fault on phase A with the ground, LL fault between phase A and B, and LLG fault on phase A and B in addition to the ground in the case where the fault duration is 10 ms.

Figure 5.28   The effect of SLG fault at PCC with 25% voltage drop: (a) positive sequences of the grid voltage; (b) grid voltage; (c) grid current; and (d) active and reactive power.

The results illustrated the effective values of grid voltage, current, and power as well as the voltage sag level during, before, and after the occurrence of the fault. On the other hand, Figure 5.31 shows the operations and the effects of the same items that are

tested under unsymmetrical fault at the same conditions in the case of occurrence of the most severe fault (3-ph fault).

Figure 5.29   The effect of LL fault at PCC with 50% voltage drop: (a) positive sequences of the grid voltage; (b) grid voltage; (c) grid current; and (d) active and reactive power.
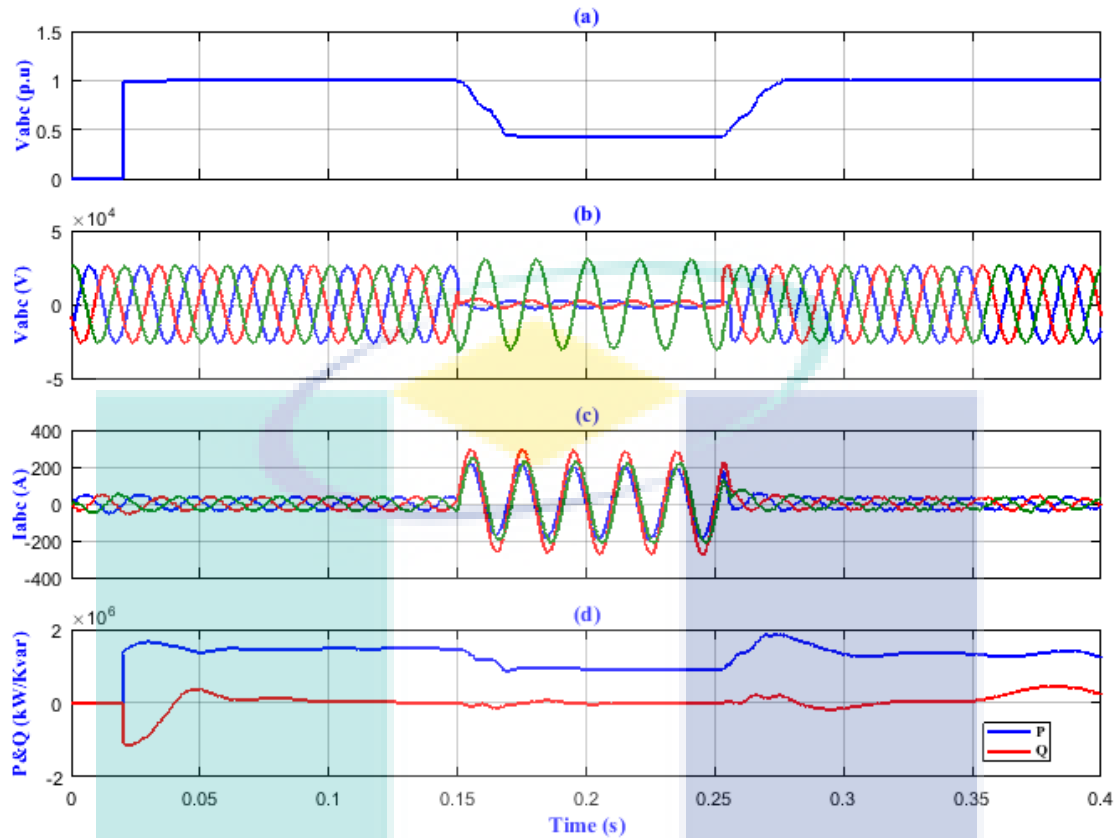
Figure 5.30   The effect of 2LG fault at PCC with 60% voltage drop: (a) positive sequences of the grid voltage; (b) grid voltage; (c) grid current; and (d) active and reactive power.

From the simulation results in Table 5.1 and Figures (5.28-5.31), it can be observed that the maximum deviation on ac current was through the SLG fault followed by 2LG fault. The lowest oscillation after a fault was within SLG fault, whereas the highest oscillation occurred after 3-ph fault. In case of SLG fault the dc-link voltage was very close to the actual value, followed by LL and LLG faults, respectively, while during the 3-ph fault, it was very far from its real value. The voltage sag level was maximum during 3-ph fault with 85%, while the minimum level was in the case of SLG fault with 25%. The maximum deviation of the voltage and power as well as in the system frequency happened during 3-ph fault occurrence. As a result, more disturbance occurred in the PV farm operation during the symmetrical fault, whereas the severity and disturbances caused by unsymmetrical fault ranked from the most dangerous to the less serious is LLG, then LL and finally SLG fault in accordance to the Simulink results.
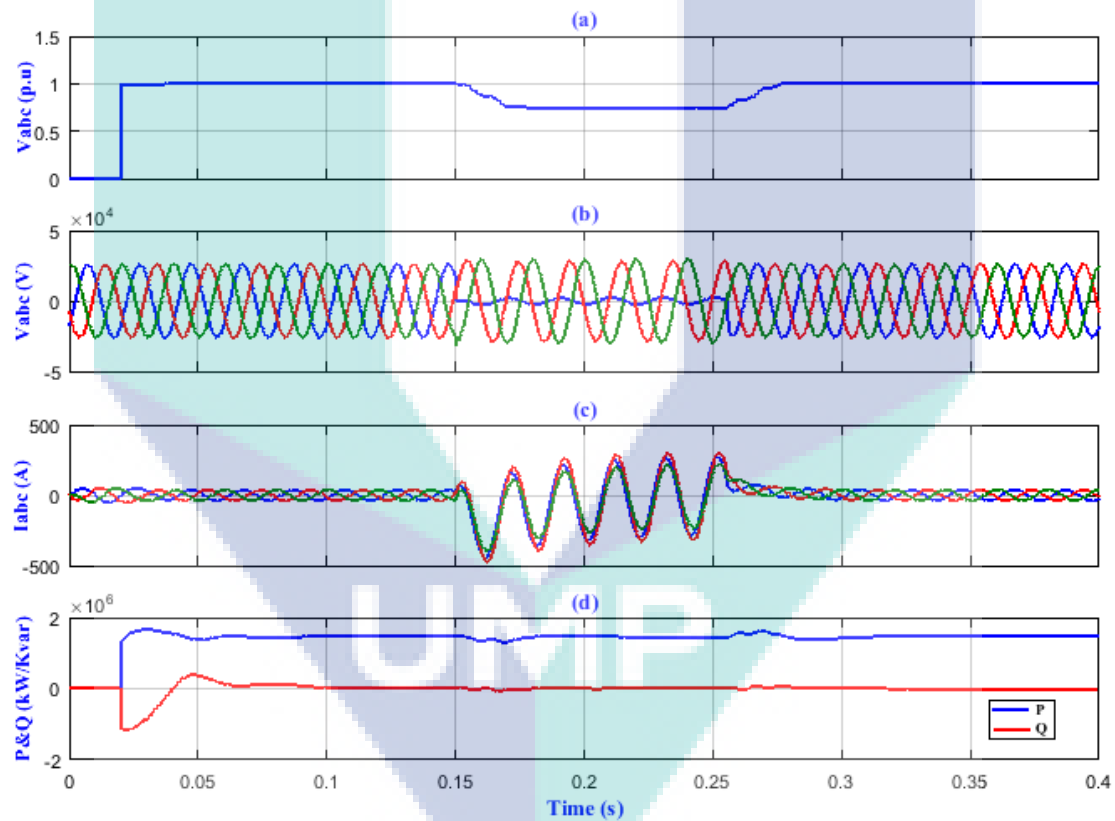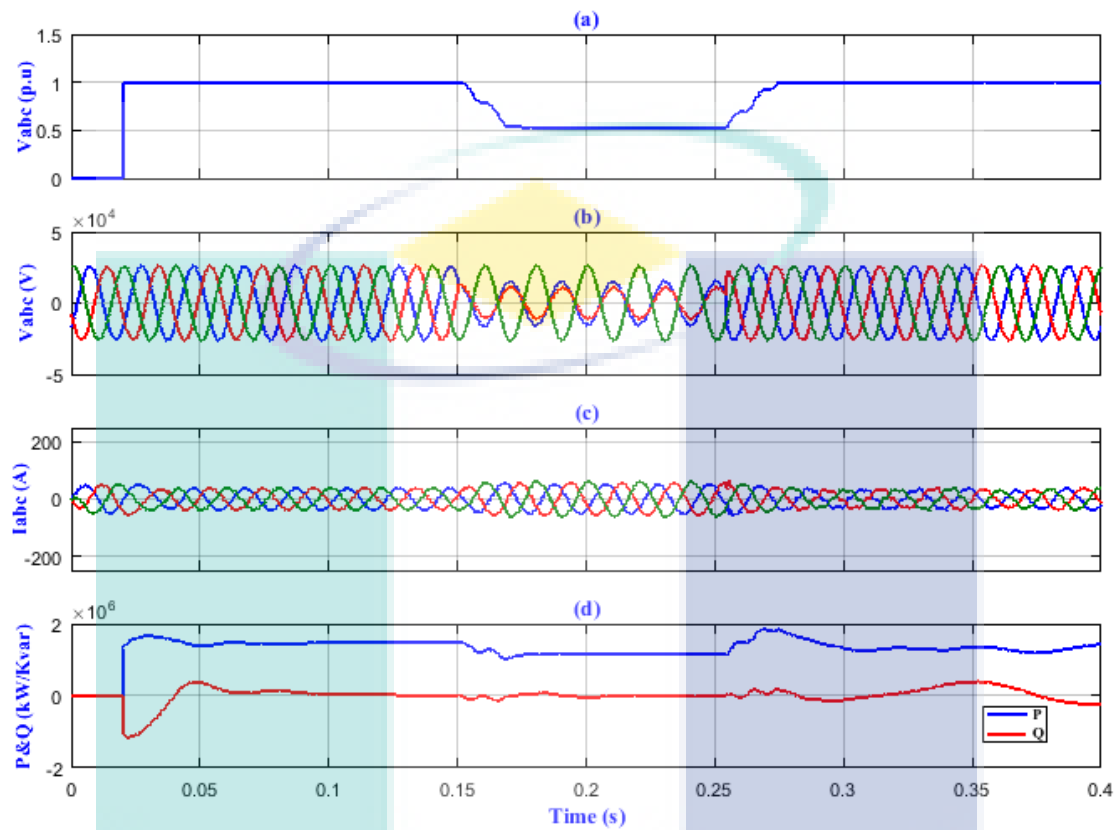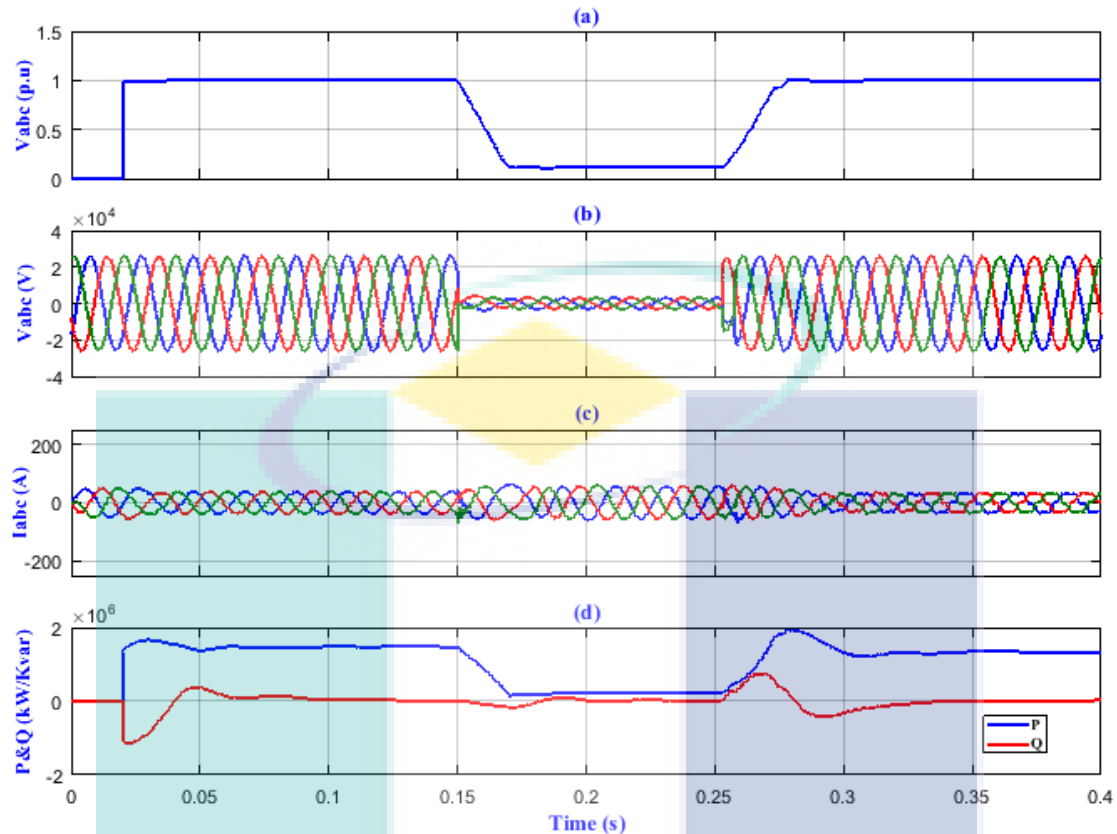
Figure 5.31   The effect of 3-ph fault at PCC with 85% voltage drop: (a) positive sequences of the grid voltage; (b) grid voltage; (c) grid current; and (d) active and reactive power.

In conclusion, the effect and behavior of the developed GCPPP dynamics results on the power system during different types of faults were like any other traditional plant and can be clearly seen when comparing with studies introduced in (Banu & Istrate, 2014; Seo, Kim, Yoon, & Jung, 2009a), in which the results are equivalent, especially the fault severity results.

5.6   Fault Ride-Through Capability Control for Inverter-Based Grid Connected Photovoltaic Power Plant

As described earlier in this thesis, fault ride-through capability is one of the challenges faced by the integration of large-scale photovoltaic power stations into electrical grid which has not been fully investigated. Therefore, this section presents the results of the comprehensive control strategy of PVPP to enhance the FRT capability based on the standards requirements and modern grid codes connection rules. The complete PVPP model shown in Figure 5.1 which is used to test the proposed FRT control

strategy has been established using Matlab/Simulink. The system is connected to the medium voltage level with nominal voltage of 33 kV and therefore the nominal current is 45.4 A (1p.u). The instantaneous values of current and voltage are measured at the PCC. In order to meet the proposed FRT requirements and other GCs standard, the developed control effectively overcomes the issues of over-current and over-voltage whereby it keeps the inverter connected and ride-through the grid faults safely, and then inject the required amount of reactive power as described in detailed in Chapter 4. The following figures show the results of the inverter FRT with dynamic voltage support (DVS) that injects an amount of reactive current during the voltage sag according to the standard requirements described, after guaranteeing that the inverter stay connected and protected from both ac over-current and dc-over voltage. It is worth to mention that all tests have been done at standard test condition (STC). The irradiation, G, is 1000 W/m^2 and the temperature, T, is 25 ºC.

The first problem addressed by the proposed control was the excessive ac-current on the ac side of the inverter using current limiter. Commercially, it is known that the PV inverter has a maximum acceptable output current at the grid side which is higher than the rated current value. This value should not be exceeded. For test purposes, as an example of grid voltage sag, a single-line-to-ground (SLG) fault occurs at the MV side of the transformer for 0.15 s time duration (according to FRT graph) as shown in Figure 5.32 is generated.
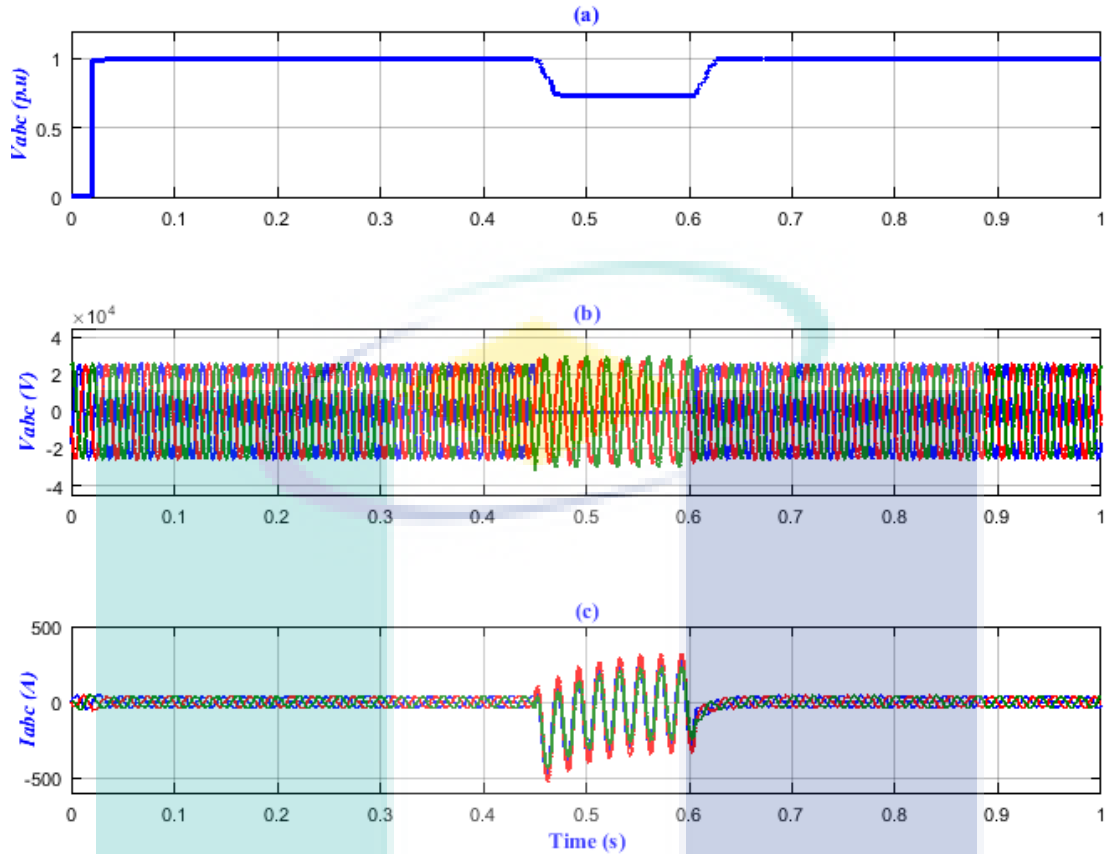
Figure 5.32   Simulation response of the PVPP with 70% voltage sag (SLG) and 30% voltage drop without current limiter: (a) positive sequence of grid voltage; (b) grid voltage; and (c) grid current.

It is obvious that the output current illustrated in Figure 5.32(c) exceeds the limits of maximum acceptable currents since it is higher than the rated current. This will lead the inverter to be disconnected from the grid, in spite of the fact that the disconnection is not applied in this simulation. To solve this issue, the proposed control applied the current limiter controller illustrated in Figure 4.6 which is used to limit the d-components of the current to an acceptable value within the required limits. Consequently, the final active reference current (output of the limiter) will be restricted considering the need for reactive current injection. As result of that, the grid currents are balanced as seen in Figure 5.33(c) as opposed to Figure 5.32(c), which illustrated the grid currents before using the current limiter. It is worthy to mention that, when working with low sun radiation or little voltage sags, the active current reference may not be limited and it goes through the limiter accordingly without being influenced.

118
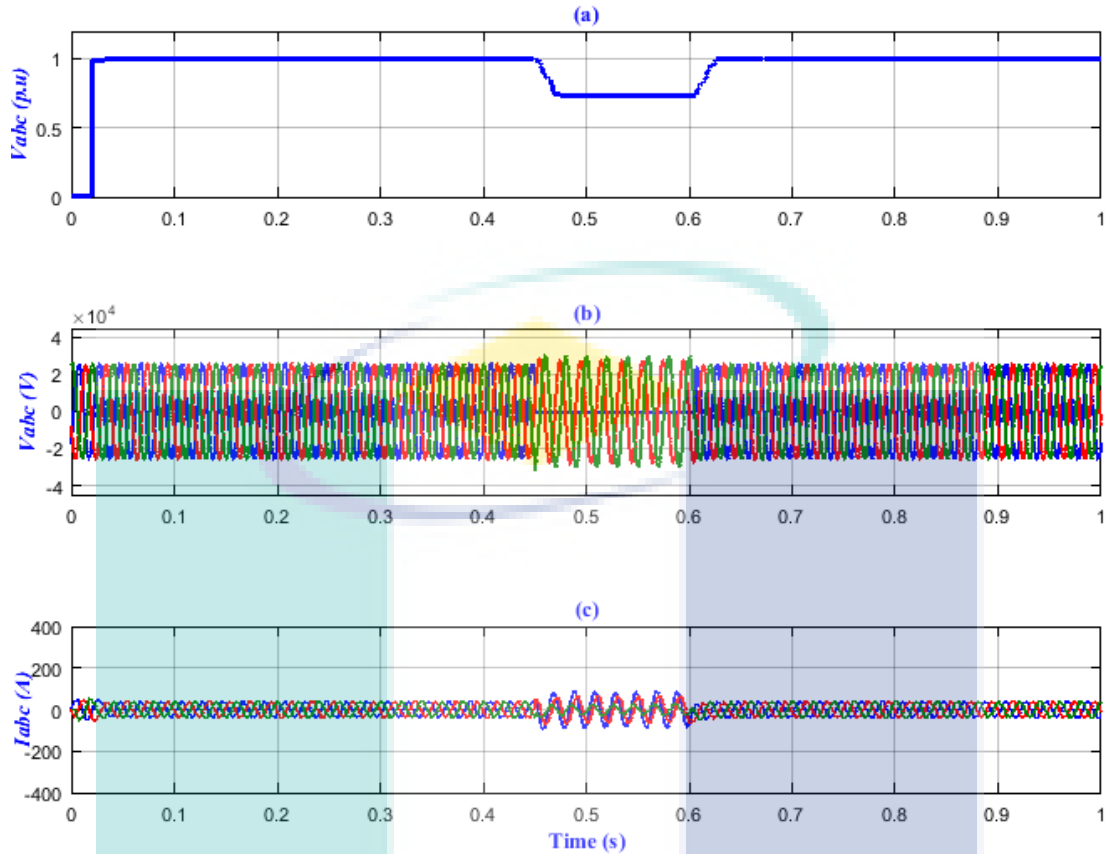
Figure 5.33　　Simulation response of the PVPP when applying 70% (SLG) voltage sag and 30% voltage drop with adding current limiter: (a) positive sequence of grid voltage; (b) grid voltage; and (c) grid current.

Next, the problem of excessive dc-voltage appeared in the dc side of the inverter during the fault was addressed using the circuit breaker controller shown in Figure 4.8. The increasing of dc-link voltage leads the maximum operating point of the PV array curve to go towards the open circuit voltage (V_{oc}) which in turn leads the array output current to decrease, as illustrated by Figure 4.7 and is proven by the simulation shown in Figure 5.34. Additionally, the deviation of MPP during voltage sag is also noticed. On the other hand, when the voltage sag is being cleared, the values of dc-link voltage, PV array current and voltage, and output power take a long time to come to the pre-fault values, as illustrated in Figure 5.34(b-d) at t=0.6s. To overcome the significant increase of dc-link voltage which causes these problems and to protect the inverter from being damaged or disconnected by over-voltage protection, the dc-chopper circuit protection scheme described in Section 4.5.3 has been used.
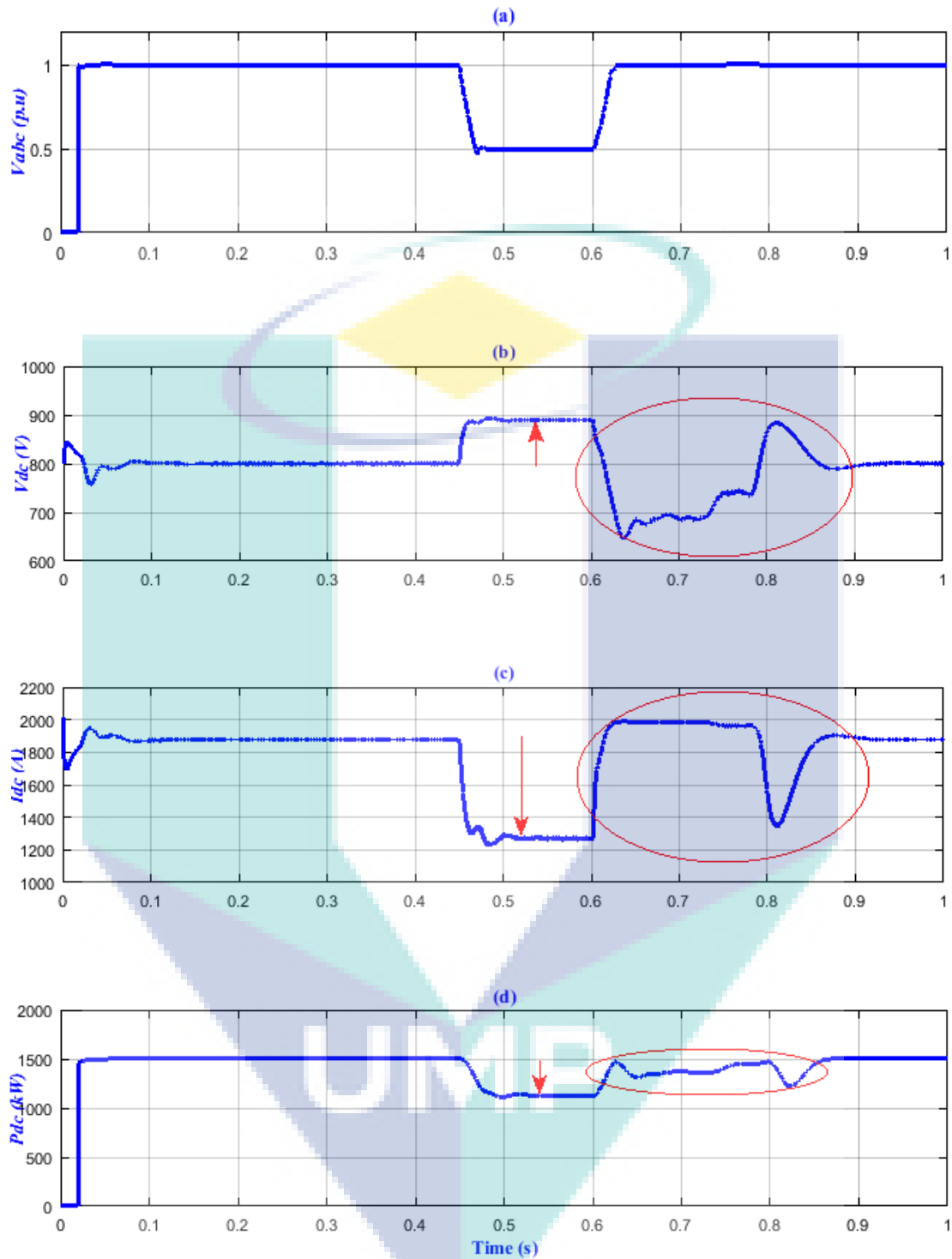
Figure 5.34   Simulation response of the PVPP with 50% three-phase voltage sag without dc chopper FRT: (a) grid voltage; (b) dc-link voltage; (c) PV array current; and (d) PV array output power.

Figure 5.35 shows the results when applying the dc-chopper circuit technique. Therefore, the effectiveness of the proposed scheme is proven by overcoming the dc-link over-voltage during fault time (0.45-0.6) s. Meanwhile, all magnitudes of the parameters

reach the pre-fault values immediately after fault clearance (after t=0.6s) as shown clearly in Figure 5.35 (a-c) as compared with Figure 5.34 (b-d) before using dc-chopper break.
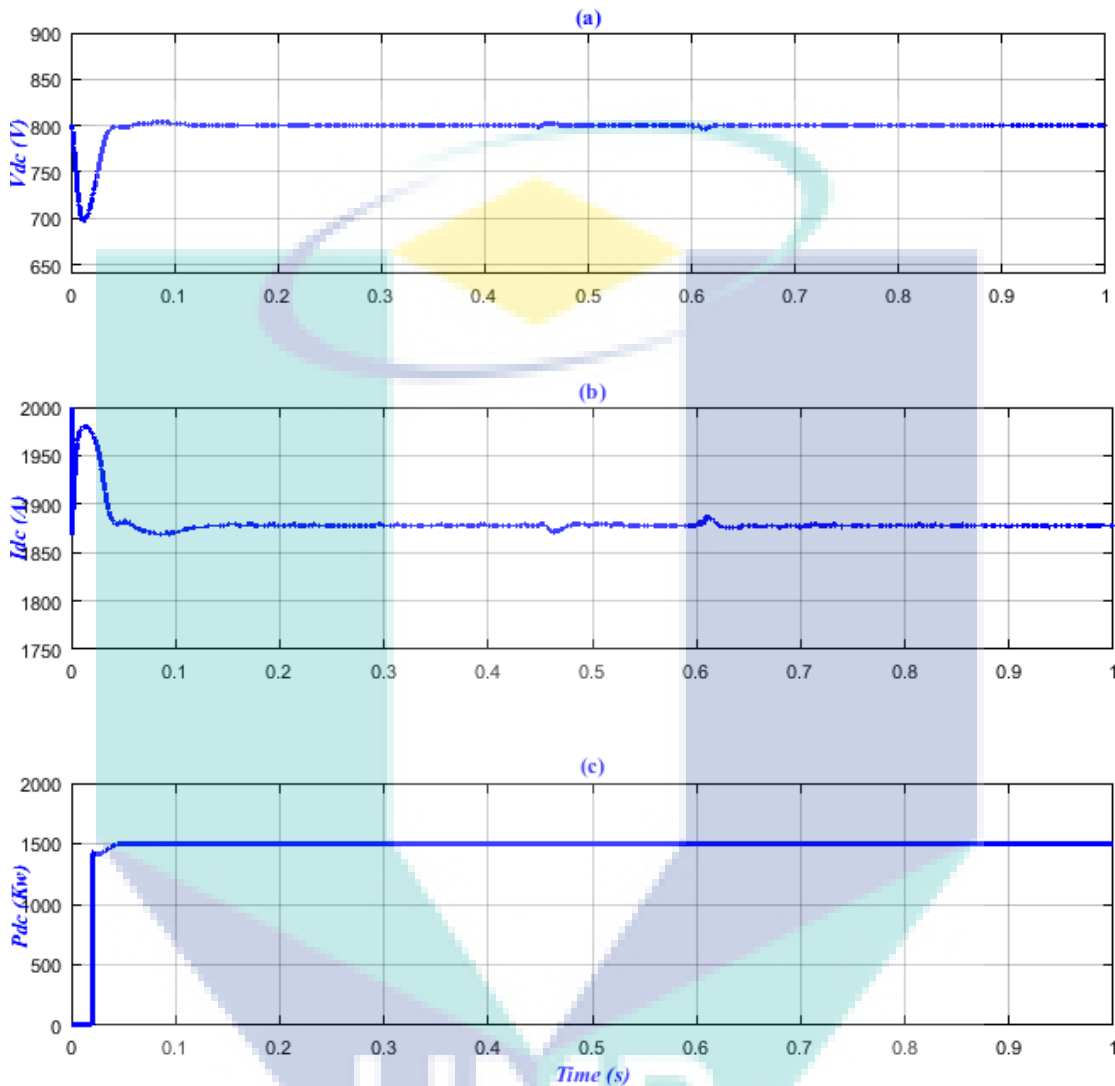
Figure 5.35   Simulation response of the PVPP with 50% three-phase voltage sag with applying of dc chopper control: (a) dc-link voltage; (b) PV array current; and (c) PV array output power.

Finally, the following figures display the reactive current injection strategy results of the proposed control test for different voltage sag scenarios and different time. In Figure 5.36, an unsymmetrical single line to ground fault leads the voltage of the affected phase at PCC to drop to 70% within 150 ms is illustrated. So, during fault time (0.45-0.6) s and based on the equations (4.8-4.10) the PV system should provide the grid with an amount of active and reactive current equivalent to 0.8 p.u and 0.6 p.u, respectively. Hence, reactive power injection during this time will support the voltage recovery. Once the voltage sag is cleared, active current, reactive current and other values back to pre-

fault values. From the figures, it is evident that, all conditions at fault period are stable, so that the inverter can withstand the fault and inject the required amount of reactive power even for a longer period of time.

Figure 5.36   Simulation results of a LVRT control strategy with an unsymmetrical SLG fault when the voltage drop by 30% from the nominal voltage in the affected phase (voltage sag 70%) for 150 ms.

Figure 5.37 describes the performance of a symmetrical three-phase fault with the worst case of voltage sag when the voltage drop is higher than 50%. In this case, the

residual voltage is only 15% of the nominal voltage. However, the FRT standard requires to provide 100% reactive current into the grid. Hereby, the inverter stays connected and support the grid with 100% (1 p.u) reactive current using the proposed method, whilst the active power is zero. This case is proved by simulation results as shown in Figure 5.37.

Figure 5.37   Simulation results of a LVRT control strategy with a symmetrical 3-phase fault when the voltage drop by 85% from the nominal voltage (voltage sag 15%) for 150 ms.

The situation in Figure 5.38 illustrates the performance in case of unsymmetrical line to line (LL) grid fault happened with 92% voltage sag within 150 ms duration. Since

the voltage is still in the dead band (from 0.9 p.u to 1.1 p.u), the voltage at the affected phases is higher than 90% of the nominal voltage ($V_{pg} > 09 V_{gn}$) and therefore, the inverter should stay connected without the injection of any reactive power. Additionally, the production of active power should stay at full generation according to the weather conditions. From the figure, it is evident that, the voltage sag is detected, but the inverter is not supporting any amount of reactive power and is kept connected until the ride-through of the fault duration according to the standard requirements.

Figure 5.39 shows the response of the inverter LVRT control strategy when an unsymmetrical two-line to ground (2LG) fault occurred with voltage dropping to 60% from its nominal value for 625 ms (duration as per the proposed Malaysian FRT and different GC requirements such as US-PREPA, China, and Romania (Cabrera-Tobar et al., 2016). So, according to the LVRT requirements shown in Figure 4.9 and equations (4.8-4.12), with voltage sag of 40%, the inverter should support 100% (1p.u) reactive current. From the figures, it is evident that the inverter supported the grid with the required value of reactive current. Since 100% reactive current is injected into the grid, the active current is zero, resulting in zero active power. When a balanced three-phase voltage sag (70%) occurred at the grid side for 625 ms, it causes the voltage to drop to 30% of its nominal value. In this case, the simulation results are shown in Figure 5.40. It can be seen that when the fault is detected at t = 0.2 s, the inverter injected the required amount of active and reactive power according to the standard requirements. As a conclusion, the results show the ability of the proposed inverter LVRT control to support the grid and voltage recovery by producing reactive power at different types of faults.
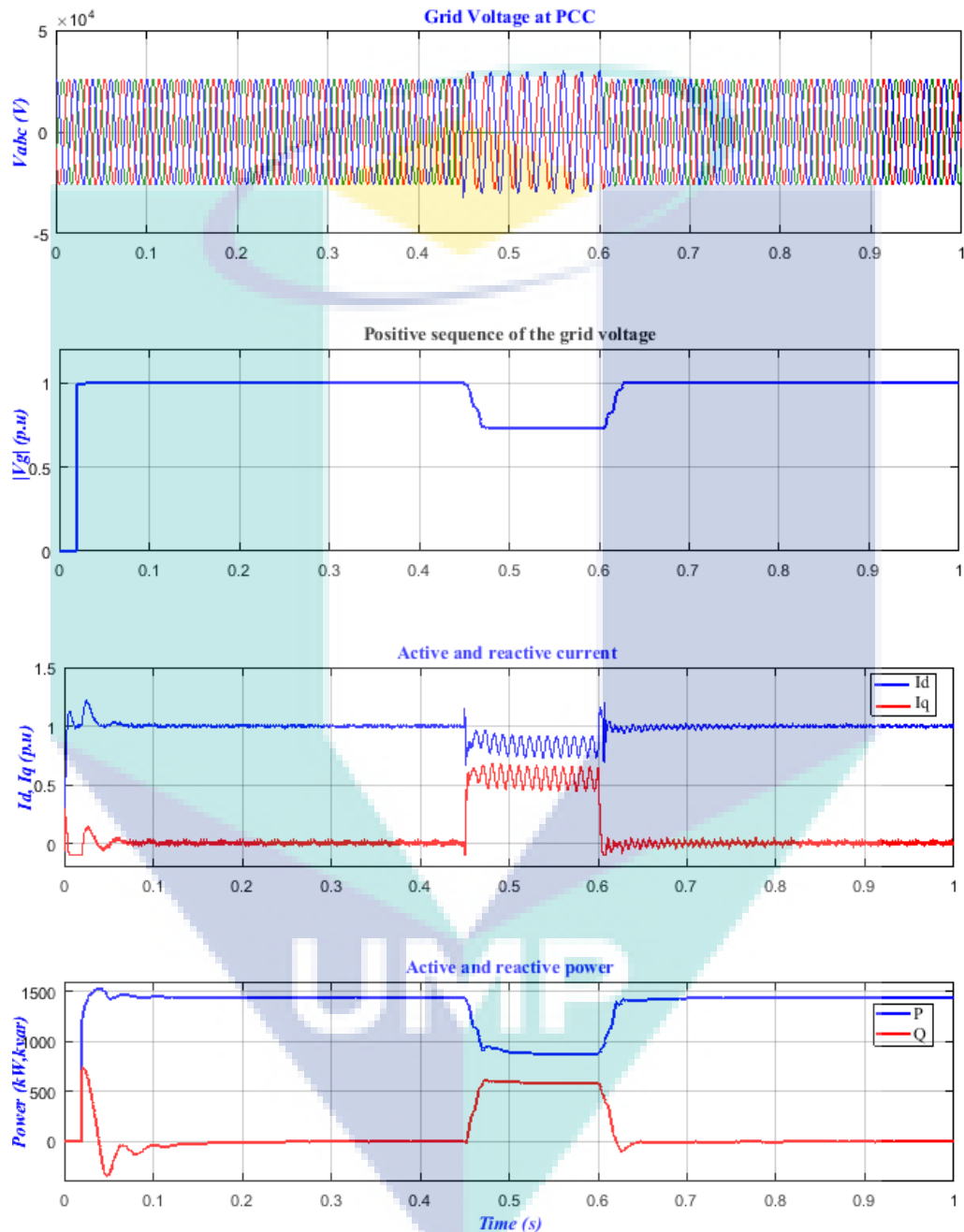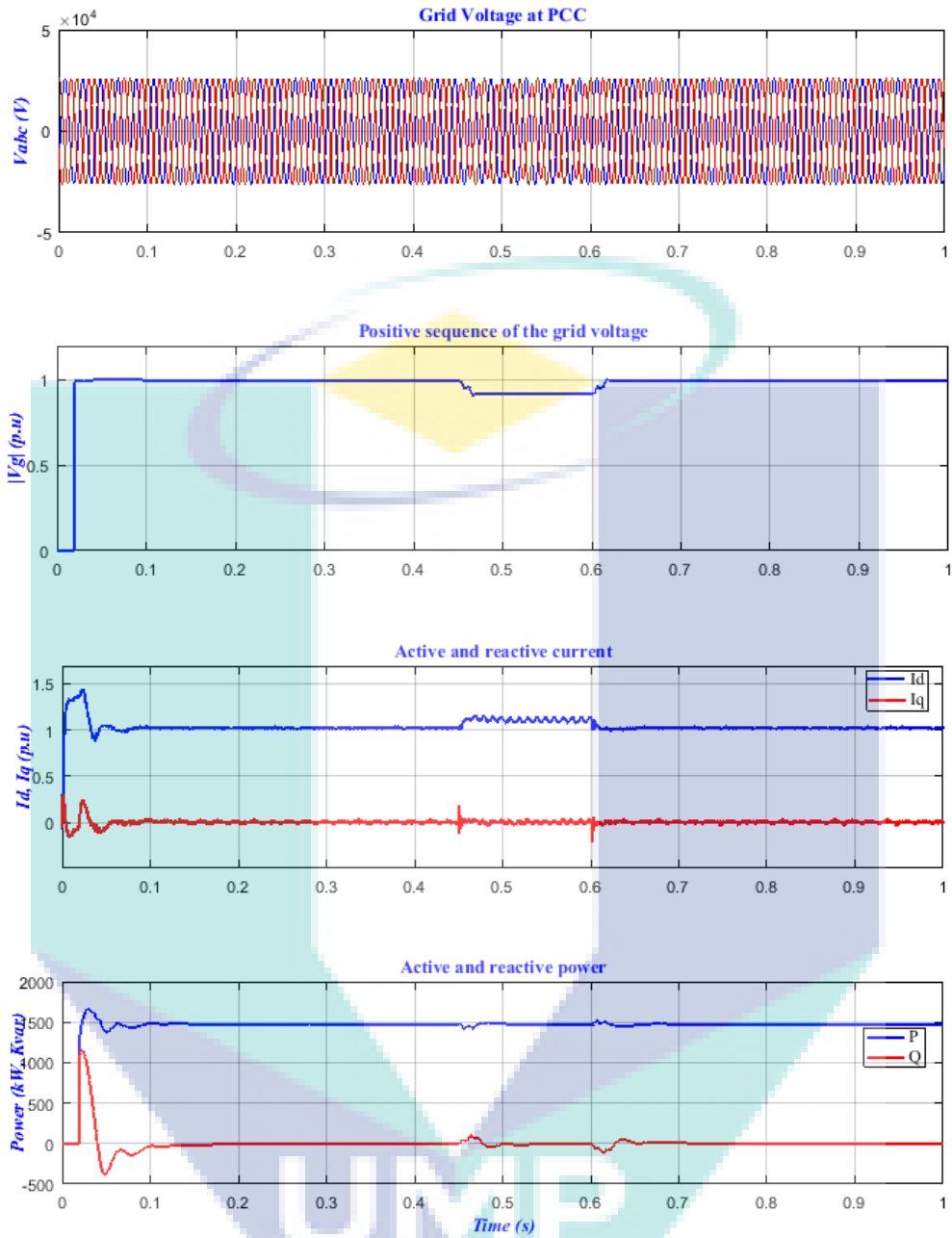
Figure 5.38   Simulation results of a LVRT control strategy with an unsymmetrical LL fault when the voltage drop by 8% from the nominal voltage in the affected phases (voltage sag 92%) for 150 ms.
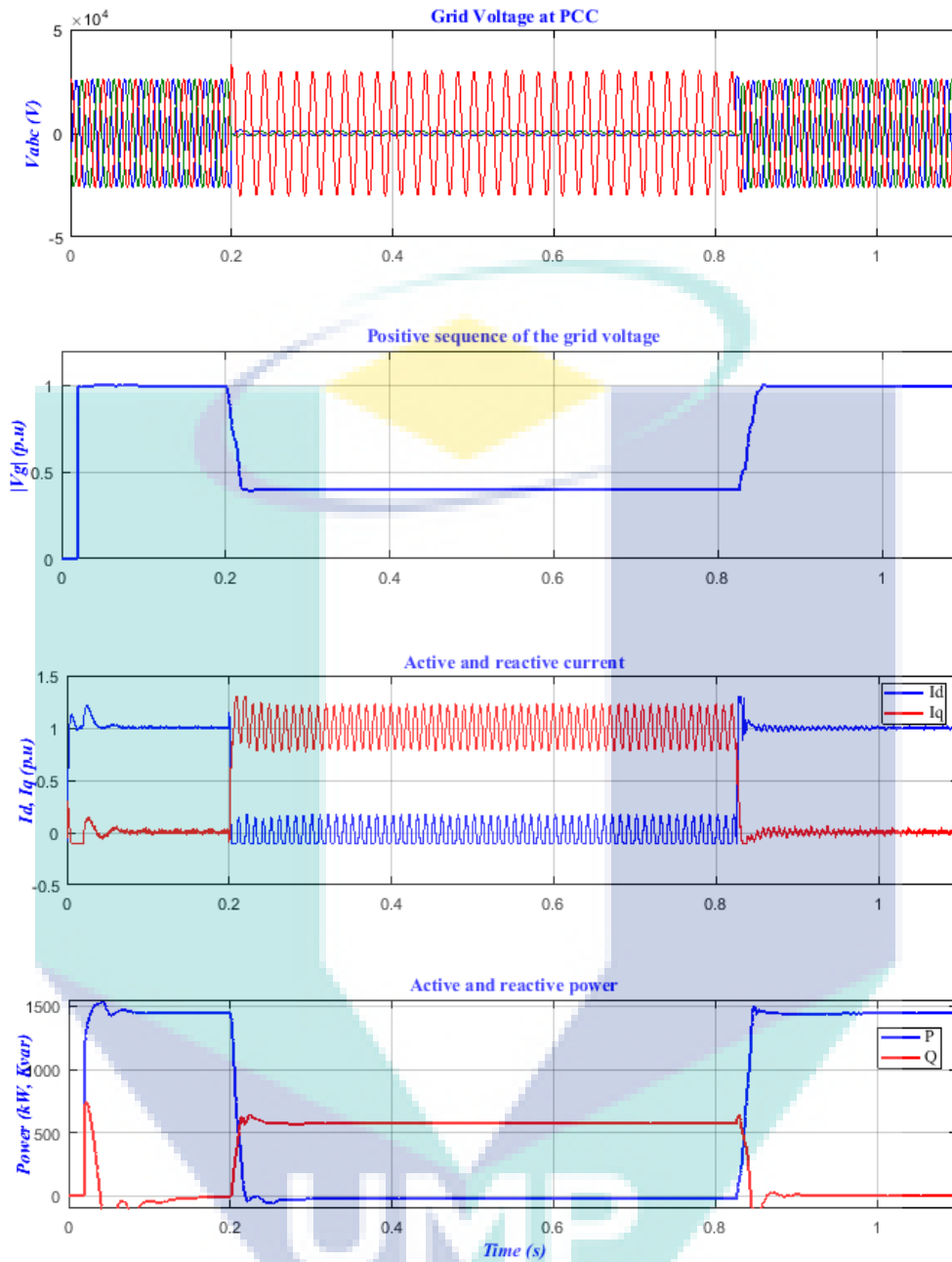
Figure 5.39   Simulation results of a LVRT control strategy with an unsymmetrical 2LG fault when the voltage drop by 60% from the nominal voltage in the affected phases (voltage sag 40%) for 625 ms.
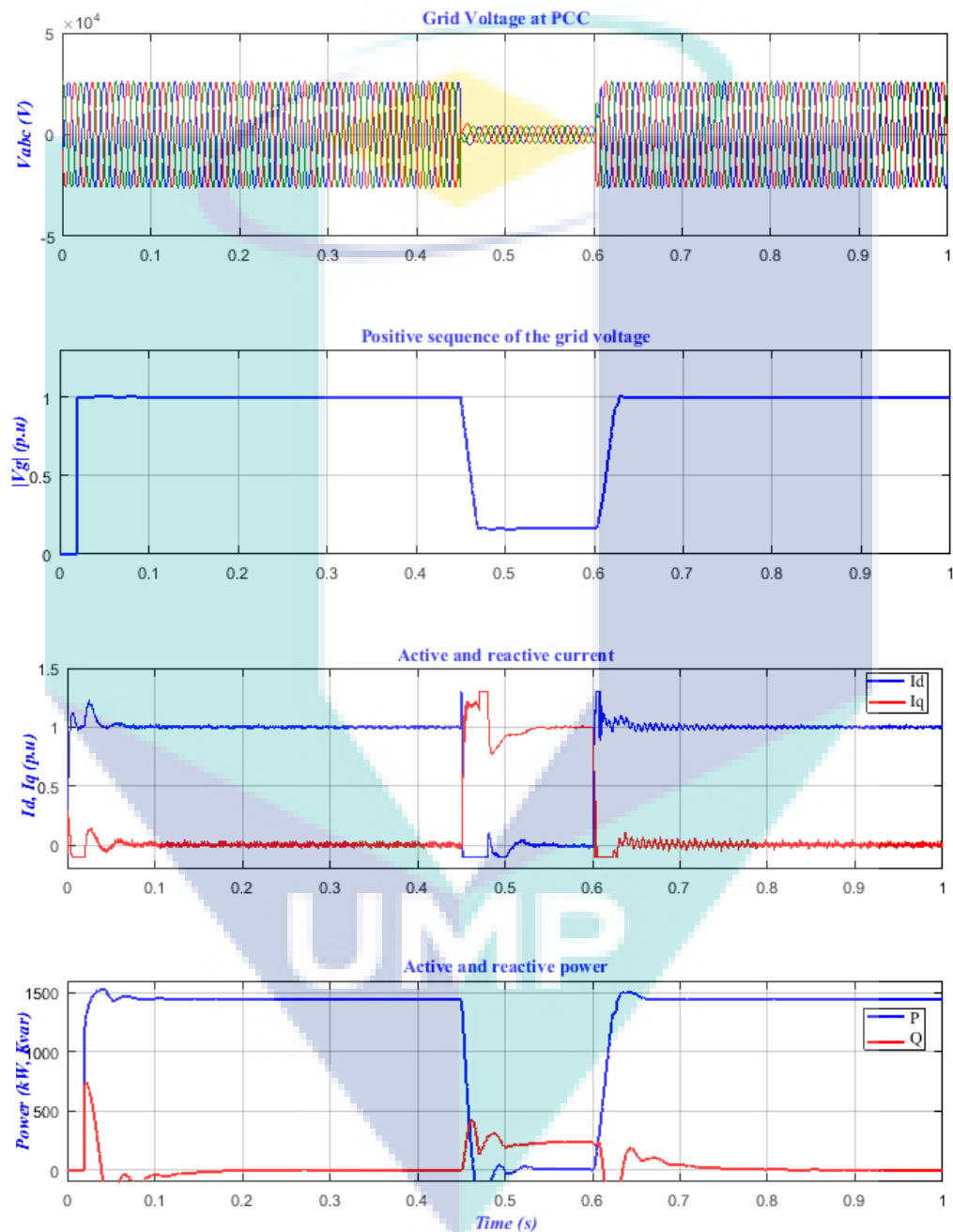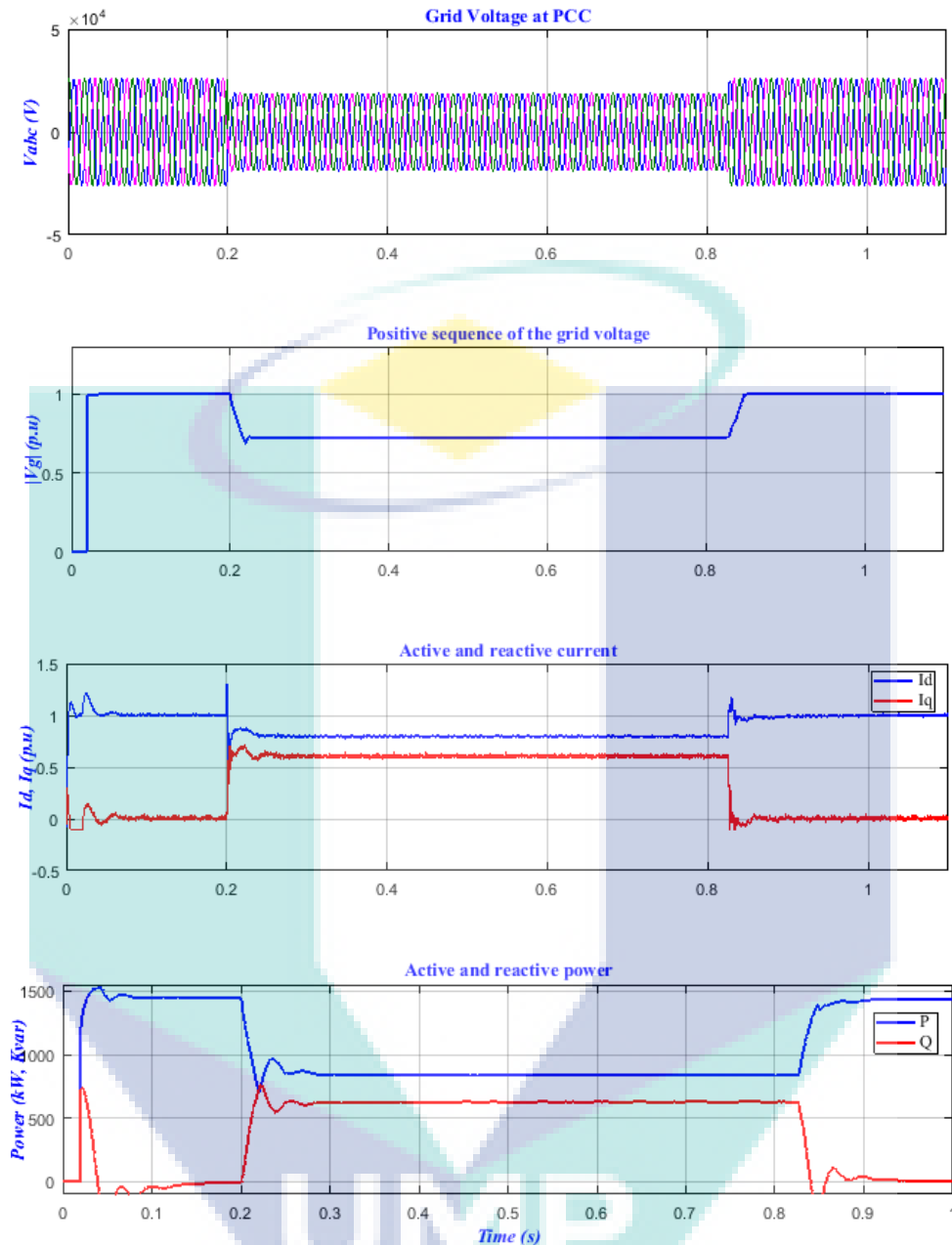
Figure 5.40   Simulation results of a LVRT control strategy with a symmetrical 3- phase fault when the voltage drop by 30% from the nominal voltage (voltage sag 70%) for 625 ms.

In general, as an example of the effectiveness of the overall FRT controller, the three-phase fault with 50% voltage drop of the nominal value is tested to illustrate the system parameter values and settling time before and after using the controller, as can be seen in Table 5.2. The simulation results of the comparison at: (*a*) steady state operation (Figure 5.41); (*b*) without FRT controller (Figure 5.42); and (*c*) with the developed FRT controller (Figure 5.43) and its parameters illustrated in the table, it is clearly that the values of dc voltage (V_{dc}), current (I_{dc}), and power (P_{dc}) as well as grid current (I_g) have

values near to the pre fault values as soon as the fault is cleared. This is because of the use of protection scheme consist of dc-chopper and current limiter, respectively. The values of active current (I_d), reactive current (I_q), power and reactive power (*P&Q*) fulfilled exactly the standard requirements of FRT as described in detail in Section 4.5.4. It is important to mention that the settling time after fault with the proposed controller is almost zero second when compared to the one without the controller (0.25s), and this is a very important feature to help the grid recovery after faults.

Table 5.2   GCPPPs parameter values with and without FRT controller.

(3-ph) Fault	V_{dc} (V)	I_{dc} (A)	P_{dc} (W)	I_g (A)	I_d (p.u)	I_q (p.u)	P (kW)	Q (kVA)	Settling time (s)
Steady-state values	799.5	1897	1515	40	1	0	1474	0	-
Without FRT	900	1250	1140	60	1.5	-0.2	1080	0.2	0.25
With FRT	800	1881	1504	42	0	1	0	750	0.01
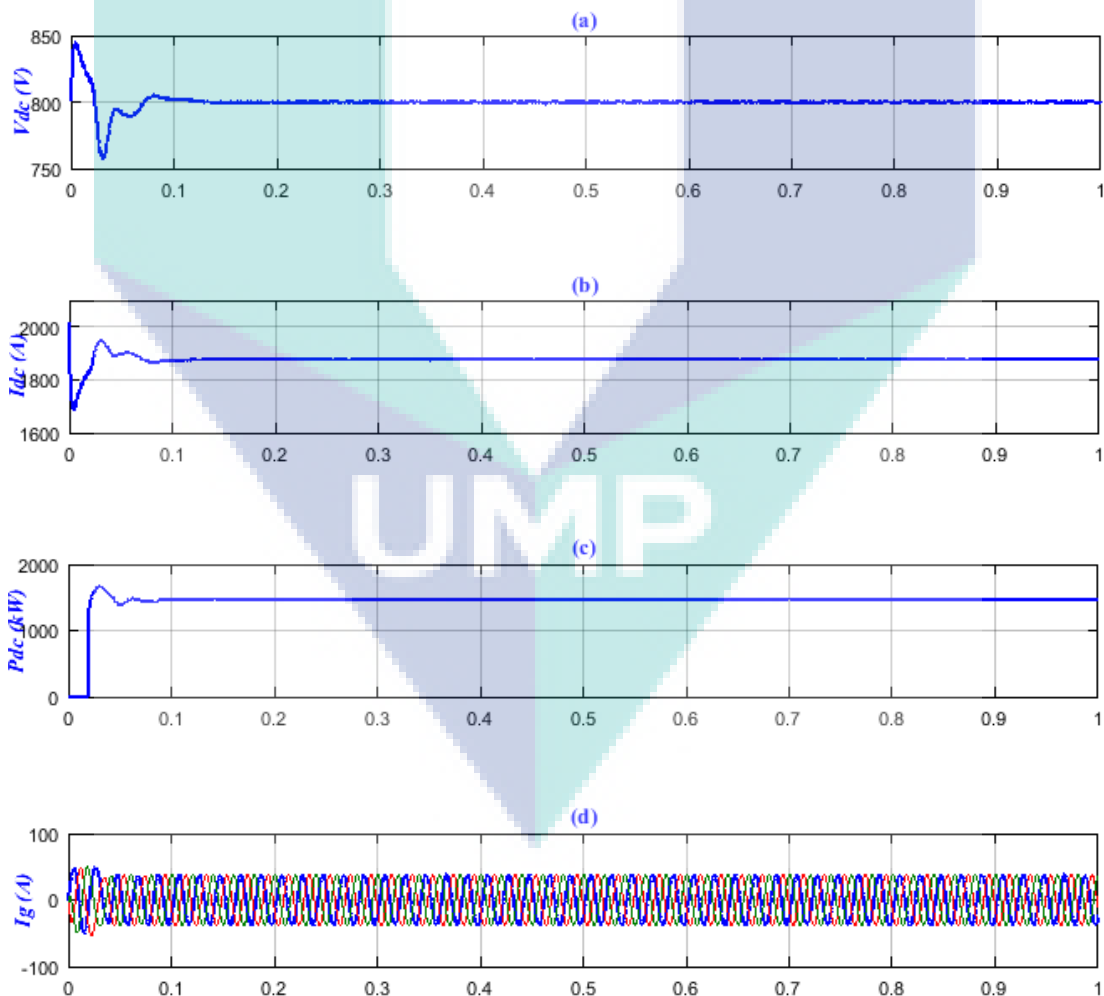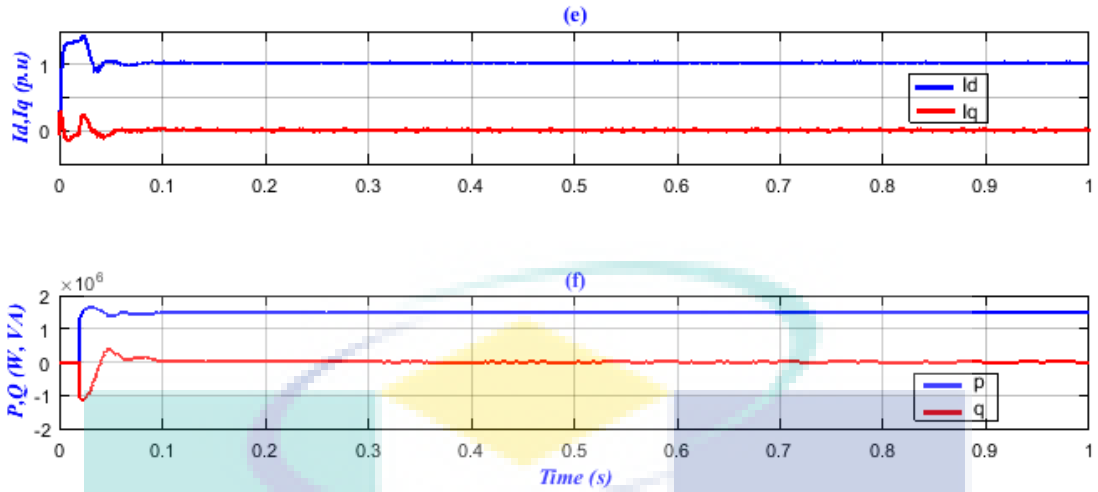
Figure 5.41   GCPPP parameters at steady state condition: (a) PV array voltage; (b) PV array current; (c) PV array output power; (d) grid current; (e) active and reactive current; and (f) active and reactive power.
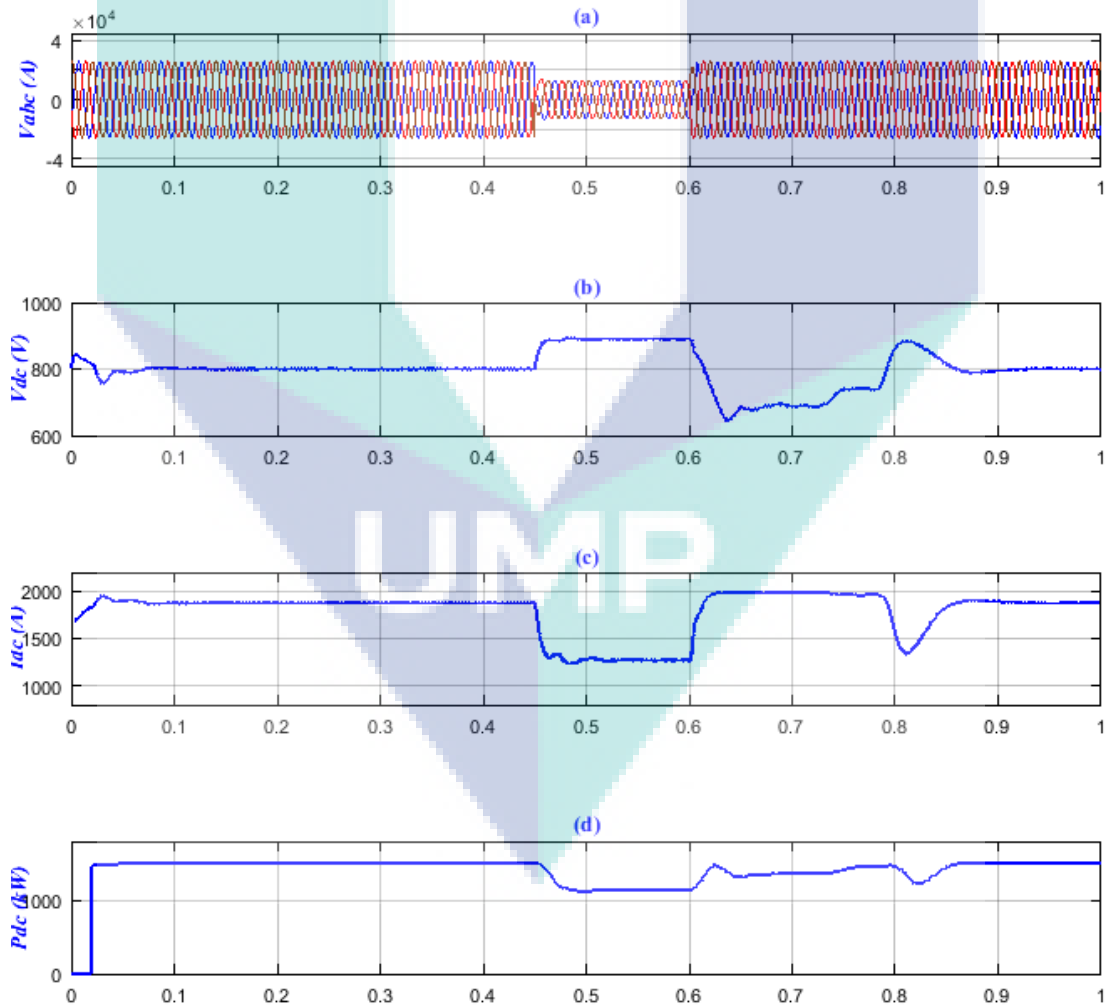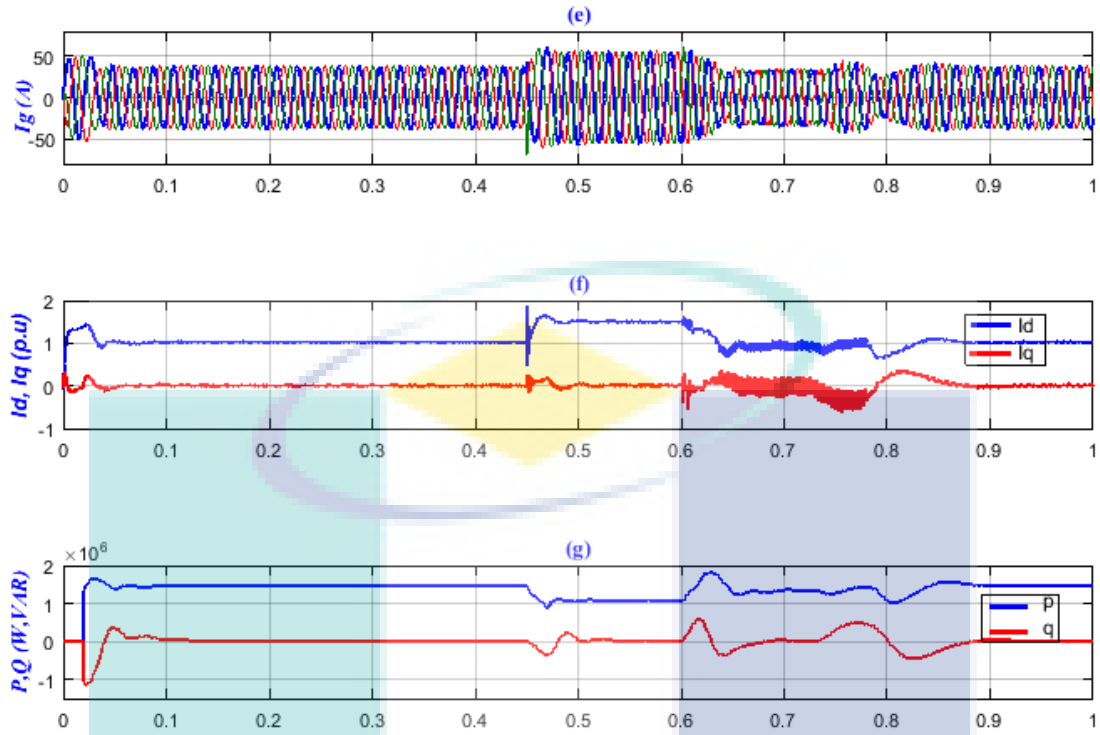
Figure 5.42   GCPPPs at the occurrence of 3-ph faults (50% sag) without FRT controller: (a) grid voltage; (b) PV array voltage; (c) PV array current; ; (d) PV array output power; (e) grid current; (f) active and reactive current; and (g) active and reactive power.
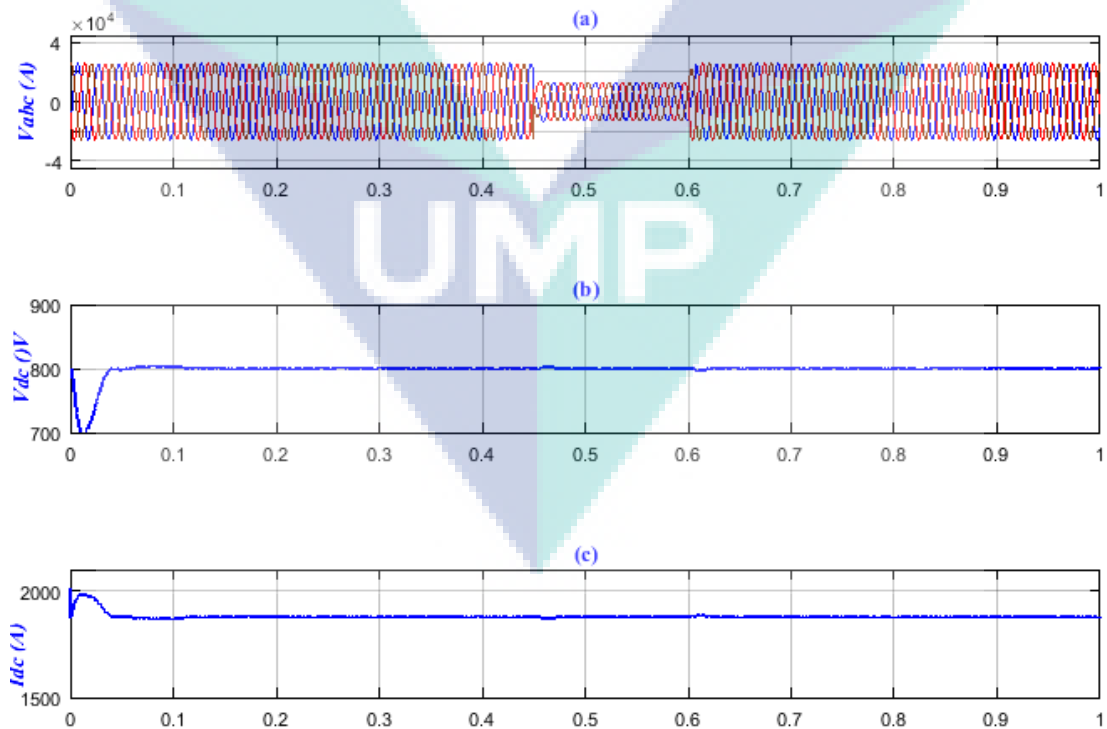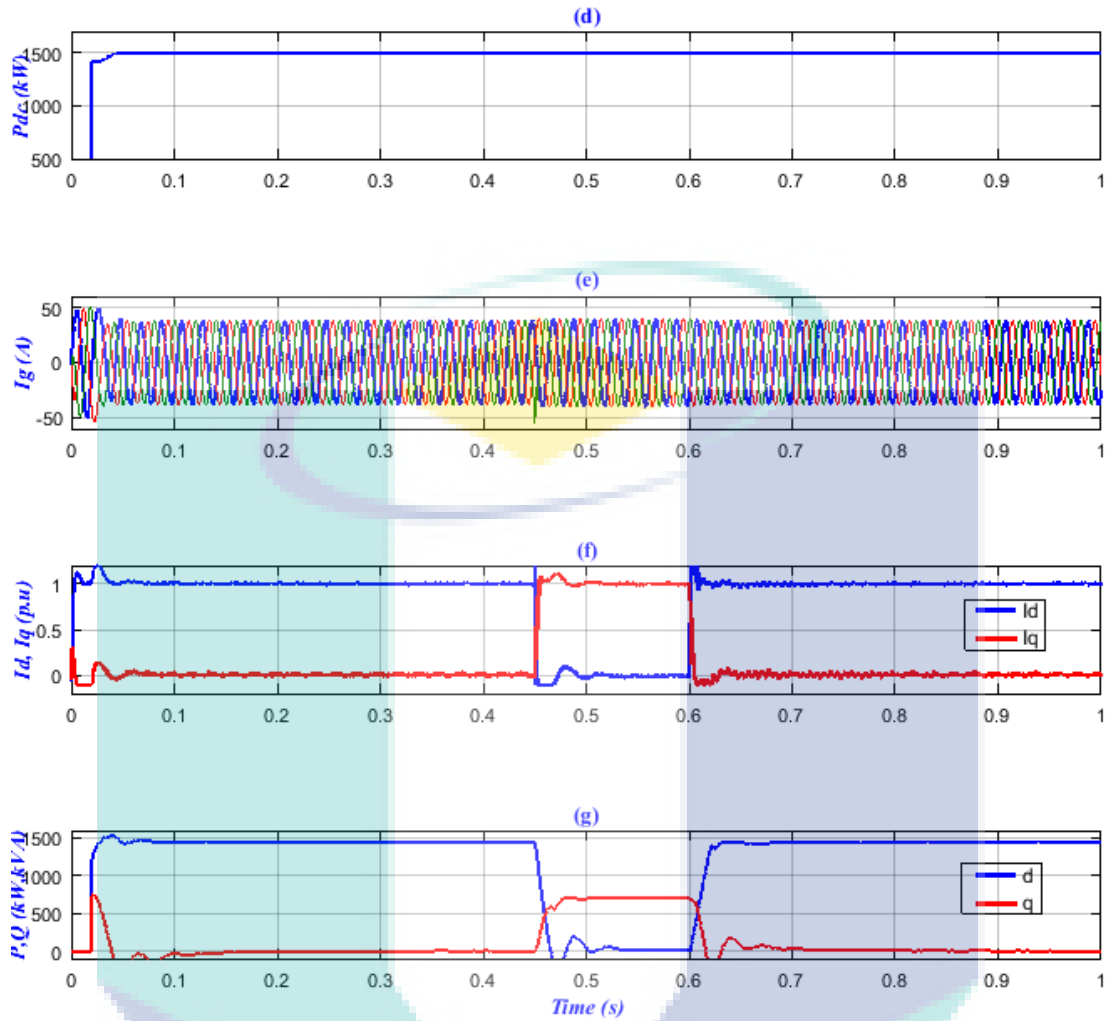
Figure 5.43   GCPPPs at the occurrence of 3-ph faults (50% sag) with FRT controller:
(a) grid voltage; (b) PV array voltage; (c) PV array current; (d) PV array output power;
(e) grid current; (f) active and reactive current; and (g) active and reactive power.

5.7   Results Comparison

This section introduces the consistency of the above results with other previous studies introduced in the literature. Some studies have been used energy storage devices which are installed in the GCPPPs to offer an ancillary service, such as active power balance and protect the inverter throughout the period of grid faults until ride-through the faults smoothly. Energy storage functions using supercapacitor that was proposed by (Kim et al., 2013; Worku & Abido, 2015), considers as one of the FRT strategies. The study introduced by (Worku & Abido, 2015) used the supercapacitor energy storage system (SCESS) control during the fault to overcome the problem of dc-link only, while excessive ac current and injection of reactive current imposed by some grid codes to support the grid and voltage recovery have not been addressed. By comparing the results

of SCESS control with this study results, it can be concluded that the proposed control has addressed the problem of excessive dc voltage successfully while all values returned to pre-fault values as soon as the fault is cleared, as seen clearly in Figure 5.44 as compared to Figure 5.35.
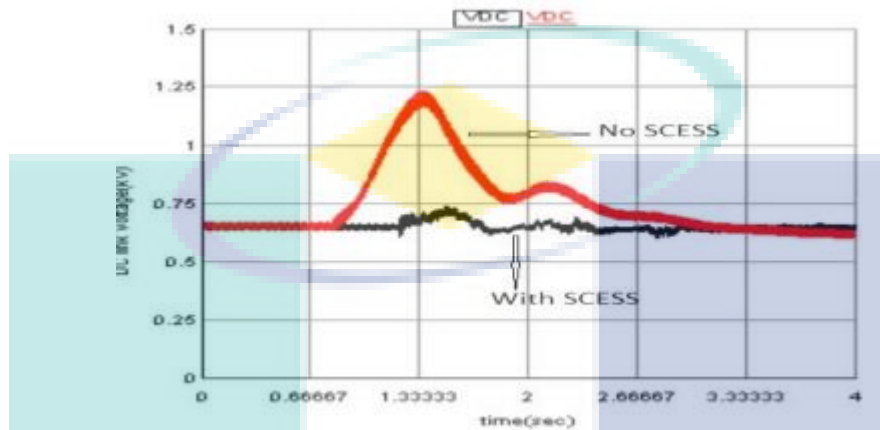
Figure 5.44   Simulation results of the SCESS control.
Source: Worku & Abido (2015).

Similarly, the batteries energy storage devices control introduced by (K. Li et al., 2015; Manikanta et al., 2017) was utilized to store the energy during the fault in order to address the over-voltage of the dc-link. The control that was proposed by (Manikanta et al., 2017) utilize the bidirectional dc-dc converter which is connected to the batteries. So, it will be in off mode during normal operation, while during the faults, the dc-link voltage is going beyond the limits specified, the controller detects this issue and activate the buck mode of bidirectional dc-dc converter to send more charge available at the dc-link to charge the battery. On the other hand, if the voltage across the dc-link is decreased to a value lower than required voltage, then the controller activates the bidirectional dc-dc converter in boost mode and the dc-link receives charged from battery. In the same manner, the study is seconded by (K. Li et al., 2015). In this study, a method of dc voltage control is adopted. Therefore, during the period of LVRT, the duty cycle of the boost circuit is adjusted to reduce the output power of the PV battery in order to restrain the dc side voltage. The behavior of these two methods is shown in Figure 5.45. It can be noted that, in comparison with the method proposed in this thesis, the (K. Li et al., 2015) dc voltage control results are similar to the proposed method, although there are some fluctuation and overshooting at the beginning and end of grid fault, but the strategy control proposed by (Manikanta et al., 2017) addressed only very high dc-link voltage.

On the other hand, a few increasing of dc-link voltage still exist and this will cause power imbalance between the both sides of the inverter.
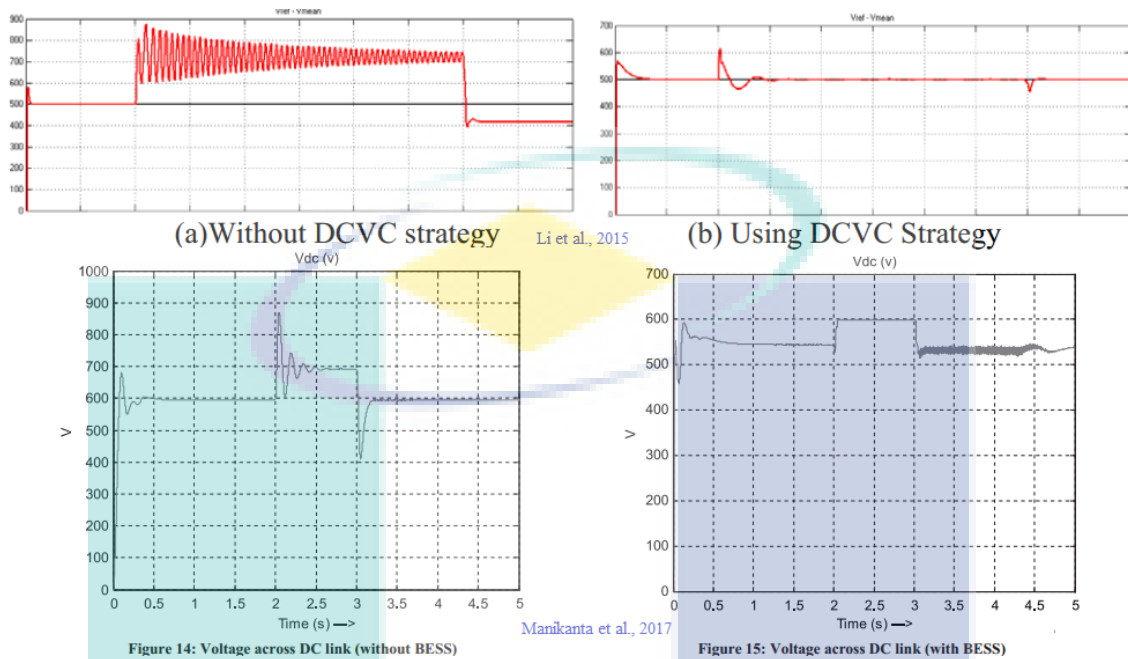
Figure 5.45   The FRT results proposed by K. Li et al.(2015) and Manikanta et al. (2017).

Although the results were compared above using energy storage methods solved the excessive dc-voltage with different efficiency, all these studies do not address excessive ac current in the ac-side as well as the injection of reactive current to support the grid and voltage recovery during grid faults which are imposed by some of grid codes. However, this type of technique is hard to be extensively applied in the industry because of the high investment price and short lifestyles cycle of energy storage units. Despite most of the above studies focused on ride-through the fault by protecting the inverter during a grid fault, a few studies dealt with reactive current injections which is the most and recent capability enforced by some grid codes. When comparing the proposed study in this thesis with the study introduced by (L. Yang et al., 2016) which used the coordination between the PV system inverter and the STATCOM to deal with the grid faults. It can be noticed that the STATCOM inject the required reactive current to support the voltage recovery during the fault. Although STATCOM is effective to inject reactive current according to the standard requirements as observed in Figure 5.46, this method has not addressed the high ac-current and increasing dc-link voltage during grid faults. In addition, it increases the complexity and cost due to adding an external hardware to the system and does not deal with inverter protection.
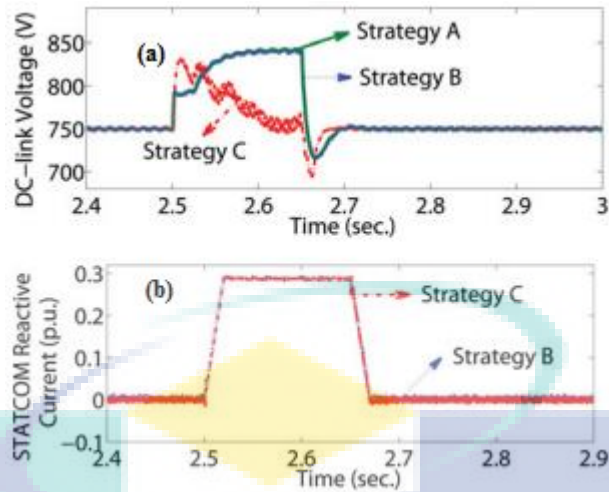
Figure 5.46   The response of using STATCOM device for LVRT when the voltage at PCC drops to 15% for 625ms: (a)dc-link Voltage, and (b)injected RC by STATCOM.
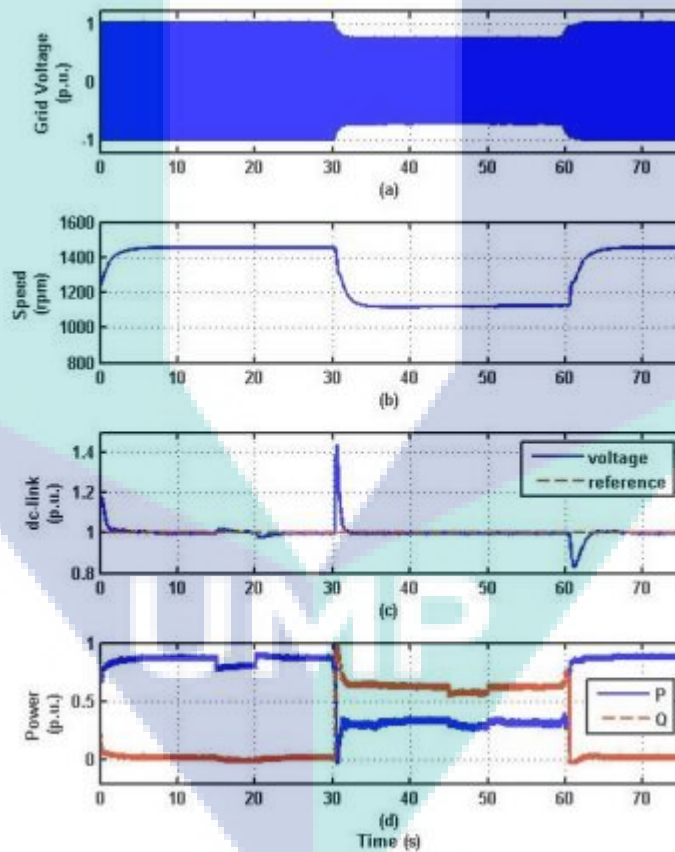
Figure 5.47   Simulation results of a LVRT control strategy (a) grid voltage, (b) speed of the wind, (c) Voltage of the dc-link, and (d) the injected active and reactive power.

Source: Merabet & Labib (2017).

On the other hand, the method applied the FRT controller using the inverter itself as the method proposed in this thesis without extra hardware is the control of grid tied wind energy conversion system with LVRT capability proposed by (Merabet & Labib,

134

2017). The study proposed two modes of operation during normal operation and grid faults. During grid faults, the regulation of dc-link voltage was controlled by the dc-dc converter while the injection of reactive and active current is achieved by the inverter control to meet the requirements of new grid codes. The simulation results presented addressed the excessive dc-link voltage to enhance the FRT capability as well as mitigate voltage sag by a ride-through the grid fault safely with reactive current injection to support the grid during faults, as seen in Figure 5.47. As a conclusion, the results of the proposed FRT control method in this thesis is compatible with the GC requirements, which is an important indicator for the results' verification. In addition, as compared to other methods, this method not only effectively suppresses the ac over-current as well as the dc-link over-voltage and protect the inverter during the voltage sag, but also to provide grid support through active and reactive power control at all types of faults. Furthermore, once the fault is cleared, all values are recovered to pre-fault values directly.

5.8   Summary

In view of the above discussion, this research presents an overall new control strategy for single-stage three-phase-PVPP connected to the electrical power grid in the faulty mode of operation to ride-through the fault and support the grid based on the proposed Malaysian LVRT requirements and other GCs. The results prove that the comprehensive control strategy enables the PVPP to withstand grid faults, to allow the inverter to remain connected, to continuously produce electricity, and to absorb excessive energy while injecting the required reactive power under various types of fault to meet the modern GCs' standard requirements. Furthermore, once the fault is cleared, all values are recovered to pre-fault values directly. The simulation results are presented to validate the performance of the proposed control strategy. This chapter also shows the results of designing and modeling of PVPP that are used to apply the proposed FRT control. The results show that the proposed PVPP is compatible with TNB requirements. The dynamic behaviors of the PVPP under all types of grid faults, and the results of modeling, design, and simulation of the PV array and GCPPPs parts have been provided. It can be summarized that the future PVPPs can offer some ancillary services for the grid during abnormal conditions like conventional power plants. The conclusion and future work in addition to recommendations will be provided in the next chapter.

CHAPTER 6

CONCLUSION

6.1   Introduction

Dwindling industrial costs and increasing efficiency of the PV module together with the features of PV system has led to the rise of PV power plants (PVPPs) connection to the power system. The integration of these PVPPs can have a major effect on the utility grid and has led to strict requirements enforced by the grid codes (GCs). It requires the PVPPs to stay linked at the connection point for the duration of grid faults and assist the grid with a reactive power injection. This thesis presented a detailed design and development of the fault-ride through (FRT) capability using the inverter control for an electrical power grid integrated large-scale PVPP taking in consideration TNB technical regulation. Therefore, under abnormal situations, the proposed strategies had been developed to keep the connectivity of the PVPPs under voltage sag situations, protect the inverter, and assist the grid with reactive power injection as required by the GCs that is known as FRT capability requirement. Additionally, after fault clearance, all values return to pre-fault values to enhance the system recovery and stability. This chapter presents the main conclusion of the research as well as the recommendations for future work.

6.2   Conclusions

With an ever-increasing PVPPs penetration into utility grids, some of GCs impose FRT requirements in order to ensure the secure, reliable, and economic operation of the power system. On the basis of FRT requirements, this research presented the potential operation of a large-scale three-phase PVPP connected to the power grid under grid faults to fulfil these requirements. Therefore, the inverter is developed to operate in two modes of operations which are steady state operation mode and abnormal or FRT operation mode. When voltage sag occurs, the control strategy proposed some modifications to

enable the PVPP to ride-through all types of grid faults according to proposed FRT requirements as well as different GCs and countries, as the changes are typically only in the depth and duration of the voltage sag. These adjustments include fault detection unit in order to inform the control to convert from normal operation mode into a faulty mode of operation. Then, the control developed dc chopper brake circuit and current limiter, which efficiently protects the system from over-voltage and -current, respectively, and also improves the FRT capability. The proposed control is effective when the system is switched to grid fault operation mode by enabling the PVPP to continue electricity production and suppress excessive energy. In addition, once the fault is cleared, all values are reset to the pre-fault values and ride through the fault smoothly. This control also achieved a very important feature imposed by some GCs for enhancing the FRT capability via injecting reactive current to support power grid and voltage recovery. As a consequence, the developed GCPPP offer ancillary capability during and after fault period. The ancillary capability consists of the FRT and reactive power control. These ancillary services can doubtlessly prevent fault cascading event which can lead to major problems, enhance the recovery process from the fault event, and improve the power system stability

As a result, the validity of the proposed control to perform the transient behavior, protect the semiconductor device, and ride through voltage sag has been demonstrated by the simulation results. In spite of the fact that the performance is dependent on the control strategy and detection method, the proposed control methods show excellent performance concerning sag detection, keep the connectivity of the inverter, protect the system from both over-voltage and over-current, and injected the required amount of reactive power to support voltage recovery until ride-through different types of voltage sag safely, which is proven by various case studies performed by simulations.

In order to apply the FRT capability control based on the proposed Malaysian FRT and standard requirements, the design and develop of large-scale PVPP integrated to the grid according to the standards concerning the penetration of PV system to the medium and low voltage network has been achieved. Thus, a complete GCPPP including, modulation of the solar module was done and presented based on the fundamental circuit equation of PV module, PV array design and sizing, MPPT strategy is utilized to ensure that the solar energy is captured and converted as much as possible, self-commuted VSI

topology which is preferred for MV connection, suitable inverter control, RL filter for harmonic mitigation and PLL for synchronization purposes were carried out using Simulink. The PVPP has been built and connected to the distribution system of the grid in accordance to the TNB interconnection method via a step up transformer to ensure that its regulation has been tested and validated. In addition, the dynamics of the proposed PVPP when the fault occurred at the grid side has been tested, and found that the symmetrical fault has a higher impact on the grid-connected PV system operation than non-symmetrical faults. The outcomes of this test show that the PV system output relies on the type of the fault and this is so consistent with previous studies. In general, the developed model satisfies the requirements and its environment became a suitable for adding FRT control without compromising the safety, stability and normal operational issues of the power system. Additionally, it can help the development of Malaysian standards regarding PV integration to the power system and promote application of grid-connected PV system.

6.3   Attainment of research objectives

This section describes the attainment of the research that support the completion of research goals. The general research objective was addressed by completing four specific research objectives. An overview of these objectives as well as a summary of contribution, achievement and how they were addressed are given in a point-by-point manner for every objective as follows:

i.   The design of comprehensive large-scale model of grid connected-PVPP is achieved in which the theoretical calculation and sizing results matched the simulation results. In addition, the PVPP is designed to be compatible with TNB technical regulations concerning the PV penetration into the utility grid. These regulations including the PV-grid connection method, PV inverter type, nominal voltage operating range within 5% were achieved. Furthermore, the total harmonic distortion of voltage and current has been decreased to less than 5%. The design of appropriate filter and increasing the switching frequency lead the current and voltage THD decreased from 9.2% and 2.8% into 0.74% and 0.15%, respectively. The voltage unbalance also did not exceed the required limits (1%) and achieved 0.2% at PCC. The power factor was a unity which is higher than 0.9 imposed by the standards. Finally, the frequency fluctuation was within $\pm$ 0.1 Hz

and $\pm$ 0.2 Hz during steady-state and faults events, respectively which is a computable with the frequency standard given.

ii.   The FRT requirement has been proposed as new requirement of the Malaysian grid code. Based on the literature, the FRT capability available for all countries obtained and compared. The most suitable FRT capability for Malaysia is the US FRT requirements. In addition, this research developed the inverter control to operate at two modes. These modes are the steady-state and FRT operation modes. In order to convert from steady-state into FRT mode during the fault, the fast and precise RMS detection method is developed. As a result, once the fault is occurred, the inverter has to switch to the FRT mode and inject the required amount of reactive current depending in the depth of voltage sag as imposed by the standards requirements. The decoupling strategy is used to decuple the active and reactive current and calculate the required amount of injected active and reactive current into the grid automatically based on the fault type. At this time, the feed-forward strategy is used also for smooth fluctuation of the dc-link voltage. In sum, the injection of reactive current was achieved and therefore support the grid and voltage recovery without using extra hardware.

iii. This research developed a protection method addressing the over-current, and over-voltage that occurs during the faults. Once the fault occurred, the dc-chopper circuit and current limiter is developed to overcome these two issues, respectively. Therefore, ensure the inverter connectivity as well as protect it and other semiconductor devices from damage. The effectiveness of dc-chopper shown by absorbing the excessive dc voltage via switching on the IGBT and allow the chopper resistor to absorb the excessive voltage during grid faults period. Moreover, the current limiter restrains the ac current to be with the required limits. As result, the excessive dc-voltage and ac-current was limited and permits to the power, voltage and current to recover speedily to per-fault values as soon as the fault is clear without time delay. Furthermore, permits the inverter to inject the reactive current without being disconnected.

iv.   The results illustrate that the overall proposed FRT control strategy is effective, not only to improve the capability of ride-through faults safely and keep the inverter connected, but also to provide grid support through active and reactive

power control at different type of faults based on the FRT standard requirements. In addition, ensure the safety of the system equipment and ensure all values return to pre-fault values as soon as the fault is cleared within almost zero second as compared to the strategy without FRT control which needs around 0.25 s.

6.4 Future Recommendations

Some recommendations for future work that can be done are listed in this section:

i. Over the recent days, the distribution generators such as PVPPs have been replacing the power system conventional generators slowly. Therefore, in this stage, the next generation of PV inverter should be provided with FRT capability control, as has been achieved in this thesis. In this regard, it is recommended that, in addition to FRT, the next generation of the PV inverter may be provided by the active power control through frequency control. Thus, during grid disturbances, the PVPP has to activate frequency control to prevent the frequency from large deviation by decreasing the amount of active power output injected into the grid, like traditional generating plants.

ii. The studies may be extended considering the FRT control performance with different power converters, different inverter control techniques, and different current controls, such as H^{∞} and model predictive control also may be developed, tested, and compared with this research in the future.

iii. As described in this research, the FRT requirements differ from country to another. Thus, this difference has led to the inefficiency and extra costs imposed on PVPPs manufacturers and PV system developers. As a result, the global harmonization of these rules is recommended in order to assist the developers of PV system as well as PV manufacturer to achieve the required balance between the cost and the international standards.

REFERENCES

Abdul Kadir, A. F., Khatib, T., & Elmenreich, W. (2014). Integrating photovoltaic systems in power system: power quality impacts and optimal planning challenges. *International Journal of Photoenergy, 2014*.

Abu-Jasser, A. (2010). A stand-alone photovoltaic system, case study: a residence in Gaza. *Journal of Applied Sciences in Environmental Sanitation, 5*(1), 81-91.

AEMC. (2015). Template for Generator Compliance Programs Review 2015. Retrieved 20-June, 2017, from http://www.aemc.gov.au/Markets-Reviews-Advice

Afshari, E., Farhangi, B., Yang, Y., & Farhangi, S. (2017). *A low-voltage ride-through control strategy for three-phase grid-connected PV systems.* Paper presented at the Power and Energy Conference at Illinois (PECI), 2017 IEEE.

Ahmad, S., Ab Kadir, M. Z. A., & Shafie, S. (2011). Current perspective of the renewable energy development in Malaysia. *Renewable and Sustainable Energy Reviews, 15*(2), 897-904.

Akorede, M. F. (2012). *Enhancing the solar energy potential in malaysia using the concentrated photovoltaic (CPV) technology.* Paper presented at the Planet under Pressure 2012 Conferences.

Australian Energy Market Commission (AEMC). (2016). National Electricity Rules Version 80. Retrieved 12-Jun, 2017, from http://www.aemc.gov.au/Energy-Rules/National-electricity-rules/Rules/National-Electricity-Rules-Version-80

Ayub, M., Gan, C. K., & Kadir, A. F. A. (2014). *The impact of grid-connected PV systems on Harmonic Distortion.* Paper presented at the Innovative Smart Grid Technologies-Asia (ISGT Asia), 2014 IEEE.

Azevedo, G. M., Vazquez, G., Luna, A., Aguilar, D., & Rolan, A. (2009). *Photovoltaic inverters with fault ride-through capability.* Paper presented at the 2009 IEEE International Symposium on Industrial Electronics.

Azit, A., Sulaiman, S., Hussein, Z., Balakhrisnan, M., Busrah, A., Devaraju, P., . . . Ismail, M. (2012). TNB technical guidebook on grid-interconnection of photovoltaic power generation system to LV and MV networks (pp. 1-38): Tenaga Nasional Berhad, Malaysia.

Badrzadeh, B., & Halley, A. (2015). Challenges associated with assessment and testing of fault ride-through compliance of variable power generation in Australian national electricity market. *IEEE Transactions on Sustainable Energy, 6*(3), 1160-1168.

Bae, Y., Vu, T.-K., & Kim, R.-Y. (2013). Implemental control strategy for grid stabilization of grid-connected PV system based on German grid code in symmetrical low-to-medium voltage network. *IEEE Transactions on Energy Conversion, 28*(3), 619-631.

Banu, I. V., & Istrate, M. (2014). *Study on three-phase photovoltaic systems under grid faults.* Paper presented at the Electrical and Power Engineering (EPE), 2014 International Conference and Exposition on.

Barge, S. A., & Jagtap, S. (2013). Harmonic Analysis of Sinusoidal Pulse Width Modulation. *International Journal of Advanced Electrical and Electronics Engineering, 2*(5), 13-16.

Basso, T., Hambrick, J., & DeBlasio, D. (2012). Update and review of IEEE P2030 Smart Grid Interoperability and IEEE 1547 interconnection standards *2012 IEEE PES Innovative Smart Grid Technologies (ISGT)*.

Basso, T. S., & DeBlasio, R. (2004). IEEE 1547 series of standards: interconnection issues. *IEEE Transactions on power electronics, 19*(5), 1159-1162. doi: 10.1109/TPEL.2004.834000

Bellia, H., Youcef, R., & Fatima, M. (2014). A detailed modeling of photovoltaic module using MATLAB. *NRIAG Journal of Astronomy and Geophysics, 3*(1), 53-61.

Benz, C. H., Franke, W.-T., & Fuchs, F. W. (2010). *Low voltage ride through capability of a 5 kW grid-tied solar inverter.* Paper presented at the Power Electronics and Motion Control Conference (EPE/PEMC), 2010 14th International.

Bică, D., Dulău, M., Muji, M., & Dulău, L. I. (2016). Photovoltaic Power Plant Grid Integration in the Romanian System–Technical Approaches *Renewable Energy-Utilisation and System Integration*: InTech.

Blaabjerg, F., Teodorescu, R., Liserre, M., & Timbus, A. V. (2006). Overview of control and grid synchronization for distributed power generation systems. *IEEE Transactions on Industrial Electronics, 53*(5), 1398-1409.

Blooming, T. M., & Carnovale, D. J. (2006). *Application of IEEE Std 519-1992 harmonic limits.* Paper presented at the Pulp and Paper Industry Technical Conference, 2006. Conference Record of Annual.

Bonaldo, J. P., Schiavon, G., Paredes, H. K. M., & Pomilio, J. A. (2017). *Multifunctional operation of current controlled VSI based on the harmonic content of PCC voltage.* Paper presented at the Power Electronics for Distributed Generation Systems (PEDG), 2017 IEEE 8th International Symposium on.

Bouraiou, A., Hamouda, M., Chaker, A., Sadok, M., Mostefaoui, M., & Lachtar, S. (2015). Modeling and simulation of photovoltaic module and array based on one and two diode model using Matlab/Simulink. *Energy Procedia, 74*, 864-877.

Bundesverband der Energieund Wasserwirtschaft (BDEW). (2008). Technische Richtlinie Erzeugungsanlagen am Mittelspannungsnetz – Richtlinie für Anschluss und Parallelbetrieb von Erzeugungsanlagen am Mittelspannungsnetz. Retrieved June, 2017, from https://www.bdew.de/

Cabrera-Tobar, A., Bullich-Massagué, E., Aragüés-Peñalba, M., & Gomis-Bellmunt, O. (2016). Review of advanced grid requirements for the integration of large scale photovoltaic power plants in the transmission system. *Renewable and Sustainable Energy Reviews, 62*, 971-987.

Carrasco, J. E.-G., Tena, J., Ugena, D., Alonso-Martinez, J., Santos-Martin, D., & Arnaltes, S. (2013). Testing low voltage ride through capabilities of solar inverters. *ELECTR POW SYST RES, 96*, 111-118. doi: doi.org/10.1016/j.epsr.2012.10.011

Castilla, M., Miret, J., Camacho, A., Matas, J., & de Vicuña, L. G. (2014). Voltage support control strategies for static synchronous compensators under unbalanced voltage sags. *IEEE Transactions on Industrial Electronics, 61*(2), 808-820.

CEI-Comitato Elettrotecnico Italiano. (2014). Reference technical rules for the connection of active and passive consumers to the HV and MV electrical networks of distribution Company. Retrieved 23-Aug., 2016, from http://www.ceiweb.it/

Center, F. S. E. (2001). Grid-connected photovoltaic system design review and approval: FSEC-CP.

Cha, H., Vu, T.-K., & Kim, J.-E. (2009). *Design and control of Proportional-Resonant controller based Photovoltaic power conditioning system.* Paper presented at the Energy Conversion Congress and Exposition, 2009. ECCE 2009. IEEE.

Charles, J.-P., Hannane, F., El-Mossaoui, H., Zegaoui, A., Nguyen, T., Petit, P., & Aillerie, M. (2014). Faulty PV panel identification using the Design of Experiments (DoE) method. *International Journal of Electrical Power & Energy Systems, 57*, 31-38.

Chen, P.-C., Chen, P.-Y., Liu, Y.-H., Chen, J.-H., & Luo, Y.-F. (2015). A comparative study on maximum power point tracking techniques for photovoltaic generation systems operating under fast changing environments. *Solar Energy, 119*, 261-276.

Chen, S., Lai, Y., Tan, S.-C., & Tse, C. K. (2008). Analysis and design of repetitive controller for harmonic elimination in PWM voltage source inverter systems. *IET Power Electronics, 1*(4), 497-506.

Chen, T.-H., Yang, C.-H., & Yang, N.-C. (2013). Examination of the definitions of voltage unbalance. *International Journal of Electrical Power & Energy Systems, 49*, 380-385.

Chine, W., Mellit, A., Pavan, A. M., & Kalogirou, S. (2014). Fault detection method for grid-connected photovoltaic plants. *Renewable Energy, 66*, 99-110.

Chua, S. C., & Oh, T. H. (2012). Solar energy outlook in Malaysia. *RENEW SUST ENERG REV, 16*(1), 564-574. doi: doi.org/10.1016/j.rser.2011.08.022

Chuah, D. G., & Lee, S. (1981). Solar radiation estimates in Malaysia. *Solar Energy, 26*(1), 33-40.

Cleveland, F. (2008). *IEC 61850-7-420 communications standard for distributed energy resources (DER).* Paper presented at the Power and Energy Society General Meeting-Conversion and Delivery of Electrical Energy in the 21st Century, 2008 IEEE.

Crăciun, B.-I., Kerekes, T., Séra, D., & Teodorescu, R. (2012). *Overview of recent grid codes for PV power integration.* Paper presented at the Optimization of Electrical and Electronic Equipment (OPTIM), 2012 13th International Conference on.

de Carvalho, R., Nielson, R., Lima, C., Kopcak, I., Vieira, F., & de Araújo, S. (2013). *Operational conditions analyses of distributed generation (DG) connected on power distribution grid based on ieee Std. 1547.* Paper presented at the Innovative Smart Grid Technologies Latin America (ISGT LA), 2013 IEEE PES Conference On.

de Souza, V. R. F. B., Alves Filho, M., & de Oliveira, K. C. (2016). *Analysis of power quality for photovoltaic systems connected to the grid.* Paper presented at the Harmonics and Quality of Power (ICHQP), 2016 17th International Conference on.

Desai, H. P., & Patel, H. (2007). *Maximum power point algorithm in PV generation: An overview.* Paper presented at the 2007 7th International Conference on Power Electronics and Drive Systems.

Diaz-Franco, F., Vu, T., El Mezyani, T., & Edrington, C. S. (2016). *Low-voltage ride-through for PV systems using model predictive control approach.* Paper presented at the North American Power Symposium (NAPS), 2016.

Ding, G., Gao, F., Tian, H., Ma, C., Chen, M., He, G., & Liu, Y. (2016). Adaptive DC-link voltage control of two-stage photovoltaic inverter during low voltage ride-through operation. *IEEE Transactions on power electronics, 31*(6), 4182-4194.

Economic Plan Unit. (2015). 9th,10th and 11th Malysian plane.   Retrieved 25, Jan, 2016, from http://www.epu.gov.my/en/home

Elrayah, M. O. M. (2017). *Performance Analysis of Grid Connected Photovoltaic System.* Sudan University of Science and Technology.

Energinet, D. (2015). Technical regulation 3.2. 2 for PV power plants with a power output above 11 kW. *Tech. Rep.*

Energy Commission Malaysia. (2010). The Malaysian grid and distribution codes. Retrieved 11-Aug., 2016, from http://www.tnb.com.my/business/malaysian-grid-code.html

Energy Commission Malaysia (ECM). (2017). Grid Code for Peninsular Malaysia. Retrieved 16-June, 2017, from http://st.gov.my

Etxegarai, A., Eguia, P., Torres, E., Buigues, G., & Iturregi, A. (2017). Current procedures and practices on grid code compliance verification of renewable power generation. *Renewable and Sustainable Energy Reviews*.

Farhoodnea, M., Mohamed, A., Shareef, H., & Zayandehroodi, H. (2013). Power quality analysis of grid-connected photovoltaic systems in distribution networks. *Przeglad Elektrotechniczny (Electrical Review), 2013*, 208-213.

Figueira, H. H., Hey, H. L., Schuch, L., Rech, C., & Michels, L. (2015). *Brazilian grid-connected photovoltaic inverters standards: A comparison with IEC and IEEE.* Paper presented at the Industrial Electronics (ISIE), 2015 IEEE 24th International Symposium on.

Foley, A., & Olabi, A. G. (2017). Renewable energy technology developments, trends and policy implications that can underpin the drive for global climate change. *Renewable and Sustainable Energy Reviews, 68*, 1112-1114. doi: http://dx.doi.org/10.1016/j.rser. 2016.12.065

Foster, S., Xu, L., & Fox, B. (2006). *Grid integration of wind farms using SVC and STATCOM.* Paper presented at the Universities Power Engineering Conference, 2006. UPEC'06. Proceedings of the 41st International.

Fuchs, E., & Masoum, M. A. (2011). *Power quality in power systems and electrical machines*: Academic press, Boston.

García-Sánchez, T., Gómez-Lázaro, E., & Molina-García, A. (2014). *A Review and Discussion of the Grid-Code Requirements for Renewable Energy Sources in Spain.* Paper presented at the International Conference on Renewable Energies and Power Quality (ICREPQ'14), Cordoba, Spain April.

GB/T. (2012). Technical Rule for PV Power Station Connected to Power Grid. *Chinese Enterprise Standards*.

Gevorgian, V., & Booth, S. (2013). Review of PREPA technical requirements for interconnecting wind and solar generation. *National Renewable Energy Laboratory: Golden, CO, USA*.

Ghaib, K., & Ben-Fares, F.-Z. (2017). A design methodology of stand-alone photovoltaic power systems for rural electrification. *Energy conversion and management, 148*, 1127-1141.

Gkavanoudis, S. I., & Demoulias, C. S. (2014). A combined fault ride-through and power smoothing control method for full-converter wind turbines employing Supercapacitor Energy Storage System. *Electric Power Systems Research, 106*, 62-72.

Global Status Report. (2017). Renewables 2016 Global Status Report-REN21. Retrieved 22 February, 2017, from http://www.ren21.net/wp-content/uploads/2016/06/GSR_2016_ Full_Report.pdf

Gonen, T. (2016). *Electric power distribution engineering*: CRC press.

Grainger, J. J., & Stevenson, W. D. (1994). *Power system analysis*: McGraw-Hill.

Guo, X.-Q., Wu, W.-Y., & Gu, H.-R. (2011). Phase locked loop and synchronization methods for grid-interfaced converters: a review. *Przeglad Elektrotechniczny, 87*(4), 182-187.

Hasanien, H. M. (2016). An Adaptive Control Strategy for Low Voltage Ride Through Capability Enhancement of Grid-Connected Photovoltaic Power Plants. *IEEE Transactions on Power Systems, 31*(4), 3230-3237.

Hassaine, L. (2016). Power Converters and Control of Grid-Connected Photovoltaic Systems *Renewable Energy in the Service of Mankind Vol II* (pp. 497-504): Springer.

Hassaine, L., OLias, E., Quintero, J., & Salas, V. (2014). Overview of power inverter topologies and control structures for grid connected photovoltaic systems. *Renewable and Sustainable Energy Reviews, 30*, 796-807.

Hojabri, M., & Soheilirad, M. (2014). *Harmonic Distortion in an Off-Grid Renewable Energy System with Different Loads.* Paper presented at the Proceedings of the International MultiConference of Engineers and Computer Scientists.

Honrubia-Escribano, A., Ramirez, F. J., Gómez-Lázaro, E., Garcia-Villaverde, P. M., Ruiz-Ortega, M. J., & Parra-Requena, G. (2018). Influence of solar technology in the economic performance of PV power plants in Europe. A comprehensive analysis. *Renewable and Sustainable Energy Reviews, 82*, 488-501.

Hossain, J., & Mahmud, A. (2014). *Renewable energy integration: challenges and solutions*: Springer Science & Business Media.

Hossain, M. K., & Ali, M. H. (2014). *Low voltage ride through capability enhancement of grid connected PV system by SDBR.* Paper presented at the T&D Conference and Exposition, 2014 IEEE PES.

Huang, T., Shi, X., Sun, Y., & Wang, D. (2014). *Three-phase photovoltaic grid-connected inverter based on feedforward decoupling control.* Paper presented at the Materials for Renewable Energy and Environment (ICMREE), 2013 International Conference on.

IEEE power and energy society. (2009). Electrical Power System Competition EPSCOM 2009,Project Based Learning (PBL). *1*, 1-34.

IEEE Std. 929-2000. (2000). IEEE Recommended Practice for Utility Interface of Photovoltaic (PV) Systems. *IEEE Std 929-2000*, i. doi: 10.1109/IEEESTD.2000.91304

International Energy Agency (IEA). (2017). 2016 snapshot of global photovoltaic markets. Retrieved 22-June, 2017, from http://www.iea-pvps.org/index.php?id=267

Ishaque, K., Salam, Z., & Lauss, G. (2014). The performance of perturb and observe and incremental conductance maximum power point tracking method under dynamic weather conditions. *Applied Energy, 119*, 228-236.

Islam, G. M. S., Al-Durra, A., Muyeen, S. M., & Tamura, J. (2011, 7-10 Nov. 2011). *Low voltage ride through capability enhancement of grid connected large scale photovoltaic system.* Paper presented at the IECON 2011 - 37th Annual Conference of the IEEE Industrial Electronics Society.

Islam, M. R., Guo, Y., & Zhu, J. (2014). Power Converters for Small-to Large-Scale Photovoltaic Power Plants *Power Converters for Medium Voltage Networks* (pp. 17-49): Springer.

Jafar, A. H., Al-Amin, A. Q., & Siwar, C. (2008). Environmental impact of alternative fuel mix in electricity generation in Malaysia. *Renewable Energy, 33*(10), 2229-2235.

Jain, S., & Agarwal, V. (2007). New current control based MPPT technique for single stage grid connected PV systems. *Energy conversion and management, 48*(2), 625-644.

Jana, J., Saha, H., & Bhattacharya, K. D. (2016). A review of inverter topologies for single-phase grid-connected photovoltaic systems. *Renewable and Sustainable Energy Reviews*.

Jayakrishnan, R., & Sruthy, V. (2015). *Fault ride through augmentation of microgrid.* Paper presented at the Advancements in Power and Energy (TAP Energy), 2015 International Conference on.

Jenkins, N., & Thornycroft, J. (2017). Grid Connection of Photovoltaic Systems: Technical and Regulatory Issues *McEvoy's Handbook of Photovoltaics (Third Edition)* (pp. 847-876): Elsevier.

Johari, A., Hafshar, S. S., Ramli, M., & Hashim, H. (2011). *Potential use of solar photovoltaic in Peninsular Malaysia.* Paper presented at the Clean Energy and Technology (CET), 2011 IEEE First Conference on, Kuala Lumpur, Malaysia.

Kale, M., & Ozdemir, E. (2005). An adaptive hysteresis band current controller for shunt active power filter. *Electric Power Systems Research, 73*(2), 113-119.

Kamarzaman, N. A., & Tan, C. W. (2014). A comprehensive review of maximum power point tracking algorithms for photovoltaic systems. *Renewable and Sustainable Energy Reviews, 37*, 585-598.

Kanjiya, P., Singh, B., Chandra, A., & Al-Haddad, K. (2013). "SRF Theory Revisited" to Control Self-Supported Dynamic Voltage Restorer (DVR) for Unbalanced and Nonlinear Loads. *IEEE Transactions on Industry Applications, 49*(5), 2330-2340.

Khan, M. J., & Mathew, L. (2017). Different kinds of maximum power point tracking control method for photovoltaic systems: a review. *Archives of Computational Methods in Engineering, 24*(4), 855-867.

Kim, S.-T., Kang, B.-K., Bae, S.-H., & Park, J.-W. (2013). Application of SMES and grid code compliance to wind/photovoltaic generation system. *IEEE Transactions on Applied Superconductivity, 23*(3), 5000804-5000804.

Klapp, D., & Vollkommer, H. T. (2014). *Application of an intelligent static switch to the point of common coupling to satisfy IEEE 1547 compliance.* Paper presented at the Power Engineering Society General Meeting, 2007. IEEE, Tampa, FL, USA.

Kobayashi, H. (2012). *Fault ride through requirements and measures of distributed PV systems in Japan.* Paper presented at the 2012 IEEE Power and Energy Society General Meeting.

Kothari, D. P., & Nagrath, I. (2003). *Modern power system analysis*: Tata McGraw-Hill Education.

Kumar, L. A., & Surekha, P. (2015). Solar PV and Wind Energy Conversion Systems.

Kurokawa, K., Komoto, K., van der Vleuten, P., & Faiman, D. (2007). Energy from the desert: Practical proposals for Very Large Scale Photovoltaic Systems: Earthscan: London.

Lammert, G., Boemer, J. C., Premm, D., Glitza, O., Ospina, L. D. P., Fetzer, D., & Braun, M. (2017). *Impact of fault ride-through and dynamic reactive power support of photovoltaic systems on short-term voltage stability.* Paper presented at the PowerTech, 2017 IEEE Manchester.

Latran, M. B., & Teke, A. (2015). A novel wavelet transform based voltage sag/swell detection algorithm. *International Journal of Electrical Power & Energy Systems, 71*, 131-139.

Lauria, D., & Coppola, M. (2014). Design and control of an advanced PV inverter. *Solar Energy, 110*, 533-542.

Lee, J.-S., & Lee, K. B. (2013). Variable dc-link voltage algorithm with a wide range of maximum power point tracking for a two-string PV system. *Energies, 6*(1), 58-78.

Li, K., Qian, J., Wu, H., Li, T., & Yang, J. (2015). *Research on Low Voltage Ride through of the Grid-Connected PV System.* Paper presented at the International Conference on Advances in Energy, Environment and Chemical Engineering (AEECE-2015).

Li, Y., Li, R., Liu, H., Cai, H., & Dong, J. China's Distributed Generation of Electric Power-Current Situation And Prospect.

Liu, Y.-J., Lan, P.-H., Lin, H.-H., Chiu, T.-Y., & Chen, H.-W. (2013). *Power conditioner interconnection test system of distributed resources based on IEEE 1547 standard.* Paper presented at the Future Energy Electronics Conference (IFEEC), 2013 1st International.

Lu, C., Zhou, Z., Jiang, A., Luo, M., Shen, P., & Han, Y. (2016). *Comparative performance evaluation of phase-locked loop (PLL) algorithms for single-phase grid-connected converters.* Paper presented at the Power Electronics and Motion Control Conference (IPEMC-ECCE Asia), 2016 IEEE 8th International.

Lu, S.-y., Wang, L., Ke, S.-c., Chang, C.-h., & Yang, Z.-h. (2014). *Analysis of measured power-quality results of a PV system connected to Peng-Hu Power System.* Paper presented at the Industry Applications Society Annual Meeting, 2014 IEEE.

Magoro, B., & Khoza, T. (2012). Grid connection code for renewable power plants connected to the electricity transmission system or the distribution system in South Africa. *no. November*.

Mahela, O. P., & Shaik, A. G. (2017). Comprehensive overview of grid interfaced solar photovoltaic systems. *Renewable and Sustainable Energy Reviews, 68*, 316-332.

Mahmoud, M. M., & Ibrik, I. H. (2006). Techno-economic feasibility of energy supply of remote villages in Palestine by PV-systems, diesel generators and electric grid. *RENEW SUST ENERG REV, 10*(2), 128-138. doi: doi.org/10.1016/j.rser.2004.09.001

Manikanta, B., Kesavarao, G., & Talati, S. (2017). LVRT of Grid Connected PV System with Energy Storage. *International Science Press, 10*(5), 75-86.

Mekhilef, S., Safari, A., Mustaffa, W., Saidur, R., Omar, R., & Younis, M. (2012). Solar energy in Malaysia: current state and prospects. *Renewable and Sustainable Energy Reviews, 16*(1), 386-396.

Merabet, A., & Labib, L. (2017). *Control system for dual-mode operation of grid-tied photovoltaic and wind energy conversion systems with active and reactive power injection.*, saint mary's university, Halifax, Nova Scotia, Canada.

Merabet, A., Labib, L., & Ghias, A. M. (2017). Robust Model Predictive Control for Photovoltaic Inverter System with Grid Fault Ride-Through Capability. *IEEE Transactions on Smart Grid*.

Milanovic, J. V., & Zhang, Y. (2010). Modeling of FACTS devices for voltage sag mitigation studies in large power systems. *IEEE transactions on power delivery, 25*(4), 3044-3052.

Mohammad, N., Quamruzzaman, M., Hossain, M. R. T., & Alam, M. R. (2013). Parasitic effects on the performance of DC-DC SEPIC in photovoltaic maximum power point tracking applications. *Smart Grid and Renewable Energy, 4*(01), 113.

Mohseni, M., & Islam, S. M. (2012). Review of international grid codes for wind power integration: Diversity, technology and a case for global standard. *Renewable and Sustainable Energy Reviews, 16*(6), 3876-3890.

Neumann, T., & Erlich, I. (2012). *Modelling and control of photovoltaic inverter systems with respect to German grid code requirements.* Paper presented at the 2012 IEEE Power and Energy Society General Meeting.

Nugroho, A. (2010). The impact of solar chimney geometry for stack ventilation in Malaysia's single storey terraced house. *Malaysia's Geography*, 163-177.

Obi, M., & Bass, R. (2016). Trends and challenges of grid-connected photovoltaic systems–A review. *Renewable and Sustainable Energy Reviews, 58*, 1082-1094.

Omar, A. M., & Zainuddin, H. (2014). Modeling and Simulation of Grid Inverter in Grid-Connected Photovoltaic System. *International Journal of Renewable Energy Research (IJRER), 4*(4), 949-957.

Ong, H., Mahlia, T., & Masjuki, H. (2011). A review on energy scenario and sustainable energy in Malaysia. *Renewable and Sustainable Energy Reviews, 15*(1), 639-647.

Orłowska-Kowalska, T., Blaabjerg, F., & Rodríguez, J. (2014). *Advanced and intelligent control in power electronics and drives,T. Orłowska-Kowalska (Ed.).* (Vol. 531): Springer.

Pannell, G., Zahawi, B., Atkinson, D. J., & Missailidis, P. (2013). Evaluation of the performance of a DC-link brake chopper as a DFIG low-voltage fault-ride-through device. *IEEE Transactions on Energy Conversion, 28*(3), 535-542.

Parvez, M., Elias, M., Rahim, N., & Osman, N. (2016). Current control techniques for three-phase grid interconnection of renewable power generation systems: A review. *Solar Energy, 135*, 29-42.

Patel, D., Goswami, A. K., & Singh, S. K. (2015). Voltage sag mitigation in an Indian distribution system using dynamic voltage restorer. *International Journal of Electrical Power & Energy Systems, 71*, 231-241.

Perpinias, I., Papanikolaou, N., & Tatakis, E. (2015). Fault ride through concept in low voltage distributed photovoltaic generators for various dispersion and penetration scenarios. *Sustainable Energy Technologies and Assessments, 12*, 15-25.

Petrović, I., Šimić, Z., & Vražić, M. (2014). Advanced PV Plant Planning based on Measured Energy Production Results-Approach and Measured Data Processing. *Advances in Electrical and Computer Engineering, 14*(1), 49-54.

Pigazo, A., Liserre, M., Mastromauro, R. A., Moreno, V. M., & Dell'Aquila, A. (2009). Wavelet-based islanding detection in grid-connected PV systems. *IEEE Transactions on Industrial Electronics, 56*(11), 4445-4455.

Preda, T. N., Uhlen, K., & Nordg, D. E. (2012, 29-30 May 2012). *An overview of the present grid codes for integration of distributed generation.* Paper presented at the Integration of Renewables into the Distribution Grid, CIRED 2012 Workshop.

Ram, J. P., Babu, T. S., & Rajasekar, N. (2017). A comprehensive review on solar PV maximum power point tracking techniques. *Renewable and Sustainable Energy Reviews, 67*, 826-847.

Red Electrica. (2008). Technical requirements for wind power and photovoltaic installationsand any generating facilities whose technology does not consist on asynchronous generator directly connected to the grid, issued by RedElectrica, October 2008, O.P. 12.2 Restricted to the technicalrequirements of wind power and photovoltaic facilities (draft).   Retrieved 23-Aug

2016, from (translated in English by: www.aeolica.es)

Reddy, K. R., Babu, N. R., & Sanjeevikumar, P. (2018). A Review on Grid Codes and Reactive Power Management in Power Grids with WECS *Advances in Smart Grid and Renewable Energy* (pp. 525-539): Springer.

Ruiz, A. (2011). System aspects of large scale implementation of a photovoltaic power plant.

Saad, N. H., El-Sattar, A. A., & Mansour, A. E.-A. M. (2016). Improved particle swarm optimization for photovoltaic system connected to the grid with low voltage ride through capability. *Renewable Energy, 85*, 181-194.

Sannino, A., Miller, M. G., & Bollen, M. H. (2000). *Overview of voltage sag mitigation.* Paper presented at the Power Engineering Society Winter Meeting, 2000. IEEE.

Saravanan, S., & Babu, N. R. (2016). Maximum power point tracking algorithms for photovoltaic system–A review. *Renewable and Sustainable Energy Reviews, 57*, 192-204.

Seo, H.-C., Kim, C.-H., Yoon, Y.-M., & Jung, C.-S. (2009a). *Dynamics of grid-connected photovoltaic system at fault conditions.* Paper presented at the Transmission & Distribution Conference & Exposition: Asia and Pacific, 2009.

Seo, H.-C., Kim, C.-H., Yoon, Y.-M., & Jung, C.-S. (2009b). *Dynamics of grid-connected photovoltaic system at fault conditions.* Paper presented at the 2009 Transmission & Distribution Conference & Exposition: Asia and Pacific.

Shah, R., Mithulananthan, N., Bansal, R., & Ramachandaramurthy, V. (2015). A review of key power system stability challenges for large-scale PV integration. *Renewable and Sustainable Energy Reviews, 41*, 1423-1436.

Shahnia, F., Ghosh, A., Ledwich, G., & Zare, F. (2011). *Voltage correction in low voltage distribution networks with rooftop PVs using custom power devices.* Paper presented at the IECON 2011-37th Annual Conference on IEEE Industrial Electronics Society.

Shahnia, F., Majumder, R., Ghosh, A., Ledwich, G., & Zare, F. (2011). Voltage imbalance analysis in residential low voltage distribution networks with rooftop PVs. *Electric Power Systems Research, 81*(9), 1805-1814.

Silvestre, S., Chouder, A., & Karatepe, E. (2013). Automatic fault detection in grid connected PV systems. *Solar Energy, 94*, 119-127.

Singh, B., Chandra, A., & Al-Haddad, K. (2014). *Power quality: problems and mitigation techniques*: John Wiley & Sons.

Smith, J. C., Hensley, G., & Ray, L. (1995). IEEE Recommended Practice for Monitoring Electric Power Quality. *IEEE Std*, 1159-1995.

Subudhi, B., & Pradhan, R. (2013). A comparative study on maximum power point tracking techniques for photovoltaic power systems. *IEEE Transactions on Sustainable Energy, 4*(1), 89-98.

Suruhanjaya Tenaga. (2016). Guidelines on Large-Scale Solar Photovoltaic Plant for Connection to Electricity Network (pp. 1-672). energy commision malaysia

Tan, C. N. (2014). Solar-Powered Digital Water Meter With Wireless Capability.

Tenaga, K., & dan Air, T. H. (2011). Handbook on the Malaysian Feed-in-Tariff for the Promotion of Renewable Energy. *Ministry of Energy, Green Technology and Water, Malaysia*.

Tenaga Nasional Berhad. (2005). Technical Guidebook for the Connection of Generation to the Distribution Network. *Tenaga Nasional Berhad*.

Teodorescu, R., Blaabjerg, F., Liserre, M., & Loh, P. C. (2006). Proportional-resonant controllers and filters for grid-connected voltage-source converters. *IEE Proceedings-Electric Power Applications, 153*(5), 750-762.

Teodorescu, R., & Liserre, M. (2011). *Grid converters for photovoltaic and wind power systems* (Vol. 29): John Wiley & Sons.

Theologitis, I.-T. (2011). Comparison of existing PV models and possible integration under EU grid specifications.

Timbus, A., Liserre, M., Teodorescu, R., Rodriguez, P., & Blaabjerg, F. (2009). Evaluation of current controllers for distributed power generation systems. *IEEE Transactions on power electronics, 24*(3), 654-664.

Tohidi, S., & Behnam, M.-i. (2016). A comprehensive review of low voltage ride through of doubly fed induction wind generators. *Renewable and Sustainable Energy Reviews, 57*, 412-419.

TOPSUN solar modules. (2017). 400Wp Topsun S400 PV module Retrieved 22/Jan, 2017, from http://topsun.kr/english/product/images/New%20Brochure.pdf

Troester, E. (2009). *New German grid codes for connecting PV systems to the medium voltage power grid.* Paper presented at the 2nd International workshop on concentrating photovoltaic power plants: optical design, production, grid connection.

Ünlu, M., Camur, S., Beser, E., & Arifoglu, B. (2015). A Current-Forced Line-Commutated Inverter for Single-Phase Grid-Connected Photovoltaic Generation Systems. *Advances in Electrical and Computer Engineering, 15*(2), 85-92.

VanderMeulen, A., & Maurin, J. (2010). Current source inverter vs. Voltage source inverter topology. *Technical Data TD02004004E, Eaton*.

Viet, N. H., & Yokoyama, A. (2010). *Impact of fault ride-through characteristics of high-penetration photovoltaic generation on transient stability.* Paper presented at the Power System Technology (POWERCON), 2010 International Conference on.

Villalva, M. G., Gazoli, J. R., & Ruppert Filho, E. (2009a). *Analysis and simulationof the P&O MPPT algorithm using alinearized PV array model.* Paper presented at the Power Electronics Conference, 2009. COBEP'09. Brazilian.

Villalva, M. G., Gazoli, J. R., & Ruppert Filho, E. (2009b). Comprehensive approach to modeling and simulation of photovoltaic arrays. *IEEE Transactions on power electronics, 24*(5), 1198-1208.

Vu, T. T., Tuyen, N. D., & Bang, N. L. H. (2016). Control Method for Reducing a THD of Grid Current at Three-Phase Grid-Connected Inverters Under Distorted and Unbalanced Grid Voltages. *PROCEEDING of Publishing House for Science and Technology, 1*(1).

Wang, G., Zhao, K., Shi, J., Chen, W., Zhang, H., Yang, X., & Zhao, Y. (2017). An iterative approach for modeling photovoltaic modules without implicit equations. *Applied Energy, 202*, 189-198.

Worku, M. Y., & Abido, M. A. (2015). *Grid-connected PV array with supercapacitor energy storage system for fault ride through.* Paper presented at the Industrial Technology (ICIT), 2015 IEEE International Conference on.

Woyte, A., & Goy, S. (2017). Large grid-connected photovoltaic power plants: Best practices for the design and operation of large photovoltaic power plants *The Performance of Photovoltaic (PV) System* (pp. 321-337): Elsevier.

Wu, H., & Tao, X. (2009). *Three phase photovoltaic grid-connected generation technology with MPPT function and voltage control.* Paper presented at the 2009 International Conference on Power Electronics and Drive Systems (PEDS), Taipei, Taiwan.

Wu, Y.-K., Lin, J.-H., & Lin, H.-J. (2017). Standards and guidelines for grid-connected photovoltaic generation systems: A review and comparison. *IEEE Transactions on Industry Applications*.

Yang, B., Li, W., Zhao, Y., & He, X. (2010). Design and analysis of a grid-connected photovoltaic power system. *IEEE Transactions on power electronics, 25*(4), 992-1000.

Yang, L., Liu, W., Peng, G., Chen, Y.-G., & Xu, Z. (2016). Coordinated-Control Strategy of Photovoltaic Converters and Static Synchronous Compensators for Power System Fault Ride-Through. *Electric Power Components and Systems, 44*(15), 1683-1692.

Yang, Y., & Blaabjerg, F. (2013). Low-voltage ride-through capability of a single-stage single-phase photovoltaic system connected to the low-voltage grid. *International Journal of Photoenergy, 2013*.

Yang, Y., Blaabjerg, F., & Zou, Z. (2013). Benchmarking of grid fault modes in single-phase grid-connected photovoltaic systems. *IEEE Transactions on Industry Applications, 49*(5), 2167-2176.

Yang, Y., Enjeti, P., Blaabjerg, F., & Wang, H. (2013). *Suggested grid code modifications to ensure wide-scale adoption of photovoltaic energy in distributed power generation systems.* Paper presented at the Industry Applications Society Annual Meeting, 2013 IEEE.

Yang, Y., Zhou, K., & Blaabjerg, F. (2013). *Harmonics suppression for single-phase grid-connected PV systems in different operation modes.* Paper presented at the

Applied Power Electronics Conference and Exposition (APEC), 2013 Twenty-Eighth Annual IEEE.

Yibre, M., & Abido, M. (2013). *Supercapacitors for wind power application.* Paper presented at the Renewable Energy Research and Applications (ICRERA), 2013 IZhang, Y., Ma, L., & Zheng, T. Q. (2011). *Application of feedback linearization strategy in voltage fault ride-through for photovoltaic inverters.* Paper presented at the IECON 2011-37th Annual Conference on IEEE Industrial Electronics Society.

Zhu, Y., Yao, J., & Wu, D. (2011). *Comparative study of two stages and single stage topologies for grid-tie photovoltaic generation by PSCAD/EMTDC.* Paper presented at the Advanced Power System Automation and Protection (APAP), 2011.
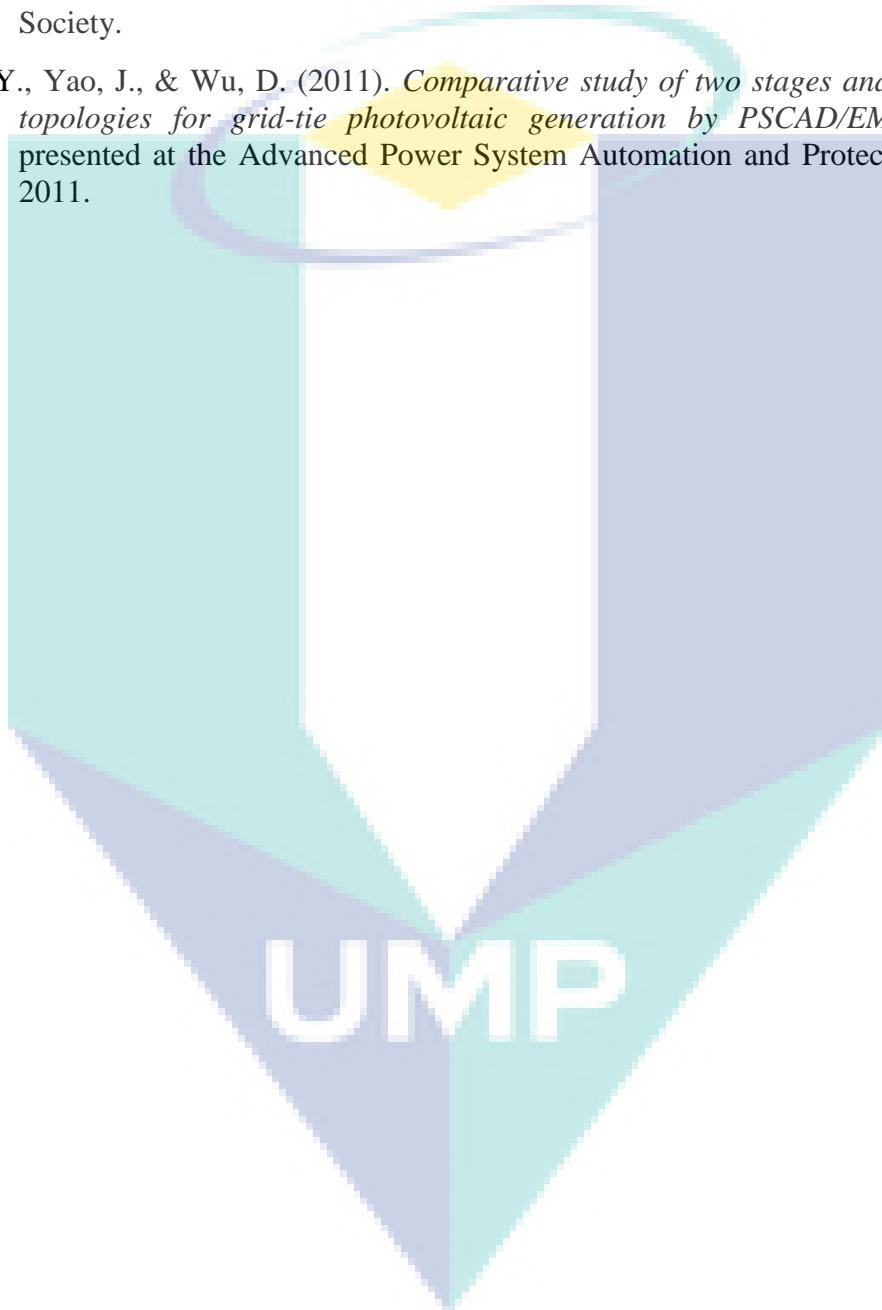
TOP SUN S400 PV MODULE DATASHEET

Electrical Specification

	TS-S390	TS-S395	TS-S400	TS-S405	TS-S410	TS-S415	TS-S420	TS-S425	TS-S430
Nominal power [Wp]	390	395	400	405	410	415	420	425	430
Voltage at nominal power [V]	49.38	49.53	49.80	50.06	50.32	50.58	50.82	51.05	51.35
Current at nominal power [A]	7.92	7.98	8.04	8.10	8.15	8.21	8.27	8.33	8.38
Open-circuit voltage [V]	59.62	59.71	60.00	60.38	61.06	61.25	61.44	61.63	61.82
Short-circuit current [A]	8.42	8.49	8.56	8.66	8.77	8.84	8.92	8.99	9.07
Module efficiency level [%]	15.25	15.41	15.60	15.80	15.99	16.19	16.38	16.58	16.77
Output tolerance [%]	±2	±2	±2	±2	±2	±2	±2	±2	±2

Performance under standard test conditions (STC) : 1000W/m², 25°C, AM 1.5
Mechanical load at 5400 Pa/m² has been performed

Mono Crystalline Solar Module
PV system installer
PV Module Manufacturing Business

Mechanical characteristics

Solar cells	96 monocrystalline 6"silicon cells [156mm(6.14in) x156mm(6.14in)]
Front cover	Low iron tempered glass 4.0mm(0.15in)
Back cover	White polyester
Frame	Silver anodized aluminum
Output Cables	4㎟(0.15in) cables with polarized weatherproof connectors, IEC certified, Length 1.25m(49.21in)
Junction box	4 bypass diodes
Dimensions (HxWxT)	1960(77.16in) x 1308(51.50in) x 40 mm(1.57in)
Weight	35.5 kg(78.26lbs)

Thermal characteristics

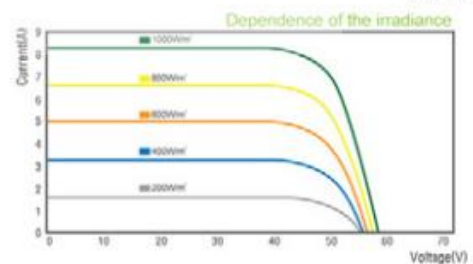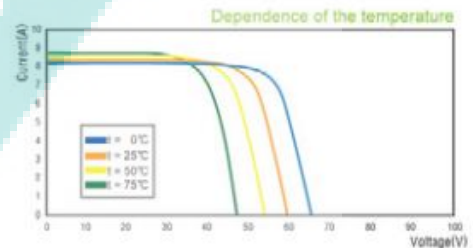|	
Temperature coefficients of Isc	0.05 %/K
Temperature coefficients of Voc	-0.40 %/K
Temperature coefficients of Pm [%]	-0.49 %/K
NOCT	47°C ±2

Limits

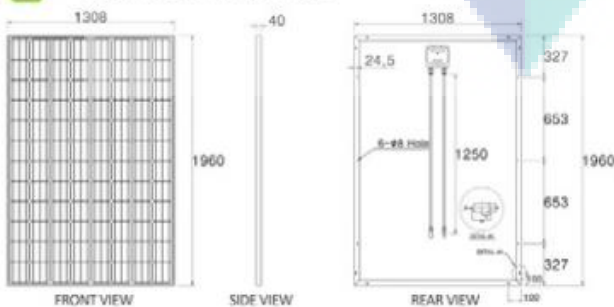|	
Operating Temperature	-40°F to +194°F (-40°C to +90°C)
Storage Temperature	-40°F to +194°F (-40°C to +90°C)
Maximum System Voltage	DC 1,000V

Warranty

10years for product defect

10years for 90% power output

25years for 80% power output

I-V Curve

Dependence of the temperature

Dependence of the irradiance

Technical Drawings

FRONT VIEW   SIDE VIEW   REAR VIEW

APPENDIX B

VOLTAGE SAG DETECTION IN GRID-CONNECTED PHOTOVOLTAIC POWER PLANT FOR LOW VOLTAGE RIDE-THROUGH CONTROL

Two various methods of sags detection which aid in calculating the needed amount of reactive current has been introduced. The RMS strategy is based on calculating the *d-q* component of the voltage grid using the following equation:

$$V_{gp} = \sqrt{V_{gd}^2 + V_{gq}^2}$$

Where V_{gd} is the *d*-component of the grid voltage whilst V_{gq} is the *q*-component of the grid voltage. The second detection method is based on calculating the positive sequence component magnitude of the three-phase grid voltage as expressed in the following equation:

$$V_{gp} = \frac{1}{3}(V_a + aV_b + a^2V_c)$$

Where *a* is the operator that shifts the vector counter-clockwise by an angle of 120 degrees, and a^2 fulfills a phase shift by 240 degrees counter-clockwise.

As described in the thesis, it is obvious that the inverter should convert from normal operation to faulty status of operation as soon as the grid sag is detected. Thus, a fast and precise detection method unit is an essential part for an efficient fault ride-through control. The flow chart shown in Figure B.1 illustrates the methodology and performance of the two proposed methods. The inputs are represented by (V_{gd} and V_{gq}) or (V_{abc} and *a*) for RMS and positive sequence methods, respectively in order to calclute the present grid voltage (V_{gp}). It should be mentioned that the value of present grid voltage is equal to the nominal grid voltage in normal operation without faults. But when the fault occurs, the V_{gp} is considered as a vector $V_{gp} = (V_{gp1}, V_{gp2,.....} V_{gpn})$, in which V_{gpi} represents the current grid voltage with regards to fault *i*, where *i* =1…*n* and *n* is the number of faults. As a result, for each value of V_{gpi}, the process will be passed through the following steps:

i. Compute the present grid voltage V_{gpi}. According to the LVRT standard requirements in the grid codes, the amount of injected reactive current will be

identified based on the value of V_{gp}. It is known that the nominal grid V_{gn} is almost one in p.u calculations, consequently identifying the value of present grid voltage is the most important step.

ii. In compliance with the standard that is divided into three regions as described in Section 4.5.4 in the thesis, the value of V_{gpi} will determine the amount of injected reactive current (I_{qr}) according to proper and complex inverter control.

iii. The output is the reactive current I_{qr}.

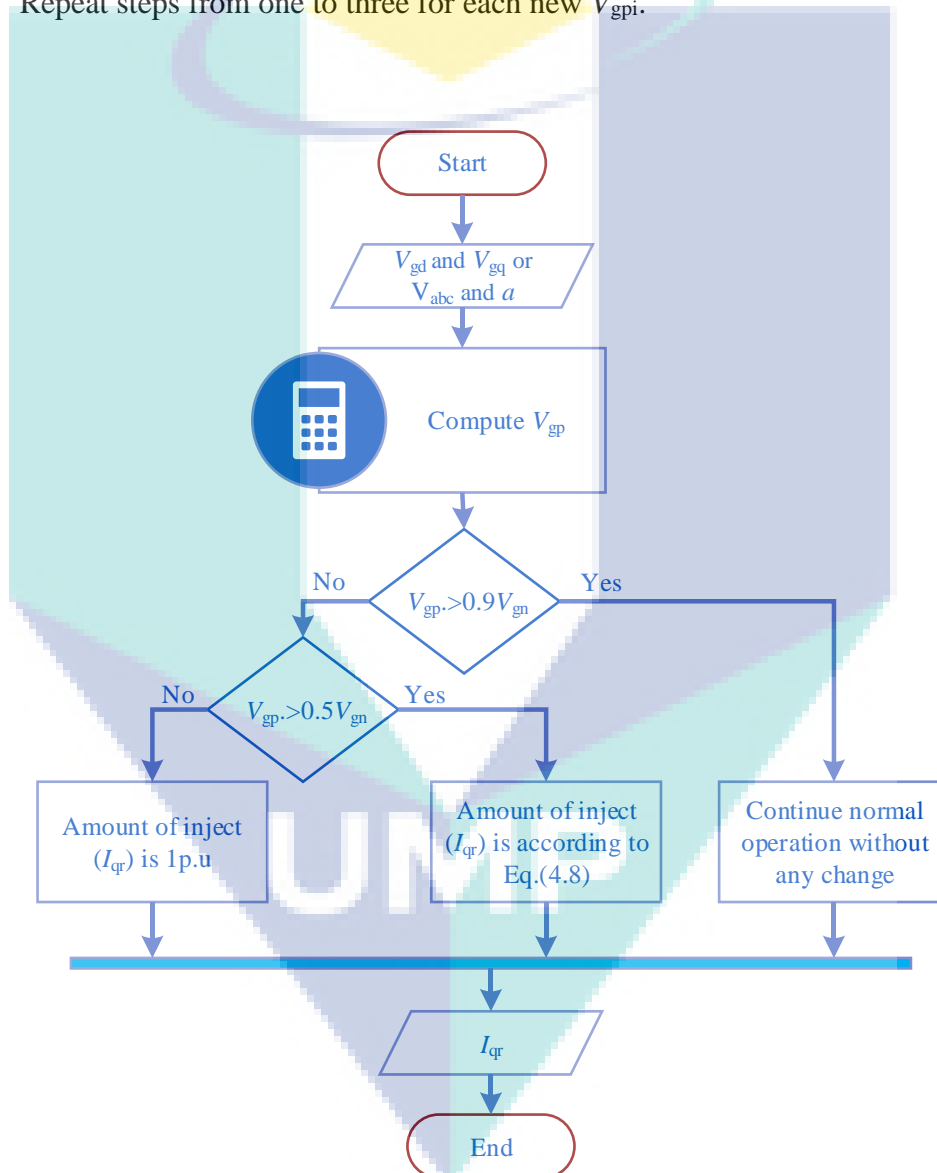iv. Repeat steps from one to three for each new V_{gpi}.

Figure B.1   Flow chart describes the operation for the detection methods.

The two sag detection methods proposed in this study have been experimentally validated for LVRT control in GCPPP using Simulink. A three-phase voltage sag that occurs at the grid side had been used as an example to test these sag detection methods.

According to the three regions of LVRT standard requirements that are previously described, as an example, the three-phase fault for testing purposes had been identified with 70% grid voltage sags.
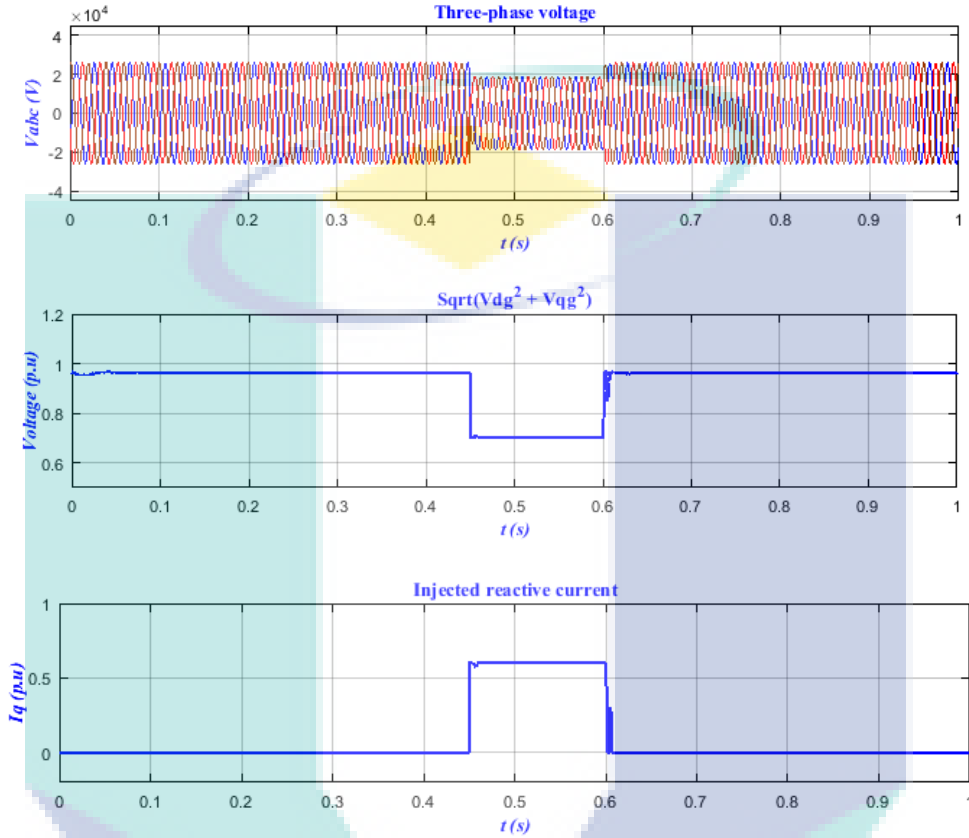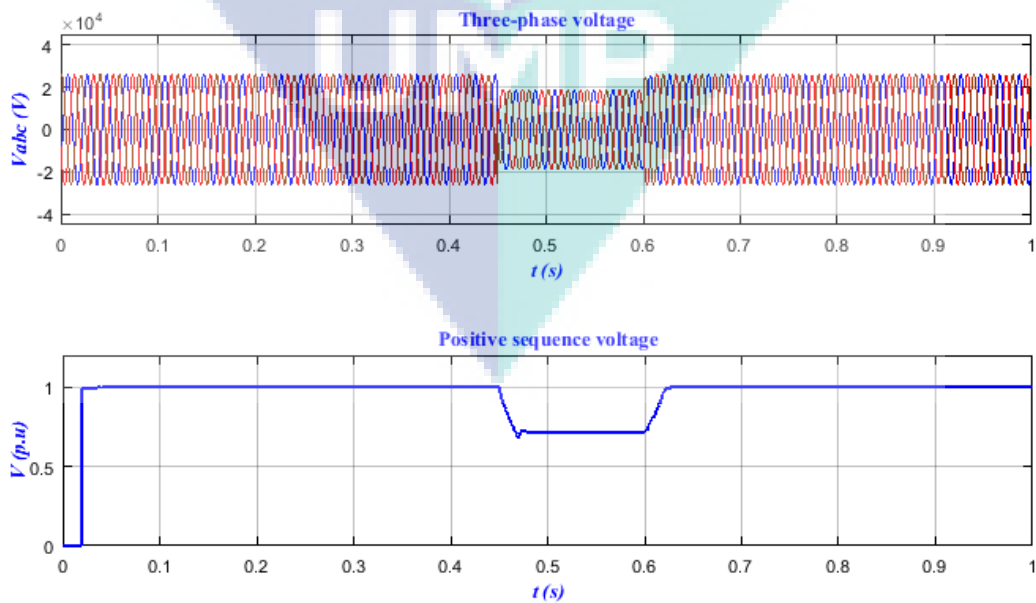

Figure B.2   RMS detection method for LVRT control during 70% three-phase voltage sag.
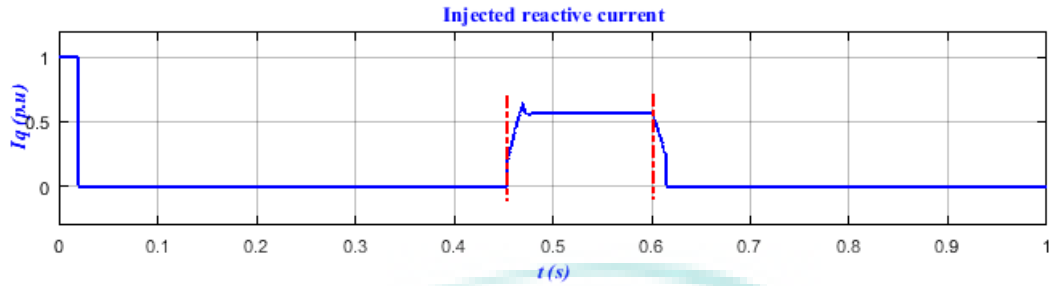
Figure B.3   Positive sequence detection method for LVRT control during 70% 3-ph voltage sag.

As a result and based on the LVRT standard requirements of GCs discussed above, the value of injected current should be 0.6 p.u. In conclusion, the two methods have satisfied the requirement conditions concerning the voltage detection, sag depth, and the amount of injected reactive current. However, the response in RMS method was faster and more accurate than positive sequence method. As it can be seen in Figure B.3   there is a delay in response at the beginning when the positive sequence method had been applied. Not only in the beginning, but also before and after the occurrence of grid faults (0.45-0.6) s. However, the RMS strategy was more accurate and effective without any delay in response which can be seen clearly in Figure B.2. Although the simulation results of the proposed methods show excellent performance concerning sag detect, identify the level of voltage sags, and amount of injected reactive current. The positive sequence detection method has some delay in response while the RMS detection algorithm is faster and more precise. In conclusion, it was found that RMS detection algorithm is preferred for a more accurate and efficient LVRT control, and therefore used in the proposed FRT control in this research.

(D-Q) TRANSFORMATION

The *dq* transformation is the process of the transform from three-phase (*abc*) system into constant *dq* rotating coordinate system via two steps. The first step is the transformation of the three-phase stationary coordinate system to the two-phase so-called stationary coordinate system *αβ*, and second step is the transformation of the *αβ* stationary coordinates system to the *dq* rotating coordinate system, as can be explained by the following figure and equations:
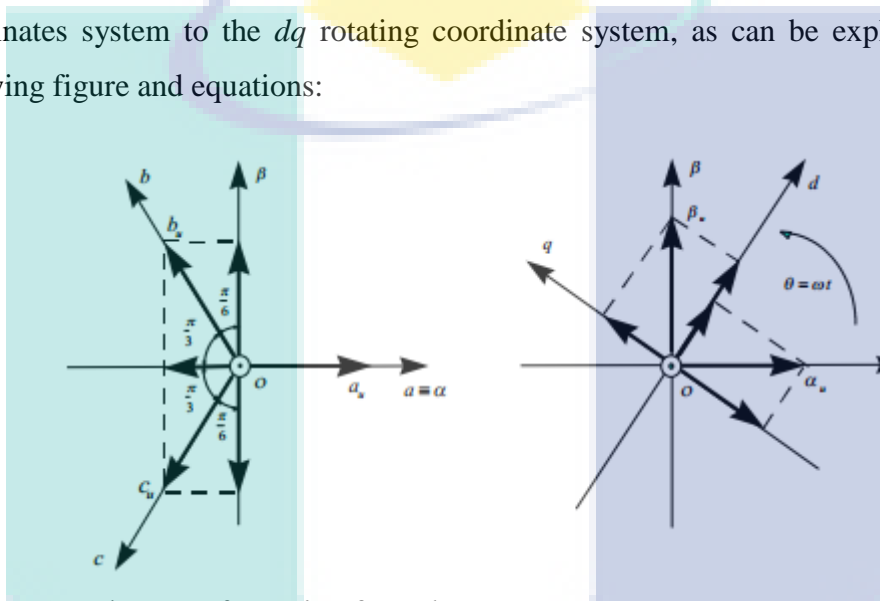

Figure B.1 Park's transformation from three-phase to rotating *dq0* coordinate system

Assuming a balanced three-phase system (X_o=0), a 3-ph vector representation transforms to *dq* vector representation (zero-axis component is 0) through the transformation matrix *T*, defined as:

$$T = \begin{bmatrix} \cos(wt) & \cos(wt - \frac{2\pi}{3}) & \cos(wt + \frac{2\pi}{3}) \\ -\sin(wt) & -\sin(wt - \frac{2\pi}{3}) & -\sin(wt + \frac{2\pi}{3}) \end{bmatrix}$$

$$\begin{bmatrix} \alpha & \beta & 0 \end{bmatrix} = \begin{bmatrix} a & b & c \end{bmatrix} \times \frac{2}{3} \times \begin{bmatrix} 1 & 0 & \frac{1}{2} \\ -\frac{1}{2} & \frac{\sqrt{3}}{2} & \frac{1}{2} \\ -\frac{1}{2} & -\frac{\sqrt{3}}{2} & \frac{1}{2} \end{bmatrix},$$

$$[d \quad q \quad 0] = [\alpha \quad \beta \quad 0] \times \begin{bmatrix} \cos\theta & -\sin\theta & 0 \\ \sin\theta & \cos\theta & 0 \\ 0 & 0 & 1 \end{bmatrix}$$

$$[d \quad q \quad 0] = [a \quad b \quad c] \times \frac{2}{3} \times \begin{bmatrix} \cos\theta & -\sin\theta & \frac{1}{2} \\ \cos(\theta - \frac{2\pi}{3}) & -\sin(\theta - \frac{2\pi}{3}) & \frac{1}{2} \\ \cos(\theta + \frac{2\pi}{3}) & -\sin(\theta + \frac{2\pi}{3}) & \frac{1}{2} \end{bmatrix}$$

It can be concluded that the transformation from X_{abc} (3-ph coordinates) to X_{dq} (dq rotating coordinates) that called Park's transformation, is obtained through the multiplication of the vector X_{abc} by the matrix T:

$$X_{dq} = T \times X_{abc}$$

The inverse transformation matrix (from dq to abc) is defined as:

$$X_{abc} = T^{-1} \times X_{dq}$$

$$T^{-1} = \begin{bmatrix} \cos(wt) & -\sin(wt) \\ \cos(wt - \frac{2\pi}{3}) & -\sin(wt - \frac{2\pi}{3}) \\ \cos(wt + \frac{2\pi}{3}) & -\sin(wt + \frac{2\pi}{3}) \end{bmatrix}$$

LIST OF PUBLICATIONS

Journal papers:

1. **Ali Q. Al-Shetwi**, Muhamad Zahim Sujod, and Frede Blaabjerg. (2018). "Low voltage ride-through capability control for single-stage inverter-based grid-connected photovoltaic power plant." *Solar Energy.* Vol. 159 (2018): 665-681. DOI: 10.1016/j.solener.2017.11.027. (*ISI Indexed, IF=4.374).*

2. **Ali Q. Al-Shetwi**, and Muhamad Zahim Sujod. (2018). "Modeling and Control of Grid-Connected Photovoltaic Power Plant with Fault Ride-Through Capability." Transaction of ASME. *Journal of Solar Energy Engineering.* Vol. 140, No. (2) (2018): 021001-021001-8. DOI: 10.1115/ 1.4038 591. (*ISI Indexed, IF=1.367).*

3. **Ali Q. Al-Shetwi**, and Muhamad Zahim Sujod. (2018). "Grid-connected photovoltaic power plants: A review of the recent integration requirements in modern grid codes." *International Journal of Energy Research.* Vol. 42, No. (5). (2018): 1849-1865. DOI: 10.1002/er.3983 (*ISI Indexed, IF=3.009).*

4. **Ali Q. Al-Shetwi**, and Muhamad Zahim Sujod. (2018). "Modeling and Design of Photovoltaic Power Plant Connected to the MV Side of the power Grid with TNB Technical Regulation Compatibility." *Electrical Engineering.* (*ISI Indexed, IF=1.269, Under Revised).*

5. **Ali Q. Al-Shetwi**, and Muhamad Zahim Sujod. (2018). "Harmonic Distortion and Voltage Unbalance Study of Photovoltaic Power Plant Connected to the Malaysian Grid." *Journal of Telecommunication, Electronic and Computer Engineering (JTEC).* Vol. 10, No. (1-2) (2018): 1-6. (*Scopus*).

6. **Ali Q. Al-Shetwi**, and Muhamad Zahim Sujod. (2018). "Voltage Sag Detection in Grid Connected Photovoltaic Power Plant for LVRT Control." *Recent Advances in Electrical & Electronic Engineering*. (*Scopus, Under Review*).

7. **Ali Q. Al-Shetwi**, and Muhamad Zahim Sujod. (2016). "Modeling And Simulation of Photovoltaic Module with Perturb and Observe MPPT Algorithm Using MATLAB" *ARPN Journal of Engineering and Applied Sciences*. Vol. 11, No. (20). (2016): 12033-12038. (*Scopus*).

8. **Ali Q. Al-Shetwi**, and Muhamad Zahim Sujod. (2015). "A review of the fault ride through requirements in different grid codes concerning penetration of PV system to the electric power network." *ARPN Journal of Engineering and Applied Sciences*. Vol. 10, No. (21) (2015): 9906-9912. (*Scopus*).

9. **Ali Q. Al-Shetwi**, Muhamad Zahim Sujod, A. Al Tarabsheh and Ibrahim A. Altawil. (2016). "Design and Economic Evaluation of Electrification of Small Villages in Rural Area in Yemen Using Stand-Alone PV System*," International Journal of Renewable Energy Research-IJRER*, Vol. 6, No. (1). (2016):289-298. DOI: 10.1234/ijrer.v6i1.3212.g6785. (*Scopus and emerging Web of Science - Thomson Reuters-outside the scope*).

Proceeding:

1. **Ali Q. Al-Shetwi**, and Muhamad Zahim Sujod. (2016). "Modeling and dynamics study of large scale PV system connected Malaysian grid under different fault conditions." *Proceeding of the IEEE International Conference of Advances in Electrical, Electronic and Systems Engineering (ICAEES), Putrajaya, Malaysia, 14-16 November 2016.* pp. 488-494. IEEE. DOI: 10.1109/ICAEES .2016. 78880 94. (*Scopus*).

2. **Ali Q. Al-Shetwi**, and Muhamad Zahim Sujod. (2016). "Sizing and Design of PV Array for Photovoltaic Power Plant Connected Grid Inverter." *Proceeding of the 3rd National Conference on Postgraduate Research, Pekan, Malaysia, 24-25 September 2016.* pp. 193-199.